Tomas Bata University in Zlín
Faculty of Technology

Doctoral Thesis

Curing of Visible Light Curing Resin Based Dental Composites

Vytvrzování dentálních materiálů

Thomas Haenel MSc

Submitted to Tomas Bata University in Zlín

Faculty of Technology

Zlín, July 2016

Doctoral study programme: P2808 Chemistry and Materials Technology

Degree course: 2808V006 Technology of Macromolecular
Substances

Supervisor: Prof. Ing. Berenika Hausnerová, Ph.D.

Consultant: Prof. Dr.-Ing. Bernhard Möginger

Keywords: visible light curing resin based composites, photo-polymerization, dielectric analysis, reaction kinetics, light distribution, hardness testing, viscoelastic properties

Klíčová slova: fotokompozit, vytvrzování světlem, dielektrická analýza, kinetika vytvrzování, distribuce záření, tvrdost, viskoelastické vlastnosti

ABSTRACT

During the last 50 years, a broad range of visible light curing resin based composites (VLC RBC) was developed for restorative applications in dentistry. Correspondingly, the technologies of light curing units (LCU) have changed from UV to visible blue light, and there from quartz tungsten halogen over plasma arc to LED LCUs increasing their light intensity significantly.

In this thesis, the influence of the curing conditions in terms of irradiance, exposure time and irradiance distribution of LCU on reaction kinetics as well as corresponding mechanical and viscoelastic properties were investigated.

Different experimental methods were used to determine time dependent degree of conversion (*DC*), depth of cure (*DoC*), hardness distribution and post-curing kinetics. Dynamic mechanical indentation technique was implemented on a dynamic mechanical analyzer to determine local viscoelastic properties on a scale of 100 to 300 μm.

To evaluate the data several quantitative approaches were applied. A novel DC-function based on a time dependent reaction constant is presented to produce intrinsically final DC-values less than 100 % and better representation DC-data. The novel *DC*-function shows that the kinetics of the curing reaction is mainly determined by the reaction time constant which depends on the irradiance of the LCU. The *DC* reached 45 % after time corresponding to the reaction time constant. It was shown that the reaction rate depends on the square root of irradiance for the investigated composites.

A new method to determine *DoC* in a user-independent and automatized manner was presented which can be applied to any depth dependent property of light curing composites. Due to the mathematical description, the properties at *DoC* have decreased to 88 % of their plateau values, and are thus not arbitrary.

Furthermore, the irradiance distribution of the LCU is reflected in the distribution of mechanical properties. Longer exposure times increase the hardness level, but do not level out the imprinted patterns. This is in accordance with long term hardness measurements revealing that the kinetics of the post-curing has a logarithmic time dependency, and is also determined by the locally introduced irradiance. Samples irradiated with different exposure times produced hardness curves which could be shifted to a master curve on the logarithmic time axis allowing for long term predictions of the hardness, and indirectly the *DC*.

RESUME

Reaction kinetics and resulting mechanical and viscoelastic properties of visible light curing resin based composites (VLC RBC) at various curing conditions are investigated. A novel degree of conversion (DC) function was determined, providing improved representation of DC-data. Further, this DC-function shows that the kinetics of the curing reaction is mainly determined by the reaction time constant which depends on the irradiance of the light curing units (LCU) under examination. The irradiance distribution of the LCU is reflected in the distribution of mechanical properties. Longer exposure times increase the hardness level, but do not level out the imprinted patterns. Samples irradiated with different exposure times produced hardness curves which could be shifted to a master curve allowing for long term predictions of the hardness, and indirectly the DC. A new method to determine depth of cure in a user-independent and automatized manner was presented which can be applied to any depth dependent property of light curing composites.

RESÜMME

Dieser Studie befasst sich mit der Reaktionskinetik und den resultierenden mechanischen und viskoelastischen Eigenschaften von lichthärtenden Dentalkompositen (VLC RBC) in Abhängigkeit der Belichtungsbedingungen. Während dieser Studie wurde eine neue Umsatzfunktion entwickelt, die zu einer Verbesserung der Darstellung der Umsatzdaten führt. Anhand dieser Funktion kann gezeigt werden, dass die Reaktionskinetik hauptsächlich durch die Reaktionszeitkonstante bestimmt wird, die vor allem von der Intensität der verwendeten Belichtungslampen abhängt. Die Intensitätsverteilung der Belichtungslampen spiegelt sich in der Verteilung der mechanischen Eigenschaften der Dentalkomposite wieder. Eine Verlängerung der Belichtungszeit führt dabei zu einer Steigerung der Härte, allerdings nicht zu einem Ausgleich der ungleichmäßigen Verteilung der mechanischen Eigenschaften. Die Belichtung von Proben mit unterschiedlichen langen Zeiten liefert Härteverläufe, die über die Verschiebung zu einer Masterkurve, die Vorhersage von Härteverläufen über einen längeren Zeitraum ermöglichen. Eine neue Methode wurde zur automatischen und benutzerunabhängigen Bestimmung der Aushärtetiefe entwickelt. Dies neue Methode kann auf verschiedene tiefenabhängige Eigenschaften von Dentalkompositen angewendet werden.

CONTENTS

LIST OF PAPERS

The following papers are included in the presented doctoral thesis:

P-I **Qualitative beam profiling of light-curing units for resin based composites.**
T. Haenel, B. Hausnerová, J. Steinhaus, B. Moeginger;
European Journal of Prosthodontics and Restorative Dentistry 2016, accepted.

P-II **Initial Reaction Kinetics of two Resin Based Dental Composites.**
T. Haenel, B. Hausnerová, J. Steinhaus, R. Price, B. Moeginger.
Submitted to *Dental Materials, July 2016.*

P-III **Examining exposure reciprocity in a resin based composite using high irradiance levels and real-time degree of conversion values.**
D. Selig, T. Haenel, B. Hausnerová, B. Moeginger, D. Labrie, B. Sullivan, R. Price.
Dental Materials, 2015, vol. 31, 583-593.

P-IV **Determining depth of cure (DoC) of VLC RBC intrinsically using a new evaluation procedure to profiles of depth dependent hardness, mass loss after solvent extraction and post-reaction enthalpy.**
T. Haenel, B. Hausnerová, M. Dopadlo, J. Steinhaus, B. Moeginger.
Submitted to *Dental Materials, July 2016.*

P-V **Effect of the irradiance distribution from light curing units on the local micro-hardness of the surface of dental resins.**
T. Haenel, B. Hausnerová, M. Dopadlo, J. Steinhaus, B. Moeginger. R. Price, B. Sullivan, B. Moeginger.
Dental Materials 2015, vol. 31, 93-104.

P-VI **Investigation of the Post-curing Behavior and Kinetics of a Dental Composite.**
T. Haenel, B. Hausnerová, L. Kehret, J. Steinhaus, B. Moeginger
Submitted to *Dental Materials, July 2016.*

1 STATE OF THE ART

Visible light curing dental resin based composites (VLC RBC) are used in different applications such as restoration, cavity liners, pit and fissure sealants, core and buildups, inlays, onlays, crowns, provisional restorations, cements for single or multiple tooth prostheses and orthodontic devices, endodontic sealers, and root canal posts [1]. Therefore, the investigation of their properties, health effects due to elution, and time dependent changes is still important to improve the performance of VLC RBCs.

1.1 Dental composites

1.1.1 History of polymer based dental composites

The use of polymers e.g. polystyrene (PS) or polymethylmethacrylate (PMMA) in dentistry for artificial teeth started in the 1930s [2,3]. These self-curing materials exhibited significant problems such as high shrinkage and low bonding with the dentin. In 1948 Oskar Haggers developed the first bonding agent, a dental adhesive based on glycerophosphoric acid dimethacrylate providing the ability to bind a polymer chemically to the dentin [4–6]. Unfortunately, the product called "Servitron" was not stable under humid conditions [7]. Between the late 1950s and the early 1960s Ray Bowen developed a silica reinforced composites based on bisphenol A glycidyl methacrylate (Bis-GMA) and triethylene glycol dimethacrylate (TEGDMA) because of the unacceptable quality of commercial products, Fig. 1 [8,9]. The first commercial resin based dental composites were self-curing materials e.g. Adaptic (Dentsply, USA). The great problem for dentists was the limited application time after mixing [4]. The first photo-polymerization systems were introduced by the chemical industry in the mid-1960s but not for the use in dentistry [10]. These UV-curing composites systems required light of wavelengths between 310 to 400 nm. The first UV-light curing unit was introduced to dentistry in 1973 [11]. Dentsply presented the first commercial UV-curing dental material named "Nuva fil" in the same year [12–14]. However, curing with UV-light caused eye defects to dentists and their assistants, generated ozone in concentration not allowed by regulations [15,16], and could lead to burnings of patients' tissue [14,17–19].

The chemical industry introduced visible light curing (VLC) monomer systems especially for printing, coating or adhesives [20]. The use of camphorquinone with a tertiary amine as co-initiator gave the photo-curing systems the ability for fast curing [14,18]. The first VLC RBCs was placed by Dr. Mohamed Bassoiuny at Turner School of Dentistry in Manchester at the 24 February 1976 [18]. The first commercial VLC RBC accepted by the American Dental Association was "Fulfil" (Dentsply, USA) in 1981 [13].

During the next twenty years the mechanical and polymerization properties - especially shrinkage, degree of conversion, wear resistance, lifetime or handling processes were in the focus of research and development [1,4]. Between 1970 and 1990, the filler systems changed from macro-filled composites over hybrid composites to micro-hybrid composites, Fig. 1 and Fig. 2. The nano-hybrid composites were developed in the late 1990s. Especially, the development of new filler systems improved mechanical performance and reduced shrinkage mainly because of higher filler contents in RBCs [21–23].
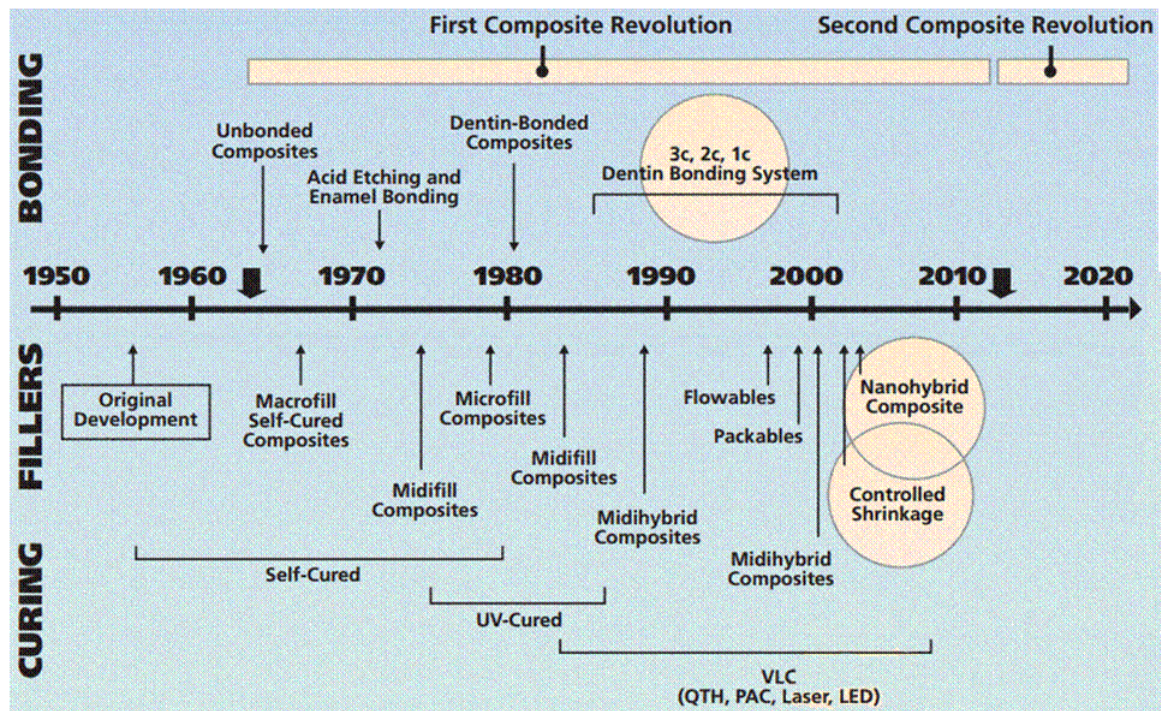

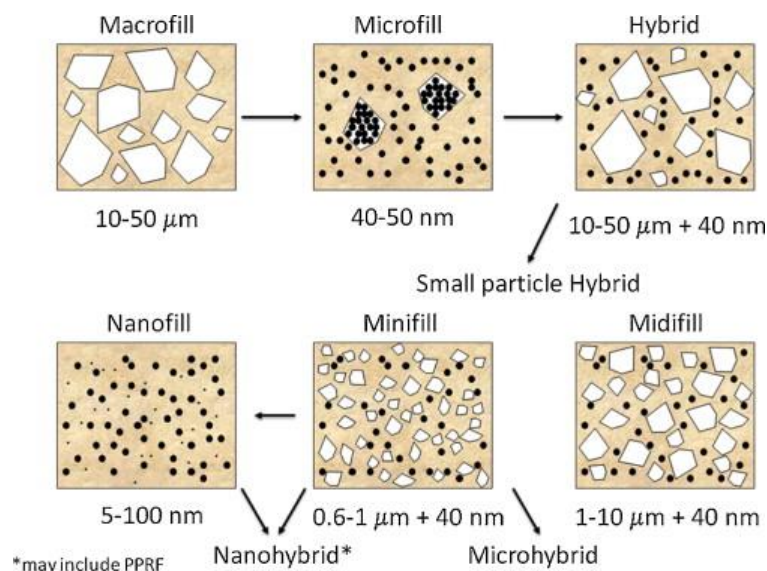Fig. 1 Development of dental composites over the last 60 years [4]

Fig. 2 Scheme of different particle sizes of VLC RCB [1]
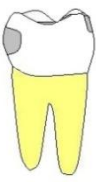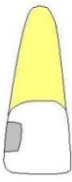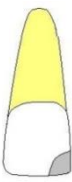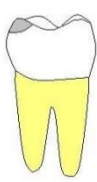
The last trend in VLC RBC is bulk fill materials developed to fill cavities with a maximum depth of 6 mm in one-step [24–27]. Despite many developments modern VLC RBCs contain resins similar to Bowen's original formula [4].

New monomers, e.g. urethane dimethacrylate (UDMA) or ethoxylated bisphenol A glycol dimethacrylate (BisEMA) were developed for lower shrinkage, better mechanical, flow or curing properties [1,28–31]. New initiators e.g. phosphine oxide, or benzoylgermanium were developed to cure VLC RBCs faster, better and deeper [31]. The components of the RBCs are discussed in the following sections.

1.1.2 Classification of RBCs

A wide range of dental restorative materials such as dental cements, amalgams, ceramics or resin based composites is available on the market. Resin-based composites are the mostly used materials for direct restorations in industrialized countries today [32]. The application of RBCs depends on the location of caries and the cavity shape. Thus, Black [33] developed a classification scheme already in the early 1900s to take into account the different requirements to each dental material, Table 1.

Table 1 Cavity Classification according to G.V. Black [34,35].

	Class I	Class II	Class III	Class IV	Class V	Class VI
Indication	Found in pits and fissures of: occlusal surfaces of premolars and molars	Found on the proximal (mesial and distal) surfaces of premolars and molars	Found on the proximal (mesial and distal) surfaces of incisors and canines.	Found on the proximal surfaces of incisors and canines, but also will involve the incisal edge.	Found on gingival third (the area near the gingiva) of the facial or lingual surfaces of any tooth.	Involve the incisal edges of anterior teeth and the occlusal surfaces

Usually RBCs are classified with respect to particle size of the filler, e.g. micro-, mini- or nanofilled composites, or viscous properties, e.g. "flowable" or "packable", Table 2 [1,36].

Table 2 Classification of resin-based composites [36] (S.279)

Class of Composite	Particle Size	Clinical Use
Traditional	1- to 50-µm glass or silica	High-stress areas
Hybrid (large particle)	(1) 1- to 20 µm (2) 40-nm silica	High-stress areas requiring improve polishability (Classes I, II, III, IV)
Hybrid (midfilling)	(1) 0.1- to 10-µm glass (2) 40-nm silica	High-stress areas requiring improve polishability (Classes III, IV)
Hybrid (minifilled/**SPF)	(1) 0.1- to 2-µm glass (2) 40-nm silica	Moderate-stress areas requiring optimal polishability (Classes III, IV)
Nanohybrid	(1) 0.1- to 2-µm particles (2) ≤100-nm nano particles	Moderate-stress areas requiring optimal polishability (Classes III, IV)
Packable hybrid	Midfilled/minifilled hybrid, but with lower filler fraction	Situations where improve condensability is needed (Classes I, II)
Flowable hybrid	Midfilled hybrid with finer particle size distribution	Situations where improved flow is needed and/or where access is difficult (Class II)

**SPF, small particle-filled

Notation and range of the particle sizes:

Macrofillers	10 to 100 µm	Minifillers	0.1 to 1 µm
Small/fine fillers	0.1 to 10 µm	Microfillers	0.01 to 0.1 µm
Midfillers	1 to 10 µm	Nanofillers	0.005 to 0.1 µm

1.1.3 Light Curing Units

VLC RBCs are cured using light curing units (LCU). They have to emit light that is suitable to activate the initiator to start the photo-polymerization [18]. Most photo-initiators have effective absorbance wavelengths between 400 and 500 nm [37,38]. Three types of LCUs are in use differing with respect to the light generation:

1. plasma arc (PAC),
2. quartz-tungsten halogen (QTH) and
3. LED LCUs.

Due to the light generation, the spectra differ significantly in the wavelength range between 400 and 500 nm, Fig. 3. PAC LCUs have irradiances up to more than 2000 mW/cm² and are used for curing of VLC RBC and dental bleaching. The disadvantage of PAC LCUs is high price, high power consumption and

restricted freedom of handling because of the power supply cable. The QTH was the mostly used LCU type until the late 1990s. The wavelength range is comparable to the PAC. The irradiance is lower than the PAC and the lifetime of the lamp, typically 30 to 50 hours in operation, is short [18,39,40].

The first LED LCUs came on the dentistry market in the late 1990s. Due to the efficient light generating process LED LCUs are operated with rechargeable batteries leading to better handling as no cable connection between charger and LED LCU is required. Compared to PAC and QTH LCUs, LED LCUs show spectra with sharp peaks having half widths of 30 nm or less, Fig. 3. The irradiance of modern LED LCUs may achieve the irradiances of PAC LCUs.
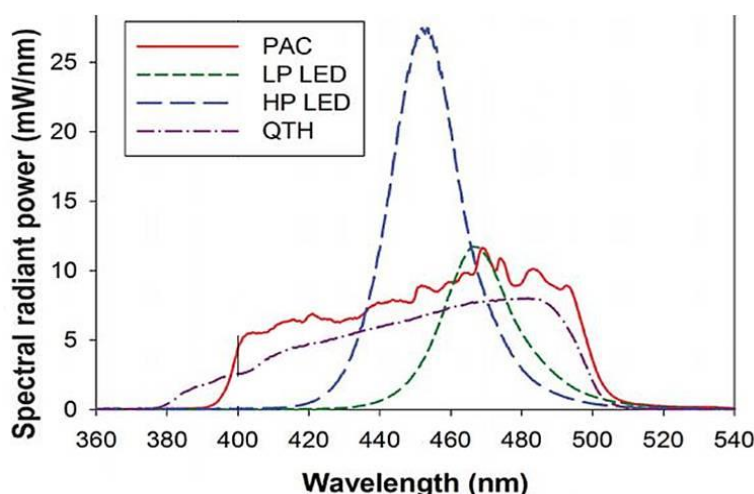
Fig. 3 Spectral emissions of 4 light curing units [41].

Some researchers identified the problem of inhomogeneous light distributions of LCUs [42–44]. Each LCU shows a characteristic light distribution, which may affect the curing performance causing locally different mechanical properties of VLC RBCs, Fig. 4.
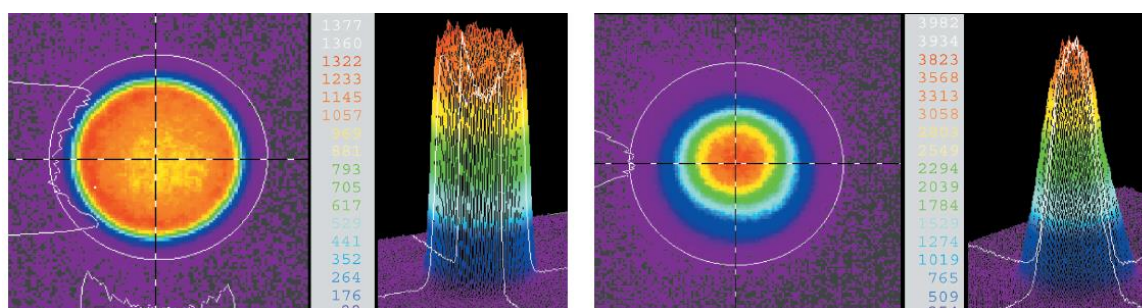
Fig. 4 Two- and three-dimensional beam profiles of: left, a LED SmartLite iQ with a homogeneous light distribution and, right a QTH Optilux 501 with a less homogeneous light distribution [42].

1.1.4 Composition of VLC RBC

VLC RBCs for dental restorations are composites based on a matrix of organic resin molecules containing inorganic fillers and additives such as initiators, accelerators, inhibitors etc.

1.1.4.1 Monomers

The monomers form the organic matrix of the VLC RBCs having a matrix content of 10 to 25 % [36]. The typical matrix contains dimethacrylate monomers [14,45]. Bowen's original matrix composition consisted of 80 % bisphenol A-glycidyl methacrylate (Bis-GMA), 10 % methyl methacrylate (MMA) and 10 % triethylene glycol dimethacrylate (TEGDMA) [4]. The important properties of monomers are [45]:

- Viscosity
- Refractive index
- Hydrophilic/hydrophobic character
- Reactivity
- Volume contraction during polymerization (ΔV_P)
- Crosslinking ability
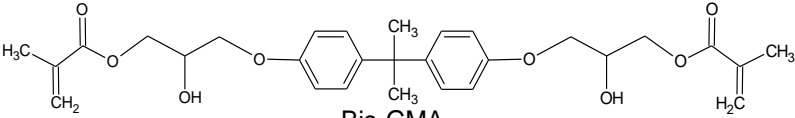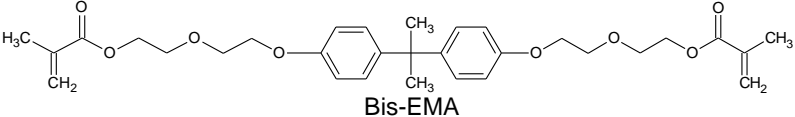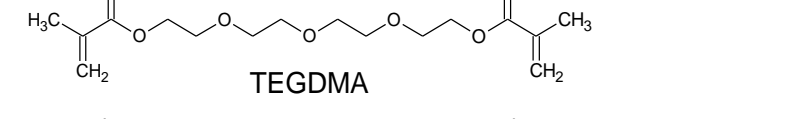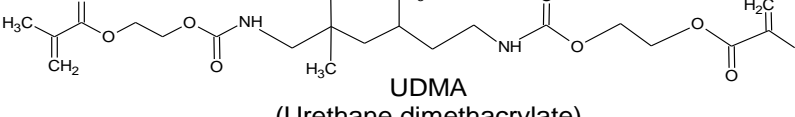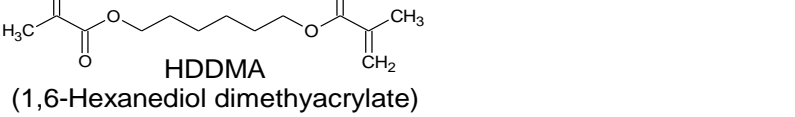
Currently Bis-GMA, Bis-EMA, UDMA and TEGDMA are used as monomers in VLC RBCs, Table 3 [28,45,46]. High viscous monomers with high molecular masses are used to avoid excessive shrinkage during polymerization. Low viscous monomers with low molecular masses are used to adjust the rheological properties of the VLC RBC [28]. New monomers were developed by modifying the molecular mass, the dipole-dipole intermolecular interaction, or the stiffness of chemical groups [47].

Ormocers are a special class of matrix materials which were introduced in the 1990s [48,49]. Ormocer stands for ORganically MOdified CERamic, which is a copolymer of organic monomers and inorganic ceramics. The advantages of ormocers are low shrinkage, abrasion resistance, or hardness.

1.1.4.2 Initiator systems

The function of the VLC RBC initiator system is the conversion of light energy from the LCU into a radical state of the initiator molecules to start the photo-polymerization. The commonly used initiator systems are composed of camphorquinone (CQ) and ethyl 4-(dimethylamino) benzoate (DABE) [14]. For bleaching products, which need to be colorless, monoacylphosphine oxid (TPO) or 1-Phenyl-1,2-propandedione (PPD) are used, Table 4 [1,18,50]. The initiator amounts of VLC RBC range typically from 0.2 to 0.5 wt% [51].

Table 3 Commonly used monomers in dental composites
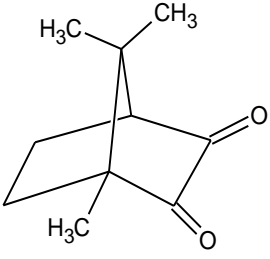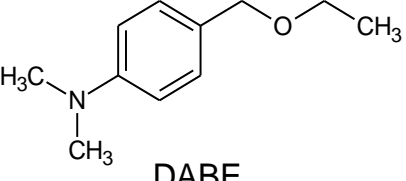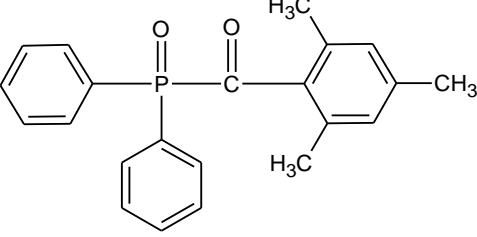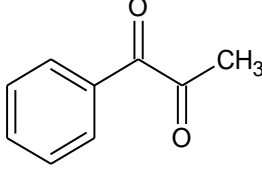
Structure	Properties
Bis-GMA (Bisphenol A glycerolate dimethacrylate)	Mol mass: 512.59 g/mol [1] Density: 1.161 g/mL [1] Viscosity: 600-1000 Pas [2] T_g: -6.6°C [52] ΔV_P: -6.0 vol% [2] Ref. index: 1.552 [1] CAS: 1565-94-2 [1]
Bis-EMA (Bisphenol A ethoxylate dimethacrylate)	Mol mass: 540 g/mol Density: 1.12 g/mL Viscosity: 3000 Pas [53] T_g: n/a ΔV_P: -5.9 vol% [2] Ref. index: 1.483 CAS: 41637-38-1
TEGDMA (Triethylene glycol dimethacrylate)	Mol mass: 286.32 g/mol [1] Density: 1.092 g/mL [1] Viscosity: 0.05 Pas [53] T_g: -52°C [3] ΔV_P: -14.5 vol% [2] Ref. index: 1.461 [1] CAS: 109-16-0 [1]
UDMA (Urethane dimethacrylate)	Mol mass: 470.56 g/mol [1] Density: 1.11 g/mL [1] Viscosity: 10 Pas [45] T_g: −38 [45] ΔV_P: -6.1 vol% [2] Ref. index: 1.483 [2] CAS: 72869-86-4
HDDMA (1,6-Hexanediol dimethyacrylate)	Mol mass: 254.32 g/mol [1] Density: 0,995 g/ml [1] Viscosity: 0.006 Pas [54] T_g: n/a ΔV_P: -6.1 vol% [2] Ref. index: 1.483 [1] CAS: 6606-59-3

[1] Sigma Aldrich Product description

[2] Ivoclar report 18

[3] BASF; Product description

Table 4 Four initiators for dental composites: (CQ/DABE) as exciplex initiator pair, TPO and PPD as initiators for bright shape dental composites (bleach product)[4] [55].

CQ	Name: Camphorquione Molar mass: 166.22 g/mol Melting point: 197-203°C CAS: 10373-78-1 Absorbance range: 400-550, 470 nm peak max
DABE	Name: Ethyl 4-(dinethylamino)benzoate Molar mass: 193.24 g/mol Density: 1.06 g/cm³ Melting point: 63-66°C CAS: 10287-53-3
TPO	Name: Diphenyl(2,4,6-trimethylbenzoyl)phosphine oxide Molar mass: 348.37 g/mol Density: 1.12 g/mL Melting point: 88-92°C CAS: 75980-60-8 Absorbance range: 230-430, 385 nm peak max
PPD	Name: 1-Phenyl 1,2-propanedione Molar mass: 348.37 g/mol Density: 1.12 g/mL Melting point: 88-92°C CAS: 75980-60-8 Absorbance range: 300-480, 393 nm peak max

1.1.4.3 Fillers

The main function of fillers is the improvement of physical and mechanical properties of VLC RBCs such as increasing stiffness, reducing shrinkage during polymerization, or improving handling properties [21]. The fillers consist of ceramics, amorphous or crystalline quartz, oxides or fluorides, and are available in different sizes and geometries, e.g. spherical or irregular. Their content in VLC RBC ranges from 50 to over 80 wt%, Fig. 5 [1,36,51,56].

Filler particles are classified as macro-, micro- and nano-fillers, Fig. 2. In the first VLC RBCs macro-fillers with particle sizes between 10 to 50 μm were used leading to materials with high stiffness and strength, but insufficient polish-ability [1,57,58]. To improve polish-ability VLC RBCs containing micro-fillers having particle sizes from 0.04 to 5 μm were developed [58]. Particles less than 100 nm are defined as nanoparticles [1,59]. Most micro-filled composites have average particle sizes of ~40 nm representing rather nano-filled composites [1,57,60]. Nevertheless, the concept of "nano" received no attention at this time.

However, the mechanical properties decreased with the introduction of micro fillers because of lower maximum filler contents [61]. Therefore, macro- and micro-fillers were combined to achieve good polishing behavior as well as high stiffness and high strength because of high filler contents. A combination of different types of fillers is called hybrid composite. The particles sizes of commercial micro-hybrid composites ranges from 0.01 to 5 μm [59,62].

Since the early 2000s nano-hybrids with particle sizes of 1 to 100 nm were introduced to micro-hybrids to further increase the filler content [63]. This led to improved mechanical, physical and handling properties, e.g. elastic moduli, shrinkage behavior or polish-ability [22,29].

Pre-polymerized fillers (PPF) are a special type of filler consisting of re-milled polymerized composites. The PPF are added as large filler particles to a composite and improve the shrinkage behavior because the content on shrinkable material decreases. The polish-ability increases due to the small particles in the PPFs, Fig. 5 [21].

| Spherical Zr/Si mixed oxide | Ba-silicate glass | Pre-polymerized resin filler |

Fig. 5 SEM pictures of different fillers with different sizes and shapes used in VLC RBCs [21,51].

1.2 Photo-polymerization
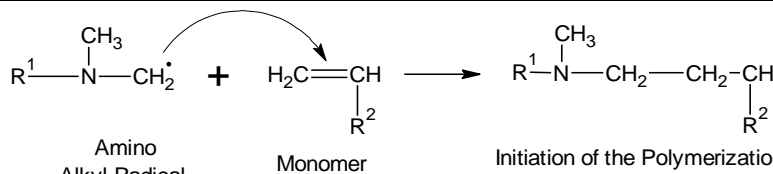
The photo-polymerization process is a light induced radical chain-growth polymerization which is divided in three processes: initiation, propagation and termination [38,56].

1.2.1 Initiation

In the case of photo-polymerization, the initiation process is started by irradiation with light, Table 5 [64–66]. The light has to have a wavelength which fits to the activation energy of the initiator molecules (I), Eq. (1) [14]. After the light activation, the initiator molecules form radicals ($R^\bullet$), Eq. (2), which start the polymerization process with the first monomer, Eq. (3). The initiation process generates two different kinds of radicals, the $CQ^\bullet$ and the $DABE^\bullet$ radicals. Due to the low reactivity of the $CQ^\bullet$, the rate of initiation (R_i) and the rate constant (k_i) of the initiation process depends mainly on the concentration of the $DABE^\bullet$.

The change of the radical concentration depends on the absorbed light intensity I_a. The quantum yield ϕ is a measure for the efficiency of the generation of radicals and describes how many photons are required for the generation of one radical. In the case of the free radical polymerization, the quantum yield ϕ corresponds to the rate constant of the initiation process k_i, Eq. (4).

Table 5 Initiation of the photo-polymerization

| **Initiation:** | $I \xrightarrow{hv} I^*$ | (1) |
| | $I^* \rightarrow R^\bullet$ | (2) |

| | $R^\bullet + M_n \xrightarrow{k_i} RM_n^\bullet$ | (3) |

| **Rate of Initiation:** | $R_i = \dfrac{d[R^\bullet]}{dt} =$ $k_i[I] = \phi I_a = \phi I_0 t\, e^{-\varepsilon c x}$ | (4) |

I = Initiator	[I] = concentration of initiator	$R^\bullet$ = Radical
[$R^\bullet$] = concentration of radicals	M = Monomer	[M] = Monomer concentration
$M_n^\bullet$ = Monomer radical	k_i = initiation rate constant	R^1, R^2…= organic groups
R_i = rate of initiation	ϕ = quantum yield	I_a =absorbed light intensity
I_0 = absorbed light on the surface	t = irradiation time	ε = extinction coefficient
c = concentration of absorbance substances		x = thickness of layers

A CQ/DABE system is used as photo-initiator in most VLC RBCs [46]. Therefore, the initiation mechanism is considered in a detailed manner. The absorbance of light energy is much higher (400 kJ/mol at $\lambda = 300$ nm) than the energy by vibration (0.4 - 40 kJ/mol) [67]. This means that the initiator molecules cannot be activated thermally. During irradiation the photo-initiator

molecule (CQ) absorbs a light quantum and changes from the ground state (S_0) to an exited state (S_n) with higher energy, Fig. 6 [64,67].
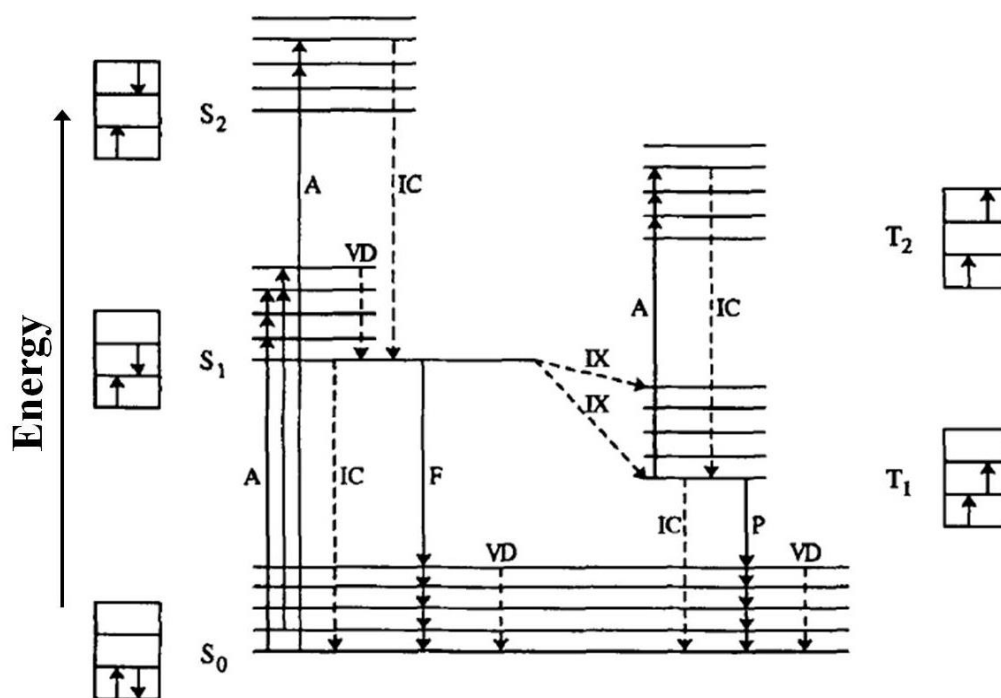
Fig. 6 Energy diagram (Jablonsky diagram) for simple molecules.
left and right: relative energy levels in spin direction of the electrons.
S0 = singlet of the ground state, S1 = first exited singlet state, S2 = second exited singlet state,
T1 first exited triplet state,T2 second exited triplet state. Perpedincular lines: transitions with (straight lines) and without (dashed lines) radiation.
A = absorption to exited singulet states, F = fluorescence, IC = internal conversion, IX = intersystem crossing, P = phosphorescence, VD = deactivation of vibration [67].

The transitions between singlet energy states are fast processes (from S_0 to S_2, S_3... $\approx 10^{-15}$s, emission from S_2, S_3..., to S_1, $\approx 10^{-11}$ to 10^{-13}s [67]). The lifetime of singlet states is too short to create radicals and to initiate the photopolymerization. However, the molecule can also transfer to a triplet state. This transfer is called a forbidden mechanism as the transfer is blocked due to quantum mechanical spin conservation and can only happen at a much lower tunneling rate than the transfer to the ground state. The triplet state has a much longer lifetime ($>10^{-4}$s [67]). This provides enough time to transfer the exited triplet state to the accelerator molecule (DABE) to form the amino alkyl radical Eq. (5).

$$\text{CQ} \xrightarrow{h\nu} \text{CQ}^* \xrightarrow{+\text{DABE}} (\text{CQ}^*, \text{DABE}) \rightarrow (\text{CQ}^{\bullet+}, \text{DABE}^{\bullet-})^* \qquad (5)$$
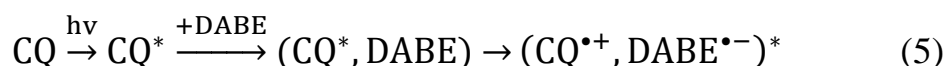
The initiation process of the system CQ/DABE is shown in Fig. 7 [14]. The CQ molecules are partly transferred to the triplet state in which they are able to react with DABE molecules to form two species of radicals (CQ radical and

amino alkyl radicals). The polymerization reaction is mainly started by the reactive DABE radicals as CQ radicals show a low reactivity [68].
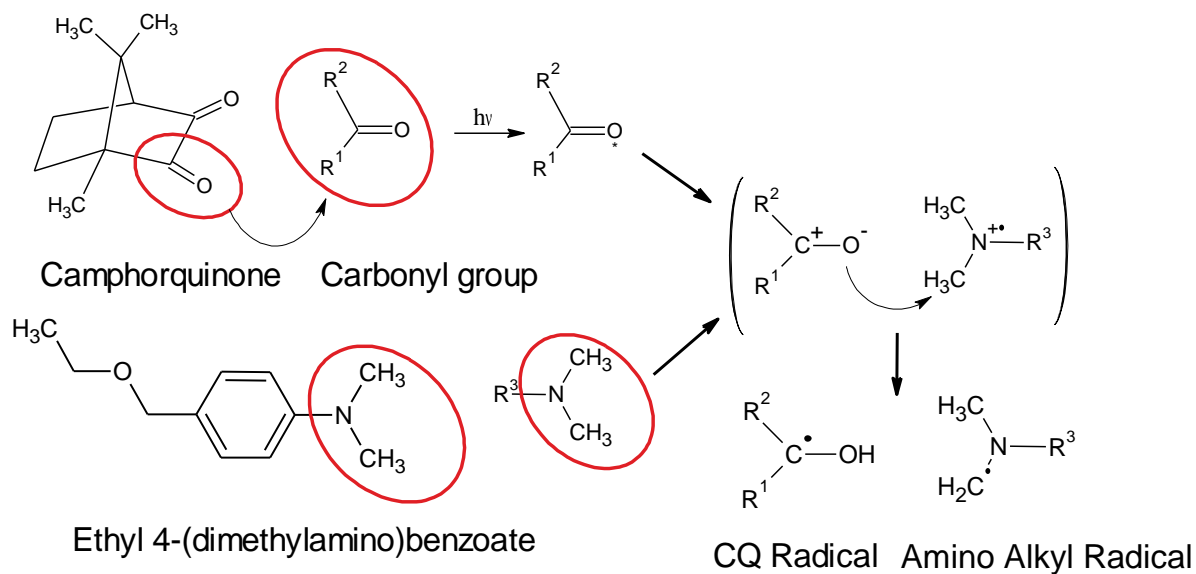
Fig. 7 Light activation of the CQ/DABE photo-initiator system [14]

Therefore, the amino alkyl radical initiates mainly the polymerization reaction, Fig. 8. The polymerization of large monomers is subjected to steric hindrances as the rests of the monomer molecules protect the reactive center, especially if it is immobilized after some polymerization steps. Furthermore, it is immediately clear that degrees of conversion (*DC*) close to 100 % cannot be expected.
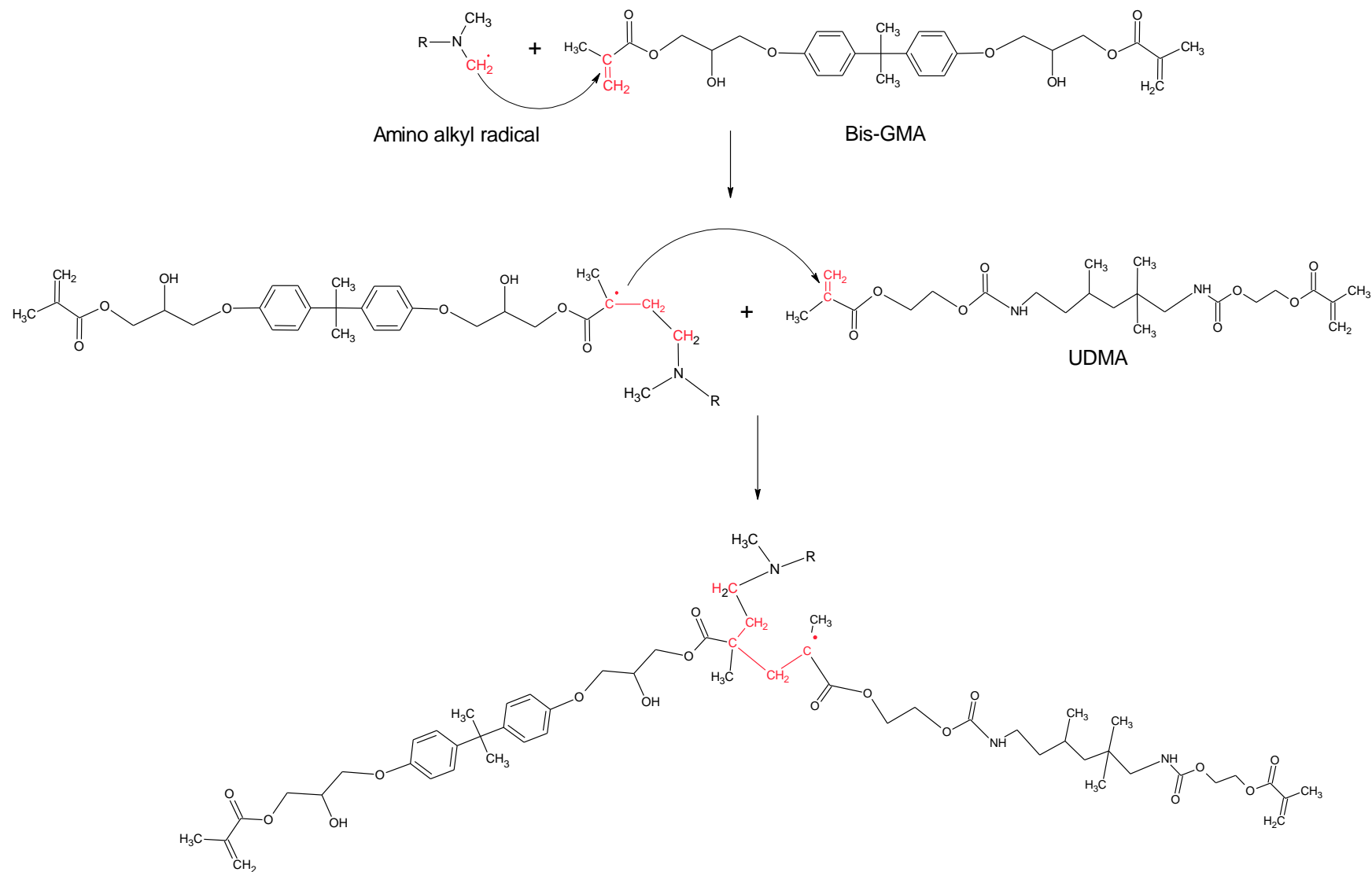
Fig. 8 Start of the polymerization with the amino alkyl radical and a Bis-GMA and UDMA monomer as example.

1.2.2 Propagation

The propagation describes the phase of chain growth during the polymerization process. It is characterized by the rate of propagation (R_p) and the corresponding rate constant of the propagation process (k_p).

Table 6 Propagation of polymer chain

	$RM_n \bullet + M$ $\xrightarrow{k_p} RM_{n+1}^{\bullet}$	(6)
Rate of Propagation	$R_p = \dfrac{-d[M]}{dt}$ $= k_p[M][RM_n^{\bullet}]$	(7)

1.2.3 Termination

The termination describes the end of the polymerization process. There are three possibilities:

Radical recombination,

Two radicals annihilate each other if two radical ends of polymer chains react and form one polymer chain or if the radical ends of polymer chains react with imitator radicals, Table 7.

Table 7 Examples of termination by radical recombination with other polymer chains

	$M_n^{\bullet} + M_m^{\bullet}$ $\xrightarrow{k_{tc}} M_{n+m}$	(8)
Rate of recombination	R_{tc} $= 2k_t[M_n^{\bullet}][M_m^{\bullet}]$	(9)

Table 8 Example for the recombination with small radicals

	$M_n^{\bullet} + R_n^{\bullet} \xrightarrow{k_{tc}} M_nR_n$	(10)
Rate of recombination	R_{tc} $= 2k_t[M_n^{\bullet}][R_n^{\bullet}]$	(11)

Disproportionation

If two radical ends of polymer chains meet, a hydrogen atom from one radical end can be transferred to the other radical end. Then, the first polymer chain exhibits an alkyl end and the other an allyl end which exhibit a carbon double bound, Table 9.

Table 9 Examples of termination by disproportionation

Polymer chain 1 Polymer chain 2/ or radical molecule	$M_n \bullet + M_m \bullet \xrightarrow{k_{td}}$ $M_n + M_m$	(12)
Rate of disproportionation	$R_{td} = 2k_t[M_n^{\bullet}][M_m^{\bullet}]$	(13)

Radical immobilization

During polymerization the molecular mass increases. This reduces the mobility of the polymer chain. At a certain molecular mass, the glass temperature exceeds ambient temperature freezing in the motion of the radical end of the polymer chain. Further polymerization is only possible if the radical end is fed by diffusing monomers.

1.2.4 Reaction kinetic of the overall polymerization process

Main topic of this work is the investigation how the viscoelastic properties are affected by the curing conditions. Also a more detailed view on the reaction kinetics, the degree of conversion (*DC*) and depth of cure (*DoC*) is presented. In general, the kinetic of the three polymerization processes is unknown. Thus, the reaction kinetics cannot be described completely. Only for the case in which initiation and termination are in the steady state the kinetics of the polymerization reaction can be described quantitatively. The overall rate of reaction R_{pol} is [69]:

$$R_{pol}(t) = \frac{d[M]}{dt} = -\frac{k_p}{k_t^{0.5}}[M](\phi I_0 e^{-\varepsilon c x})^{0.5} \qquad (14)$$

1.2.5 Degree of Conversion (*DC*) and Depth of Cure (*DoC*)

DC and *DoC* strongly depend on the light penetration and the resulting effective activation of initiator molecules with depth. The Lambert-Beer's law, Eq. (15), describes the attenuation of light if trespassing a medium:

$$I(x) = I_0 e^{-\varepsilon_\lambda \cdot c \cdot x} \qquad (15)$$

with the wavelength depended extinction coefficient (ε_λ), the concentration of the absorbance material (c), and the thickness of the layer (x). Whereby, I_0 is the incident light and $I(x)$ is the transmitted light at a certain thickness x.

In general, the extinction coefficient and the concentration of monomers can be assumed as constant during curing and summarized to the material specific absorbance coefficient a, Eq (16):

$$a = \varepsilon_\lambda \cdot c \qquad (16)$$

$$I_x = I_0 e^{-a \cdot x} \qquad (17)$$

Obviously, the rate of reaction depends on the absorbed intensity I_a Eq. (4) which decreases with depth according to the Lambert-Beer's law. Now Eq. (14) can be expressed as a function of time t and depth x. This leads to the time dependent monomer concentration:

$$[M](t,x) = M_0 e^{-\frac{k_p}{k_t^{0.5}}\phi I_a t} = M_0 e^{-\frac{k_p}{k_t^{0.5}}(\phi I_0 e^{-ax})^{0.5} t} \qquad (18)$$

Taking into account the *DoC*, it is possible to write [*M*] as a function of time t and depth x from the upper surface of the cured resin. The time and depth depending *DC(t,x)* is determined by integration of Eq. (19):

$$DC(t,x) = 1 - \frac{[M](t,x)}{M_0} = 1 - e^{-\frac{k_p}{k_t^{0.5}}(\phi I_0 e^{-ax})^{0.5} t} \qquad (19)$$

The *DC* is an important measure to characterize the curing behavior of VLC RBCs and can be determined by spectroscopic methods, such as FTIR, Raman spectroscopy, or thermal analysis, such as differential scanning calorimetry (DSC), dielectric analysis (DEA) [22,38,70–72].

The *DoC* represents the thickness of a layer with sufficient curing properties. Different methods are used in dental material science to determine *DoC*:

- Spectroscopy (Fourier transformation infrared spectroscopy (FTIR), Raman) [22,73]
- Thermal Analysis (differential scanning calorimetry (DSC), dielectric analysis (DEA) [74–76]
- Scratch Test ISO 4049 [77,78]
- Indentation measurements (Vickers, Knoop, Nanoindenter, etc.) [27,73,77]

The spectroscopic methods allow to observe the changes of *DC* in a real time and give the ability to determine the reaction kinetic at the beginning of the polymerization. A disadvantage of spectroscopic or thermal methods, especially for the determination of *DoC*, is that bulk properties are measured. This requires multiple repetitions with different layer thicknesses to determine *DoC*.

Mechanical test methods such as the ISO 4049 scratch test or hardness test are simple to use. The indentation methods allow for determination of mechanical properties on different local positions on one sample. A disadvantage of indentation methods is the low measurement speed, which avoids an observation of properties changes during curing in a real time. Additionally, determination of the depth depending properties can become a time-consuming procedure according to the numbers of indentations, Fig. 9. However, the *DoC* measurements by ISO 4049 scratch test, and also the definition of the thickness at 80 % of the maximal hardness value as a sufficient *DoC*, involves the risk of misjudgment and overestimation [27,77]. These methods are based on single values. Obviously, the resulting depth depending properties are not uniform, Fig. 9. Furthermore, a uniform definition for a sufficient *DoC* determined by other methods is currently not available.
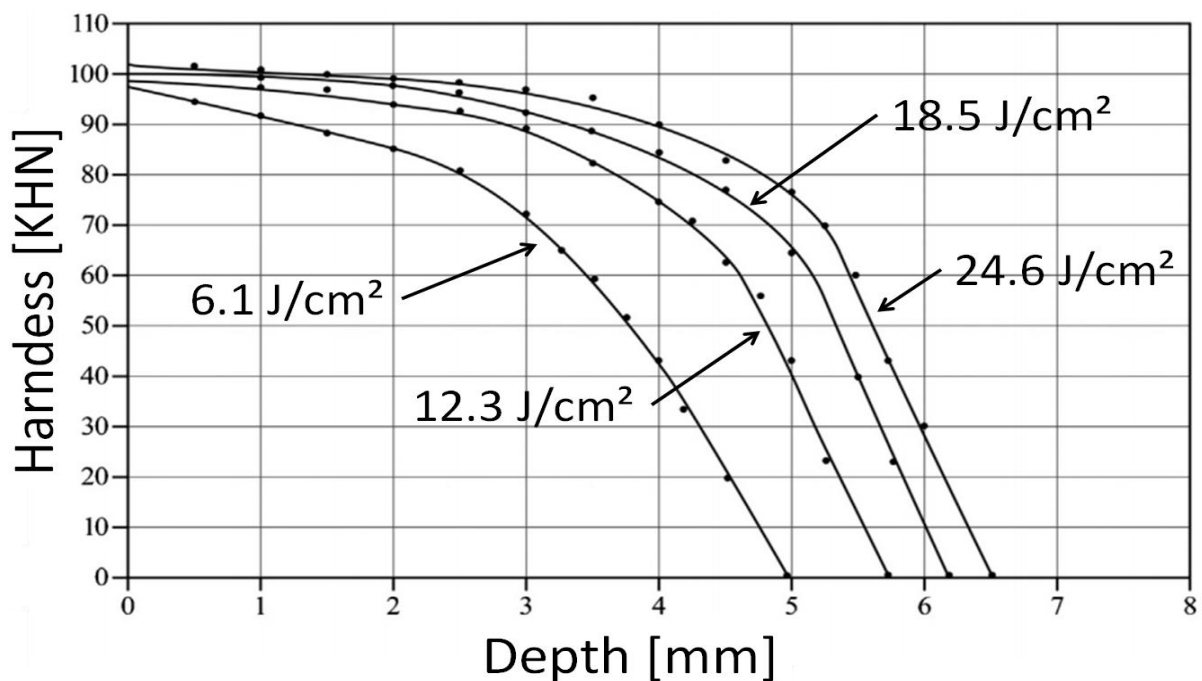
Fig. 9 Depth dependent hardness for different radiant exposures using a LCU with 600 mW/cm² [79].

1.3 Methods to determine curing state and degree of conversion (*DC*)

There are methods which allow for characterizing the curing state and determining the DC either locally or in bulk, Table 10.

Table 10 Methods allowing for the determination of *DC* of VLC RBC

Method	Quantity correlated to *DC*	Spatial resolution
FTIR	Change of absorbance of aliphatic double bonds with time	local and bulk?
Raman	Change of absorbance of aliphatic double bonds with time	bulk
DSC	time dependent heat flow of the curing enthalpy peak	bulk
DEA	time dependent ion viscosity	local and bulk

1.3.1 Infrared spectroscopy

IR radiation is absorbed partly generating molecule vibrations [80]. The frequency of the vibrations is affected by molecular bonding forces, masses of the involved atoms, or the initial vibration state. Therefore, the wavelength of the absorbed IR radiation is specific for functional groups of molecules allowing for identifying substances, Fig. 10.
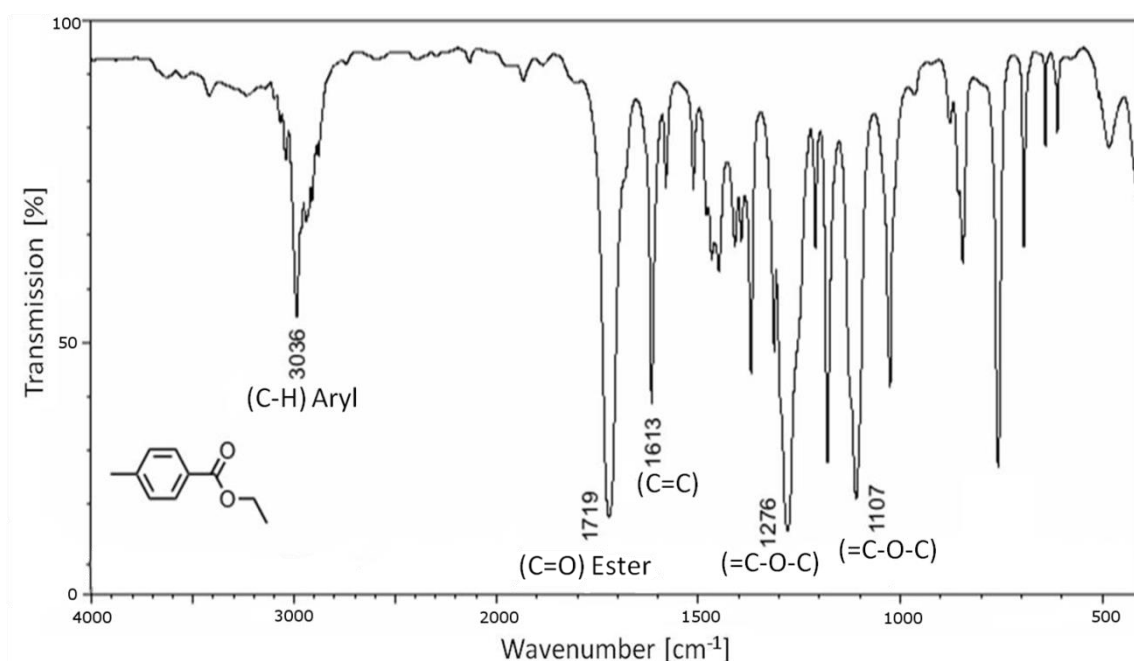
Fig. 10 Spectrum of an Ethyl 4-methylbenzoate [81]

The attenuated total reflection Fourier-transformation infrared-spectroscopy (ATR-FTIR) is often used to trace the polymerization process of VLC RBCs [72,82,83]. The sample with a defined thickness is placed above a crystal (e.g. diamond, germanium or silicon). The curing light can be placed on top of the sample and the measurement is performed at the bottom during the curing process.

The IR beam is reflected at the crystal surface and penetrates the sample a few microns as an evanescent wave [80], Fig. 11.
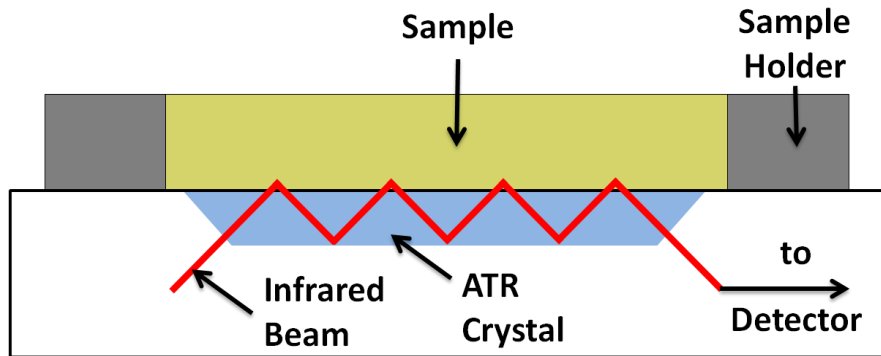
Fig. 11 Principle of ATR-spectroscopy [84]

During the polymerization, the molecular structure of the specimen is changed as the number of aliphatic C=C bounds decreases. If the VLC RBCs contains BisGMA, the aromatic C=C bounds can be used as an internal reference peak to account for e.g. baseline drifts. This allows measuring more accurate absorbance, Fig. 12. The time dependent $DC_{IR}(t)$, can be calculated by the following equation:

$$DC_{IR}(t) = \frac{\left\{\frac{\left[[Abs_{aliphatic}](t)\right]}{[Abs_{aromatic}]}\right\}_{polymer}}{\left\{\frac{\left[[Abs_{aliphatic}]\right]}{[Abs_{aromatic}]}\right\}_{monomer}} \qquad (20)$$

with *Abs* as absorption of the aliphatic or aromatic C=C bonds of the polymer or monomer, respectively, Fig. 12. For modern LCU the polymerization rate is high. Therefore, at least 8 to 10 spectra per second are required immediately after starting the irradiation to resolve and to investigate the reaction kinetics of the curing process, Fig. 12.

The curing behavior depends on e.g. irradiation time, irradiance of LCU, temperature, resin viscosity, or the chemical structure of the chosen monomer. Sideridou et. al investigated the influence of the monomer viscosity (BisGMA > UDMA > BisEMA > TEGDMA) on time dependent DC and rate of reaction (R_p) for 4 different monomers by using FTIR, Fig. 13 [85]. It is shown that the R_p increase with the increase of viscosity. This is known as the Trommsdorff-Norrish effect or gelation-point of a radical polymerization [38,85]. This effect describes the decreasing probability of radical termination because of the reduced mobility of the radicals with increasing viscosity during the polymerization. Therefore, a higher viscous monomer system restricts the mobility of the radicals, and decreases the rate of termination, but increases the R_p. However, the higher polymer chain mobility of the low-viscous monomer systems gives the ability for a higher DC, which is shown with TEGDMA in Fig. 13.
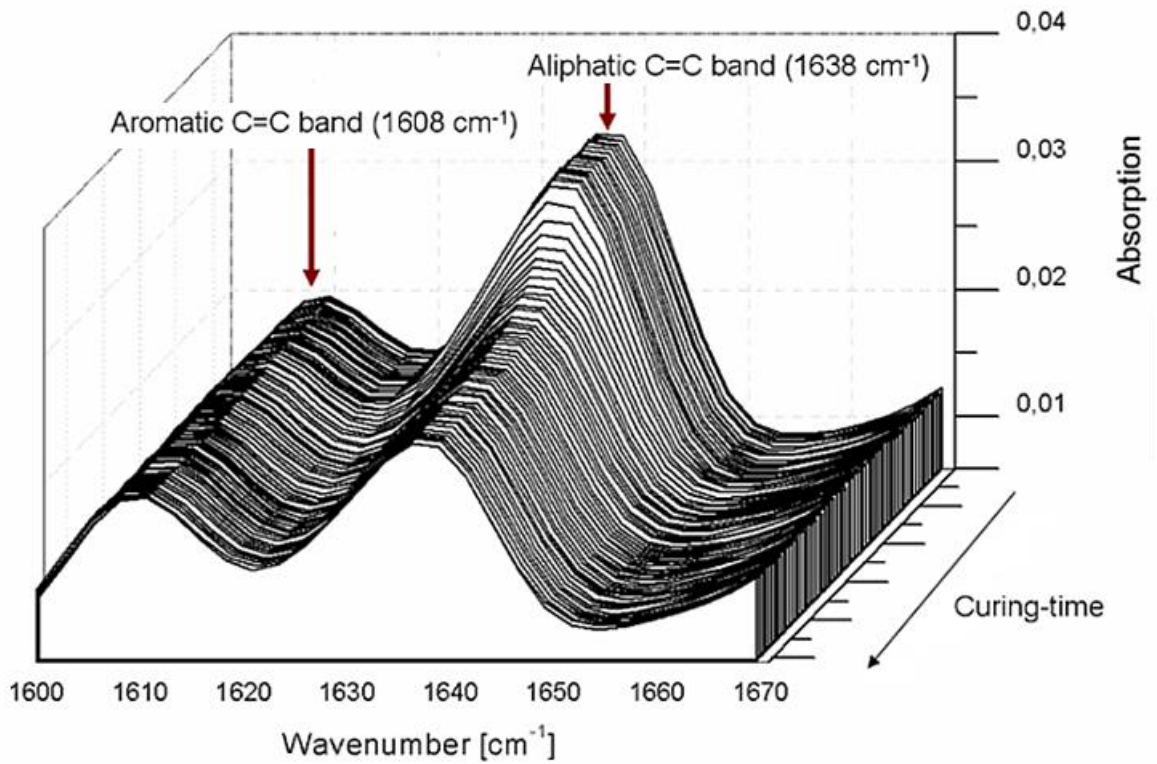
Fig. 12 Change of absorbance of aliphatic C=C bonds during the photo-polymerization observed in real-time [46].
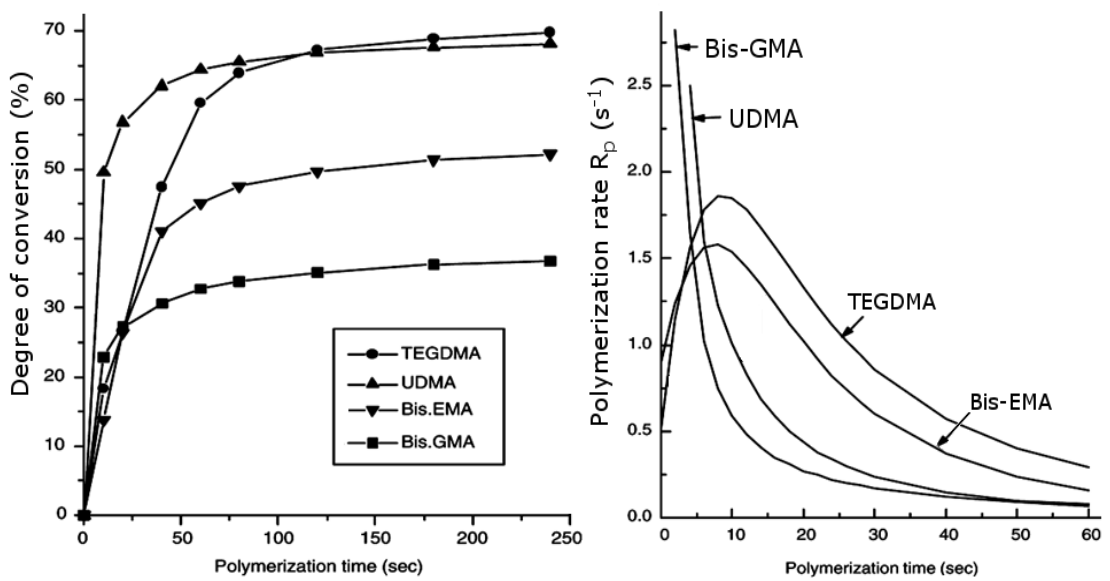
Fig. 13 Degree of conversion and reaction rate of different VLC RBC monomers determined by FTIR [85]

1.3.2 Raman Spectroscopy

Raman spectroscopy is a complementary technique to the IR-spectroscopy and can also be used to determine the *DC* of VLC RBCs [73,86–90]. It depends on the inelastic light scattering of molecules [86,87]. A sample is irradiated by monochromatic laser light. Most of the light is elastically scattered (Rayleigh scattering). Only a small portion of the light is inelastically scattered by the molecules with a shift in energy (Stokes- and anti-Stokes scattering). In the case of Stokes-scattering, the energy is transferred from the photon to a molecule decreasing the energy of the photon. In the case of Anti-Stokes scattering, the energy is transferred from a molecule to the photon, increasing its energy. As Anti-Stokes scattering is less likely, it exhibits lower peak intensities than Stokes scattering, Fig. 14.
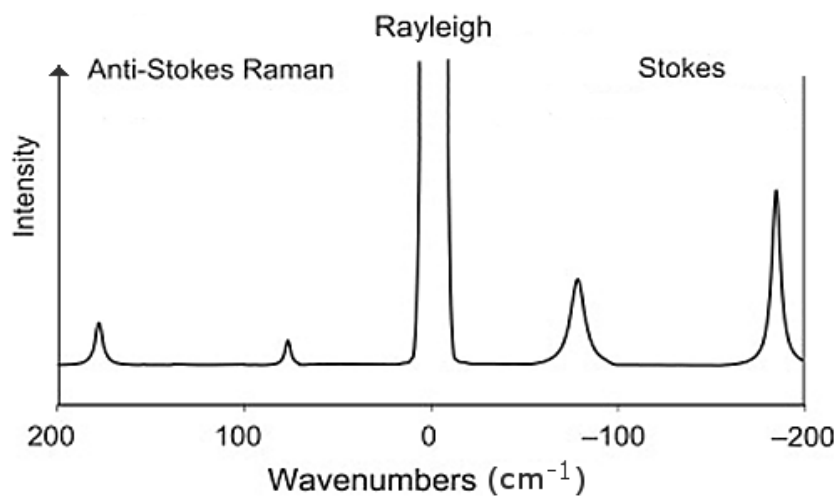
Fig. 14 Comparison of anti-Stokes and Stokes peak intensities with respect to the Rayleigh peak intensity [86]

Fluorescence caused by ingredients of the VLC RBC can overlap with the Raman scattered light [70,90]. Furthermore, laser light absorption increases the sample temperature and may cause thermal degradation [91]. The determination of the *DC* corresponds to (Eq. 20) [73,88].

1.3.3 Differential scanning calorimetry

The differential scanning calorimetry (DSC) allows for the determination of the heat flow ($\dot{Q}$) between sample and environment [92]. Typical applications are the determination of transition temperatures such as melting temperature (T_m), glass transition temperature (T_g) and decomposition temperature, enthalpies of chemical reactions and phase transitions as well as specific heat capacity (c_p). As VLC RBCs are cured under different conditions, such as exposure time, irradiance level, temperature, or thickness of layers, DSC can be used to characterize the resulting properties.

The photo-polymerization process is an exothermal reaction. Therefore, the time dependent $DC_{DSC}(t)$ can be defined by evaluating the peak of curing enthalpy in the following way, Eq. (21):

$$DC_{DSC}(t) = \frac{\int_{t_{start}^{peak}}^{t} \dot{Q}(t')dt'}{\int_{t_{start}^{peak}}^{t_{end}^{peak}} \dot{Q}(t')dt'} = \frac{\int_{t_{start}^{peak}}^{t} \dot{Q}(t')dt'}{\Delta Q_{curing}} \qquad (21)$$

with the heat flow $\dot{Q}(t)$ and curing heat ΔQ_{curing} [93]. The integral in the nominator represents the curing enthalpy released by the sample until time t which is assumed to be equivalent to the amount of reacted aliphatic double bonds. Evaluation of $DC_{DSC}(t)$ provides information about the curing kinetics of VLC RBCs, especially the rate of reaction [74,94], and allows for the identification of the influence of ingredients ratio, type of initiator, filler content, etc. [95].

Tanimoto et al. [96] investigated different monomer mixtures of UDMA/TEGDMA to determine the influence of the viscosity on the rate of reaction, Fig. 15. The decreasing viscosity, with increasing TEGDMA content, decreases the R_p. These results of the DSC correspond to the results of the FTIR in Fig. 13.
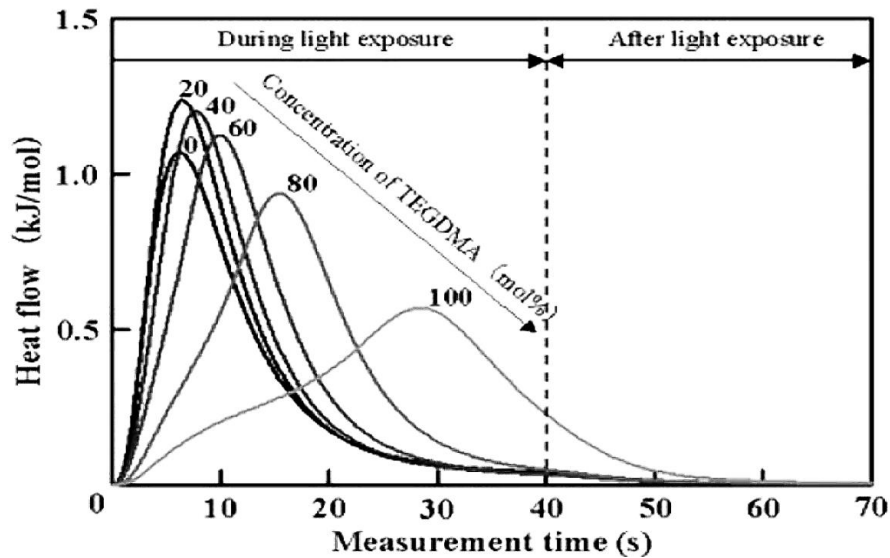
Fig. 15 Isothermal heat flows of resin mixtures with different ratios of UDMA/TEGDMA (0 to 100 % TEGDMA) [96].

The DSC can also be used to estimate the temperature rise of teeth during the exposure process caused by photo-polymerization, and light intensity [97]. Another application is the curing of thermosets at different curing temperatures to simulate the curing reaction within a mold, and to estimate cycle time and temperature increase during manufacturing process [92]. Additionally, post-curing processes caused by trapped radicals in the cured resin can be characterized by the post-reaction enthalpy [75,98]. The measured T_g after post-curing is used to evaluate the quality of the curing process [75].

1.3.4 Dielectric analysis

The dielectric analysis (DEA) allows for monitoring the change of dielectric properties of VLC RBCs during the curing process [76,99]. The DEA is a robust method, which is used for industrial applications such as the observation of curing processes of epoxy resin materials in the aerospace industry [100]. The high data acquisition rate at high frequencies allows real-time monitoring of fast curing processes such as VLC RBCs as well as a long-time observation [99,101].

In general, the sample is placed between two electrodes and an external alternating electrical field is applied leading to orientation of dipoles and generation of electric current due to the motion of ions, Fig. 16. This orientation or moving of dipoles and ions leads to a dissipation of energy by internal friction. The result is a loss in the excitation voltage input signal and a phase shift of the response current output signal. With ongoing curing of a VLC RBC the network density increases while mobility of dipoles and ions decrease. This leads to an increasing ion viscosity $\eta^{ion}(t)$, Fig. 17. The assumption $\eta^{ion}(t) \sim DC(t)$ allows for the calculation of $DC_{DEA}(t)$, Eq. (22):

$$DC_{DEA}(t) = \frac{\eta^{ion}(t) - \eta_0^{ion}}{\eta_\infty^{ion} - \eta_0^{ion}} \tag{22}$$

with the initial ion viscosity η_0^{ion} and the final ion viscosity η_∞^{ion}.
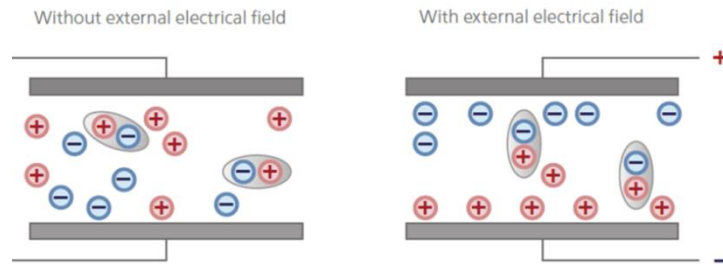
Fig. 16 Measurement principle of the DEA with dipoles and ions between two electrodes [102]
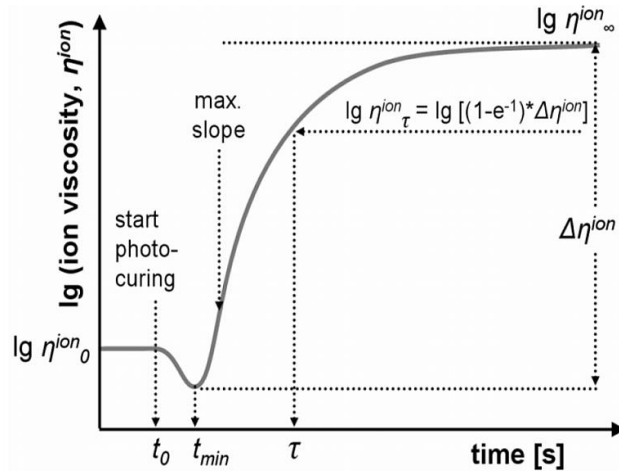
Fig. 17 Characteristic DEA curve for an VLC RBC with initial ion viscosity $lg\,\eta_0^{ion}$, final ion viscosity $lg\,\eta_\infty^{ion}$ [103].

1.4 Determination of viscoelastic properties of VLC RBCs using indentation methods

1.4.1 General introduction

Indentation methods such as hardness testing or nanoindentation allow for determining the local mechanical surface properties, and as a consequence, the influence of the curing parameters such as irradiance, exposure time, or spectral distribution of an emitted light on the properties of the VLC RBCs. In dental materials science indentation methods are used to compare DCs of different curing protocols, to determine DoC, or to map the surface hardness distribution for mechanical imaging [43,77,104,105].
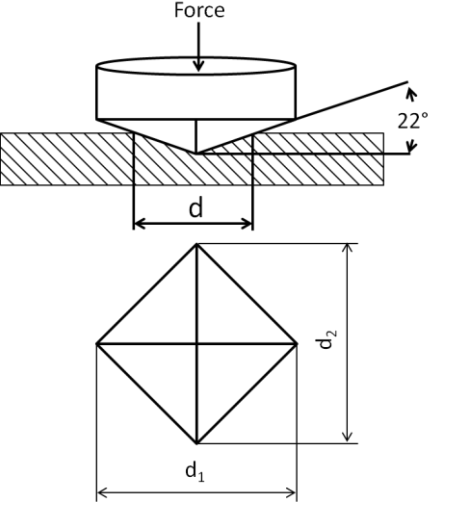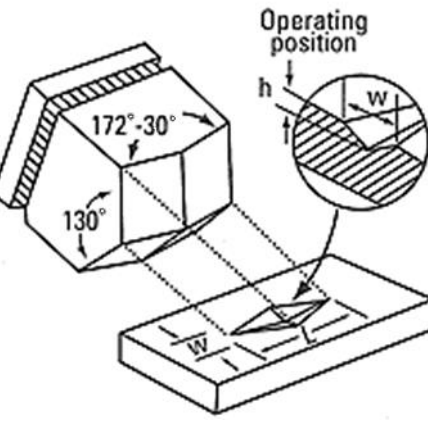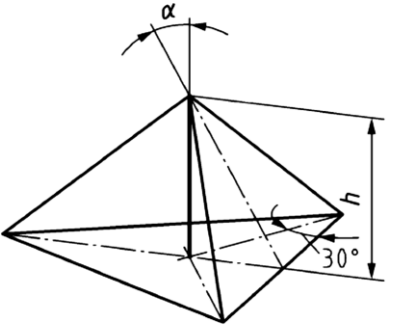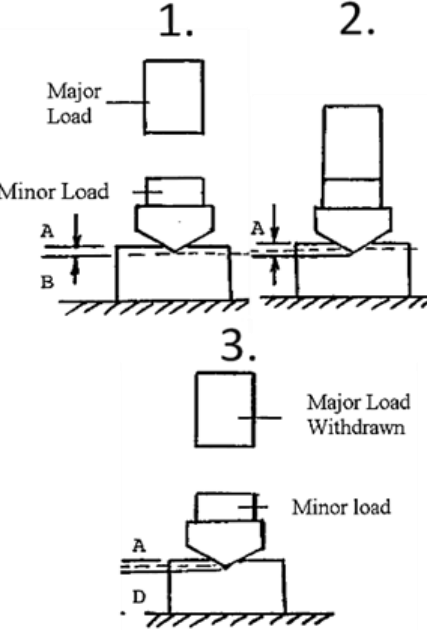
Table 11 Indentation methods and measured variables of mechanical methods to determine the mechanical and viscoelastic properties of VLC RBCs

Method	measurable quantities	spatial resolution
Hardness tester	Hardness, depth of cure	local
Atomic force microscopy (AFM)	Stiffness, surface roughness	local
Nanoindenter	Stiffness, hardness, depth of cure	local

1.4.2 Classification of hardness testing

Hardness testing methods differ with respect to indenter geometry, load or force, loading time, and evaluation procedure, Table 12. The measuring techniques differ in the operation mode: e.g. Vickers, Knoop, or Brinell measure the impression of the indentation and Rockwell, Wallace, Penetrometer, or Shore A/D measure the penetration depth. The indentation methods are classified in three load classes: macro-range, micro-range, and nano-range, Fig. 18.

Table 12 Indenter geometries, evaluation of hardness values and measurement principles of hardness tester systems.

Vickers	Knoop	Berkovich	Rockwell
		$$A_s(h) = \frac{3 \cdot \sqrt{3} \cdot \tan\alpha}{\cos\alpha} \cdot h^2$$ $$= 26.43 h^2 \quad (25)$$ $A_s(h)$ = indenter contact area α = angle (α = 65.55°) h = depth of indentation	
$HV = 0{,}102 \cdot \frac{F}{A} = 0.189 \cdot \frac{F}{d^2}$ (23)	$HK = \frac{F}{0.0702 \cdot L^2}$ (24)		
HV = Vickers hardness F = applied force d = impression diagonals A = impression area	HK = Knoop hardness F = applied force L = length of impression	$$HM = \frac{F}{A_s(h)} \quad (26)$$ HM = Martens hardness F = applied force	$HR = 100 - \frac{h}{0.002\ mm}$ (27) HR = Rockwell hardness h = depth of indentation
	Measurement	**Principle:**	
The diagonals (d) of the residual impression in the material surface are measured with a microscope and the Vickers hardness (*HV*) is calculated with the applied load, Eq. (23) [106].	The long edge of the indentation is measured with a microscope and the Knoop hardness (*HK*) is calculated with the applied load, Eq. (24) [107].	Especially used for instrumented indentation methods with low load, such as nanoindenter [106,107]. The Martens hardness (*HM*) is calculated by the ratio of the applied force and the contact area of the indenter Eq. (26).	The measure of the Rockwell hardness (*HR*) is the depth of indentation under the minor load after the indentation and is calculated by Eq (27). *HR* is available directly after the measurement on the hardness tester display [108].
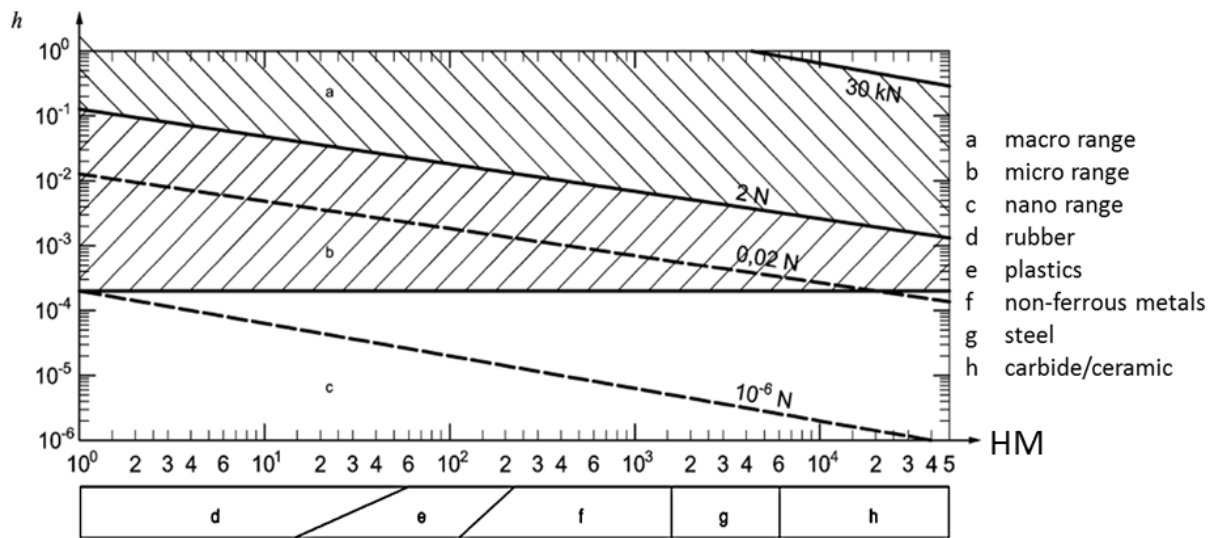
Fig. 18 Correlation between the depth of indentation (h), and the applied load for the Martens hardness (HM) [106].

Classical hardness testers perform static measurements. Many materials e.g. polymers behave mechanically time dependent - they creep if loaded. This leads to sinking-in or piling-up of the sample material, and as a consequence to non-ideal contact areas and wrong hardness values, Fig. 19 [107].
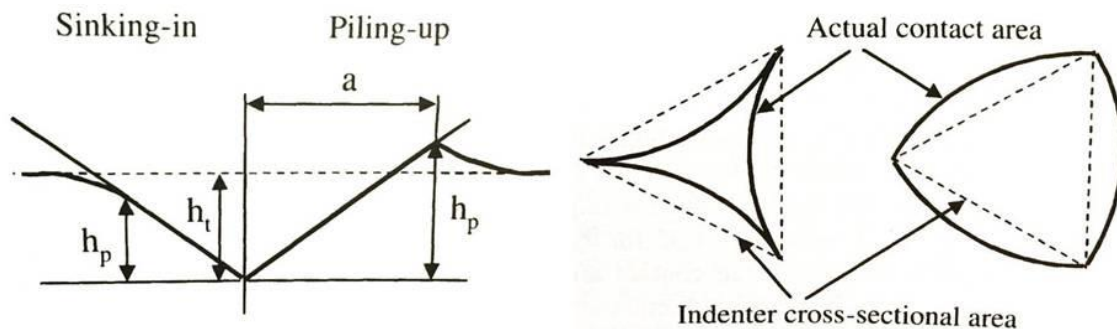
Fig. 19 Effect of piling-up and sinking-in on a material surface and the actual contact area [107]

1.4.3 Instrumented indentation techniques

Instrumented hardness tester, nanoindenter and atomic force microscopy (AFM) determine force-indentation depths curves - providing significantly more materials information such as hardness, plastic deformation energy, creep and relaxation properties and Young's modulus. The determination of the elastic modulus is based on the work of Oliver and Pharr [109]. The loading curve is followed by an unloading curve whereas the linear section of the unloading curve is used to determine Young modulus, Fig. 20.
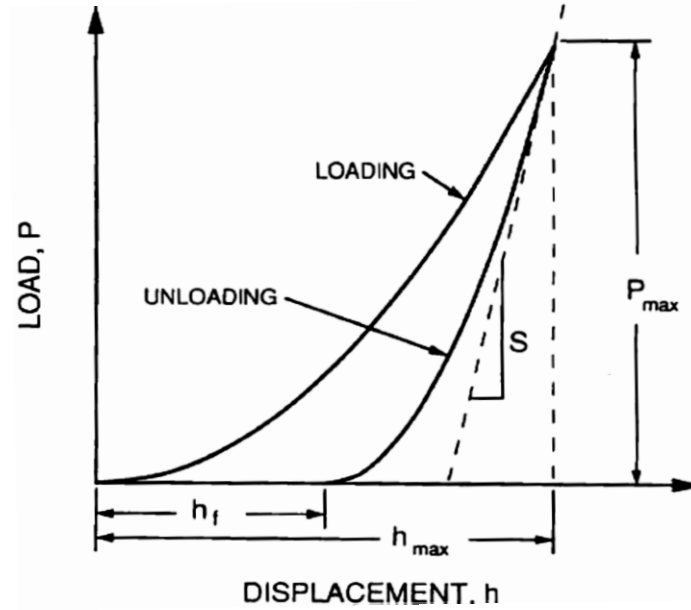
Fig. 20 Scheme of load versus indenter displacement data with loading and unloading curves, stiffness S, maximum displacement h_{max}, residual displacement h_f, and maximum load P_{max} [109].

The slope of the linear section is called stiffness and represents a measure of elasticity of a material with the contact area of the indenter A.

$$S = \frac{dP}{dh} = \frac{2}{\sqrt{\pi}} E \cdot \sqrt{A} \qquad (28)$$

The determined elastic modulus depends on moduli and Poisson's ratios of both tip (E_t, ν_t) and sample (E_s, ν_s).

$$\frac{1}{E} = \frac{1 - \nu_s^2}{E_s} + \frac{1 - \nu_t^2}{E_t} \qquad (29)$$

1.4.3.1 Atomic Force Microscopy (AFM)

The AFM allows for determining surface properties on a nano-scale, 0.1 to 10 nm, using repulsive and attractive atomic forces of surface atoms and atoms of fine tip [110–114]. AFM indentation can be used to map local mechanical properties of a surface. An AFM consists of a cantilever spring having a defined stiffness with a fine tip at the end, a laser diode, a position sensitive photo-detector, a xyz-stage for 3D positioning and a processing unit, Fig. 21.

The position of the cantilever spring tip is determined by the position of the reflected laser beam on the photo-detector [112]. The cantilever spring bends during the indentation and its deflection is detected by the laser beam. As the cantilever stiffness is known the applied load P can be calculated by the displacement of the cantilever spring.
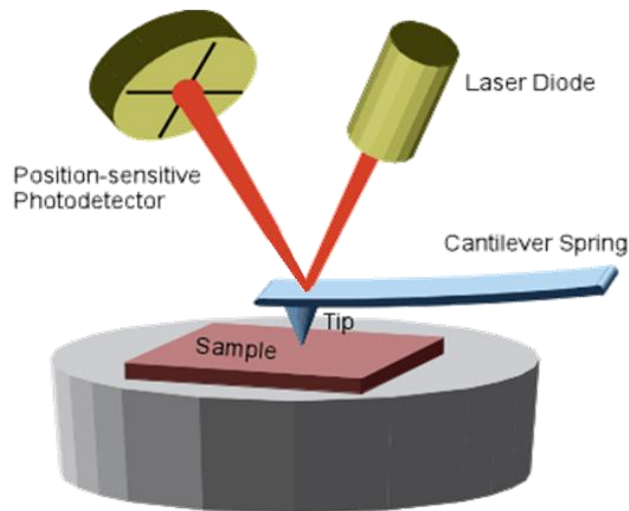
Fig. 21 Schematic setup of an AFM [115].

1.4.3.2 Nanoindenter

The nanoindenter is a type of instrumented indentation techniques to measure mechanical properties, e.g. hardness, elastic modulus, or adhesion strength, in force range of 40 and 1800 mN with lateral resolution of >10 nm [116–118]. Nanoindenters are equipped with motorized xy-stage for mechanical images and uses the typical hardness indenter geometries such as Vickers or Berkovich [116]. Furthermore, the nanoindenter can be used in dynamic mechanical mode which allows for evaluation of viscoelastic properties [116].

Its application in dental material science covers mainly determination of hardness and elastic modulus depending on curing conditions or composition of VLC RBCs [119–121]. Additionally, the mechanical properties are correlated with other material properties, such as *DC*, to investigate the relationship between mechanical and structural properties of VLC RBCs [121,122]. Another application is the determination of VLC RBC morphology due to filler content or distribution [123]. Due to the high resolution, small spatial properties such as the influence of coupling agents on the mechanical properties on the interface region are possible [124].

1.4.4 Mechanical imaging and mapping

The great advantage of instrumented indentation techniques is automation of measurement and data acquisition as well as data evaluation for mechanical mapping, Fig. 22.
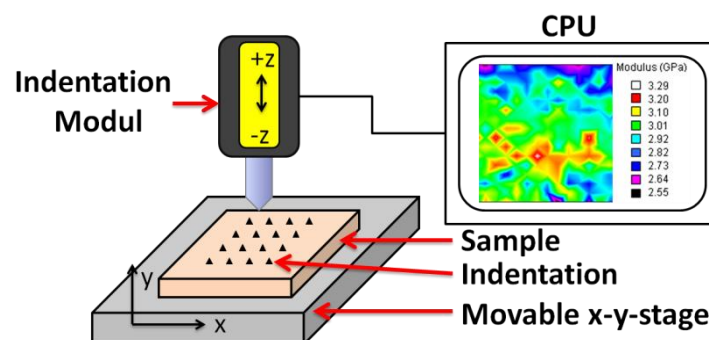
Fig. 22 Scheme of a mapping system to determine the mechanical property distribution of a sample surface.

36

Mechanical mapping visualizes local mechanical properties of a surface caused by filler particles, inclusions in alloys and polymers, or inhomogeneous curing, and is applied for AFM and nano-indenters. Nevertheless, the classical hardness tester can be used for mechanical imaging on a scale of typically 0.5 to 1 mm [43,105,125]. In dental materials science effects of the light intensity distribution of the LCU on the mechanical properties of cured VLC RBCs are of crucial interest [43,125]. Uneven intensity distributions of LCU are found again in the corresponding mechanical images of top and bottom surfaces, Fig. 23.
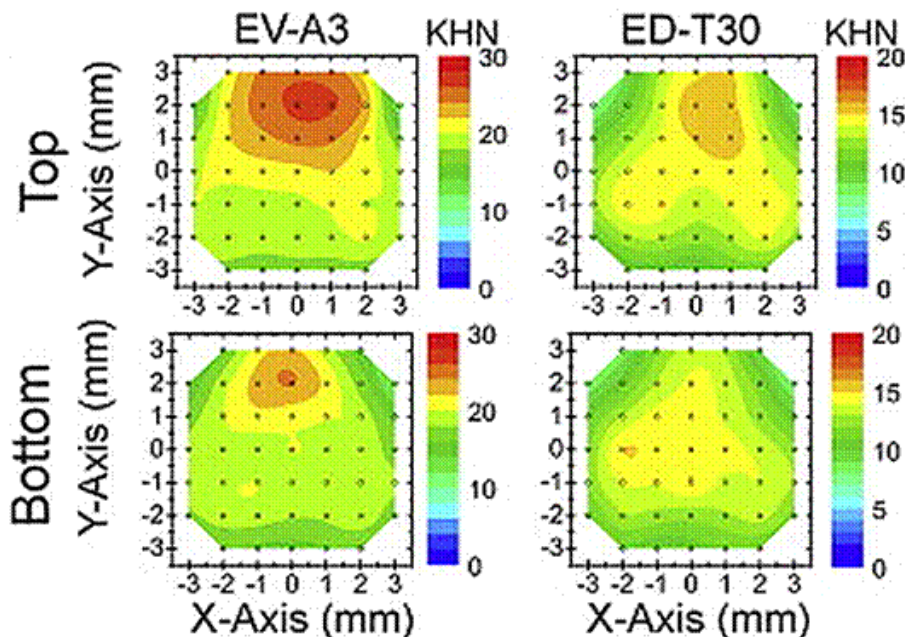
Fig. 23 Mechanical imaging by Knoop hardness testing of two different VLC RBC, Tetric Evoceram natural shade A3 (EV-A3) and Empress Direct high translucency shade Trans 30 (ED-T30), for the Top and Bottom sample side [105].

1.5 Dynamic Mechanical Analysis (DMA)

The dynamic mechanical analysis (DMA) is a method to characterize the viscoelastic behavior of materials in terms of the temperature and frequency dependent complex modulus $E^*(\omega,T)$ [92,108,126]. Besides, the determination of $E^*(\omega,T)$ further mechanical properties are available such as the storage E' and loss modulus E'', loss factor $\tan \delta(\omega)$, glass temperature T_g or the melting temperature T_m. DMA instruments allow for sample holders measuring in bending, torsion, shear, compression or tension [127].

Usually, a small sinusoidal deformation (ε) is applied to the sample and a phase-shifted stress as a response signal is measured, Fig. 24 left.
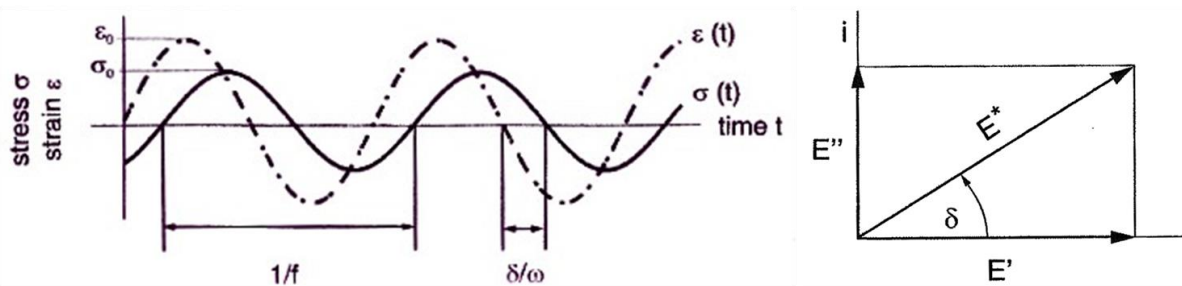
If the strain $\varepsilon(\omega,t)$, with the strain amplitude (ε_0) and angular frequency (ω), is given by

$$\varepsilon(\omega,t) = \varepsilon_0(\omega)\sin(\omega t) = \varepsilon_0(\omega)e^{i(\omega t)} \tag{30}$$

one measures the responding stress $\sigma(\omega,t)$:

$$\sigma(\omega,\text{t}) = \sigma_0(\omega)\sin(\omega t + \delta(\omega)) = \sigma_0(\omega)e^{i(\omega t + \delta(\omega))} \tag{31}$$

with the stress amplitude (σ_0) and the phase angle (δ). Now the complex modulus can be calculated by

$$E*(\omega) = \frac{\sigma_0(\omega)e^{i(\omega t)} \cdot e^{i(\delta)}}{\varepsilon_0(\omega)e^{i(\omega t)}} = \underbrace{E_0(\omega)\cos\delta(\omega)}_{E'(\omega)\,StorageModulus} + i\underbrace{E_0(\omega)\sin\delta(\omega)}_{E''(\omega)\,Loss\,Modulus} \tag{32}$$

The real part of the complex modulus $E*(\omega)$ represents the storage modulus E' and the imaginary part the loss modulus E'', Fig. 24 right. To describe the damping behavior the loss factor is defined:

$$\tan\delta(\omega) = \frac{E''(\omega)}{E'(\omega)} \tag{33}$$

The mechanical properties may change drastically during a phase transition, the contributions to the viscoelastic properties of even small portions of polymers can be detected, Fig. 25. Thus, transition temperatures can be determined very sensitively.
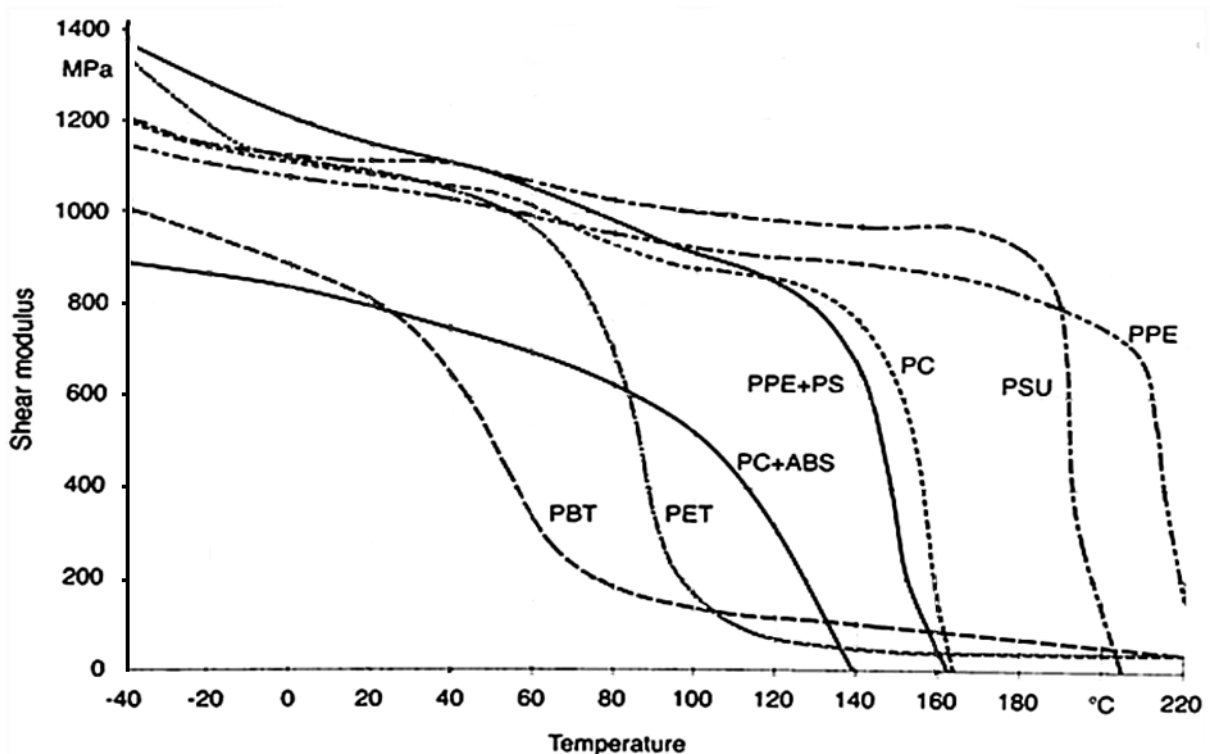
Fig. 25 Change of moduli of different polymers as a function of the temperature [92].

DMA measurements of polymers show that transition temperatures shift to higher temperatures if the frequency is increased, Fig. 26.
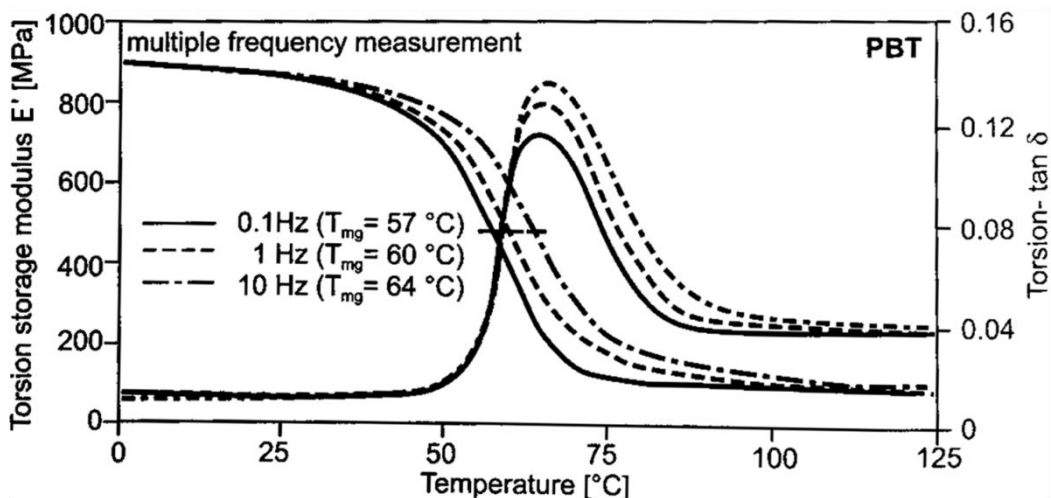
Fig. 26 Frequency dependence of storage modulus E', Tg and loss factor tan δ for PBT [92].

This behavior leads to the principles of frequency-temperature superposition and time-temperature superposition on which a master curves constructions are based, Fig. 27 [108,126]. They allow for predicting materials behavior beyond the experimentally accessible measuring range, e.g. high frequency performance of tire rubbers [128] or long time behavior of plastic pipes [129].
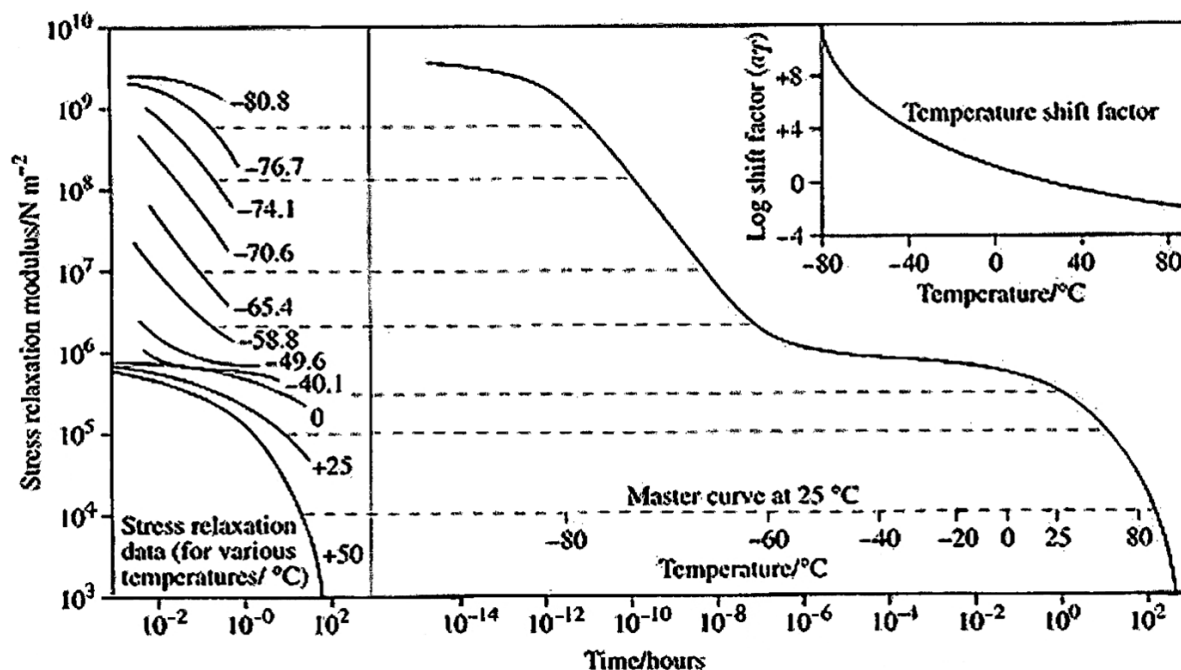
Fig. 27 Construction of the viscoelastic master curve for PIB at 25 °C reference temperature by shifting stress relaxation curves obtained at different temperatures horizontally along the time axis. The shift factor, aT varies with temperature as shown [130].

The primary curing of VLC RBC is a fast process if modern LCUs are used with endings typically within 20 to 40 seconds. In order to gain kinetic data, the primary curing process has to be measured with a time resolution of 10 data points per

seconds. This requires at least a frequency of 1 kHz. The maximum measuring frequency is typically restricted to 50 Hz for most DMA instruments. Therefore, a curing reaction can be traced if it lasts at least 3 minutes as at least 3 cycles are necessary for one reliable data point.

The stiffness evaluation requires "homogeneity", which is obeyed for self- or thermally-activated curing reactions, because the reaction starts roughly in the whole cross-section area. As photo-activation goes along with Lambert-Beer-absorption, the curing kinetics differs with respect to depth leading to gradient stiffnesses during the first phases of the curing reaction [27]. This restricts DMA to the investigation of slow photo-curing processes [131].

In the field of dental composites, the DMA is used to determine the stiffness of VLC RBC after curing to evaluate the influence of the curing conditions [132–134]. This yields the stiffness of VLC RBCs, which then can be compared to tooth properties [132,134,135].

Another application is the investigation of the kinetics of post-curing processes. As post-curing happens slowly, DMA with low frequencies (< 1 Hz) reveals a logarithmic time dependency of the post-curing process, Fig. 28.
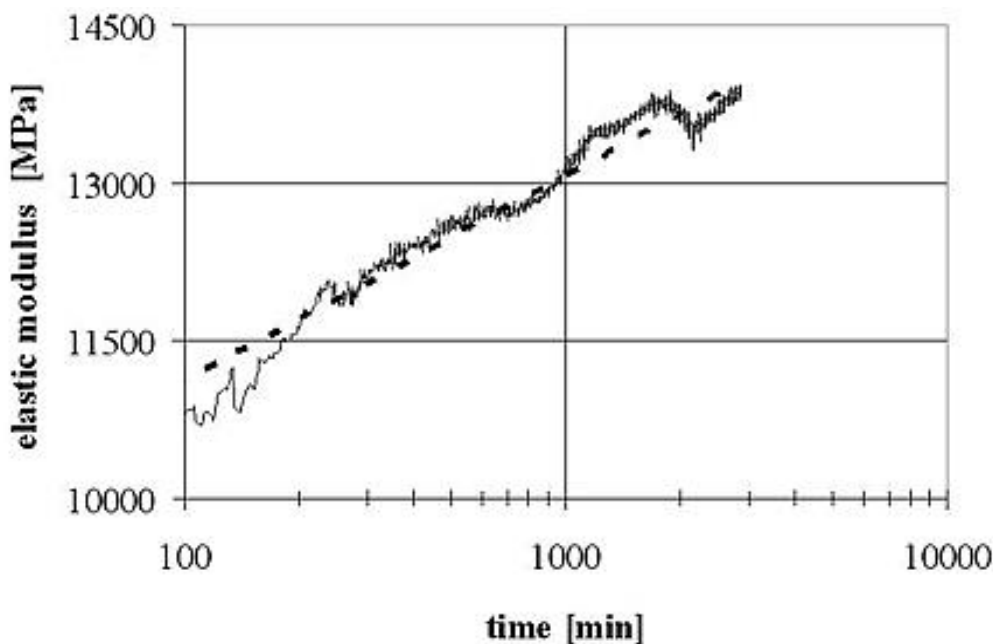
Fig. 28 DMA long-term measurement of post curing of a VLC RBC [136]

Besides the characterization of the bulk viscoelastic behavior, the DMA allows for the determination of the local viscoelastic properties in the compression mode with small size indenters [137]. Therefore, it is principally possible to determine local mechanical properties comparable with nanoindentation. Especially for the VLC RBCs with their inhomogeneous curing behavior, the DMA allows to measure these inhomogeneous local mechanical properties. Hence, it is possible to visualize the local mechanical properties as mechanical imaging.

2 METHODOLOGY AND PURPOSE OF THE WORK

Visible light curing resin based dental composites (VLC RBCs) are the most common used dental restorative materials. These materials were developed to replace amalgam based restoratives first because of elution of mercury, which may cause health problems, and second, in order to improve esthetic aspects/requirements of patients. The resulting material properties and the life time of VLC RBCs depend on the curing conditions. The main influence factors on the resulting material properties are irradiance, light distribution and spectrum of the light curing unit (LCU). The methods employed in this work shall provide information about LCU characteristics, mechanical as well as curing parameters, e.g. degree of conversion (*DC*), time dependent *DC (DC(t))*, depths of cure (*DoC*) and hardness of the VLC RBC, Fig. 29.

Until now there is no model established which can predict sufficient *DC* and *DoC* dependences on curing conditions such as irradiance or exposure time. Furthermore, there is hardly any knowledge about the influence of curing conditions on post curing, thus predictions of the surface hardness cannot be made. Generally, it is known that the LCUs emit inhomogeneous light, and therefore the curing will be inhomogeneous, e.g. surface hardness distribution. No one knows how curing conditions, such as irradiance and exposure time, influence the resulting distribution of the mechanical properties. Often, materials show inhomogeneous mechanical properties, e.g. hardness inhomogenities induced by light distribution. A dynamical mechanical analysis (DMA) has an ability to determine viscoelastic properties of materials. Unfortunately, a micro-indentation system for a commercial DMA is not available yet.

Kinetic models are necessary to predict the *DC(t)* and *DoC*. The kinetic models will have to be adjusted with measured *DC(t)* and *DoC* results for different curing conditions. To determine *DC(t)* for different curing conditions a Fourier transform infrared spectroscopy (FTIR) is used in this work. *DoC* will be measured by using differential scanning calorimetry (DSC), hardness and mass loss in strong solvent. To gain more information about the influences of the curing conditions on post curing, a master curve based superposition will be proposed. The surface hardness for VLC RBCs under different curing conditions will be measured at different times with hardness testing. Different LCUs will be characterized by ultra violet visible spectrometer (UV-Vis) for irradiance and spectra, and a laser beam profiler will be utilized for light distribution. These data will be used to compare the LCU characteristics to the distribution of the local mechanical properties of VLC RBCs measured by mechanical imaging with hardness testing.

For the development of a micro-indentation DMA an indenter system with sample holder and movable x-y stage will be adapted to the DMA to allow the determination of viscoelastic properties. A validation of this indentation method will be done by comparing the moduli measured in DMA three point bending mode with those measured in an indentation mode. The results of the mechanical imaging using DMA microindentation will be compared with the results from Knoop hardness mapping.
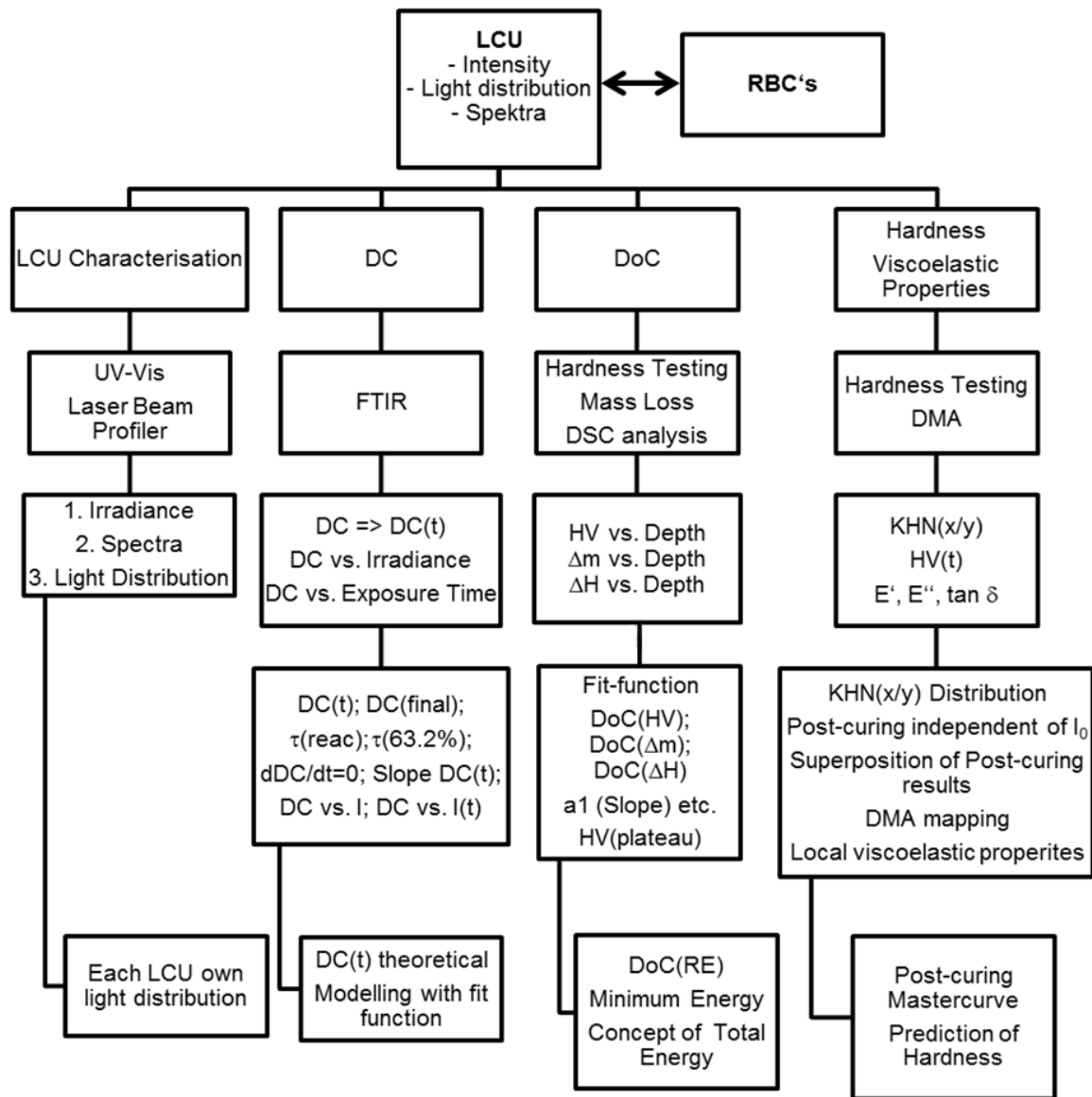
Fig. 29 Flow chart of the plant methodology and methods of the PhD thesis

3 DISCUSSION OF THE RESULTS

3.1 Characterization of dental light curing units

Mechanical properties depend on the degree of conversion which is primarily affected by the interaction of light from the LCU and the VLC RBC [39,138–140]. Therefore, emission spectra, irradiance and irradiance distribution were measured to compare the LCU properties with the resulting properties of the VLC RBC after the curing. A laser power meter, an integrating sphere equipped with an UV-Vis spectrometer and a laser beam profiler were used to characterize the properties of the LCUs. Furthermore, the energy transmission through a VLC RBC was determined by exposing samples with increasing thickness in front of an integrating sphere to determine the attenuation coefficient of the VLC RBCs.

3.1.1 Light energy and spectral measurements [P-I and P-VI]

The tested LCUs in this part of the study was the Quarz-Tungsten-Halogen (QTH) LCU Polofil Lux, the monowave LED LCU Celalux I, and the polywave LCU Bluephase 20i.

Each LCU had a characteristic spectrum and different irradiance levels, Fig. 30. Irrespective of irradiances, different spectral emissions lead to differences in the curing performance. CQ has a broad absorbance spectrum with the most effective wavelength around 460 nm [141,142]. The width at the half-maximum absorption A_{max} peaks ranges from 444 to 504 nm determining the effective CQ spectra. The monowave LED Celalux has maximum spectrum overlap of 90 % to CQ followed by the polywave Bluephase 20i Turbo with 82 % and the QTH with 70 % because of its broad spectrum. The irradiance of the Bluephase 20i Turbo is double that of the Celalux and four times that of the QTH. Thus, differences between the LCUs affect the initiation of CQ and the whole curing process with respect to the polymerization kinetics as well as the final mechanical properties of the cured composites.
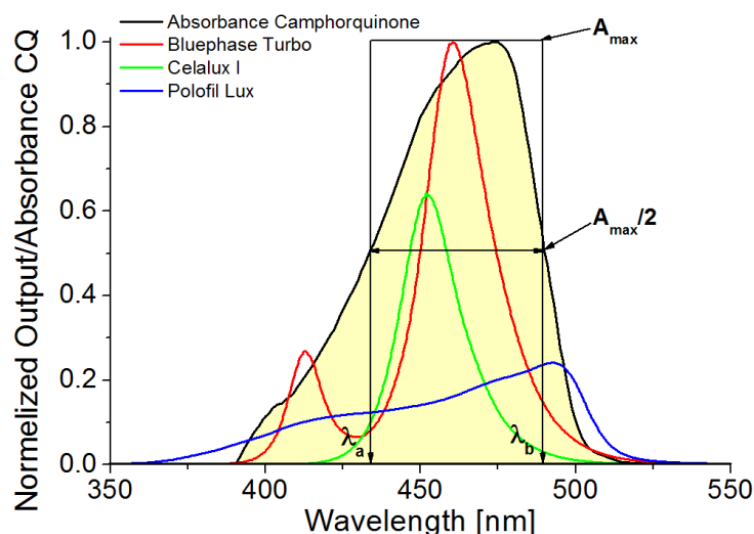
Fig. 30 Emission spectra of LCUs and absorbance spectrum of camphorquinone [P-VI].

The laser power meter and the integrating sphere show similar results and both can be considered as adequate methods to determine the irradiance of LCUs, [P-I Table 1]. However, with the integrating sphere the irradiance and the spectral distribution of an LCU can be determined by using the UV-Vis spectrometer.

The measurement of the absorbance energy through a thickness of a VLC RBC sample shows an exponential decrease of light energy, Fig. 31. Extrapolation to zero thickness shows that approximately 30 % of the light intensity is reflected at the sample surface. The decreasing light intensity within a VLC RBC is important for depth depending properties such as depth of cure [139,140].
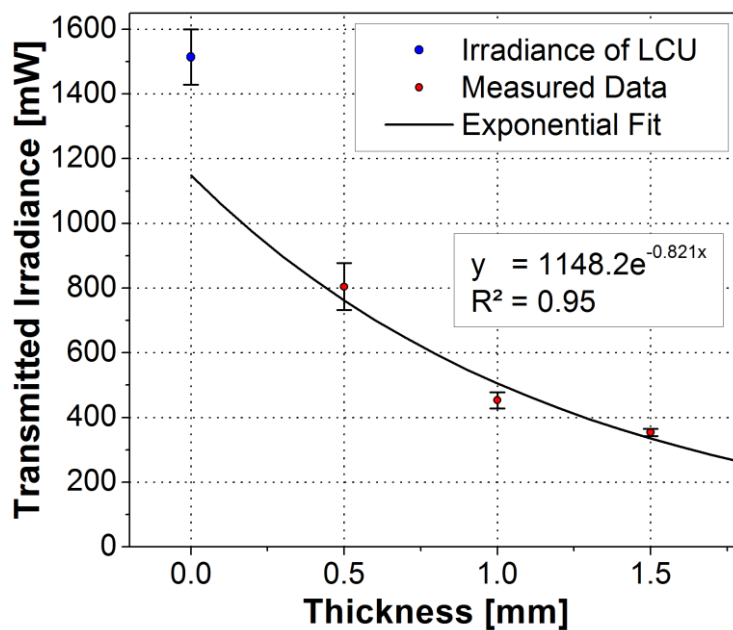
Fig. 31 Transmitted irradiance through Arabesk TOP OA2; LCU: Elipar S10 [P-VI]

3.1.2 Light distribution measurements [P-I]

The measurements of the irradiance distribution of LCUs by a laser-beam profiler show that each LCU has an individual irradiance distribution pattern, Fig. 32. This depends on the internal setup of the LCU, e.g. reflection of light by the mirrors or its design [143]. This may lead to inhomogeneous irradiance distributions with high and low intensity areas at the exit of the light guide tip. If a low irradiance area is positioned over a filling, it is insufficiently cured.
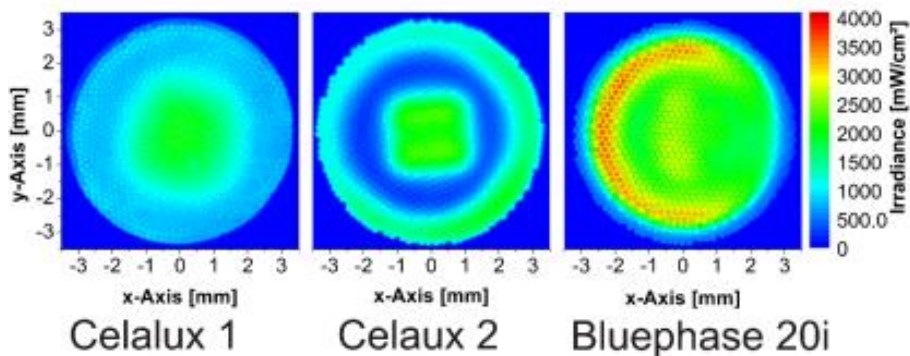
Fig. 32 Images taken by the laser-beam profiler: Celalux 1, Celalux 2 and Bluephase 20i Turbo [P-I].

A comparison of the results gained by laser beam profiler, SLR (single lens reflex) and iPad measurements produce similar pictures of intensity distributions. This allows for using SLR and iPads if only a qualitative information of the intensity distribution of LCUs is required, e.g. in a dental practice, Fig. 33. In order to get quantitatively reliable results, the use of a laser-beam profiler is required.
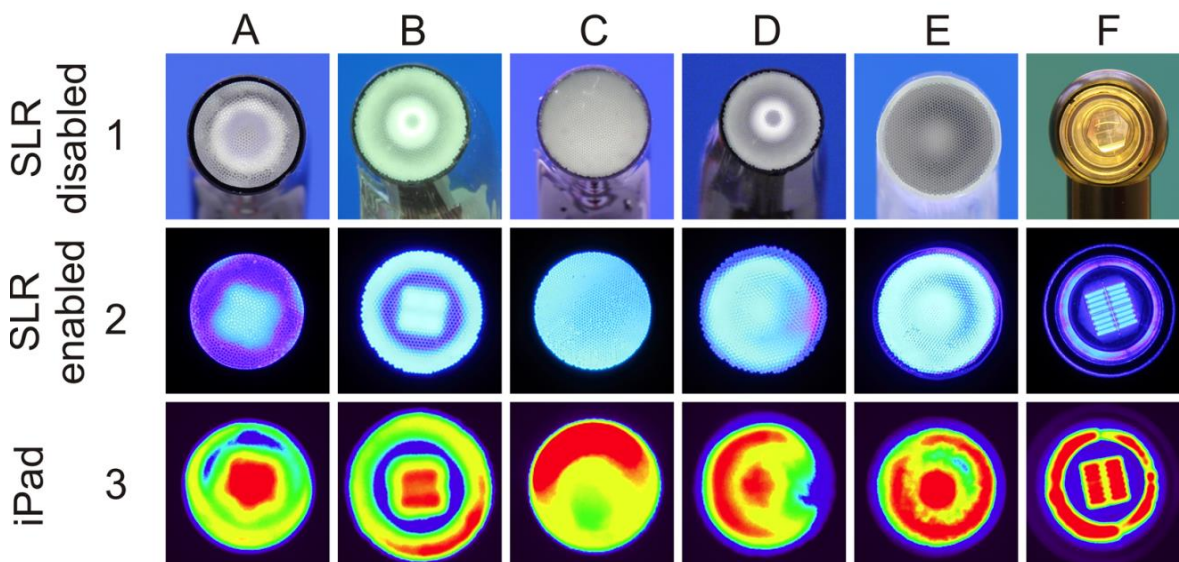
Fig. 33 Images of light guide tip exits of different LCUs inactivated and activated with SLR and iPad: A Celalux 1, B Celalux 2, C Polofil Lux, D Bluephase 20i, E Elipar S10, and F Dentsply SmartLite PS [P-I].

One has to know how the emitted light of a LCU affect the properties of a VLC RBC after irradiation to get sufficiently and homogeneously cured composites.

3.2 Kinetics of the curing reaction of VLC RBCs

The reaction kinetics describes quantitatively the change of monomer concentration during the curing process [38,69] and allows for correlating curing conditions to final properties of VLC RBCs, e.g. effect of the introduced irradiance on *DC* of sample.

The first part of the following section considers investigations and modelling the effect of irradiance on photo-polymerization reaction kinetics and corresponding *DC*. The second part considers the concept of "total energy" [144,145] which assumes that equal quantities of energy introduced in different exposure time intervals results in equivalent *DCs*.

3.2.1 Modelling reaction kinetics of VLC RBCs to describe *DC*-curves [P-II]

The reaction kinetics of the curing process was modeled using a time dependent reaction time constant to gain a novel *DC*-function taking into account the increase of viscosity due to chain growth and vitrification.

Growth reaction: $A-(DMA)_n-(DMA\bullet)+DMA \xrightarrow{k_{ucg}} A-(DMA)_{n+1}-(DMA\bullet)$

The concentration change of dimethylacrylate monomers (DMA) during curing depends on the reaction constant k_{cg}.

$$\frac{dc^{DMA}(t)}{dt}=-\underbrace{k_{ucg}*c_0^{initiator}(x)}_{=k_{cg}}*c^{DMA}(t)=-k_{cg}*c^{DMA}(t) \tag{34}$$

with c_0^{DMA} concentration of DMA monomers
    $c_0^{initator}$ concentration of radicalized initiator molecules
    k_{cg} global reaction constant.

The reaction constants k_{cg} is linked to the reaction time constant τ_{reac}^0 by

$$\tau_{reac}^0=\frac{1}{k_{ucg}*c_0^{initiator}}=\frac{1}{k_{cg}}\quad. \tag{35}$$

For the first seconds of curing the time dependent *DC* is then described by [101,146]:

$$DC(t)=1-\frac{c^{DMA}(t)}{c_0^{DMA}}=1-e^{-\frac{t}{\tau_{reac}^0}} \tag{36}$$

The curing process can be considered to consist of two steps: i) primary curing in the liquid state with highly mobile radicals and monomers representing a thermally controlled process, and ii) post-curing in the glassy state with inhibited mobility of radicals and monomers representing a diffusion controlled process. Thus, Eq. (36) overestimates the *DC* for long times and approaches "1", whereas typical *DC* values are experimentally determined between 0.5 and 0.7.

Therefore, a novel *DC*-function had to be developed which takes into account the deceleration of the reaction rate due to increasing resin viscosity and its transfer to

the glass. A possible approach is to assume a time dependent reaction time constant:

$$\tau_{reac}(t) = \tau^0_{reac}{}' + \Theta * e^{\frac{t}{\tau_{grow}}} \qquad (37)$$

with $\quad \tau^0_{reac}{}' \quad$ constant part of reaction time constant in the liquid phase

$\quad \tau_{grow} \quad$ growing time constant

$\quad \Theta \quad$ strength of the time dependent part

Note that the reaction time constant of Eq. (34) is given now by $\tau^0_{reac} = \tau^0_{reac}{}' + \Theta$. This yields the following term for the time dependent reaction constant

$$k_{cg}(t) = \frac{1}{\left\{ \tau^0_{reac}{}' + \Theta * e^{\frac{t}{\tau_{grow}}} \right\}} \qquad (38)$$

Introducing Eq. (38) to Equation (1) of P-II yields

$$\frac{dc^{DMA}(t)}{dt} = -\frac{c^{DMA}(t)}{\left\{ \tau^0_{reac}{}' + \Theta * e^{\frac{t}{\tau_{grow}}} \right\}} \qquad (39)$$

The differential equation (39) can be solved by separation the variables.

$$\int_{c(t=0)}^{c(t)} \frac{dc^{DMA}}{c^{DMA}} = -\int_0^t \frac{dt'}{\left\{ \tau^0_{reac}{}' + \Theta * e^{\frac{t'}{\tau_{grow}}} \right\}} \quad {}^5. \qquad (40)$$

Integration yields the time dependent DMA monomer concentration

$$c^{DMA}(t) = c_0^{DMA} * e^{-\frac{t}{\tau^0_{reac}{}'}} * \left(\frac{\tau^0_{reac}{}' + \Theta * e^{\frac{t}{\tau_{grow}}}}{\left(\tau^0_{reac}{}' + \Theta \right)} \right)^{\frac{\tau_{grow}}{\tau^0_{reac}{}'}} \qquad (41)$$

and the degree of conversion (*DC*) is given by

---

[5] According to Bronstein's "Taschenbuch der Mathematik" the solution of the integral on the right side of Equation (39) is found as integral 454:

$$\int \frac{dx}{b + c * e^{ax}} = \frac{x}{b} - \frac{1}{a * b} \ln\left(b + c * e^{ax}\right) \text{ with correspondences } a = \frac{1}{t_{glass}}, b = \tau^0_{reac}{}', c = \Theta$$

$$DC(t) = 1 - \frac{c^{DMA}(t)}{c_0^{DMA}} = 1 - e^{-\frac{t}{\tau_{reac}^0}} * \underbrace{\left(\frac{\tau_{reac}^0 + \Theta * e^{\frac{t}{\tau_{grow}}}}{\left(\tau_{reac}^0 \text{'} + \Theta \right)} \right)^{\frac{\tau_{grow}}{\tau_{reac}^0}}}_{correction\ term\ K(t)} \tag{42}$$

The effects of growing time constant τ_{grow} and strength Θ on calculated $DC(t)$-curves are shown in Fig. 34 and Fig. 35, respectively. A decreasing τ_{grow} leads to a flatter DC-curve with decreasing final DC-values, Fig. 34. A similar behaviour is observed for an increasing Θ, Fig. 35. This novel DC-function allows for better fits of DC measurements.
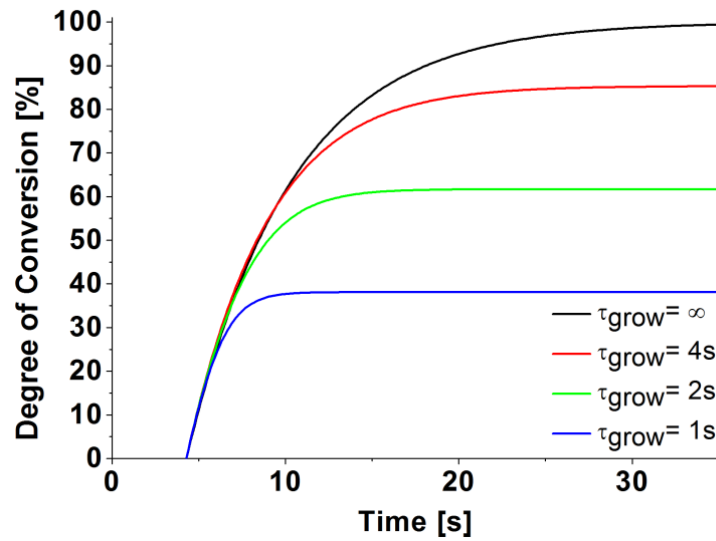
Fig. 34 Influence of growing time constant τ_{grow} on calculated DC-curves [P-II].
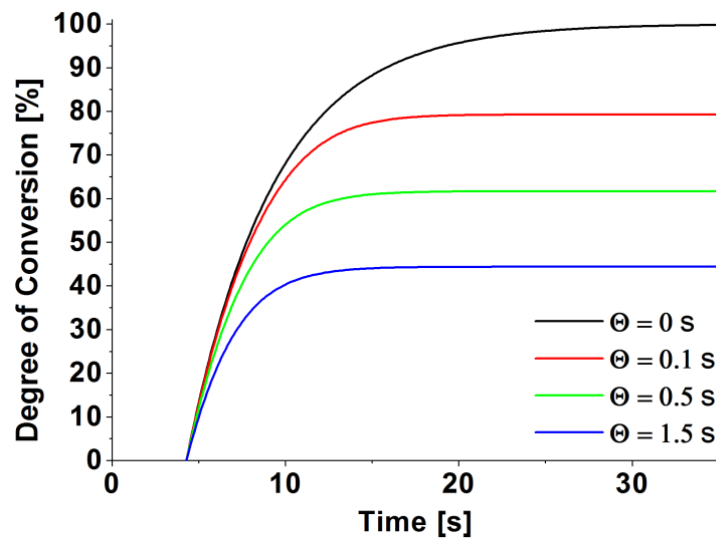
Fig. 35 Influence of strength Θ on calculated DC-curves [P-II].

Experimental *DC*-data of two commercial VLC RBCs cured with different irradiances were performed using a FTIR-ATR. Firstly, the FTIR *DC(t)* data were evaluated by a direct method to determine characteristic parameters of the curing kinetics, Fig. 36, and secondly by applying and verifying the novel *DC*-function, Eq. (42).

Direct method: Each measured *DC(t)*-curve was evaluated with respect to initial slope $m_{initial}$, reaction time $\tau_{reaction}$, the time to a degree of curing of $(1-1/e)*DC_{3min}$, and DC_{3min}, Fig. 36. The initial slope $m_{initial}$ was calculated by a linear fit of the DC-curve between the DC-baseline prior to irradiation and a *DC* of 30 %. The start time t_{start} of the curing reaction was determined by the intercept of *DC*-baseline and initial slope $m_{initial}$. DC_{3min} represents the arithmetic average of the *DC* during the last 5 s of each measurement. The degree of curing of $(1-1/e)*DC_{3min}$ is given by 63.2 % of DC_{3min}. The corresponding time represents the reaction time $\tau_{reaction}$ which is a measure of the reaction rate. The evaluation scheme is shown in Fig. 4. For example, the initial slopes $m_{initial}$ increased by a factor of 2 (Arabesk) and by a factor of 1.8 (Grandio) when the irradiance increased a factor 3.3. In general, this increase is to be expected because the concentration of radicals is directly affected by the irradiance. However, after an exposure time of 80 s all samples reached the same constant *DC* values of 68.1 % (0.6) for Arabesk and 64.1 % (1.3) for Grandio. This shows the limitation of *DC* and will not reach 100 %.
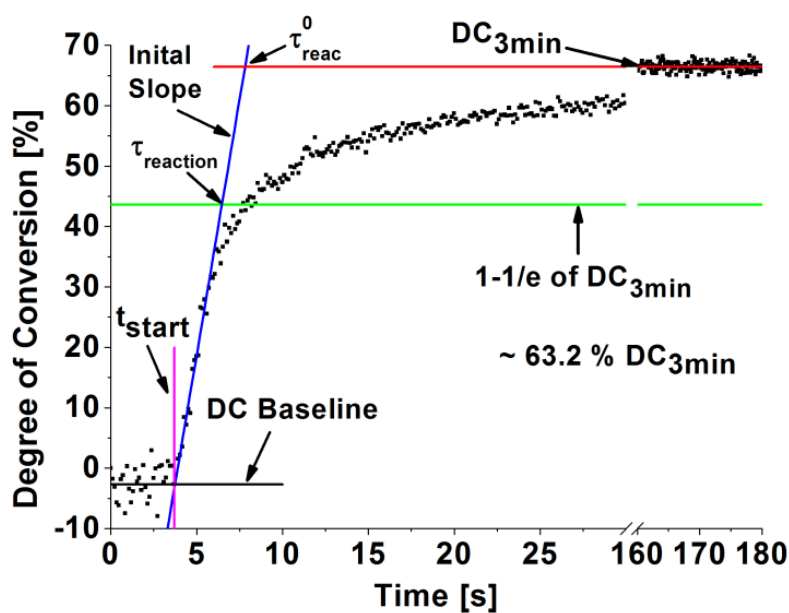
Fig. 36 Evaluation of *DC* curves to determine the characteristic parameters of the curing kinetics [P-II]

Fitting using novel *DC*-function: The novel *DC*-function provides good fits for the early stages of the curing reaction as shown in Fig. 27 for the 15 s-fit interval of *DC(t)*. The reaction time constants τ_{reac}^{0} decrease a factor 1.9 (Arabesk) and a factor 1.8 (Grandio), respectively, if the irradiance is increased a factor 3.3. This result is comparable to the results of the direct method. If the fit interval is increased to 40 s and 160 s, the fit curves increasingly differ from *DC*-data in the phase of primary

curing, but fit better for long times due to the increasing number of data points in the post-curing range, Fig. 37.
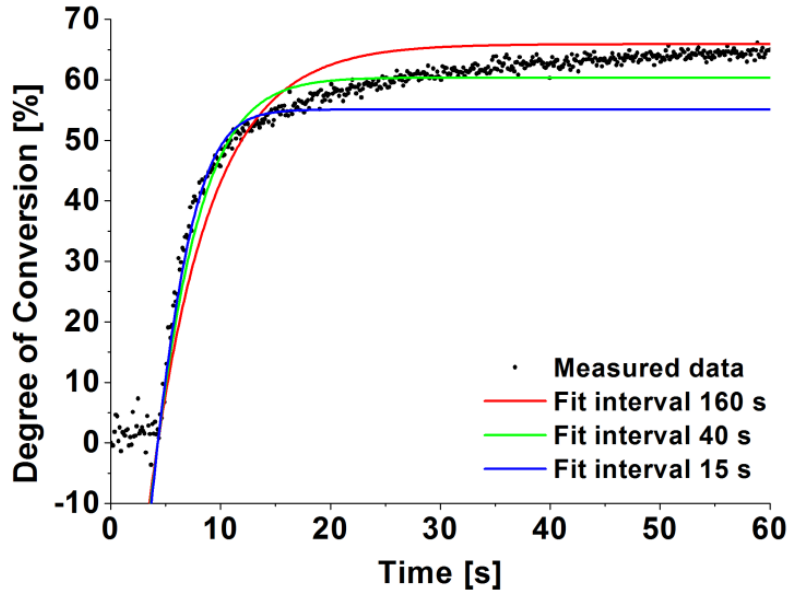
Fig. 37 Comparison of a measured *DC* curve (dots) of Arabesk fitted with respect to the time range of fit intervals of 15 s, 40 s and 160 s; LCU: Bluephase 16i

Fig. 38 shows that the reaction time constant decreases with increasing irradiance and can be well fitted by

$$\tau_{reac}^{0}(I_{LCU}) = \frac{a}{I_{LCU}^{b}} \tag{43}$$

with the parameter "*b*" close to –0.5 for both Arabesk and Grandio. This means that τ_{reac}^{0} depends reciprocally on the square root of irradiance. For the first time Eq. (14) of [69] could be verified for commercial VLC RBCs.
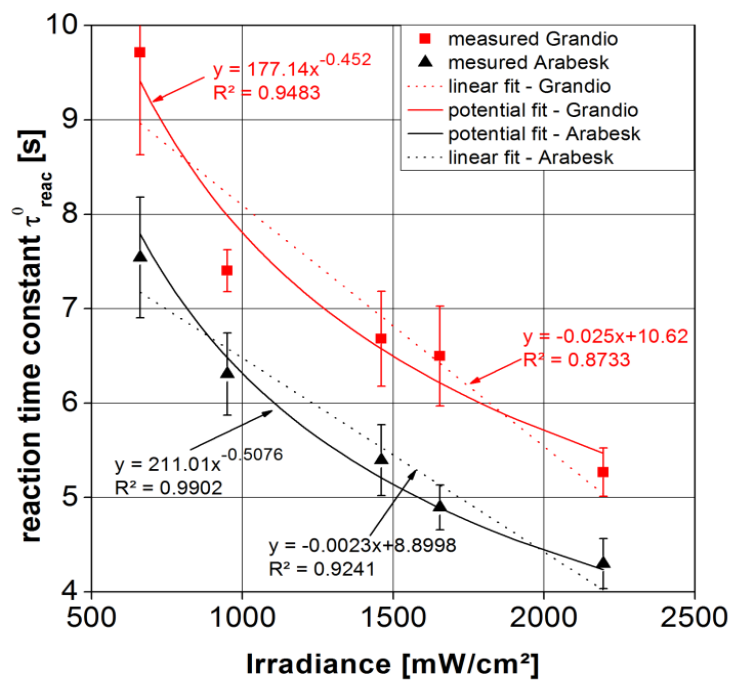
3.2.2 Evaluation of the *DC* and total energy concept [P-III]

The basic idea of "total energy concept" or "exposure reciprocity" is that the achieved *DC* of VLC RBCs depends only on equivalent amounts of energy irrespective of LCU irradiance or exposure time [97,144]. It is used to choose the optimal exposure strategy to ensure sufficient cure and to prevent overexposure with the danger of tissue damages.

Real time measurements of *DC* were performed by FTIR-ATR, [P-III Fig. 2]. The samples were irradiated with a radiant exposure of approximately 18 J/cm² with different irradiance levels and corresponding exposure times, Fig. 39. The measured *DC(t)*-curves could be well fitted by a *DC*-function considering primary curing in the liquid state at short times and post-curing at large times.

$$DC(t) = A \cdot \underbrace{\left(1 - e^{\left(-\frac{t - t_{LCU}}{\tau_{reac}^0} \right)} \right)}_{primary\,curing} \cdot \underbrace{\left(1 + B \cdot \ln \frac{t}{t_{LCU}} \right)}_{post-curing} \tag{44}$$

with t_{LCU} time at which the LCU was switched on

             A   fit parameter, achievable *DC* of primary curing

             B   fit parameter, increase of *DC* due to post-curing
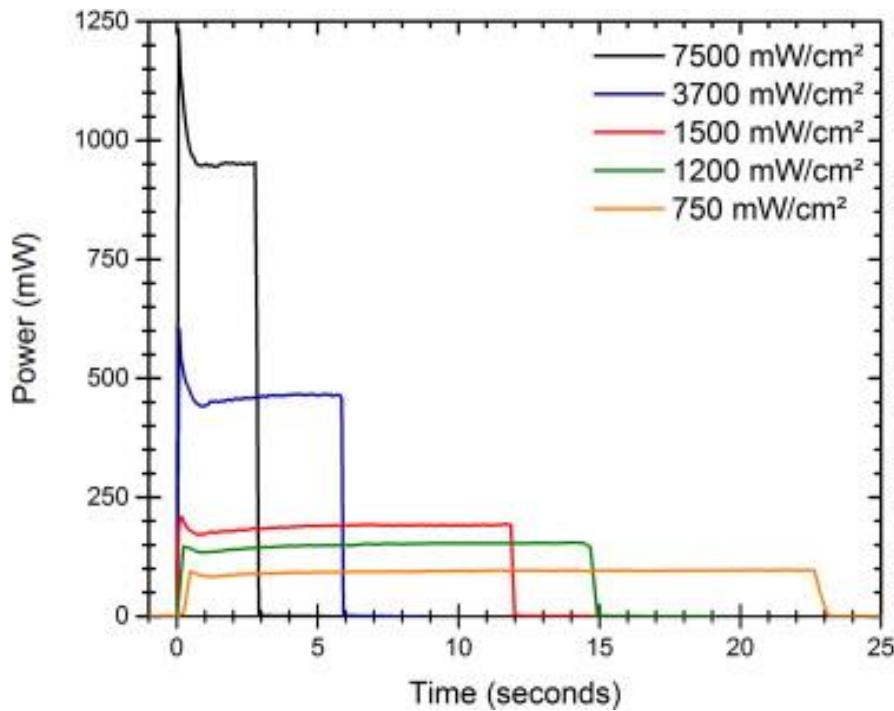
Fig. 39 Exposure time (seconds) and power (mW) at each irradiance level determined using the integrating sphere attached to the fiber optic spectrometer. The radiant exposure to specimens at each irradiance level is given by the integrals under the five graphs [P-III].

51

This *DC(t)*-function allows for the determination of specific influences of the curing conditions such as the irradiance or exposure time on measured *DC(t)* of VLC RBC. It consists of two parts. The exponential term represents the kinetics of primary curing during the initial phase of polymerization in the liquid state. The logarithmic term represents the post-curing reaction after the mobility of the monomers, radicals and polymer chains has decreased because the resin transfers to the glassy state. The fit parameter *A* limits the final *DC* of primary curing to values smaller than "1". It was found to be rather constant – final *DC*-values were 55 – 60 % – and not influenced by the irradiance. The fit parameter *B* turned out to close to constancy showing no dependency on an irradiance. The cause of *A* and *B* shows that the curing kinetics is completely determined by the reaction time constant τ_{reac}^{0} which of course changes with irradiance.

The *DC* curves in Fig. 40 show that the increase of irradiance leads to larger initial slopes due to larger rates of reaction.
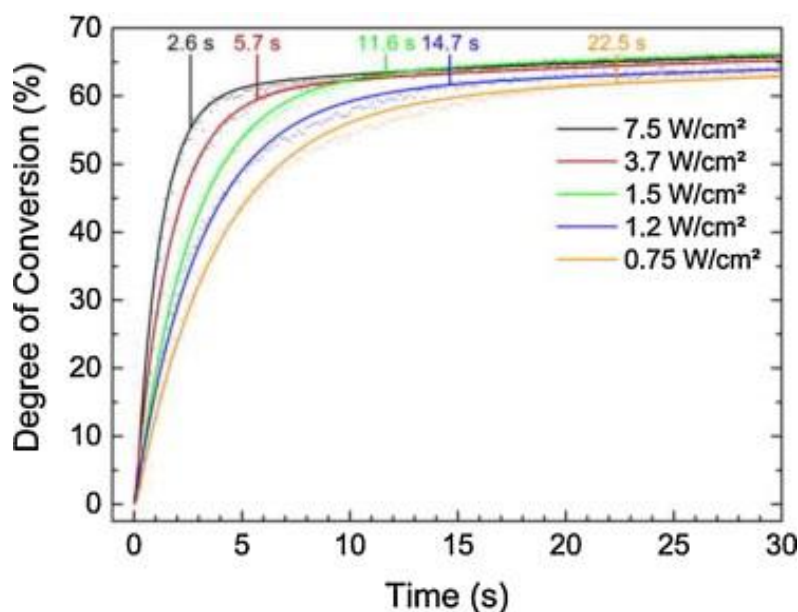
Fig. 40 Measured DC_{exp} curves and calculated DC_{fit} curves of Tetric EvoFlow shown for the first 30 s irradiated with 0.75, 1.2, 1.5, 3.7 and 7.5 W/cm2. The times of LCU turn off are indicated on each curve [P-III].

As a consequence, a sample exposed with a low irradiance level does not reach the *DC* at the same time as a highly exposed sample. With the same delivered amount of energy, the *DC* at irradiance levels below 3.7 W/cm² was higher than for irradiance levels 3.7 and 7.5 W/cm², Table 13.

Table 13 Mean exposure time, distance to sample, irradiance and calculated radiant exposure as determined using real time measurements made with the spectrometer

Mean exposure time	[s]	2.6 (0.3)	5.7 (0.2)	11.7 (0.2)	14.7 (0.1)	22.5 (0.2)
Distance to RBC	[mm]	0.0	4.5	9.0	10.5	13.5
Mean irradiance	[W/cm²]	7.5 (0.8)	3.7 (0.2)	1.5 (0.1)	1.2 (0.1)	0.75 (0.1)
Mean radiant exposure	[J/cm²]	19.6 (2.2)	21.1 (0.7)	17.4 (0.3)	17.5 (0.2)	16.7 (0.2)
DC @ (5 J/cm^2)	[%]	27.6 (2.4)	37.3 (3.1)	47.1 (2.7)a,b	46.8 (0.9)a	49.8 (1.4)a
DC @ (10 J/cm^2)	[%]	43.4 (2.3)	50.2 (3.1)	57.7 (2.8)a	56.2 (1.2)a	58.3 (1.6)a
DC @ (15 J/cm^2)	[%]	50.7 (2.5)	56.4 (3.8)	61.4 (2.8)a	60.2 (1.3)a	61.9 (1.5)a
DC_{exp} (170 s)	[%]	70.9 (2.1)	70.2 (3.7)	71.1 (2.7)	69.0 (1.2)	68.5 (1.6)
DC_{fit} (170 s)	[%]	71.0 (2.4)	70.5 (4.1)	71.1 (3.2)	69.0 (1.3)	68.9 (1.7)
Post hoc Fisher's PLSD: similar supersript letter a, b idicate no significant difference in mean values with the colum (p>0.05)						

After 170 s no significant differences in final DC_{exp} were observed between the samples. However, the real time DC as a function of the radiant exposure showed that higher irradiance level > 3.7 W/cm² (radiant exposure > 17 J/cm²) did not reach the same DC in contrast to the lower irradiance levels, Fig. 41. The concept of exposure reciprocity does not hold for high irradiance. At high irradiance levels, the exposure time is short, and thereby the initial lag time due to light initiated radical formation before the start of the polymerization has a stronger effect on the exposure reciprocity. It was found that an optimum combination of irradiance and exposure time for this material is an irradiance of 1.5 W/cm² and an exposure time of 12 s, Fig. 41 (green curve). Therefore, this method is usable to determine the optimum curing conditions to prevent an under- or overexposure of a VLC RBC only for low irradiances.
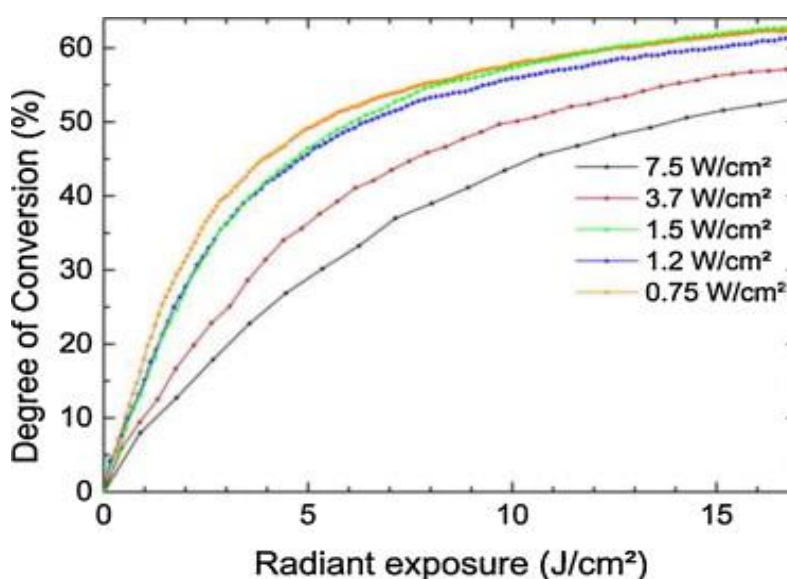
Fig. 41 Real time DC as a function of radiant exposure (J/cm2) delivered at irradiance levels of 0.75, 1.2, 1.5, 3.7 and 7.5 W/cm2 [P-III].

3.3 Effects of curing condition on the properties of VLC RBCs

The properties of VLC RBC depend on the curing conditions such as irradiance, exposure time or the irradiance distribution. Insufficient cured VLC RBCs may cause problems due to inadequate mechanical behavior or elution of monomers leading to reduced lifetimes of the restoration or health problems such as allergies.

The following section presents how depth depending properties are affected by the curing conditions especially the influence of the irradiance distribution of LCUs on the surface hardness distribution. Furthermore, the last section presents the development of an indentation method to determine viscoelastic properties locally, using a dynamic mechanical analyzer.

3.3.1 Effects of the curing time and irradiance on the depth depending properties [P-IV]

The effects of irradiance and exposure time on hardness, mass loss in THF and post reaction enthalpy were investigated as a function of depth for two commercial VLC RBCs. The depth dependent properties were evaluated using a fitting procedure. For details of the measuring as well as evaluation procedures see P-IV.

The post reaction enthalpy ΔH_R is a measure of the concentration of trapped radicals in the glassy state of the polymer matrix, Fig. 42. As the mobility of radicals depends on the density of the polymer network large ΔH_R-values indicate highly cured regions.
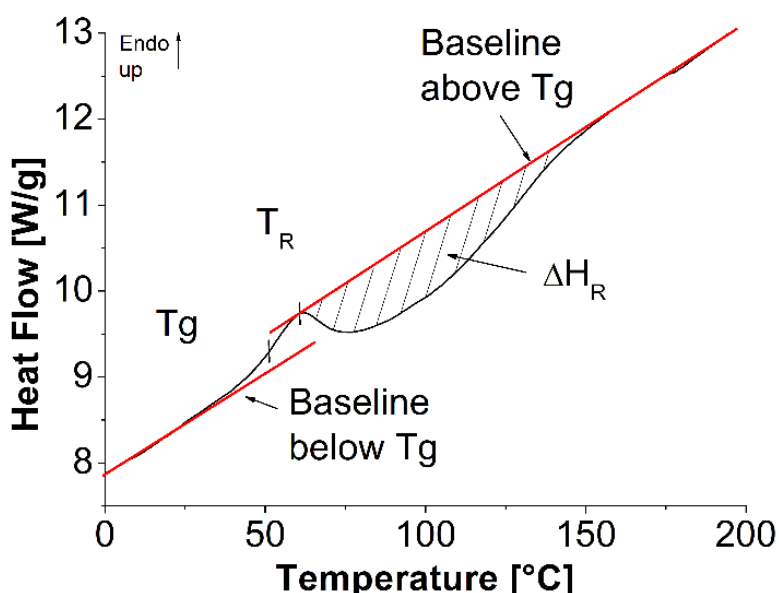
Fig. 42 Evaluation of DSC curves to determine glass transition temperature T_g, start temperature of post-reaction T_R, and post-reaction enthalpy ΔH_R [P-VI].

Hardness, relative mass loss and post-curing enthalpy show a sigmoidal depth dependency, Fig. 43. The length of the plateaus depends on irradiance and exposure

time representing the fully cured region of the sample. Then, the values of the properties change due to insufficient cure as more light is absorbed, and less radical initiation. Increasing irradiances and exposure times compensate for the low initiation rate of radicals shifting the curves to deeper depths.
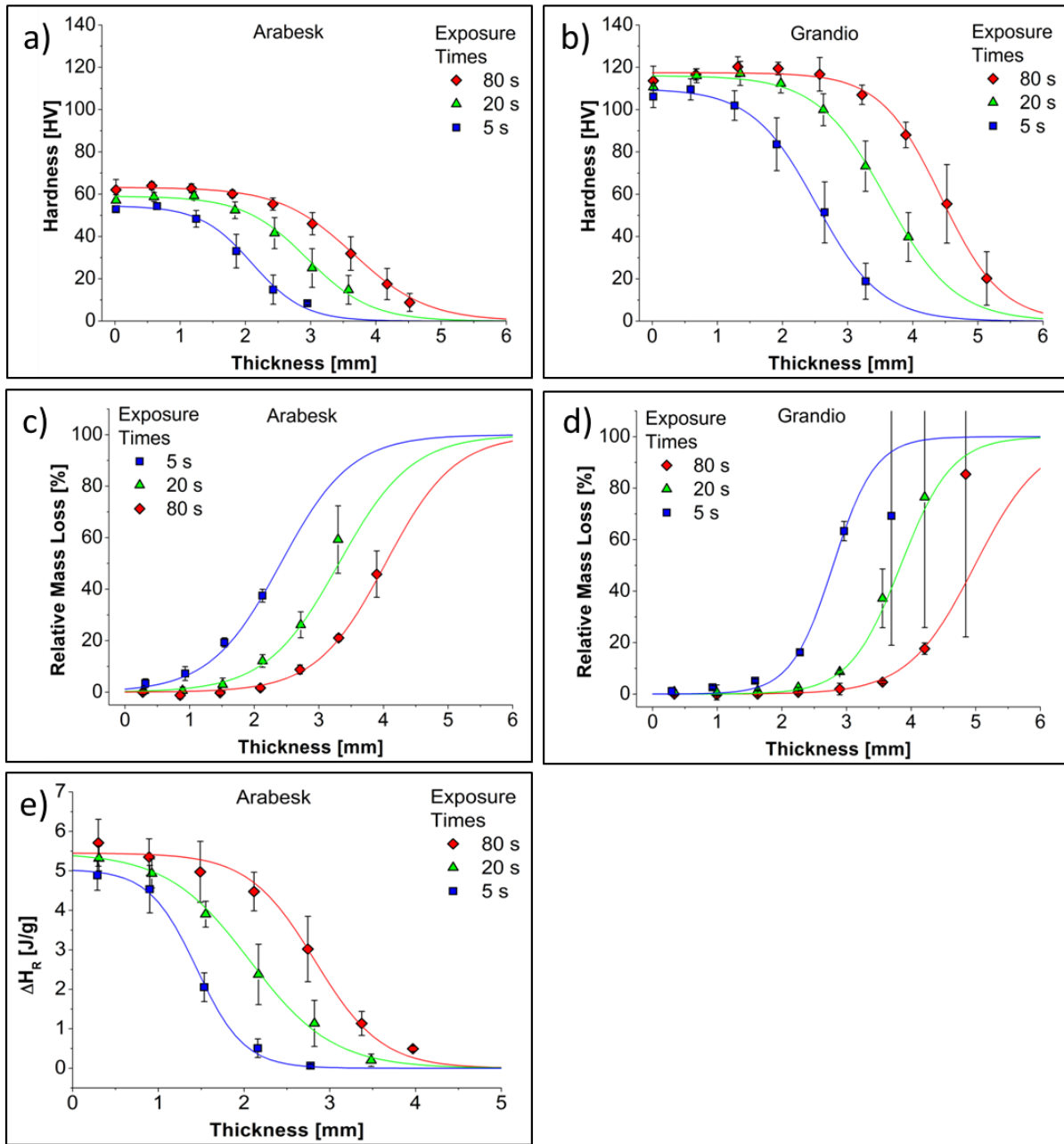
Fig. 43 Depth dependent hardness, mass loss and post reaction enthalpy of Arabesk and Grandio irradiated with Bluphase 20i Turbo

Due to the sigmoidal shape of the curves a hyperbola tangent is used to fit the depth dependent data (lines in Fig. 43). For the hardness data it is given by

$$HV(x) = \frac{HV^{Plateau}}{2} \cdot \left\{1 + tanh\left[-a_1\left(x - x_{0,1}\right)\right]\right\} \qquad (45)$$

with HV hardness
        x depth

a_1 slope at inflection point
$x_{0,1}$ depth of inflection point

The advantage of this fit function is that it takes into account all measured data (thus being user independent). Furthermore, it leads to a new definition of the "depth of cure (*DoC*) given by the relationship:

$$DoC_{HV} = x_{0,1} - \frac{1}{a_1} \qquad (46)$$

Graphically it is the depth at which the plateau value intercepts the slope at the inflection point, Fig. 44.
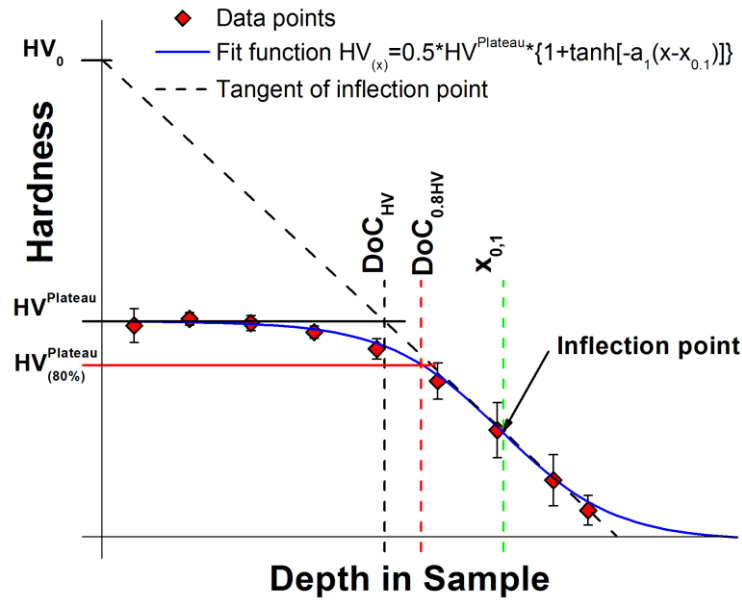
Fig. 44 Scheme of the evaluation of the depth dependent hardness measurements using the fit function with the fit parameter HV^{Plateau}, the slope at inflection point of *tanh* a_1, the depth at inflection point $x_{0,1}$, the slope of tangent of inflection point $a_{1(HV)}$, intercept of tangent of inflection point with hardness axis HV$_0$, the depth at the intercept of HV^{Plateau} and the tangent of the inflection point $DoC_{(tanh)}$, the hardness of 80 % of HV^{Plateau} HV$^{Plateau}_{(80\%)}$), and the depth at 80 % of HV^{Plateau} $DoC_{0.8HV}$.

Established methods e.g. ISO 4049 scratch test or 80 % of plateau hardness (see chapter 1.2.5) are single point methods and overestimate *DoC* compared to Eq. (46). The introduction of DoC_{HV} to Eq. (45) shows that the hardness dropped to 88 % compared to the plateau value. The correlation of DoC_{HV} and radiant exposure RE reveals a logarithmic dependency, Fig. 45.

$$DoC_{HV}(RE) = A * \ln RE + B \qquad (47)$$

with the parameters A and B describing materials properties of VLC RBC. The reduction of light intensity with depth due to Beer-Lambert-absorption law leads to the consequence that *DoC* is limited because no light will come to depth exceeding 5 times the penetration depth and the energy introduction cannot be increased at will. The evaluation also shows that a minimum radiant exposure of around 0.5 J is needed to overcome effects caused by inhibition.
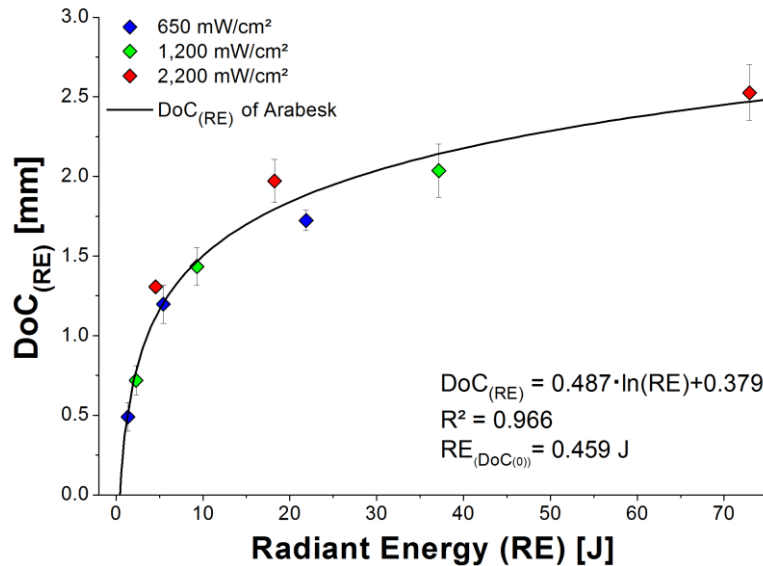
Fig. 45 *DoC* **of Arabesk depending on radiant energy compared to a logarithmic fit**

3.3.2 Effects of irradiance distribution on the mechanical surface properties [P-V]

The following section describes the influences of irradiance distribution and exposure time on the hardness distribution on the sample surfaces.

Due to their design, LCU produce different patterns of irradiance distribution, Fig. 32. This leads to locally different degrees of cure, and thus different mechanical properties reflected in the hardness distributions of the samples, Fig. 46.

The increase of the exposure time leads to an increase in the hardness values. Therefore, one may expect that an increase of the exposure time should also increase the hardness and compensate for irradiance distributions of LCU in the long term. However, areas exposed with low irradiances are always found to have lower hardness values compared to areas exposed with high irradiances, irrespective of exposure time. A homogenization does not take place meaning that an imprinted irradiation pattern is conserved it the glass transition temperature exceeds ambient temperature.

The formation of a crosslinked polymer network during photo-polymerization is a fast process. The reaction rate reaches the maximum after few seconds, Fig. 47, and the structure of the crosslinked polymer network is frozen, inhibiting compensation processes because of the inhibited mobility in the glassy state. Therefore, it can be concluded that the "total energy concept" is only applicable for bulk, and not for local properties.
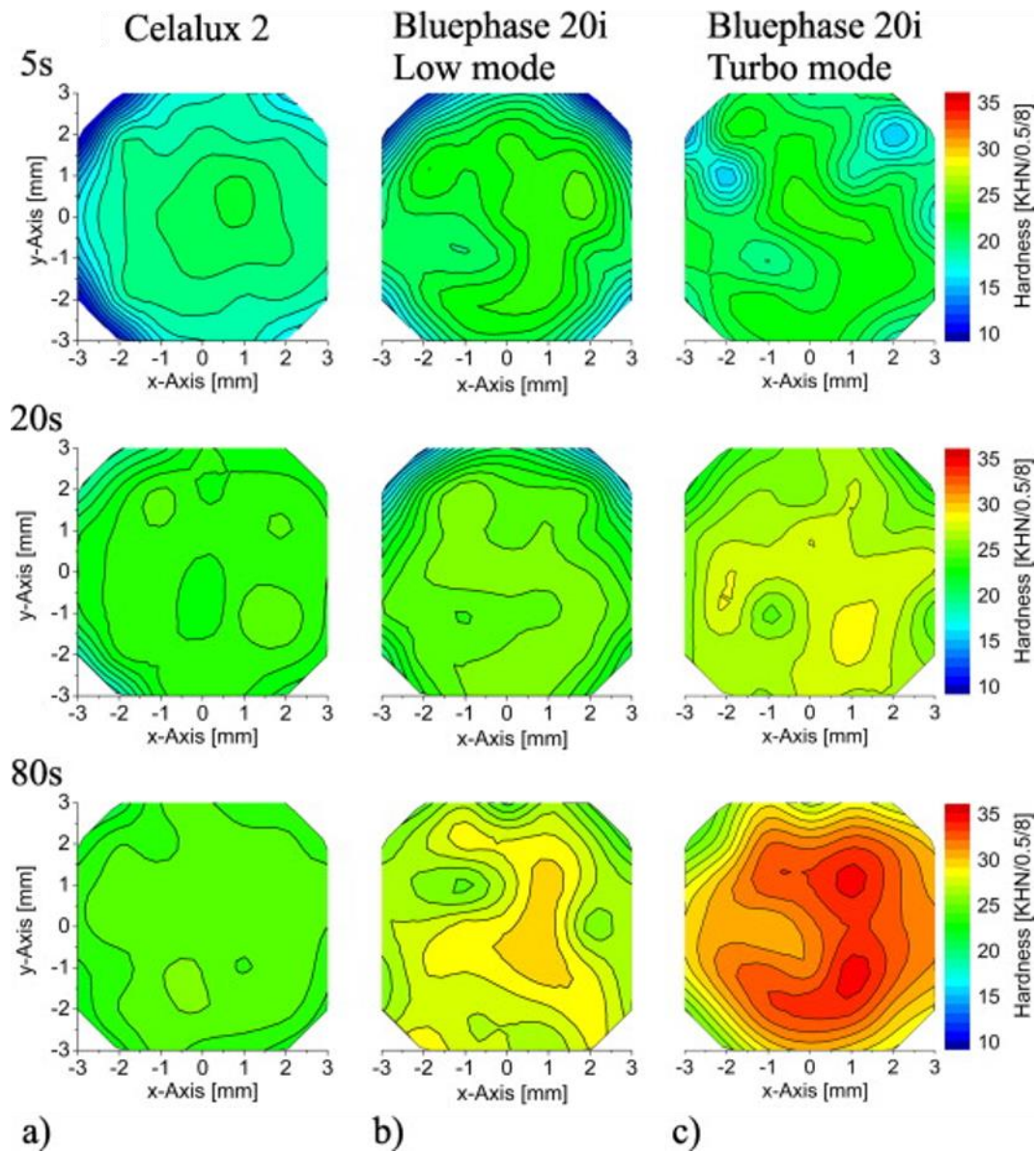
Fig. 46 Surface hardness distributions of Arabesk specimens after 5, 20 and 80 s exposure time using the Celalux® 2 (a), Low mode (b) and Turbo mode (c).
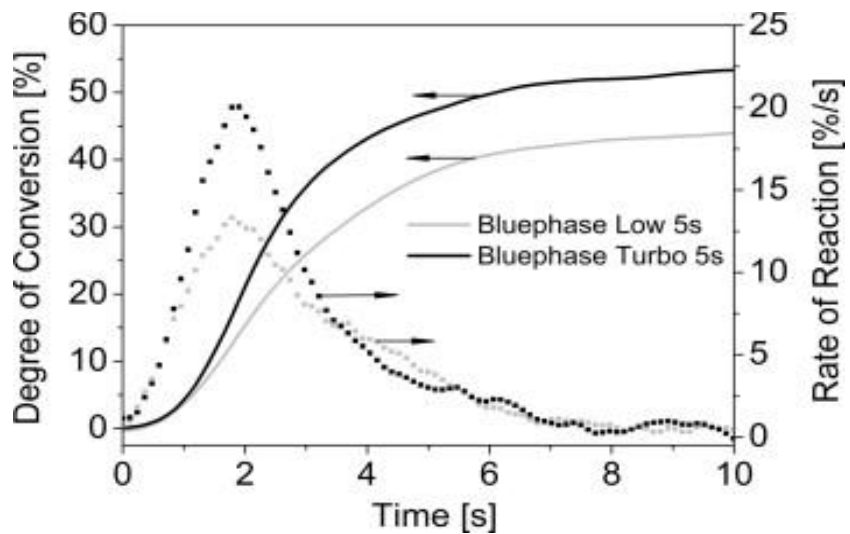
Fig. 47 Degree of conversion (*DC*) and conversion rate of Arabesk cured with Bluephase® 20i in Low and Turbo mode for 5 s

Usually, dentists are not aware of the inhomogeneity of irradiance distribution of their LCU. This leads to the risk that dental restorations are cured with too low irradiances leading to insufficient *DoC*. Therefore, it should be taken in account that the individual irradiance distribution of an LCU must be determined to achieve proper curing results by selecting correct exposure times and irradiance levels.

3.3.3 Development of a dynamic mechanical indentation method to determine local viscoelastic depth and surface properties of VLC RBCs
[not published yet]

Dynamic mechanical analysis (DMA) provides information about the viscoelastic properties with respect to effects of time, temperature and frequency. A commercial DMA requires relatively large samples, and therefore determines global bulk properties. This can be overcome if a DMA is modified to a dynamic mechanical micro-indenter allowing for determining viscoelastic properties locally.

To modify the DMA two measures were necessary:

1. Indenter holders for a high lateral resolution (a tungsten needle) and for lower lateral resolutions (Vickers, Berkovich and Rockwell indenters) were adapted to the DMA, Fig. 48.

2. A XY-movable stage was integrated to account for accurate positioning of the sample underneath the indenter.
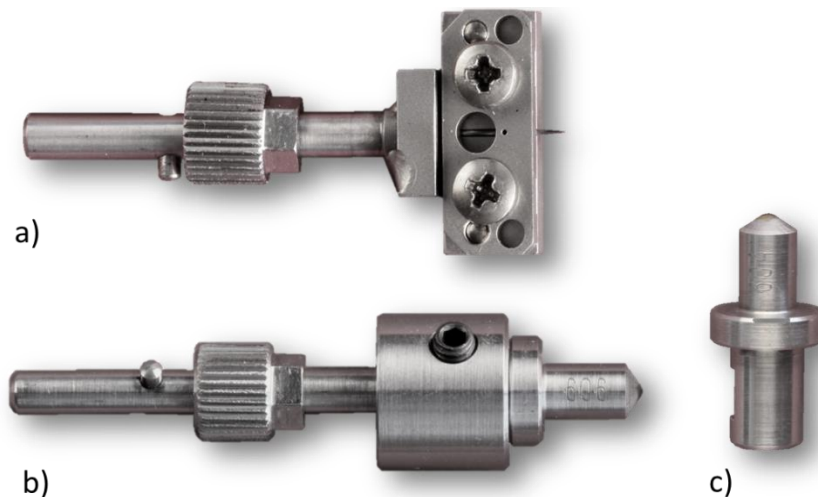
Fig. 48 Indenter holders for the DMA; a) tungsten needle indenter, b), diamond indenters with standardized geometry and c) indenter head

The complex modulus E^* is determined by the concept of Oliver & Pharr (see chapter 1.4.3).

$$S = \frac{dF}{dh} = \frac{2}{\sqrt{\pi}} E^* \cdot \sqrt{A} \tag{48}$$

with   *S*   sample stiffness
           F   load
           h   indentation amplitude of indenter into sample
           A   contact area of indenter

In the DMA indentation experiments a sinusoidal force *F(t)* generates a periodic indentation amplitude *h(t)* as a response signal. The measurements have shown that the indentation amplitudes of the diamond indenters looked rather sinusoidal, while the needle indenter has a pronounced non-sinusoidal shape, Fig. 49. This means that data generated by the diamond indenters can be directly introduced in Eq. (48), whereas the data generated by the needle indenter required a more sophisticated treatment using Fourier analysis.
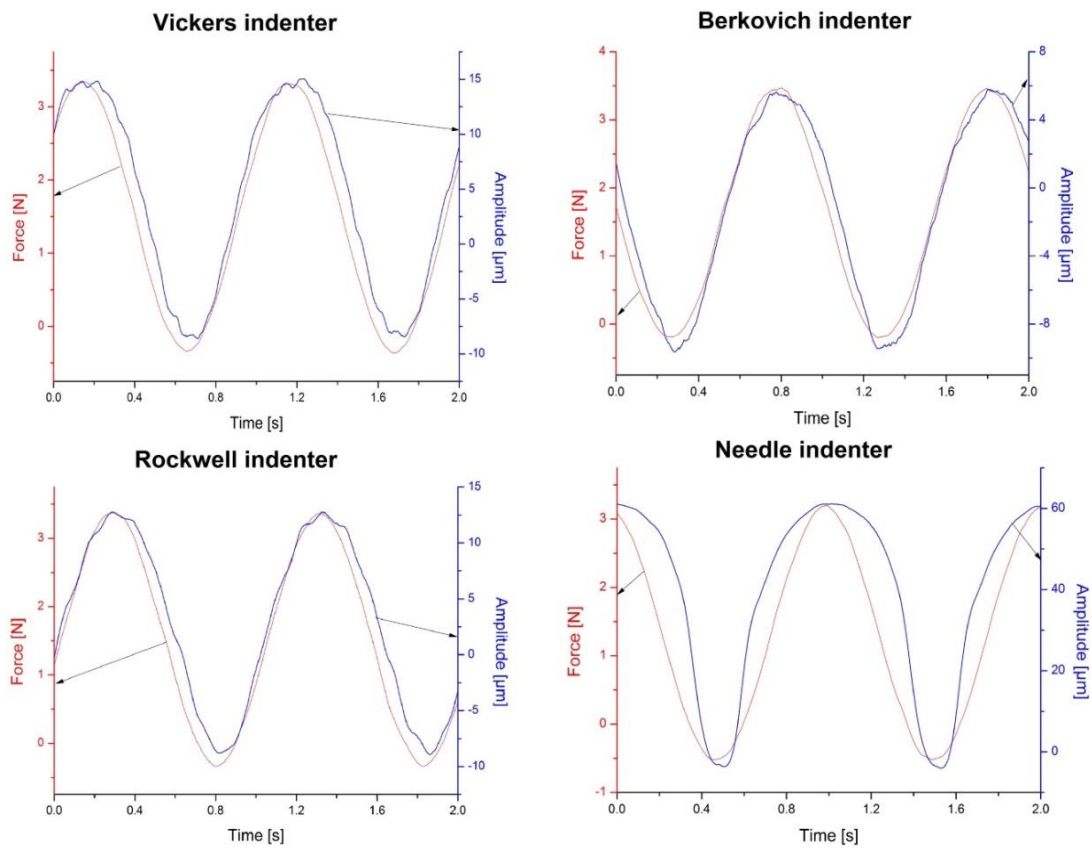
Fig. 49 Force and indentation amplitudes during DMA indentation

The complex moduli determined by DMA indentation measurements show a similar change of depth depending properties as Vickers hardness measurements, Fig. 50.
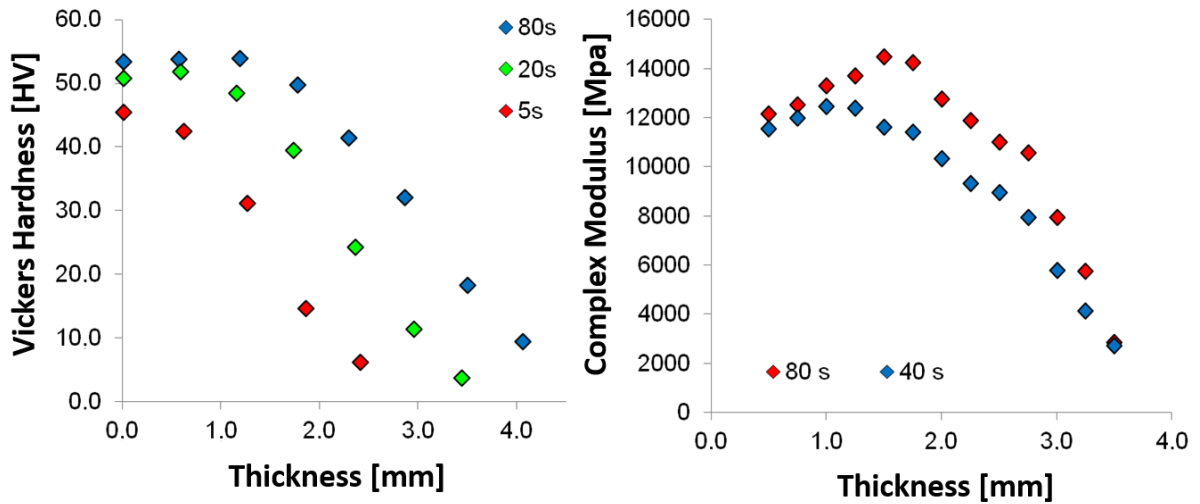
Fig. 50: hardness profile of Arabesk sample irradiated with Bluephase 20i Turbo (left); profile of complex modulus of Arabesk determined using DMA indentation

The distribution of complex moduli is comparable to results generated by hardness mapping, Fig. 51. This verifies DMA indentation as an appropriate method to determine the local viscoelastic properties. Furthermore, as the modulus of cross-linked polymers is related to the cross-link density it may provide the chance to determine cross-link density quantitatively.
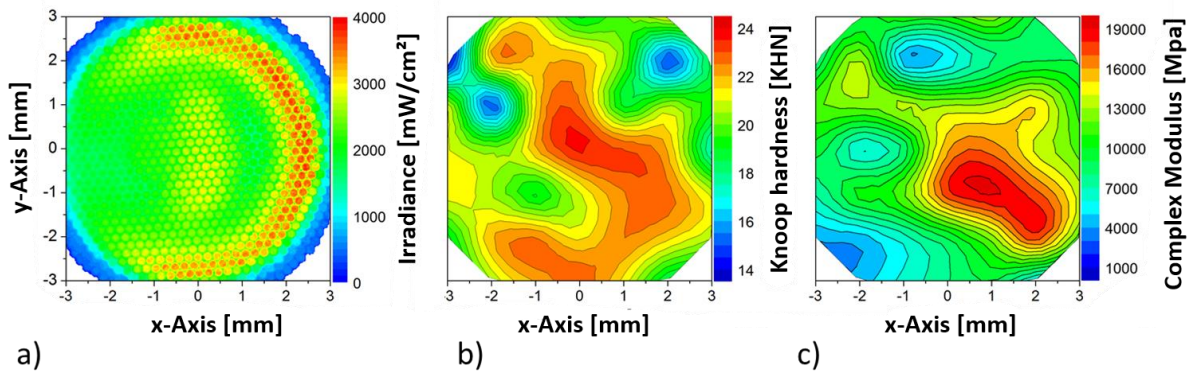
Fig. 51 Determination of the influence of the irradiance distribution (a) on hardness distribution (b) and distribution of complex module determined by DMA indentation, sample: Arabesk irradiated with Bluephase 20i Turbo for 80 s

3.4 Effects on the post-curing on hardness evolution of VLC RBCs

3.4.1 Surface hardness prediction by using a master curve post-curing concept [P-VI]

During post-curing chemical and physical properties change because of a diffusion controlled polymerization in the glassy state without any introduction of light due to trapped radicals [75]. In the reaction kinetics section, it was shown that the change from primary curing in the liquid state to post-curing in the glassy state happens after a few seconds. However, as post-curing takes place over long times it

can contribute remarkably to the final *DC*, Table 13, and further increase the mechanical properties.

During primary curing, VLC RBCs are cured to a certain degree of conversion depending on the irradiance levels of LCUs and exposure times. Therefore, hardness of the top and the bottom surfaces of the samples were measured for times of 10 minutes to one week after irradiation, Fig. 52. The top surface produced for all irradiances higher hardness values than the bottom surface. The interpretation of this result is that the kinetics of post-curing processes is determined by the conditions under which the liquid resin was transferred to the glassy state. At the bottom surface in a depth of 1 mm the light intensity is approximately half that of the top surface. If one assumes, according to the total energy concept, that radical concentration is proportional to irradiance, the cured Arabesk resin has roughly the double cross-linking density at the top surface compared to bottom surface. Both surfaces are in a glassy state, however, the molecular mobility at the bottom surface is a little bit higher due to the less cross-linked network. At first sight this should lead to a higher rate of post-curing. However, the rate of radical annihilation is also increased, especially if further irradiation generates new radicals via initiation reactions. The decrease of radical concentration subsequently decreases the rate of post-curing. Thus, "high" rates of post-curing can be expected only if the cured resin consists of a highly cross-linked network in which the radicals are bound to immobile chain ends and hardly subjected to termination reactions.
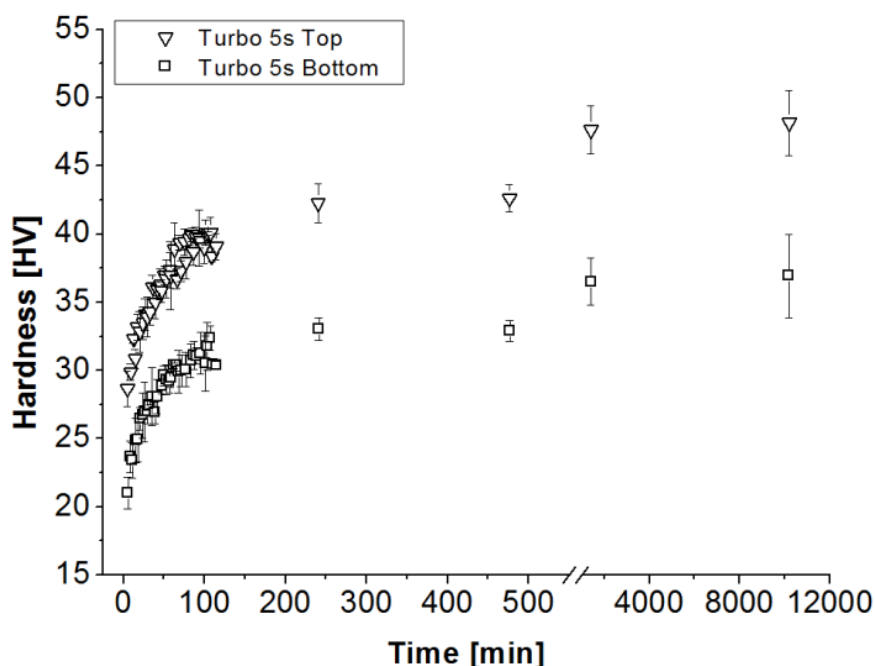
Fig. 52 Evolution of hardness for one week; Arabesk irradiated with Bluephase 20i Turbo for 5 s

Longer exposure times shift the hardness curves to higher values. The increasing hardness values seem to have a logarithmic time dependency. If the hardness values are plotted versus logarithm of time, the hardness values lay on straight lines, which clearly distinguish between top and bottom surfaces, Fig. 53.

The slopes of the hardness increase on the logarithmic time scale seem to be similar for the different irradiation times. This suggests the presence of a superposition principle for the post-curing process – short term hardness values of long irradiation times correspond to long term hardness values of short irradiation times – allowing for constructing a master curve using the function:

$$HV\left(\lg(a_{t_{irrad}} * t)\right) = a * \lg(a_{t_{irrad}} * t) + b = a * \left(\lg t + \lg a_{t_{irrad}}\right) + b \qquad (49)$$

with Vickers hardness HV, shift factor, slope a and intercept b.

Fig. 54 shows that the hardness values of different irradiation times can be shifted nicely to the master curves if shifted with the shift factors given in Table 3a and b of [P-VI]. The self-similarity implies that the kinetics of post-curing is determined by a single variable of the type $f(I_{LCU}, t_{irrad})$.
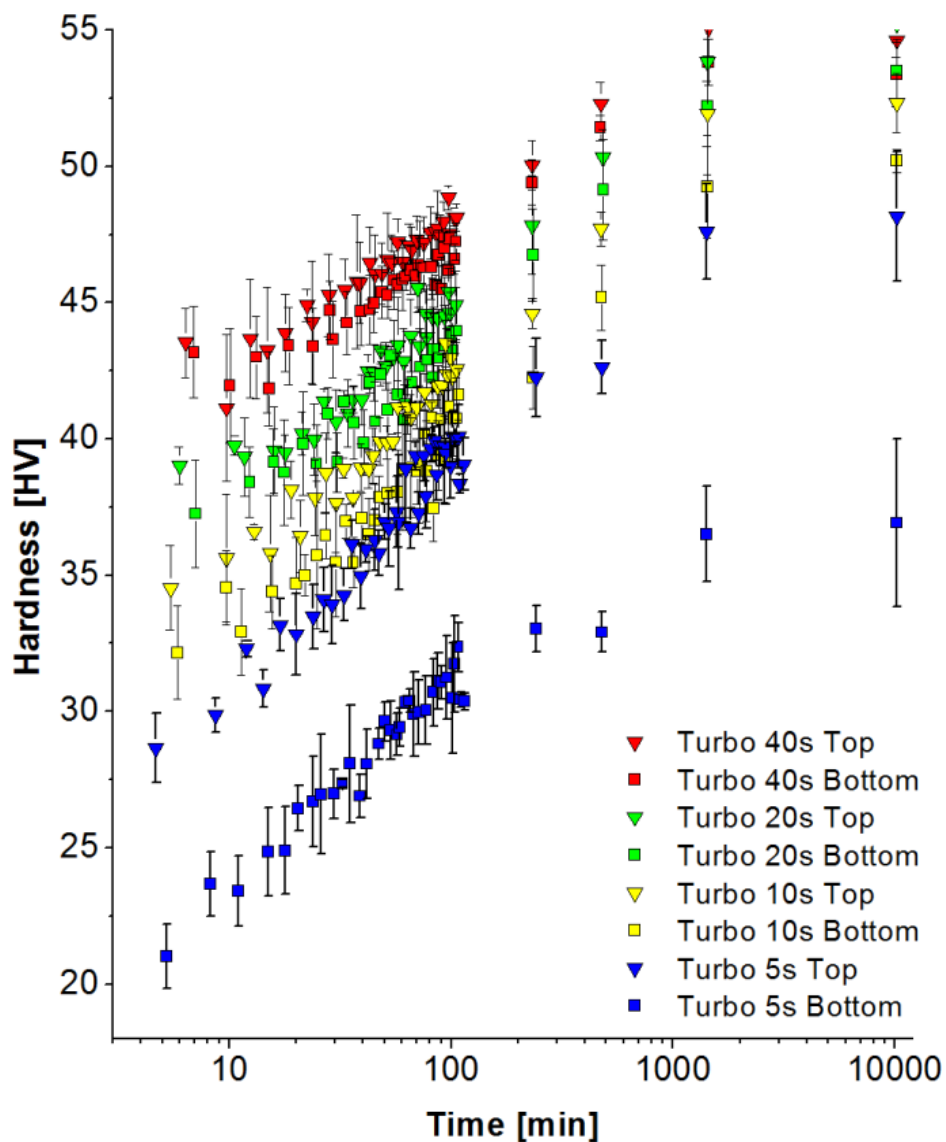
Fig. 53 Time dependent hardness values of top and bottom surface; curing conditions: 5, 10, 20 and 40 s with Bluephase 20i Turbo)
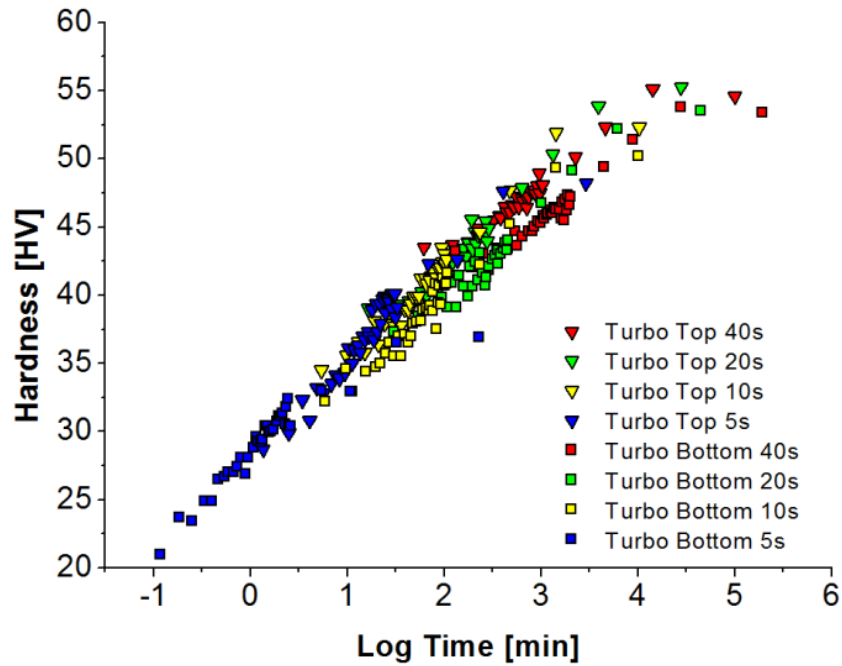
Fig. 54 Construction of master curves of top and bottom surface hardness values using the data of Fig. 53; reference data set with irradiation time of 10 s

If the master curves are fitted linearly it is found that the slopes of the hardness of the top surface are slightly larger than those of the bottom surface, Figure 6. The construction of master curves requires the definition of reference measurements which are given by hardness curves irradiated for 20 s (Polofil Lux and Celalux) and 10 s (Bluephase 20i Turbo) as these irradiation conditions correspond to radiant exposures of approximately 20 J/cm².

$$HV_{(t)Top} = 29.8 + 6.12*log\,t$$

$$HV_{(t)Bottom} = 28.4 + 5.65*log\,t$$
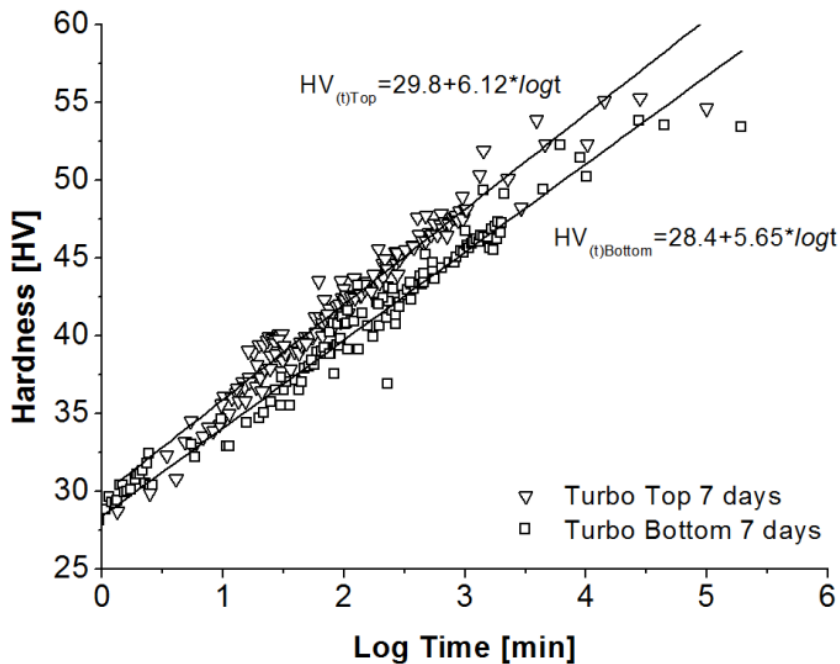
Fig. 55 Master curves of top and bottom surface hardness values with fit curves

Thus, the master curve construction is the base for predicting the post-curing state in terms of hardness, and indirectly the state of cross-linking. For Arabesk the hardness increase is predicted to be around 6 HV per decade of time. This means that the hardness would increase from 55 to 73 HV in 20 years.

4 CONCLUSIONS

In this PhD thesis the effect of the curing conditions - irradiance, exposure time and irradiance distribution of light curing units (LCUs) - on reaction kinetics as well as mechanical properties were investigated.

LCUs differ with respect to irradiance, spectrum and irradiance distribution. As this fact is not known to most dentists, their handling of LCU for curing purposes is rather arbitrary with the consequence of insufficiently cured restorations. Therefore, a simple, user-friendly method using iPad or SLR cameras was developed allowing for determining intensity distributions of LCUs.

The effects of irradiance and exposure time on reaction kinetics were investigated by FTIR-ATR to get real time degree of conversion (DC) data. In order to evaluate these DC data a novel DC-function was developed by the introduction of a time dependent reaction constant taking into account the slow-down of curing reactions due to the increase of both resin viscosity and its glass transition temperature. The novel DC-function produces intrinsically final DC-values less than 100 % and it shows that the curing kinetics is determined mainly by one quantity – the reaction time constant τ_{reac}^0 – which is a function of irradiance. Furthermore, it was shown that the reaction rates – for which the reaction time constant τ_{reac}^0 is a measure – change with the square root of the irradiance. This clearly means that the "total energy concept" fails for the considered range of irradiance. To which extent the other parameters of the novel *DC*-function – growing time constant and strength - depend on τ_{reac}^0 has to be investigated in a future. As the *DC* is around 45 % after a time corresponding to the reaction time constant τ_{reac}^0 , it might be considered as the time, in which the resin is transferred to the glassy state and post-curing starts.

As one focus of this PhD-thesis laid on the kinetics of post-curing both DC data over 160 s corresponding to 15 to 30 times τ_{reac}^0 and hardness increase over 7 days was measured. The *DC* data showed that the "total energy concept" also failed here in the high irradiance range. The evaluation of both data sets revealed that the kinetics of post-curing can be well described by a logarithmic time dependency. Surprisingly samples cured with different irradiation times produced hardness curves during post-curing allowing for constructing master curves. It was clearly shown for the investigated composites that the post-curing kinetics differs with depth. Furthermore, the master curves can be used to predict the hardness change for really long times.

With increasing irradiances and exposure times more VLC RBC is cured. The thickness of the cured layer is measured by a quantity called depth of cure (*DoC*). Although its meaning is intuitively clear, its determination is heuristic. Therefore, a new method to determine *DoC* was proposed by measuring depth dependent changes of properties (e.g. hardness, mass loss in solvent or post-reaction enthalpy) and fitting the data with a hyperbola tangent. It turned out that the *DoC* can be

simply determined as the intercept of the plateau value close to the surface with the slope of the tangent at the inflection point. The evaluation procedure also showed that the considered property has decreased to 88 % of its initial value.

Hardness mapping of sample surfaces showed that patterns of the irradiance distribution of the LCU are reflected in the hardness distribution of the surfaces. Longer irradiation times increased the hardness values in the surface but did not surprisingly level out the patterns. This means that the pattern of hardness (and corresponding DC) frozen in the moment the resin transfers to the glassy state will be maintained irrespective of further irradiation.

A new indentation method based on a commercial Dynamic Mechanical Analyser (DMA) was developed to determine local viscoelastic properties of the VLC RBC. First results showed that the measured stiffness maps correspond qualitatively to their hardness maps.

5 CONTRIBUTION TO SCIENCE AND PRACTICE

Final properties such as hardness, modulus or chemical resistance of visible light curing resin based composites depend on the curing conditions. The resulting properties are important due to their influence on the resistance of dental restorations over the lifetime. Therefore, the understanding of the influences on the curing process during irradiation as well as post-curing is important to identify the right curing strategy.

In this PhD-thesis curing behavior is connected to the resulting composites properties by reaction kinetics, degree of conversion (DC) measurements, investigations of depth depending properties and post-curing behavior. Thus, the following points are considered as relevant contributions to science and practice:

1) The investigation of reaction kinetics of commercial dental composites showed for the first time that the curing rate depends on the square root of light curing unit (LCU) irradiance and that the "total energy concept" fails for such high irradiances. The reaction kinetics is mainly governed by the reaction time constant .

2) A novel DC-function was developed which intrinsically produces final DC-values less than 100 % and better coincidence with measured data. It also indicates that separation of primary curing and post-curing should be possible.

3) Samples irradiated with different exposure times produced hardness curves during post-curing; their master curves can be constructed allowing for long term predictions of hardness evolution.

4) For high irradiances with short curing times the "total energy concept" also fails, showing that it can only be used for LCU operated with low irradiances. Thus, if dentists use high irradiance LCUs the rule "double irradiance - halve exposure time" does not apply any longer.

5) A new method to determine the depth of cure (DoC) is suggested.

6) A dynamic mechanical indentation technique was implemented on a commercial DMA machine allowing for determining viscoelastic properties locally. Furthermore, deeper insight becomes possible as these properties can be determined as a function of temperature and frequency.

ACKNOWLEDGEMENT

First of all, I would like to say thank to my supervisor Berenika Hausnerova for her help, support and her open and friendly manner. She always stood by my side and her advices help me also in slightly difficult situations. Thank you very much!

Secondly, I would like to thank my consultant and boss in Germany, Bernhard Möginger. He gave me the chance to still in the science after my master degree. He has always supported me, but also challenged and brought me to my limits. Sometimes, I lost the target, but he, like a good captain, brought me back on course. I learned a lot and for this experience, I would like to say tanks you!

Furthermore, a big thanks go to my colloquies in Germany at the Bonn-Rhein-Sieg University. A special thank go to research group with Esther van Dorp, Lara Kehret und Johannes Steinhaus. Without you, there would be no fun. Thank you very much! A special thanks go also to my colloquies Klaus Schmitz, Christina Meckelburger, Tatjana Radowitz, Astrit Beninde, Lukas Pschyklenk und Johannes Wilms and all the other in our department.

A Special thanks go to Richard Price from the Dalhousie University Halifax, Canada. My research visit was a great experience. The work with you was an enhancement in my life. Thank you very much!

Then, I would like to say thank to the support team and all members of the Tomas Bata University. Especially to LadaVojáčková, Michaela Blahová and Vladimir Pavlínek. It was a great time as a PhD student on the TBU and it was wonderful to see the growing up of the TBU over the last six years. I hope I will comeback often to visit Zlín.

Additionally, I would like to thank Andreé Barg and the VOCO GmbH for providing the dental materials and light curing units. My next thank go to the Netzsch Gerätebau GmbH and especially to Georg Storch and Tobias Pflock for their great support and help in all questions about DMA.

A special thanks go to the Ministry of Education and Research of the Federal Republic of Germany for the financial support in the Projekt FhProfUnt „Denthart" (grant no. 17081X10).

I want to say thanks to my parents for their great support in the last years. Also I would like to say thank to all my family, friends and contacts which I cannot listed here.

Last but not least, I would like to say thank you to my girlfriend, Annika. She was always by my side. I love you!

REFERENCES

[1] Ferracane, J L. Resin composite--state of the art. Dent Mater, 2011; 27:29–38.

[2] Schmidt, F. Kuenstliche Gebisse Artificial Dentures, 1932.

[3] Bauer, W. Kunststoff, 1939.

[4] Bayne, S C. Beginnings of the dental composite revolution. J Am Dent Assoc, 2013; 144:880–884.

[5] Söderholm, K-J M. Dental adhesives … how it all started and later evolved. J Adhes Dent, 2007; 9 Suppl 2:227–230.

[6] Eliades, G, Watts, D C and Eliades., T. Dental Hard Tissues and Bonding. Interfacial Phenomena and Related Properties. Berlin, 2005.

[7] Schmidseder, J, Munz, T and Allen, E P. Ästhetische Zahnmedizin. 49 Tabellen. Stuttgart, 2009.

[8] Bowen, R L. Dental filling material comprising vinyl silane treated fused silica and a binder consisting of the reaction product of bis phenol and glycidyl acrylate, 1962.

[9] Bowen, R L. Properties of a silica-reinforced polymer for dental restorations. J Am Dent Assoc, 1963; 66:57–64.

[10] Steinberg, I V. Epoxy adhesive containing acrylic acid-epoxy reaction products and photosensitizers, 1969.

[11] Lienhard, O. Instrument for transmitting ultraviolet radiation to a limited area, 1973.

[12] Waller, D. Photopolymerizable dental products, 1973.

[13] Dentsply. Esthet X micro matrix restorative. Technical Manual, 2000.

[14] Stansbury, J W. Curing Dental Resins and Composites by Photopolymerization. J Esthet Restor Dent, 2000; 12:300–308.

[15] Peterson, R W, Bostrom, R G, Coakley, J M and Ellingson, O L. Measurments of the radiation emissions from the NUVA-Lite(R) dental appliance. Rockville, 1975.

[16] Ham, W T, Mueller, H A and Sliney, D H. Retinal sensitivity to damage from short wavelength light. Nature, 1976; 260:153–155.

[17] Mills, L F, Lytle, C D, Andersen, F A, Hellman, K B and Bockstahler, L E. Review of biological effects and potential risks associated with ultraviolet radiation as used in dentistry.

[18] Rueggeberg, F A. State-of-the-art: dental photocuring--a review. Dent Mater, 2011; 27:39–52.

[19] Moysan, A, Marquis, I, Gaboriau, F, Santus, R, Dubertret, L and Morliere, P. Ultraviolet A - Induced Lipid Peroxidation and Antioxidant Defense Systems in Cultured Human Skin Fibroblasts. J Invest Dermatol, 1993; 100:692–698.

[20] Allen, R J and Chaberek, S. Labile hydrogen initiators for visible light photopolymerization, 1970.

[21] Ferracane, J L. Current Trends in Dental Composites. Crit Rev Oral Biol Med, 1995; 6:302–318.

[22] Beun, S, Glorieux, T, Devaux, J, Vreven, J and Leloup, G. Characterization of nanofilled compared to universal and microfilled composites. Dent Mater, 2007; 23:51–59.

[23] Sideridou, I D, Karabela, M M and Vouvoudi, E C. Physical properties of current dental nanohybrid and nanofill light-cured resin composites. Dent Mater, 2011; 27:598–607.

[24] Ivoclar Vivadent AG. Tetric EvoCeram Bulk Fill Instruction for use. Schaan,Lichtenstein, 2013.

[25] Voco GmbH. x-tra base instruction for use. Cuxhaven, Germany, 2013.

[26] Dentsply. SDR Smart Dentin Replacement instruction for use. Konstanz, Germany, 2014.

[27] Alrahlah, A, Silikas, N and Watts, D C. Post-cure depth of cure of bulk fill dental resin-composites. Dent Mater, 2014; 30:149–154.

[28] Peutzfeldt, A. Resin composites in dentistry: the monomer systems. Eur J Oral Sci, 1997; 105:97–116.

[29] Moszner, N and Salz, U. New developments of polymeric dental composites. Prog Polym Sci, 2001; 26:535–576.

[30] Braga, R R, Ballester, R Y and Ferracane, J L. Factors involved in the development of polymerization shrinkage stress in resin-composites: a systematic review. Dent Mater, 2005; 21:962–970.

[31] Cramer, N B, Stansbury, J W and Bowman, C N. Recent advances and developments in composite dental restorative materials. J Dent Res, 2011; 90:402–416.

[32] Stein, P S, Sullivan, J, Haubenreich, J E and Osborne, P B. Composite Resin in Medicine and Dentistry. J Long Term Eff Med Implants, 2005; 15:641–654.

[33] Heymann, H O, Swift, Jr., Edward J and Ritter, A V. Sturdevant's Art & Science of Operative Dentistry. London, 2014.

[34] Wikipedia. Greene Vardiman Black - Wikipedia, the free encyclopedia. https://en.wikipedia.org/w/index.php?oldid=680540747, 9/14/2015.

[35] Kaweckyi, N, Frye, W, Hilling, L and Schmitt, L. The Business of Dentistry. Patient Records and Record Management. http://www.dentalcare.com/media/en-US/education/ce390/ce390.pdf.

[36] Anusavice, K J, Shen, C and Rawls, H R. Phillips' Science of dental materials. Philadelphia, 2012.

[37] Chae, K H and Sun, G J. Phenylpropanedione; a new visible light photosensitizer for dental composite resin with higher efficiency than camphorquinone. Bull Korean Chem Soc, 1998; 19:152–154.

[38] Watts, D C. Reaction kinetics and mechanics in photo-polymerised networks. Dent Mater, 2005; 21:27–35.

[39] Bennett, A W and Watts, D C. Performance of two blue light-emitting-diode dental light curing units with distance and irradiation-time. Dent Mater, 2004; 20:72–79.

[40] Yaman, B C, Efes, B G, Dörter, C, Gömeç, Y, Erdilek, D and Büyükgökçesu, S. The effects of halogen and light-emitting diode light curing on the depth of cure and surface microhardness of composite resins. J Conserv Dent, 2011; 14:136–139.

[41] Labrie, D, Moe, J, Price, R B T, Young, M E and Felix, C M. Evaluation of ocular hazards from 4 types of curing lights. J Can Dent Assoc, 2011; 77:b116.

[42] Vandewalle, K S, Roberts, H W, Andrus, J L and Dunn, W J. Effect of light dispersion of LED curing lights on resin composite polymerization. J Esthet Restor Dent, 2005; 17:244-54; discussion 254-5.

[43] Arikawa, H, Kanie, T, Fujii, K, Takahashi, H and Ban, S. Effect of inhomogeneity of light from light curing units on the surface hardness of composite resin. Dent Mater J, 2008; 27:21–28.

[44] Price, R B T, Fahey, J and Felix, C M. Knoop microhardness mapping used to compare the efficacy of LED, QTH and PAC curing lights. Oper Dent, 2010; 35:58–68.

[45] Stansbury, J W. Dimethacrylate network formation and polymer property evolution as determined by the selection of monomers and curing conditions. Dent Mater, 2012; 28:13–22.

[46] Steinhaus, J. Real-time Investigation of Curing Mechanisms of Thermoset Resins for Medical and Technical Applications. Dissertation. Dissertation. Zlin, 2015.

[47] Lendenmann, U, Roulet, J-F, Moszner, N, Vogel, K, Burtscher, P, Heintze, S and Peschke, A. R&D Report Nr.18
. The Secrets of Composites. Schaan, Lichtenstein, 2007.

[48] Wolter, H, Storch, W and Ott, H. New Inorganic/Organic Copolymers (Ormocer®s) for Dental Applications. Mater Res Soc Symp Proc, 1994; 346.

[49] Hartmann. Admira: A filling system based on ormocer. A filling system based on ormocer. Cuxhaven, Germany, 2003.

[50] Neumann, M G, Miranda, W G, Schmitt, C C, Rueggeberg, F A and Correa, I C. Molar extinction coefficients and the photon absorption efficiency of dental photoinitiators and light curing units. J Dent, 2005; 33:525–532.

[51] Klapdohr, S and Moszner, N. New Inorganic Components for Dental Filling Composites. Monatsh Chem, 2005; 136:21–45.

[52] Pereira, S G, Osorio, R, Toledano, M and Nunes, T G. Evaluation of two Bis-GMA analogues as potential monomer diluents to improve the mechanical properties of light-cured composite resins. Dent Mater, 2005; 21:823–830.

[53] Gonçalves, F, Kawano, Y, Pfeifer, C, Stansbury, J W and Braga, R R. Influence of BisGMA, TEGDMA, and BisEMA contents on viscosity, conversion, and flexural strength of experimental resins and composites. Eur J Oral Sci, 2009; 117:442–446.

[54] Odell, P and Goredema, A. Inks for ink jet printing curable by UV light initiated free radicals. Xerox Corporation, 2006.

[55] Esstech Inc. Dental Photoinitiators. http://www.esstechinc.com/blog/dental-photoinitiators/, 1/21/2016.

[56] van Noort, R. Introduction to dental materials. Edinburgh, 2009.

[57] Lambrechts, P and Vanherle, G. Structural evidences of the microfilled composites. J Biomed Mater Res, 1983; 17:249–260.

[58] Lutz, F and Phillips, R W. A classification and evaluation of composite resin systems. J Prosthet Dent, 1983; 50:480–488.

[59] Sideridou, I D, Karabela, M M and Spyroudi, C S. Dynamic mechanical analysis of a hybrid and a nanohybrid light-cured dental resin composite. J Biomater Sci Polym Ed, 2009; 20:1797–1808.

[60] Bayne, S C. Dental biomaterials: where are we and where are we going? J Dent Educ, 2005; 69:571–585.

[61] Bayne, S C, Heymann, H O and Swift, Jr., Edward J. Update on dental composite restorations. J Am Dent Assoc, 1994; 125:687–701.

[62] Scheibe, K, Almeida, K, Medeiros, I S, Costa, J F and Alves, Cláudia Maria Coêlho. Effect of different polishing systems on the surface roughness of microhybrid composites. J Appl Oral Sci, 2009; 17:21–26.

[63] Khurshid, Z, Zafar, M, Qasim, S, Shahab, S, Naseem, M and AbuReqaiba, A. Advances in Nanotechnology for Restorative Dentistry. Materials, 2015; 8:717–731.

[64] Green, G E, Stark, B P and Zahir, S A. Photocross-Linkable Resin Systems. J Macromol Sci Polym Rev, 1981; 21:187–273.

[65] Odian, G. Principles of Polymerization (Fourth Edition). Hoboken, 2004.

[66] Marchi Netto, A, Steinhaus, J, Hausnerova, B, Moeginger, B and Blümich, B. Time-Resolved Study of the Photo-Curing Process of Dental Resins with the NMR-MOUSE. Appl Magn Reson, 2013; 44:1027–1039.

[67] Elias, H-G. Chemische Struktur und Synthesen. Weinheim, 2009.

[68] Jakubiak, J, Allonas, X, Fouassier, J P, Sionkowska, A, Andrzejewska, E, Linden, L and Rabek, J F. Camphorquinone–amines photoinitating systems for the initiation of free radical polymerization. Polymer, 2003; 44:5219–5226.

[69] Andrzejewska, E. Photopolymerization kinetics of multifunctional monomers. Prog Polym Sci, 2001; 26:605–665.

[70] Stansbury, J W and Dickens, S. Determination of double bond conversion in dental resins by near infrared spectroscopy. Dent Mater, 2001; 17:71–79.

[71] Trujillo, M, Newman, S M and Stansbury, J W. Use of near-IR to monitor the influence of external heating on dental composite photopolymerization. Dent Mater, 2004; 20:766–777.

[72] Calheiros, F C, Daronch, M, Rueggeberg, F A and Braga, R R. Influence of irradiant energy on degree of conversion, polymerization rate and shrinkage stress in an experimental resin composite system. Dent Mater, 2008; 24:1164–1168.

[73] Santos, G B, Medeiros, I S, Fellows, C E, Muench, A and Braga, R R. Composite depth of cure obtained with QTH and LED units assessed by microhardness and micro-Raman spectroscopy. Oper Dent, 2007; 32:79–83.

[74] Breschi, L, Cadenaro, M, Antoniolli, F, Sauro, S, Biasotto, M, Prati, C, Tay, F R and Di Lenarda, R. Polymerization kinetics of dental adhesives cured with LED: correlation between extent of conversion and permeability. Dent Mater, 2007; 23:1066–1072.

[75] Leprince, J G, Leveque, P, Nysten, B, Gallez, B, Devaux, J and Leloup, G. New insight into the "depth of cure" of dimethacrylate-based dental composites. Dent Mater, 2012; 28:512–520.

[76] Steinhaus, J, Moeginger, B, Grossgarten, M, Rosentritt, M and Hausnerova, B. Dielectric analysis of depth dependent curing behavior of dental resin composites. Dent Mater, 2014; 30:679–687.

[77] Moore, B K, Platt, J A, Borges, G, Chu, T-M G and Katsilieri, I. Depth of cure of dental resin composites: ISO 4049 depth and microhardness of types of materials and shades. Oper Dent, 2008; 33:408–412.

[78] Flury, S, Hayoz, S, Peutzfeldt, A, Hüsler, J and Lussi, A. Depth of cure of resin composites: Is the ISO 4049 method suitable for bulk fill materials? Dent Mater, 2012; 28:521–528.

[79] Erickson, R L, Barkmeier, W W and Halvorson, R H. Curing characteristics of a composite - part 1: cure depth relationship to conversion, hardness and radiant exposure. Dent Mater, 2014; 30:e125-33.

[80] Cammann, K (Ed.). Instrumentelle analytische Chemie. Verfahren, Anwendungen und Qualitätssicherung. Heidelberg, 2001.

[81] IR Spectrum. https://www.chemie.uni-kl.de/fachrichtungen/oc/kubik/img/oc3_ir_4.gif.

[82] Oréfice, R, Discacciati, J, Neves, A, Mansur, H and Jansen, W. In situ evaluation of the polymerization kinetics and corresponding evolution of the mechanical properties of dental composites. Polym Test, 2003; 22:77–81.

[83] Wendl, B, Droschl, H and Kern, W. A comparative study of polymerization lamps to determine the degree of cure of composites using infrared spectroscopy. Eur J Orthod, 2004; 26:545–551.

[84] PerkinElmer. FTIR Spectroscopy: Attenuated Total Reflectance (ATR). Shelton.

[85] Sideridou, I, Tserki, V and Papanastasiou, G. Effect of chemical structure on degree of conversion in light-cured dimethacrylate-based dental resins. Biomaterials, 2002; 23:1819–1829.

[86] Larkin, P. Infrared and Raman spectroscopy: Principles and spectral interpretation. Amsterdam, 2011.

[87] Bumbrah, G S and Sharma, R M. Raman spectroscopy – Basic principle, instrumentation and selected applications for the characterization of drugs of abuse. Egyptian J For Sci, 2015.

[88] Pianelli, C, Devaux, J, Bebelman, S and Leloup, G. The micro-Raman spectroscopy, a useful tool to determine the degree of conversion of light-activated composite resins. J Biomed Mater Res, 1999; 48:675–681.

[89] Shin, W, LI, X, Schwartz, B, Wunder, S and Baran, G. Determination of the degree of cure of dental resins using Raman and FT-Raman spectroscopy. Dent Mater, 1993; 9:317–324.

[90] Xu, J, Butler, I S, Gibson, D and Stangel, I. High-pressure infrared and FT-Raman investigation of a dental composite. Biomaterials, 1997; 18:1653–1657.

[91] Chase, D B. Fourier transform Raman spectroscopy. J Am Chem Soc, 1986; 108:7485–7488.

[92] Ehrenstein, G W, Riedel, G and Trawiel, P. Thermal analysis of plastics. Theory and practice. Munich, 2004.

[93] Steinhaus, J, Hausnerova, B, Moeginger, B, Harrach, M, Guenther, D and Moegele, F. Characterization of the auto-curing behavior of rapid prototyping materials for three-dimensional printing using dielectric analysis. Polym Eng Sci, 2015; 55:1485–1493.

[94] Maffezzoli, A, Pietra, A, Rengo, S, Nicolais, L and Valletta, G. Photopolymerization of dental composite matrices. Biomaterials, 1994; 15:1221–1228.

[95] Schneider, L F J, Pfeifer, C S C, Consani, S, Prahl, S A and Ferracane, J L. Influence of photoinitiator type on the rate of polymerization, degree of conversion, hardness and yellowing of dental resin composites. Dent Mater, 2008; 24:1169–1177.

[96] Tanimoto, Y, Hayakawa, T and Nemoto, K. Analysis of photopolymerization behavior of UDMA/TEGDMA resin mixture and its composite by differential scanning calorimetry. J Biomed Mater Res Part B Appl Biomater, 2005; 72:310–315.

[97] Emami, N and Soderholm, K-J M. How light irradiance and curing time affect monomer conversion in light-cured resin composites. Eur J Oral Sci, 2003; 111:536–542.

[98] Wu, W and Fanconi, B M. Post-curing of dental restorative resin. Polym Eng Sci, 1983; 23:704–707.

[99] Rosentritt, M, Shortall, A C and Palin, W M. Dynamic monitoring of curing photoactive resins: a methods comparison. Dent Mater, 2010; 26:565–570.

[100] McIlhagger, A, Brown, D and Hill, B. The development of a dielectric system for the on-line cure monitoring of the resin transfer moulding process. Compos Part A Appl Sci Manuf, 2000; 31:1373–1381.

[101] Steinhaus, J, Hausnerova, B, Haenel, T, Großgarten, M and Moeginger, B. Curing kinetics of visible light curing dental resin composites investigated by dielectric analysis (DEA). Dent Mater, 2014; 30:372–380.

[102] Dielectric Cure Monitoring. Method, Technique, applications. Selb, 2015.

[103] Steinhaus, J, Moeginger, B, Großgarten, M and Hausnerova, B. Evaluation of dielectric curing monitoring investigating light-curing dental filling composites. Materials Engineering, 2011:30–35.

[104] Ferracane, J L. Correlation between hardness and degree of conversion during the setting reaction of unfilled dental restorative resins. Dent Mater, 1985; 1:11–14.

[105] Price, R B T, Labrie, D, Rueggeberg, F A, Sullivan, B, Kostylev, I and Fahey, J. Correlation between the beam profile from a curing light and the microhardness of four resins. Dent Mater, 2014; 30:1345–1357.

[106] DIN EN ISO 14577-1 Metallic materials - Instrumented indentation test for hardness and materials parameters - Part 1: Test method (ISO/DIS 14577-1:2012); German version prEN ISO 14577-1:2012. Berlin, 2012; 77.040.10.

[107] Fischer-Cripps, A C. Nanoindentation. New York, NY, 2002.

[108] Grellmann, W and Seidler, S. Polymer Testing. s.l., 2012.

[109] Oliver, W C and Pharr, G M. An improved technique for determining hardness and elastic modulus using load and displacement sensing indentation experiments. J Mater Res, 1992; 7:1564–1583.

[110] Binnig, G, Quate and Gerber. Atomic force microscope. Phys Rev Lett, 1986; 56:930–933.

[111] Salerno, M, Patra, N and Diaspro, A. Atomic force microscopy nanoindentation of a dental restorative midifill composite. Dent Mater, 2012; 28:197–203.

[112] Jandt, K D. Atomic force microscopy of biomaterials surfaces and interfaces. Surf Sci, 2001; 491:303–332.

[113] Bhushan, B and Koinkar, V N. Nanoindentation hardness measurements using atomic force microscopy. Appl. Phys. Lett., 1994; 64:1653.

[114] Marshall, G W, Marshall, S J, Kinney, J H and Balooch, M. The dentin substrate Structure and properties related to bonding. J Dent, 1997; 25:441–458.

[115] Institut für Physik. AFM (Atomic Force Microscope). Principles. http://www.physik.uni-greifswald.de/scientific-groups/helm/methods/afm-atomic-force-microscope.html?L=1, 2/4/2016.

[116] Nanovea. Mechanical Tester.

[117] Keysight Nano Indenter G200. USA, 2014.

[118] NanoForce Nanomechanical Testing System. Enabling Nwe Discoveroes in Nanomechanics, 2015.

[119] Willems, G, Celis, J P, Lambrechts, P, Braem, M and Vanherle, G. Hardness and Young's modulus determined by nanoindentation technique of filler particles of dental restorative materials compared with human enamel. J Biomed Mater Res, 1993; 27:747–755.

[120] Drummond, J L. Nanoindentation of Dental Composites. J Biomed Mater Res Part B Appl Biomater, 2006; 78:27–34.

[121] Lin-Gibson, S, Sung, L, Forster, A M, Hu, H, Cheng, Y and Lin, N J. Effects of filler type and content on mechanical properties of photopolymerizable composites measured across two-dimensional combinatorial arrays. Acta Biomater, 2009; 5:2084–2094.

[122] Mohamad, D, Young, R J, Mann, A B and Watts, D C. Post-polymerization of dental resin composite evaluated with nanoindentation and micro- Raman spectroscopy. Arch Orofac Sci, 2007; 2:26–31.

[123] Willems, G, Lambrechts, P, Braem, M, Celis, J P and Vanherle, G. A classification of dental composites according to their morphological and mechanical characteristics. Dent Mater, 1992; 8:310–319.

[124] Ho, E and Marcolongo, M. Effect of coupling agents on the local mechanical properties of bioactive dental composites by the nano-indentation technique. Dent Mater, 2005; 21:656–664.

[125] Naderi, M, Saeed-Akbari, A and Bleck, W. Quantitative and qualitative investigation of the heterogeneous microstructures using surface hardness mapping and dilatation data. Mater Lett, 2008; 62:1132–1135.

[126] Ferry, J D. Viscoelastic properties of polymers. New York, 1980.

[127] Dynamic Mechancial Analysis Method, technique, Applications. DMA 242 E. Selb.

[128] Ramorino, G, Vetturi, D, Cambiaghi, D, Pegoretti, A and Ricco, T. Developments in dynamic testing of rubber compounds. Assessment of non-linear effects. Polym Test, 2003; 22:681–687.

[129] Frank, A, Pinter, G and Lang, R W. Prediction of the remaining lifetime of polyethylene pipes after up to 30 years in use. Polym Test, 2009; 28:737–745.

[130] Introduction to polymers. www.open.edu/openlearn/science-maths-technology/science/chemistry/introduction-polymers/content-section-5.3.1, 2/13/2016.

[131] Jian, Y, He, Y, Zhao, L, Yang, W and Nie, J. Dynamic mechanical analysis of elastic modulus development of dental composites. Polym Compos, 2013; 34:580–586.

[132] Emami, N and Söderholm, K-J M. Dynamic mechanical thermal analysis of two light-cured dental composites. Dent Mater, 2005; 21:977–983.

[133] Vidal Mesquita, R. Dynamic mechanical analysis of dental composite resins. Dissertation. Dissertation. Tübingen, 2006.

[134] Ferracane, J L and Greener, E H. The effect of resin formulation on the degree of conversion and mechanical properties of dental restorative resins. J Biomed Mater Res, 1986; 20:121–131.

[135] Lovell, L G, Lu, H, Elliott, J E, Stansbury, J W and Bowman, C N. The effect of cure rate on the mechanical properties of dental resins. Dent Mater, 2001; 17:504–511.

[136] Steinhaus, J, Frentzen, M, Rosentritt, M and Moeginger, B. Dielectric Analysis of Short-Term and Long-Term Curing of Novel Photo-Curing Dental Filling Materials. Macromol Symp, 2010; 296:622–625.

[137] Herrmann, V. Charakterisierung von Elastomeren mittels dynamischer Indentation und vergleichender Methoden. Dissertation. Dissertation. Aachen, 2002.

[138] D'Alpino, P H P, Svizero, N R, Pereira, J C, Rueggeberg, F A, Carvalho, R M and Pashley, D H. Influence of light-curing sources on polymerization reaction kinetics of a restorative system. American journal of dentistry, 2007; 20:46–52.

[139] Jandt, K D and Mills, R W. A brief history of LED photopolymerization. Dent Mater, 2013; 29:605–617.

[140] Aravamudhan, K, Rakowski, D and Fan, P L. Variation of depth of cure and intensity with distance using LED curing lights. Dental materials : official publication of the Academy of Dental Materials, 2006; 22:988–994.

[141] Price, R B T, Labrie, D, Rueggeberg, F A and Felix, C M. Irradiance differences in the violet (405 nm) and blue (460 nm) spectral ranges among dental light-curing units. Journal of esthetic and restorative dentistry : official publication of the American Academy of Esthetic Dentistry … [et al.], 2010; 22:363–377.

[142] Nomoto, R. Effect of light wavelength on polymerization of light-cured resins. Dental materials journal, 1997; 16:60–73.

[143] Price, R B T, Rueggeberg, F A, Labrie, D and Felix, C M. Irradiance uniformity and distribution from dental light curing units. Journal of esthetic and restorative dentistry : official publication of the American Academy of Esthetic Dentistry … [et al.], 2010; 22:86–101.

[144] Peutzfeldt, A and Asmussen, E. Resin Composite Properties and Energy Density of Light Cure. Journal of Dental Research, 2005; 84:659–662.

[145] Leprince, J G, Hadis, M, Shortall, A C, Ferracane, J L, Devaux, J, Leloup, G and Palin, W M. Photoinitiator type and applicability of exposure reciprocity law in filled and unfilled photoactive resins. Dental materials : official publication of the Academy of Dental Materials, 2011; 27:157–164.

[146] Selig, D, Haenel, T, Hausnerova, B, Moeginger, B, Labrie, D, Sullivan, B and Price, R B T. Examining exposure reciprocity in a resin based composite using high irradiance levels and real-time degree of conversion values. Dental materials : official publication of the Academy of Dental Materials, 2015; 31:583–593.

ABBREVIATIONS

AFM	Atomic force microscopy
ATR	Attenuated total reflection
BisEMA	Ethoxylated bisphenol-A dimethacrylate
BisGMA	Bisphenol A glycidyl methacrylate
CQ	Camphorquinone
DABE	Ethyl 4-aminobenzoate
DC	Degree of conversion
DEA	Dielectric analysis
DMA	Dynamic mechanical analysis
DoC	Depth of cure
DSC	Differential scanning calorimetry
Eq.	Equation
FTIR	Fourier transformation infrared spectroscopy
HK	Knoop hardness
HM	Martens hardness
HV	Vickers harndess
LCU	Light Curing Unit
LED	Light emitted diode
MMA	Methyl methacrylate
PAC	Plasma arc
PMMA	Polymethylmethacrylate
PPD	1-Phenyl-1,2-propandedione
PPF	Pre-polmerized fillers
PS	Polystyrene
QTH	Quartz-tungsten halogen
RBC	Resin based composite
RBC	Resin based composite
SEM	Scanning electron microscope
TEGDMA	Triethylene glycol dimethacrylate
TPO	Monoacylphosphine oxid
UDMA	Urethane dimethacrylate
UV	Ultra violet
VLC	Visible light curing
VLC RBC	Visible light curing resin based composites

SYMBOLS

A	Imprint area (indentation)
$Abs_{aliphatic}$	Absorbance of aliphatic C=C-bonds
$Abs_{aromatic}$	Absorbance of aromatic C=C-bonds
c	Concentration
c_p	Heat capacity
d	Diagonal
DC	Degree of conversion
$DC(t,x)$	Time and depth dependent DC
$DC_{DEA}(t)$	Time dependent DC determined by Dielectric analysis
$DC_{DSC}(t)$	Time dependent DC determined by Differential scanning calorimetry
$DC_{IR}(t)$	Time dependent DC determined by infrared spectroscopy
E	Elastic modulus
E_t	Elastic modulus of indenter
E_s	Elastic modulus of sample
$E(\omega, T)$	Frequency and temperature dependent complex modulus
E'	Storage modulus
E''	Loss modulus
F	Force
ΔH	Reaction enthalpy
ΔH_{calc}	Calculated reaction enthalpy
ΔH_{obs}	Observed reaction enthalpy
HK	Knoop hardness
HM	Martens hardness
HV	Vickers hardness
h_{max}	Maximal indentation displacement
I_a	Absorbed light intensity
$I(x)$	Transmitted light at a certain thickness
I_0	Incident light intensity
k_i	Initial rate constant
k_P	Propagation rate constant
k_t	Termination rate constant
P	Load (indentation)

$\dot{Q}(t)$	Heat flow	
$\Delta Qcuring$	Curing heat	
R	Rate of propagation	
R_{tc}	Rate of combination	
R_{td}	Rate of disproportionation	
R_{pol}	Rate of polymerization (rate of reaction)	
R_i	Rate of initiation	
S_0	Ground state	
S_n	Exited state	
t	Time	
t_{irr}	Irradiation time (VLC RBC kinetics)	
T_g	Glass transition temperature	
T_m	Melting temperature	
T_R	Post-reaction temperature	
ΔV_P	Volume contraction	
x	Thickness/depth	

GREEK SYMBOLS

α	Tip angle of indenter
δ	Phase angle
$tan\ \delta$	Loss factor
ε_0	Strain amplitude
ε_λ	Wavelength dependent extinction coefficient
$\varepsilon(\omega,t)$	Time and frequency dependent strain (dynamic mechanical analysis)
η_0^{ion}	Initial ion viscosity
η_{min}^{ion}	Minimum ion viscosity
η_∞^{ion}	Final ion viscosity
$\eta^{ion}(t)$	Time dependent ion viscosity
λ	Wavelength
v_s	Poisson's ratio of sample
v_t	Poisson's ratio of indenter
σ_0	Stress amplitude
$\sigma(t,\omega)$	Time and frequency dependent stress
ϕ	Quantum yield
ω	Angular frequency

CHEMICAL SYMBOLS

$C=C$	Carbon-carbon double bonds
I	Initiator molecules
$[I]$	Concentration of initiator
M	Monomer
$M_n\bullet$	Monomer radical
$[M]$	Concentration of monomers
$M0$	Initial Monomer concentration
$R\bullet$	Radical
$[R\bullet]$	Concentration of radicals
$R_1, R_2...$	Organic groups

PUBLICATIONS, POSTERS AND PRESENTATIONS

Publications in the context of this doctoral work:

– Qualitative beam profiling of light-curing units for resin based composites. T. Haenel, B. Hausnerová, J. Steinhaus, B. Moeginger. Eur J Prosthodont Rest Dent, 2016, accepted.

– Initial Reaction Kinetics of two Resin Based Dental Composites. T. Haenel, B. Hausnerová, J. Steinhaus, R. Price, B. Moeginger. Submitted to Dent Mater, July 2016.

– Examining exposure reciprocity in a resin based composite using high irradiance levels and real-time degree of conversion values. D. Selig, T. Haenel, B. Hausnerová, B. Moeginger, D. Labrie, B. Sullivan, R. Price. Dent Mater, 2015, vol. 31, 583-593.

– Determining depth of cure (DoC) of VLC RBC intrinsically using a new evaluation procedure to profiles of depth dependent hardness, mass loss after solvent extraction and post-reaction enthalpy. T. Haenel, B. Hausnerová, M. Dopadlo, J. Steinhaus, B. Moeginger. Submitted to Dent Mater, July 2016.

– Effect of the irradiance distribution from light curing units on the local microhardness of the surface of dental resins. T. Haenel, B. Hausnerová, J. Steinhaus, R.B.T. Price, B. Sullivan, B. Moeginger. Dent Mater 2015, vol. 31, 93-104.

– Investigation of the Post-curing Behavior and Kinetics of a Dental Composite. T. Haenel, B. Hausnerová, L. Kehret, J. Steinhaus, B. Moeginger. Submitted to Dent Mater, July 2016.

Other Publications in English language:

– Correlation of shear and dielectric ion viscosity of dental resins – Influence of composition, temperature and filler content. J. Steinhaus, B. Hausnerová, T. Haenel, D. Selig, F. Duvenbeck, B. Moeginger. Dent Mater, 2016; 32(7): 899-907.

– Effect of a Broad-Spectrum LED Curing Light on the Knoop Microhardness of Four Posterior Resin Based Composites at 2, 4 and 6-mm Depths. M. Alshaafi, T. Haenel, B. Sullivan, D. Labrie, M. Alqahtani, R.B.T. Price. J Dent, 2016; 45:14-18.

– Curing Kinetics of Visible Light Curing Dental Resin Composites Investigated by Dielectric Analysis (DEA). J. Steinhaus, B. Hausnerová, T. Haenel, M. Großgarten, B. Moeginger. Dent Mater. 2014; 30(3): 837-380.

Conference Presentations:

- A New Evaluation Method to Determine Depth Depending Properties of Visible Light Curing Resin Based Composites. T. Haenel, M. Dopadlo, R.B.T. Price, B. Hausnerová, J. Steinhaus, Esther van Dorp, B. Moeginger. 2015, IADR (International Association for Dental Research), Antalya, Turkey, oral poster presentation

- A New Approach to Model Thermal Expansion of Semi Crystalline Polymers. E. van Dorp, T. Haenel, J. Steinhaus, D. Reith, O. Bruch, B. Hausnerová, B. Moeginger. 2015. PPS 2015

- Modeling curing kinetics and degree of conversion of visible light curing resin based composites (VLC RBC) using a time dependent reaction constant. B. Moeginger, T. Haenel, J. Steinhaus, B. Hausnerová, R.B.T. Price. 2015; European Dental Materials, Nürnberg, Germany, oral poster presentation.

- Effect of composition on the curing behaviour of visible light-curing resins measured with dielectric analysis. J. Steinhaus, D- Selig, T. Haenel, B. Moeginger, B. Hausnerová. 2015. European Dental Materials, Nürnberg, Germany, oral poster presentation.

- Effect of Thickness on the Properties of Bulk Cured Resins. M. Alshaafi, M.Q. Alqahtani, T. Haenel, R.B.T. Price, J. Fahey. 2013; IADR Seattle, poster presentation.

- Real-time observation of the degree of conversion of dental resins having a wide range of CQ-concentrations using ATR-FTIR. T. Haenel, R.B.T. Price, D. Labrie, B. Moeginger, J. Steinhaus, B. Hausnerová. 2012. AODES (Academy of Operative Dentistry), Leuven, Belgium. poster presentation.

- Hardness Mapping of Light-Cured Composites to Identify Inhomogeneous Curing. T. Haenel, B. Hausnerová, L. Kehret, J. Steinhaus, B. Moeginger. IADR 2011, Budapest, Hungary. Publications in the context of this doctoral work:

Academic Apprenticeship

- Lecturer in the bachelor program "Chemistry and material sciences" in the course "Poylmer and compounds"

- Lecturer in the bachelor program "Forensic Science" in the course "Poylmer and compounds"

- Lecturer in the bachelor program "Forensic Science" in the course "Forensic microscopy"

Research visit

− Research visitor on the Dalhousie University, Halifax, Canada, Oct. 2011 to February 2012, Issue: Investigations of the influences of light exposure on the photo-polymerization kinetics and mechanical properties of visible light curing resin based dental composites.

CURRICULUM VITAE

Date and place of birth	February 20th, 1980 in Remscheid, Germany
Permanent Address	von-Liebig-Str. 20
	53359 Rheinbach
	Phone: (+49) 2241 865 766
	E-Mail: thomas.haenel@h-brs.de
Education	
since 09/2010	PhD studies at Tomas Bata University Zlín, Faculty of Technology,
09/2007 – 02/2010	Master studies in "Applied Polymer Science" at FH Aachen, University of Sciences
09/2003 – 07/2007	Bachelor studies in "Chemistry and Material Sciences" at FH Bonn-Rhein-Sieg, University of Applied Sciences
09/1996-01/2000	Vocational education in aircraft mechanics at 15th German Army Aviator Battalion, Rheine, Germany
Work Experience	
since 09/2010	Bonn-Rhein-Sieg University of Applied Sciences, Rheinbach, Germany, Faculty of Natural Sciences, Scientific Assistance research group "Polymer Materials"
02/2008-08/2009	German Aerospace Center, Cologne, Germany, Research Assistance, Institute of Material Physics in Space,
01/2001-07/2002	Express Airways, Troisdorf, Germany, Maintenance Aircraft machinist,
03/2000-12/2000	Military Service at: 15th German Army Aviator Battalion, Rheine, Germany

PAPER I

Authors

Thomas Haenel * ‡
(*PostNominalLetters*)

Berenika Hausnerová § ^
(*PostNominalLetters*)

Johannes Steinhaus § ‡
(*PostNominalLetters*)

Bernhard Moeginger ‡
(*PostNominalLetters*)

Address for Correspondence

Thomas Haenel * ‡

Email: thomas.haenel@fh-brs.de

* Bonn-Rhein-Sieg, University of Applied Sciences, Department of Natural Sciences, Justus-von Liebig Str. 20, 53359 Rheinbach, Germany

§ Centre of Polymer Systems, University Institute, Tomas Bata University in Zlin, Zlin, Czech Republic

‡ Bonn-Rhein-Sieg, University of Applied Sciences, Department of Natural Sciences, Rheinbach, Germany

^ Tomas Bata University in Zlin, Faculty of Technology, Department of Production Engineering, Zlin, Czech Republic

Qualitative Beam Profiling of Light Curing Units for Resin Based Composites

ABSTRACT

This study investigates two technically simple methods to determine the irradiance distribution of light curing units that governs the performance of a visible-light curing resin-based composites. Insufficient light introduction leads to under-cured composites with poor mechanical properties and elution of residual monomers. The unknown irradiance distribution and its effect on the final restoration are the main critical issues requiring highly sophisticated experimental equipment. The study shows that irradiance distributions of LCUs can easily be determined qualitatively with generally available equipment. This significantly helps dentists in practices to be informed about the homogeneity of the curing lights.

INTRODUCTION

UV or visible-light cured (VLC) resin-based composites (RBC) were established in dentistry in the late 1970s.[1, 2] During the last 40 years, the light curing unit (LCU) has changed from quartz-tungsten halogen (QTH) to plasma arc lamps (PAC) and argon ion laser and further to light emitting diodes (LED).[3] The current states of art of LCUs are polywave LED LCUs, known as third generation LCUs. These emit in several wavelength ranges to activate different types of photoinitiators.[4] Nevertheless, the older techniques such as QTH or PAC are still in use.[3]

Typically, two kinds of basic LCUs are used. The first type has a light guide tip which directs the light from the light source to the restoration. These light guide tips are fiber optics of high optical quality. Therefore, the shape of the light source or parts of the internal design is often recognizable on the light guide tip exit (hereinafter called the tip exit). The second type is exclusive to LED LCUs which have LEDs on a rod end with a lens or a window in front of them.

Moseley *et al.*[5] showed in the 1980s that LCUs exhibit an inhomogeneous irradiance distribution across the tip exits. The first studies were performed with photocells or optical fibers connected with a UV-Vis spectrometer which were positioned in front of the tip exits to scan the irradiance distribution.[5, 6] Vandewalle *et al.* [7] used a digital camera known as "laser-beam profiler" to take images indirectly onto a target screen of an entire tip exit in one shot to determine the irradiance distribution.

Several studies showed that the irradiance distribution affects the mechanical properties of RBCs.[6–10] The degree of conversion and the resulting mechanical properties depend on the irradiance delivered to the RBC.[11–15] Areas of VLC RBCs exposed to a high irradiance show higher hardness values than those exposed to lower irradiance.[6,9] Low irradiance leads not only to a lower surface hardness but also to lower depth of cure causing under-cured or uncured layers at the bottom of the restoration.

EJPRD

An issue for dentists is that they do not know to what extent the irradiance output of their LCU is inhomogeneous. In the case of pronounced irradiance inhomogeneity, the curing process depends strongly on the position of the tip exit above the restoration yielding possibly insufficient final material properties.

In the present study two different methods are investigated to qualitatively determine the irradiance distribution from LCUs. The first method was to take images of the irradiance distribution of activated LCUs with a single lens reflex camera (SLR) in "true color". The second method was to image the irradiance distribution with the iPad using the "thermal camera" program in pseudo color. The results were compared to images performed with a laser-beam profiler as the reference method.

MATERIALS AND METHODS

Six different LCUs were tested in this study, Table 1. Five LCUs were equipped with fiber optic light guide tips and one with a window in front of the LED. A laser-beam profiler, a SLR and an iPad were used to determine the irradiance or irradiance distribution of these LCUs. The quantitative light measurement values with integrated sphere and laser-beam profiler are denoted as irradiance while the qualitative light measurements with the SLR and the iPad are denoted as intensity. The experimental equipment is listed in Table 2.

POWER OUTPUT MEASUREMENT AND BEAM PROFILING

The power output of the LCUs was measured to ensure the correct functioning of the LCUs in respect to the manufacturer specifications. The power output of a Celalux 1, Celalux 2 and Bluephase 20i was firstly measured with an integrated sphere (Labs sphere) connected to a UV-Vis spectrometer by integrating the spectra between the wavelengths $l_{min}=350nm$ and $l_{max}=550nm$. Secondly, these three LCUs were measured

with a laser power meter (Thorlabs PM100D) to compare both methods and to ensure that the laser power meter delivers comparable results to the integrated sphere.

The power output of a Polofil Lux, Elipar S10, and Smart-Lite PS were measured only with the laser-power meter after the results of the integrating sphere and laser power meter corresponding was checked. The irradiances were calculated by dividing power output through the effective tip exit area determines by measuring the diameter by a caliper.

The irradiance distributions of Celalux 1, Celalux 2 and Bluephase 20i were determined using the laser-beam profiler as the reference method. The LCUs were placed in contact to a frosted glass shield (DG2X2-1500, Thor Laboratories, Newton, NJ, USA) in front of the laser-beam profiler, Figure 1. A neutral density filter set (ND1/ND2, Ophir optics) was placed between the laser-beam profiler and the optic to prevent overexposure of the laser-beam profiler. The intensity images were represented in arbitrary units and had to be transferred to irradiance in mW/cm² with the calibration factor fcal

$$f_{cal} = \frac{P_{out}}{I_{total} \cdot A_{pixel}} \qquad (1)$$

whereby Pout is the total power output in mW of a LCU, Itotal is the total amount of all arbitrary units of the image, and Apixel is the area of one pixel of the laser-beam profiler.

Then the irradiance per pixel Irpixel is given by:

$$\mathrm{Ir_{pixel}} = f_{cal} \cdot \mathrm{I_{pixel}} \qquad (2)$$

with the intensity of one pixel Ipixel in arbitrary units.

IMAGING OF THE LCUS WITH SLR AND IPAD

As SLR camera was used a Canon EOS 60D with a 18-200mm lens. The SLR images were shot with inactivated and activated LCUs. The LCUs were mounted on a stand with a distance of 80 cm to the SLR and the focal length was 200mm. The aperture of the camera lens was between 13 and 20 and the length of exposure was chosen to prevent overexposure between 1/5000 s and 1/8000 s.

Table 1. Light curing units				
Unit	**Manufacturer**	**Type**	**Irradiance [mW/cm²]**	
			Integrated Sphere	Laser Power Meter
Celalux 1	Voco GmbH, Cuxhaven, Germany	Monowave LED LCU	1172 (6.2)	1107 (30.2)
Celalux 2			1264 (9.5)	1255 (33.7)
Polofil Lux		Quartz Tungsten Halogen	n/a	1156 (2.2)
Bluephase 20i	Ivoclar Vivadent, Schaan, Lichtenstein	Polywave LED LCU	2222 (24.2)	2211 (15.1)
Elipar S10	3M ESPE AG, Seefeld, Germany	Monowave LED LCU	n/a	1117 (2.1)
SmartLite PS	Dentsply DeTrex GmbH, Konstanz, Germany	Monowave LED LCU	n/a	1246 (34.9)

Table 2. Experimental equipment

Canon 60d	Canon, Ota, Tokyo, Japan	SLR Camera (Resolution: 18 Megapixel)
Canon EF 18-200 mm		Zoom lenses, Model EF-S 18-200/1:3,5-5,6 IS
iPad 2	Apple Inc., Cupertino CA, USA	Tablet PC, Model A1396 (GSM) (Resolution front camera: 0.3 Megapixel)
DHG Light Control Filter ND 8	Dörr, Neu-Ulm, Germany	Neutral density filter, Optical Density: 0.9
LabSphere 6"	LabSphere, North Sutton, NH, USA	Integrated Sphere
Ocean Optics USB4000	Ocean Optics, Dunedin, FL, USA	UV-Vis Spectrometer
LBA USB-L070 Beam Profiler	Ophir-Spiricon, Logan, UT, USA	Laser Beam Profiler (Resolution 0.3 Megapixel)
Stackable Filter ND1/ND2		Neutral Density Filter, Light transmission ND1 ~ 10%, ND2 ~ 1%
Thorlabs PM100D	Thorlabs GmbH, Dachau, Germany	Power Meter
Thorlabs S310C		Thermal Sensor
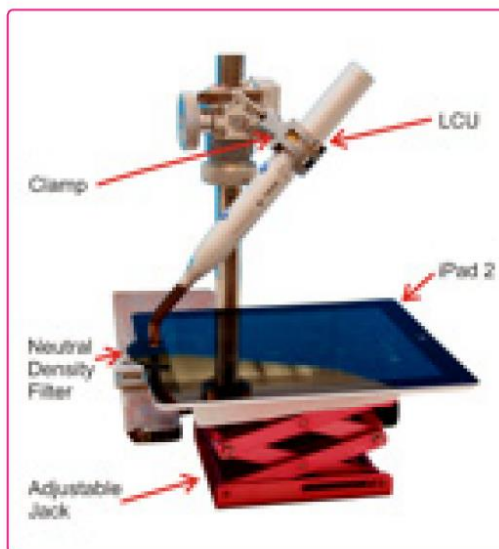
Figure 2: Experimental Setup with an iPad as detector

The iPad images were collected with the "thermal camera" function of the standard installed camera program "photo booth". The iPad was placed on an adjustable jack, Figure 2. Due to the high radiant power from the sources, two neutral density filters (ND 8, Dörr, Neu-Ulm, Germany) were used to prevent overexposure. These filters were placed in front of the camera on an iPad (Apple Inc. Cupertino, CA) to avoid overexposure.

The light guide tip exits were fixed parallel to the iPad surface over the front camera. The LCUs were moved up and down until focused images were shown on the screen. Depending on the LCU the distances between the tip exits and the camera were in a range of 5 to 15cm. The different distances are necessary because of the different focus of the light beam from the LCUs and the autofocus operation of the iPad. The settings of length of exposure and aperture were automatically chosen by the program and are not under the control of the user.

RESULTS

The power outputs and the calculated irradiances of the six tested LCUs correspond to the manufacturer's data, Table 1.[16-20] Both methods, the integrated sphere and the laser power meter delivered similar results, Table 1. The images of the laser-beam profiler, Figure 3, look very similar to the activated tip exit SLR and iPad images for Celalux 1, Celalux 2, and Bluephase 20i, Figure 4 A, B and D which were tested with all three methods. The center spot areas for Celalux 1 and Celalux 2 are clearly seen in each image. Additionally, the laser-beam profiler and iPad images show the higher irradiance area at the 5 o'clock position. The lack of irradiance at the 3 o'clock position and the c-shaped high irradiance area around the center spot of the Bluephase 20i is also shown in each activated image. Furthermore, the SLR image shows a purple spot at the 3 o'clock position, Figure 4 D2.
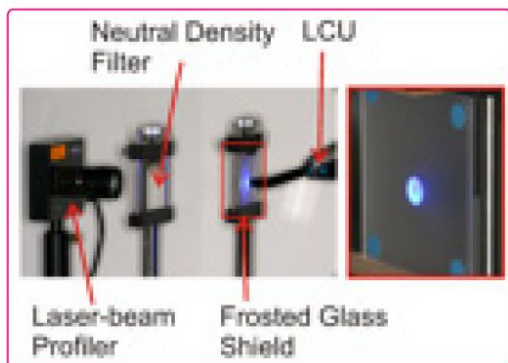
Figure 1: right, experimental setup of the laser-beam profiler with a Bluephase 20i in front of the frosted glass shield; left, shining Bluephase 20i through the frosted glass shield

This spot is caused by the 410nm area of the polywave LED chip of the Bluephase 20i.

The images of the inactivated tip exits of Celalux 1, Celalux 2, and Bluephase 20i do not correspond with the other methods, Figure 4 A1, B1, and D1. However, the Polofil Lux, Elipar S10 and SmartLite PS disabled SLR images correspond with the activated SLR and iPad images.

Imaging of very homogeneous LCUs such as Polofil Lux, Figure 4 C3, is difficult with the iPad as the difference in irradiance between the highest and lowest levels of output is used to create the pseudo color image. On very homogeneous LCUs a small deviations of parallelism between tip exit and camera may pretend an inhomogeneous irradiance distribution. In this case the position of the irradiance distribution is not fixed and is moving with a change of the angle. Additionally, the automatic adjustment generates the same pseudo color image of the intensity distribution which is qualitatively identical, but different with respect to the irradiance level, Figure 5.
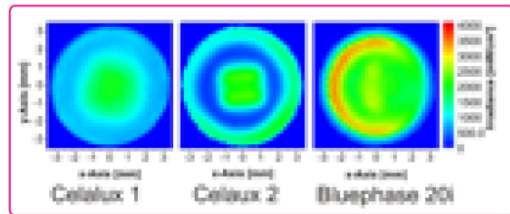
Figure 3: Laser-beam profiler images of Celalux 1, Celalux 2 and Bluephase 20i in Turbo Mode
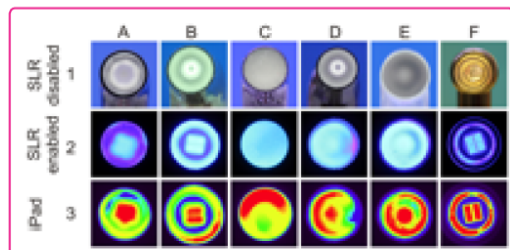
Figure 4: Images of light guide tip exits inactivated and activated with SLR and iPad: A Celalux 1, B Celalux 2, C Polofil Lux, D Bluephase 20i, E Elipar S10, and F Dentsply SmartLite PS
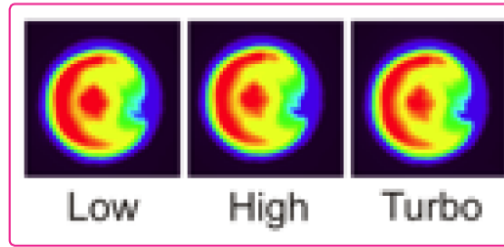
Figure 5: Pseudo color images of Bluephase 20i in Low, High, and Turbo mode made with iPad

DISCUSSION

Each LCU has a characteristic distribution of irradiance which may affect the quality of a restoration.[5–9, 21] The clinician should endeavor to understand the distribution of the irradiance from a LCU. The three different methods laser-beam profiler, SLR and iPad give the user the ability to determine the irradiance and intensity distributions of LCUs.

The laser-beam profiler as the reference method has the highest experimental effort of all methods and is not practicable for a normal clinical practice. Additionally, the laser-beam profiler setup is slightly different from the SLR and iPad setup with the frosted glass shield as target for the LCU light beam. The frosted glass shield is the projection screen and it is necessary to determine the irradiance distribution with increasing distance from the LCU to a surface. A resulting irradiance distribution depending on the distance cannot be displayed without a target. Price *et al* show the influence on the irradiance distribution and output, which show that the top hat factor as measure for the inhomogeneity is not change with increasing distance.[22] However, the output is change and this may cause of insufficient curing intensified by lack of irradiance cause of inhomogeneous irradiance distribution. Damages of the frosted glass shield or incorrect alignment of the LCUs can cause in reflections and incorrect presentation of the irradiance distribution. Nevertheless, for the determination of an irradiance distribution at 0mm, a frosted shield is not necessary because of the exit window of the light guide tip which is the target in the SLR and iPad setup.

The results show that each LCU has a characteristic irradiance distribution which differs from each other. The SLR has the highest resolution of the three methods and provides the best image quality, Table 1. However, the SLR images of the inactive light guide tips do not coincide with the real intensity distribution in all cases, Figure 4. Therefore, this method is inappropriate to determine the intensity distribution. Additionally, the visual examination of an active light guide tip by eye sight is extremely hazardous and totally contraindicated.

90

The comparison between the images of activated LCUs with the laser-beam profiler, SLR and iPad imaging shows that all the above methods are suitable to determine the irradiance distribution.

The SLR imaging of the activated LCU in "true color" shows similar intensity distribution as the laser-beam profiler for the tested LCUs Celalux 1 and 2 and Bluephase 20i with both methods. SLR imaging is advantageous due to the lower experimental effort, e.g. an adjustable jack is not necessary. However, the SLR images provide a lower contrast than the laser-beam profiler and the iPad imaging, Figure 3 and 4. Nevertheless, the results show that SLR imaging is an appropriate method to qualitatively characterize the intensity distribution of activated LCUs.

The iPad imaging in pseudo color shows similar intensity distribution as the laser-beam profiler. The experimental effort is slightly higher than the SLR imaging considering the precise parallel adjustment of the tip exit above the iPad camera is required. Furthermore, focusing is easier with an SLR. Nevertheless, the iPad imaging gives a good qualitative overview of the intensity distribution to the clinician.

In contrast to the clinical situation, the used experimental setups in this study were fixed cameras in relation to the LCUs. The dentist cannot stabilize the LCU in relation to the restoration during the irradiation by hand. The movement of the light guide tip over the restoration may have a positive effect to diminish the intensity distribution effects of the LCU. However, some facts seem to be at odd to this assumption. The specific intensity distribution is normally unknown to the user and the movement of the LCU in relation to the restoration is arbitrary, which leads to a not reproducible curing. Additionally, the amount of energy to the restoration depends on the user and their level of instruction and training.[23] Instructed user delivered a higher amount of energy to the restoration as not trained user, which can lead to an insufficient curing of the restoration. Therefore, a user without the knowledge and awareness to the intensity distributions of LCU would likely not lead to a positive result. Furthermore, the fast curing processes of VLC-RBCs exceed the vitrification point in the first few second after the start of exposure.[9, 24] As a result, the pattern of the intensity distribution is shown in the formed polymer network of the restoration. This reduces the chance to diminish the impact of very inhomogeneous intensity distribution of LCUs by moving.

In summary, the SLR and iPad imaging are both adequate methods for a qualitative estimation of the intensity distribution on LCUs. Due to the pseudo color images, the iPad imaging is easier to interpret compared to the images from the SLR camera. Both methods allow the user to quickly and qualitatively determine the intensity distribution of any LCU and help guide choice of the best position above the restoration for exposure. In general, all SLRs should suitable to determine the intensity distribution of LCUs provided that the SLR is not overexposed.

CONCLUSION

The three methods of LCU imaging showed the same qualitative irradiance distribution for the tested LCUs. The laser-beam profiler images can be scaled to represent the irradiance values. The SLR images have a higher resolution than the laser-beam profiler, but the contrast is often too low. The iPad images have a lower resolution than SLR images but the option of pseudo colorization results in irradiance distribution is very similar to the laser-beam profiler. The pseudo color iPad imaging is a useful tool for the qualitative evaluation of irradiance distribution. Furthermore, the tip exit images of inactive LCUs give no reliable information about the intensity distribution.

Additionally, it is clear that the irradiance distribution is governed by the internal design but the user has to consider where the highest intensity area of a LCU is to ensure a proper curing for restorations.[10]

ACKNOWLEDGEMENTS

REFERENCES

1. Rueggeberg FA. State-of-the-art: Dental photocuring—A review. *Dent Mater* 2011; **27**:39–52.

2. Ferracane JL. Resin composite—State of the art. *Dent Mater* 2011; **27**:29–38.

3. Jandt KD, Mills RW. A brief history of LED photopolymerization. *Dent Mater* 2013; **29**:605–17.

4. Price RBT, Felix CA, Andreou P. Third-generation vs a second-generation LED curing light: effect on Knoop microhardness. *Compend Contin Educ Dent* 2006; **27**:490-6.

5. Moseley H, Strang R, Stephen KW. An assessment of visible-light polymerizing sources. *J Oral Rehabil* 1986; **13**:215–24.

6. Arikawa H, Kanie T, Fujii K, Takahashi H, Ban S. Effect of inhomogeneity of light from light curing units on the surface hardness of composite resin. *Dent Mater J* 2008; **27**:21–8.

7. Vandewalle KS, Roberts HW, Andrus JL, Dunn WJ. Effect of Light Dispersion of LED Curing Lights on Resin Composite Polymerization. *J Esthet Restor Dent* 2005; **17**:244–54.

8. Price RBT, Fahey J, Felix CM. Knoop microhardness mapping used to compare the efficacy of LED, QTH and PAC curing lights. *Oper Dent* 2010; **35**:58–68.

9. Haenel T, Hausnerová B, Steinhaus J, Price RBT, Sullivan B, Moeginger B. Effect of the irradiance distribution from light curing units on the local micro-hardness of the surface of dental resins. *Dent Mater* 2015; **31**:93–104.

10. Price RBT, Rueggeberg FA, Labrie D, Felix CM. Irradiance uniformity and distribution from dental light curing units. *J Esthet Restor Dent* 2010; **22**:86–101.

11. Cook WD. Factors affecting the depth of cure of UV-polymerized composites. *J Dent Res* 1980; **59**:800–8.

12. Cook WD. Spectral Distributions of Dental Photopolymerization Sources. *J Dent Res* 1982; **61**:1436–8.

13. Ferracane JL. Correlation between hardness and degree of conversion during the setting reaction of unfilled dental restorative resins. *Dent Mater* 1985; **1**:11–4.

14. DeWald JP, Ferracane JL. A Comparison of Four Modes of Evaluating Depth of Cure of Light-activated Composites. *J Dent Res* 1987; **66**:727–30.

15. Uhl A, Mills RW, Vowles RW, Jandt KD. Knoop hardness depth profiles and compressive strength of selected dental composites polymerized with halogen and LED light curing technologies. *J Biomed Mater Res* 2002; **63**:729–38.

16. Voco GmbH. Celalux - LED Curing Light Instruction of Use. *Cuxhaven*; 2007.

17. Voco GmbH. Celalux 2: Neuste Technik für Ihre Praxis. *Cuxhaven*; 2010.

18. Ivoclar Vivadent. Bluephase 20i: *Licence to cure*; LED for every use.

19. 3M ESPE. LED Technology - Here to Stay - 3M: *A dentist's guide to understanding the latest advances in curing technology*; 2002.

20. Dentsply DeTrey GmbH. SmartLite PS - Pen-style high power LED curing light. *Konstanz*; 2003.

21. Vandewalle KS, Roberts HW, Rueggeberg FA. Power distribution across the face of different light guides and its effect on composite surface microhardness. *J Esthet Restor Dent* 2008; **20**:108-17.

22. Price RB, Labrie D, Whalen JM, Felix CM. Effect of distance on irradiance and beam homogeneity from 4 light-emitting diode curing units. *J Can Dent Assoc* 2011; **77**:1-10.

23. Price RBT, McLeod ME, Felix CM. Quantifying light energy delivered to a Class I restoration. *J Can Dent Assoc* 2010; **76**:1-8.

24. Lovell LG, Lu H, Elliott JE, Stansbury JW, Bowman CN. The effect of cure rate on the mechanical properties of dental resins. *Dent Mater* 2001; **17**:504–11.

P6   ·   Qualitative Beam Profiling of Light Curing Units for Resin...

92

PAPER II

Journal of
Dental Research

Initial Reaction Kinetics of two Resin Based Dental Composites

| Abstract: | The curing behavior of two resin based composites Arabesk TOP and Grandio (both from VOCO) was investigated using a FT-IR spectrometer (Bruker Tensor 27, Mid IR) in the attenuated total reflectance mode. Four irradiance levels (666, 954, 1,281, and 2,222 mW/cm²) were used. To resolve the kinetics of the curing reaction, 7 to 8 spectra were recorded each second. The degree of conversion (DC) was determined via the ratio of the intensity of aliphatic and aromatic carbon-carbon double bond bands for each spectrum to produce time dependent DC curves. These were fitted using a novel DC(t)-function that assumes the curing behavior of dental RBCs has a time dependent reaction constant. The scatter in the data was at most 2 to 3% during curing. The novel DC-function provided excellent fitting of the data for the first 15 s after the light was turned on. The irradiance dependent reaction time constants were between 4.3 and 7.5 s for Arabesk and 5.3 and 9.7 s for Grandio. This DC(t) function takes into account that the reaction rates slow down not only because the monomer is consumed, but also because the viscosity increases within the RBC. The function also produced a calculated final DC in the order of 50% for both RBCs, independently of the irradiance. Furthermore, the DC exhibited a reciprocal square root dependency on the irradiance level, thus indicating that exposure reciprocity does not hold for these RBCs. The final DC was around 50% and it was concluded that the DC(t)-function only describes the kinetics of "primary curing", and a quantitative separation between primary curing and post-curing must exist. After three reaction time constants have elapsed, the initial reaction can be considered to have ended and all further changes in DC can be attributed to post-curing. |

1   Introduction

Visible light curing resin based composites (VLC RBC) have replaced amalgam as the material of choice in developed countries, and with the adoption of the Minimata Convention, there will soon be a global phase down in the use of amalgam [1–4]. Adequate photo-curing is required for light-activated VLC RBC restorations to reach the manufacturer's intended properties and it is believed that this is a basic requirement for the predictable long-term clinical success of resin restorations [5–7]. The initiator system used in many dental resins often consists of light sensitive camphorquinone (CQ) and accelerator molecules [2,8]. Blue light excites the CQ molecules to a triplet state from which they may then react with accelerator molecules to form two radicals [9,10].

Initiation reaction $\qquad CQ_{triplet}^* + A \xrightarrow{k_i} \underbrace{CQ\bullet}_{\text{radicals with low reactivity}} + \underbrace{A\bullet}_{\text{radicals with high reactivity}}$ (I)
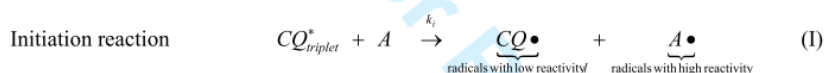
with $\qquad k_i \qquad$ reaction constant of initiation reaction.

Subsequent curing reactions are started by amine radicals with adjacent dimethacrylate monomers (DMA) [10–13]:

Start reaction: $\qquad A\bullet + DMA \xrightarrow{k_s} A-(DMA)\bullet$ (II)

Growth reaction: $\qquad A-(DMA)_n-(DMA\bullet) + DMA \xrightarrow{k_p} A-(DMA)_{n+1}-(DMA\bullet)$ (III)
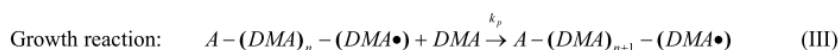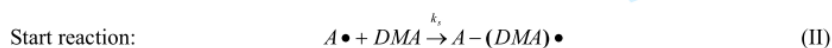
with $\qquad k_s \qquad$ reaction constant of start reaction

$\qquad k_p \qquad$ reaction constant of the polymerization of the chain growth

As the radical concentration increases, radical annihilation becomes more probable due to increased termination reactions in which either CQ or amine radicals react with the radical ends of growing polymer chains or the radical ends of two polymer chains recombine.

Theoretical considerations of the reaction kinetics of VLC RBC usually assume that an equilibrium exists between initiation and termination [13,14] and this allows for solving the rate equation [13]. However, the curing rate will slow down if the growing polymer chains reach a length at which their glass transition temperature T_g exceeds the ambient temperature. The chain growth then becomes diffusion controlled [15] and at this point one can assume that the concentration of mobile radicals becomes constant.

Since the start reaction is very quick, the rate equation of polymerization is determined by the reaction constant k_p.

$$\frac{dc^{DMA}(t)}{dt} = -k_p * c_{rad}(t) * c^{DMA}(t) \tag{1}$$

with c_0^{DMA} concentration of DMA monomers

          c_{rad} concentration of radicalized initiator molecules

Equation (1) cannot be integrated because in most cases, $c_{rad}(t)$ is unknown. At high irradiance levels, most of the initiator molecules are radicalized quickly because the number of photons outnumbers the number of initiator molecules [16]. Thus, equilibrium is reached after a short initiation time and the radical concentration becomes constant. The rate equation is then rewritten as [17]:

$$\frac{dc^{DMA}(t)}{dt} = -k_p * c_{0,rad} * c^{DMA}(t) \tag{2}$$

with $c_{0,rad}$ radical concentration in the equilibrium

Equation (2) yields the time dependent concentration of DMA monomers

$$c^{DMA}(t) = c_0^{DMA} * e^{-k_p * c_{0,rad} * t} = c_0^{DMA} * e^{-\frac{t}{\tau_{reac}^0}}. \tag{3}$$

The product $k_p * c_{0,rad}$ represents a reciprocal time. Thus, a reaction time constant τ_{reac}^0 can be defined as the point when 63% of the monomers have reacted.

$$\tau_{reac}^0 = \frac{1}{k_p * c_{rad}} \tag{4}$$

The aspect of interest is the time dependent degree of conversion (DC).

$$DC(t) = 1 - \frac{c^{DMA}(t)}{c_0^{DMA}} = 1 - e^{-\frac{t}{\tau_{reac}^0}}. \tag{5}$$

Equation (5) can be directly used to fit *DC(t)* curves [18] and indirectly for ion viscosity curves that have been determined by dielectric analysis [17] if its kinetics are related to the *DC(t)*.

$$\eta^{ion}(t) = \eta_0^{ion} + \left(\eta_\infty^{ion} - \eta_0^{ion}\right) * \left(1 - \frac{c^{DMA}(t)}{c_0^{DMA}}\right) = \eta_0^{ion} + \left(\eta_\infty^{ion} - \eta_0^{ion}\right) * DC(t). \tag{6}$$

with $\eta^{ion}(t)$ ion viscosity

η_0^{ion} initial ion viscosity (before curing)

η_∞^{ion} final ion viscosity.

Equation (4) produces good fits for time intervals that do not exceed twice the reaction time constant τ_{reac}^0. However, it fails for longer times as DC_{final} tends to "1" whereas experiments show DC_{final} of 0.5 to 0.7 [19–21]. Therefore, equation (5) was supplemented by additional fit parameters:

$$DC(t) = A - B * e^{-\frac{t}{\tau_{reac}^0}}. \tag{7}$$

The fit parameters A and B represent the maximum DC and should be identical, but instead they are different in the fitting process. This indicates that equation (7) cannot produce a reasonable fit [18]. Ilie et al [22], has suggested a second exponential to attribute for post-curing in the glassy state. This improved the quality of the fit, but produced i) still non-zero values for A [18] and ii) allowed post-curing to occur from time zero.

Lovell et al found that the glass transition of many dental resins occurs when the DC reaches 30 to 40% [23]. Then, the viscosity of the resin increases during the ongoing curing reaction and the curing rate slows down [24]. In the liquid resin, the reaction rate is high and changes little [14]. However, if the glass temperature of the resin exceeds ambient temperature, the curing rate decreases significantly [24], thus, the reaction constant k_p must depend on time. The objective of this was to develop a novel DC-function based on a time dependent reaction constant that generates a DC_{final} that is les than 100%. This should allow an improved evaluation of initial reaction kinetics to verify if exposure reciprocity is a valid concept.

2   Theoretical considerations

The reaction time constant has the following time dependency

$$\tau_{reac}(t) = \tau_{reac}^0{}' + \Theta * e^{\frac{t}{\tau_{grow}}}. \tag{8}$$

with $\tau_{reac}^0{}'$ constant part of reaction time constant

Θ initial strength of time dependent part whereas $\Theta \ll \tau_{reac}^0{}'$

τ_{grow} characteristic growing time constant of time dependent part.

As curing starts, the reaction time constants of equations (4) and (8) have to be identical leading to $\tau_{reac}^0 = \tau_{reac}^0{}' + \Theta$. With ongoing curing, the time dependent part should increase exponentially. Introducing equation (8) to equation (2) leads to

$$\frac{dc^{DMA}(t)}{dt} = -\underbrace{k_p * c_{0,rad}}_{is\ to\ be\ time\ dependent} * c^{DMA}(t) = -\frac{c^{DMA}(t)}{\left\{\tau_{reac}^0{}' + \Theta * e^{\frac{t}{\tau_{grow}}}\right\}}. \tag{8}$$

Separation for variables yields

$$\int_{c(t=0)}^{c(t)} \frac{dc^{DMA}}{c^{DMA}} = -\int_0^t \frac{dt'}{\left\{ \tau_{reac}^0 ' + \Theta * e^{\frac{t'}{\tau_{grow}}} \right\}} \cdot 1 . \qquad (9)$$

Integration provides the monomer concentration

$$c^{DMA}(t) = c_0^{DMA} * e^{-\frac{t}{\tau_{reac}^0 '}} * \left(\frac{\tau_{reac}^0 ' + \Theta * e^{\frac{t}{\tau_{grow}}}}{\left(\tau_{reac}^0 ' + \Theta \right)} \right)^{\frac{\tau_{grow}}{\tau_{reac}^0 '}} . \qquad (10)$$

and the degree of conversion (DC)

$$DC(t) = 1 - \frac{c^{DMA}(t)}{c_0^{DMA}} = 1 - e^{-\frac{t}{\tau_{reac}^0 '}} * \underbrace{\left(\frac{\tau_{reac}^0 ' + \Theta * e^{\frac{t}{\tau_{grow}}}}{\left(\tau_{reac}^0 ' + \Theta \right)} \right)^{\frac{\tau_{grow}}{\tau_{reac}^0 '}}}_{correction\ term\ K(t)} . \qquad (11)$$

For short times ($t \rightarrow 0$), K(t) approaches "1", equation (5) and (11) become identical. For long times ($t \rightarrow \infty$), the DC approaches

$$DC_{final} \underset{t \rightarrow \infty}{=} 1 - \left(\frac{\Theta}{\tau_{reac}^0 ' + \Theta} \right)^{\frac{\tau_{grow}}{\tau_{reac}^0 '}} = constant < 1 . \qquad (12)$$

Due to $\Theta << \tau_{reac}^0 '$ the correction term $K(t)$ restricts DC$_{final}$ to values below "1" representing the maximum DC achieved by "primary curing". Shorter characteristic growing time constants τ_{grow} and larger initial strengths Θ produce $DC(t)$-curves with lower DC$_{final}$. For the values $\tau_{grow} = \infty$ and $\Theta = 0$ equation (5) is reproduced.

---

[1] According to Bronstein's "Taschenbuch der Mathematik" the solution of the integral on the right side of Equation (1.8) is found as integral 454:

$$\int \frac{dx}{b + c * e^{ax}} = \frac{x}{b} - \frac{1}{a * b} \ln \left(b + c * e^{ax} \right) \qquad \text{with correspondences} \quad a = \frac{1}{t_{glass}}, b = \tau_{reac}^0, c = \Theta$$

1
2
3
4
5
6
7
8
9
10
11
12
13
14
15
16
17
18
19
20
21
22
23
24
25
26
27
28
29
30
31
32
33
34
35
36
37
38
39
40
41
42
43
44
45
46
47
48
49
50
51
52
53
54
55
56
57
58
59
60

3   Materials and methods

3.1   Materials and Light Curing Units

Two VLC RBCs were investigated: the microhybrid composites Arabesk TOP, shade OA2 and the nanohybrid composites Grandio shade OA2 (both from VOCO), Table 1. In the following text the composites are called Arabesk and Grandio, respectively. The specimens were cured using three light curing units (LCU), the mono-wave LCU Bluephase 16i (Ivoclar Vivadent), Celalux I (VOCO) and the poly-wave LCU Bluephase 20i (Ivoclar Vivadent) operated in the Low, High and Turbo modes, Table 1. The irradiances were additionally determined in the 4 mm diameter center region of the light beam according to the method described in [18].

3.2   Determination of Degree of Cure (DC) by ATR FT-IR Spectroscopy

The VLC RBCs were packed in 1 mm thick Delrin® rings with D_{out}=15 mm and D_{in}=4 mm, centrically placed over the Golden Gate ATR diamond of the FT-IR spectrometer (Bruker Tensor 27, Mid IR) and covered with a Mylar® strip. A glass slide was used to press and flatten the sample to the thickness of 1 mm. The experimental setup is shown in Figure 1.

The specimens were irradiated for maximum of 160 s. The curing light was immediately restarted for times exceeding the maximum exposure time of the LCU. Five specimens (n = 5) were made for each exposure time and LCU. The *DC* was recorded at the bottom surface in real time at room temperaturę (23°C). The parameters setting of the FT-IR were:

- Total measurment time   180 s

- Scan mode   6 recorded spectra in double side mode per second

- Resolution   8 cm-1

- Scan rate   7 to 8 scans/s

The DC was determined by the changing ratio of the absorbance band of the aliphatic C=C double bound ($Abs_{(Aliphatic)}$) to the absorbance of the uncured state in the wave number range 1645 to 1620 cm^{-1}. To reduce scatter between two measurements and to account for changing refraction index the absorbance of the aliphatic band was normalized to the absorbance of the aromatic band ($Abs_{(Aromatic)}$) in the wave number range 1620 to 1590 cm^{-1}. The peak areas were determined using baseline type B of the OPUS software v 6.5 (Bruker). The FT-IR equipment was calibrated based on a technique reported by Rueggeberg et al [25].

$$DC = 100\,\% * \left[1 - \frac{0.141\left[\frac{Abs_{(Aliphatic)}}{Abs_{(Aromatic)}}\right]^2_{Polymer} + 1.1424\left[\frac{Abs_{(Aliphatic)}}{Abs_{(Aromatic)}}\right]_{Polymer}}{0.141\left[\frac{Abs_{(Aliphatic)}}{Abs_{(Aromatic)}}\right]^2_{Monomer} + 1.1424\left[\frac{Abs_{(Aliphatic)}}{Abs_{(Aromatic)}}\right]_{Monomer}} \right] \tag{13}$$

3.3 Evaluation of DC curves

3.3.1 Direct evaluation of DC curves

Each DC curve was evaluated with respect to initial slope $m_{initial}$, reaction time $\tau_{reaction}$ which is the time to a degree of cure of $(1-1/e)*DC_{3\,min}$, and DC_{3min}. The initial slope $m_{initial}$ was calculated by a linear fit between the DC-baseline before irradiation and a DC of typically 30%. The start time t_{start} of the curing reaction was determined by the intercept of DC-baseline and $m_{initial}$. DC_{3min} represents the arithmetic average of the DC during the last 5 s of each measurement. The degree of cure at $(1-1/e)*DC_{3min}$ is given by 63.2% of DC_{3min}. The corresponding time represents the reaction time $\tau_{reaction}$ which is a measure for the time after

101

which the resin is to have been fully light cured. The evaluation protocol is reported in Figure 2.

3.3.2 Fitting of DC curves

Curve fitting was performed to determine;

- Reaction time constant τ_{reac}^0

- Characteristic growing time constant τ_{grow}

- Initial strength Θ of time dependent part

The fit procedure consisted of two steps. In the first step, equation (5) was used in the form;

$$DC(t) = 1 - \frac{c^{DMA}(t)}{c_0^{DMA}} = 1 - e^{-\frac{t - t_{start}}{\tau_{reac}^0}} \tag{14}$$

to fit the data between 0 s to maximum 7 s where t_{start} denotes the start of the light curing reaction. This produced the start values of τ_{reac}^0 for the second step in which growing time constant τ_{grow} and initial strength Θ were determined for constant τ_{reac}^0. In order to account for effects of the length of fit intervals on parameter values and quality of the fits, the fit procedure was carried out at three time intervals: 15 s, 40 s and 160 s.

4   Results

4.1   Direct evaluation of *DC(t)* and characteristic kinetics parameters

The initial slopes $m_{initial}$ increased a factor of 2 for Arabesk, and by a factor of 1.8 for Grandio, while irradiance increased by a factor 3.3. The corresponding R^2-values of the slopes are between 0.91 and 0.95 due to the scatter of the DC-data. Corresponding to the initial slopes, the reaction times $\tau_{reaction}$ decreased by a factor of 2.3 for Arabesk and a factor of 2.0 for Grandio, Table 2. The increase in the initial slopes and the decrease in the reaction times were not proportional to the irradiance levels used in this study. The data shows that Arabesk exhibits initial slopes that are typically a factor 1.32 (0.07) higher than those of Grandio for the corresponding irradiation conditions. In contrast, the reduction in the reaction times seems to be less affected by only a factor of 1.13 (0.08). After an irradiation time of 160 s, all samples reached the same DC values of 68.1% (0.6) for Arabesk and 64.1% (1.3) for Grandio.

4.2   Evaluation of the DC data using curve fitting with the novel DC-function

The fit results of the measured *DC(t)*–curves are shown in Table. The parameters determined for a fit interval of 15 s produce calculated DC curves which represent the *DC* data obtained during the first 20 s of curing, Figure 3. The fitted curves differ a little bit more at the higher irradiances and correspondingly faster conversion rates. This means that the fit intervals must to be shortened and related to the reaction time constant τ_{reac}^0. e.g for Arabesk the fit interval of 15 s corresponds to $2 * \tau_{reac}^0$ when light cured with Bluephase 20i Low, but to $3 * \tau_{reac}^0$ when cured with the Celalux unit. The calculated DC-curves achieved an asymptotic DC_{final} after 20 s, which is below the measured values, as shown in Figure 3. Larger fit interval of 40 s or 160 s, respectively, let the calculated DC-curves differ by more and more from the measured

DC data in the range of short times, but produced better values for $DC_{3\,min}^{fit}$, because the large number of data points of the DC plateau increases its impact on the fitting process.

The reaction time constants τ_{reac}^{0} decrease a factor of 1.9 (Arabesk) and a factor of 1.8 (Grandio) when the irradiance is increased by a factor 3.3, Table 3. The corresponding reaction times $\tau_{reaction}$, Table 2, are lower than the reaction time constants τ_{reac}^{0} determined by curve fitting, Table 3, because τ_{reac}^{0} refers always to a DC_{final} of 100% whereas $\tau_{reaction}$ refers to the DC_{3min}-values of 68.1% (0.8) for Arabesk and 64.1% (1.4) for Grandio, respectively.

The initial strengths Θ are found to be less than one tenth of the corresponding reaction time constants τ_{reac}^{0}, demonstrating that its initial contribution is small. With increasing irradiance, the initial strengths Θ decrease by a factor of 2.3 (Arabesk) and by a factor of 1.4 (Grandio) for the 15 s fit. However, this decrease was not significant with respect to the standard deviations (SD). If the fit intervals are extended to 40 s or 160 s, Θ increases typically a factor 3 or 6, respectively, for both Arabesk and Grandio and this is due to the greater number of data points of the DC-plateau

As the irradiance increases, the characteristic growing time constants τ_{grow} decrease by a factor of 1.7 Arabesk or by 1.5 for Grandio, respectively. τ_{grow} is typically 1/4 to 1/3 the reaction time constants τ_{reac}^{0} for all fit intervals, Table 3. Thus, one might assume a constant relation between τ_{grow} and τ_{reac}^{0}. For longer fit intervals the characteristic growing time constants τ_{grow} increase and this compensates for effects of larger initial strengths of Θ.

The $DC_{3\min}^{fit}$-values increase with the length of the fit interval and reach constant values of 65.6% (0.8) for Arabesk and 63.3% (0.3) for Grandio, respectively. These values are slightly below the experimentally determined DC_{3min}-values reported in Table 2.

4.3 Effects of irradiance on reaction time constants

Figure 4 shows the reaction time constants τ_{reac}^0 determined for 15 s fit intervals versus the effective irradiances of the LCU. The data was fitted using both a linear as well as a potential function given by

$$\tau_{reac}^0(I_{LCU}) = a * I_{LCU}^b \qquad (15)$$

with fit parameters "a" and "b". For the potential fit the parameter "b" turned out to be "-0.51" for Arabesk (R^2=0.99) and "-0.45" for Grandio (R^2=0.95). The fit curves according to equation (14) exhibit significantly better R^2-values than the linear fits with R^2=0.92 (Arabesk) and R^2=0.87 (Grandio), respectively. This indicates that the reaction time constants do not depend reciprocally on irradiance. The determined values of parameter b are close to "-0.5", thus, the reaction time constants τ_{reac}^0 depend almost reciprocally on the square root of irradiance.

5 Discussion

The aim of this paper is to investigate the curing kinetics of two VLC RBCs during their early stages and how the kinetics depend on the irradiance from the LCU. Therefore, the time dependent degree of cure was determined using FT-IR with a sampling rate of 7 to 8 points/s.

105

These measurements provided a sufficient number of data points each second to test and verify DC-functions for the first 10 to 20 s of the curing reaction. This time interval is considered here as "primary curing".

Since the DC-functions given by equations (4) and (5) are not satisfactory, a novel DC-function, equation (11), was derived. This novel DC-function was based on the assumption that the reaction constant is not constant, but instead is time dependent because the conversion rate slows down during the curing process viscosity increases and due to the glass transition temperature of the resin. Thus, a time dependent correction is added to the equation (4);

$$K(t) = \left(\frac{\tau^0_{reac}{}' + \Theta * e^{\frac{t}{\tau_{grow}}}}{\left(\tau^0_{reac}{}' + \Theta \right)} \right)^{\frac{\tau_{grow}}{\tau^0_{reac}{}'}} . \qquad (16)$$

leading to equation (11). This prevents the DC from reaching 100% and it significantly increases the time range with good fitting of data, Figure 5.

In equation (4) the reaction time constant τ^0_{reac} represents the quantity determining the curing kinetics of VLC RBCs because it indicates the time to reach a conversion of 63%. If one checks the conversion of both Arabesk and Grandio after the time $t = \tau^0_{reac}{}'$ one finds typically a conversion of 45%. Lovell et al [23] suggest that dental resins transfer to the glassy state when they reach conversion levels of 30 to 40%. Thus, the resins of Arabesk and Grandio are almost certainly in the glassy state after $\tau^0_{reac}{}'$ and the mobility of monomers has been drastically reduced at this time. Under these circumstances, few triplet activated CQ molecules are available to react with accelerator molecules to form any new radicals. Therefore, radical generation comes almost to an end once the resin reaches the glassy state despite the fact that further light is delivered. At this point, the kinetics of radical annihilation and further curing become diffusion controlled. Thus, any polymerization reaction in the

glassy state takes place under similar conditions as the post-curing processes after turning off the LCU.

Teshima et al [26] investigated the radical generation using radical traps and found that irradiance caused a linear increase of radical concentration. However, their LED LCU delivered an irradiance of 160 mW/cm² and required approximately 250 s to radicalize all the CQ-molecules. In the present study, LCUs delivered 4 to 13 times greater irradiance levels. Their radicalization times should be between 20 and 60 s and at least 4 times longer than the reaction time constants τ_{reac}^0 given in Table 3. Thus, without radical annihilation processes one can expect maximum that one fourth of the initiator molecules will be radicalized.

The curing rate of VLC RBCs depends on the available light intensity and decreases exponentially with cross-sectional distance x from the surface [27] according to

$$\frac{dc^{DMA}(t,x)}{dt} = -\frac{k_p}{\sqrt{k_t}} * c^{DMA}(t) * \left(\Phi * I_0 \, e^{-\frac{x}{d}} \right)^{0.5} \tag{17}$$

with rate constant of polymerization k_p, rate constant of termination k_t, quantum yield Φ, initial intensity I_0 and light penetration depth d. Consequently reaction time constants τ_{reac}^0 increase correspondingly, and the deeper into the VLC RBC, the longer the time to transfer the resin to the glassy state. Therefore, in principle, one can distinguish 3 regions whose borders are time dependent:

1. Highly cured regions close to the surface that are above the glass temperature where curing and radical generation is diffusion controlled in spite of further irradiation. Therefore, the reaction rate approaches almost that of post-curing processes.

2. Curing regions where primary curing takes place so long as the temperature is below glass temperature.

3. Uncured regions where the light has generated no radicals and no curing takes place.

In that context, the reaction time constant τ^0_{reac}' represents the time after which a VLC RBC has transferred to the glassy state. Primary curing takes place only for times not exceeding τ^0_{reac}' whereas for longer times the kinetics of VLC RBCs are mainly determined by diffusion controlled post-curing processes. This now provides a tool to separate between primary curing where the reaction kinetics are given by equation (11), and post-curing where the reaction kinetics appear to depend logarithmically on time [18].

For very long times, the new DC-function reaches the value $DC^{primary\ curing}_{final}$, given by equation (12). Fitting the DC-curves for a time interval of $1.5\tau^0_{reac}$ produces values of $DC^{primary\ curing}_{final}$ between 49.8 and 52.3% (Arabesk) and 49.2 and 51.1% (Grandio). This can be interpreted that primary curing accounts for approximately 50% DC and that the increase in $DC_{3\,min}$ to 68% (Arabesk) and 64% (Grandio), respectively, Table 2, must be attributed to post-curing.

As the reaction time constant τ^0_{reac} is reciprocal to the conversion rate, the irradiance dependency of curing reactions can now be investigated, Figure 4. The analysis shows that the reaction time constants τ^0_{reac} depend reciprocally on the square root of irradiance – values of parameter b are close to "0.5" as predicted by rate equation (16) that was derived for initiator systems generating two radicals in the initiation reaction [13] and [14] – and not reciprocally as required by exposure reciprocity. Thus, the investigated VLC RBCs Arabesk and Grandio do not obey exposure reciprocity at a depth of 1mm if cured with irradiances between 660 mW/cm² and 2200 mW/cm². However, one has to keep in mind that the collection of DC-data at deeper depths e.g. 2 mm would have produced much larger reaction time constants that may then be fitted with similar R²-values for both linear and potential fits depending on the

standard deviations. This would explain in a simple why some researchers have found evidence for exposure reciprocity, but only under certain conditions [e.g. 28].

6 Conclusions

The novel DC-function reproduces the actual DC-data excellently during the initial curing reactions. The reaction time constant $\tau_{reac}^{0}{}'$ is a measure for the conversion rate in the liquid resin as well as the time to glass transition at which point primary curing ends. It depends reciprocally on the square root of irradiance meaning that exposure reciprocity breaks down at higher irradiance levels. Furthermore, DC_{final} was found to be around 50% for both resin based composites, thus, a separation between the primary curing and post-curing aspects must exist.

References

1. Shawkat ES, Shortall AC, Addison O and Palin WM. Oxygen inhibition and incremental layer bond strengths of resin composites. Dental materials, 2009; 25:1338–1346.

2. Leprince J, Lamblin G, Truffier-Boutry D, Demoustier-Champagne S, Devaux J, Mestdagh M and Leloup G. Kinetic study of free radicals trapped in dental resins stored in different environments. Acta Biomaterialia, 2009; 5:2518–2524.

3. Heintze SD and Rousson V. Clinical effectiveness of direct class II restorations - a meta-analysis. Journal of adhesive dentistry, 2012; 14:407–431.

4. Dental restorative materials and the Minamata Convention on Mercury. Guidelines for successful implementation. Geneva-Cointrin, 2012.

5. Bayne SC. Correlation of clinical performance with 'in vitro tests' of restorative dental materials that use polymer-based matrices. Dental materials, 2012; 28:52–71.

6. Leprince JG, Palin WM, Hadis MA, Devaux J and Leloup G. Progress in dimethacrylate-based dental composite technology and curing efficiency. Dental materials, 2013; 29:139–156.

7. Shortall AC, Felix CJ and Watts DC. Robust spectrometer-based methods for characterizing radiant exitance of dental LED light curing units. Dental Materials, 2015; 31:339–350.

8. Gauthier MA, Stangel I, Ellis TH and Zhu XX. Oxygen inhibition in dental resins. Journal of dental research, 2005; 84:725–729.

9. Green GE, Stark BP and Zahir SA. Photocross-Linkable Resin Systems. Journal of Macromolecular Science, Part C, 1981; 21:187–273.

10. Stansbury JW. Curing Dental Resins and Composites by Photopolymerization. J Esthet Restor Dent, 2000; 12:300–308.

11. Cook WD. Photopolymerization kinetics of dimethacrylates using the camphorquinone/amine initiator system. Polymer, 1992; 33:600–609.

12. Anseth KS and Bowman CN. Kinetic Gelation model predictions of crosslinked polymer network microstructure. Chemical Engineering Science, 1994; 49:2207–2217.

13. Young RJ and Lovell PA. Introduction to polymers. CRC Press, 2011.

14. Andrzejewska E. Photopolymerization kinetics of multifunctional monomers. Progress in Polymer Science, 2001; 26:605–665.

15. Fox TG and Loshaek S. Influence of molecular weight and degree of crosslinking on the specific volume and glass temperature of polymers. J. Polym. Sci., 1955; 15:371–390.16. Watts DC. Reaction kinetics and mechanics in photo-polymerized networks. Dental materials, 2005; 21:27–35.

17. Steinhaus J, Hausnerova B, Haenel T, Großgarten M and Möginger B. Curing kinetics of visible light curing dental resin composites investigated by dielectric analysis (DEA). Dental materials, 2014; 30:372–380.

18. Selig D, Haenel T, Hausnerová B, Moeginger B, Labrie D, Sullivan B and Price, Richard B T. Examining exposure reciprocity in a resin based composite using high irradiance levels and real-time degree of conversion values. Dental materials, 2015; 31:583–593.

19. Ferracane JL. Correlation between hardness and degree of conversion during the setting reaction of unfilled dental restorative resins. Dental materials, 1985; 1:11–14.

20. Stansbury JW and Dickens SH. Network formation and compositional drift during photo-initiated copolymerization of dimethacrylate monomers. Polymer, 2001; 42:6363–6369.

21. Amirouche-Korichi A, Mouzali M and Watts DC. Effects of monomer ratios and highly radiopaque fillers on degree of conversion and shrinkage-strain of dental resin composites. Dental materials, 2009; 25:1411–1418.

22. Ilie N, Keßler A and Durner J. Influence of various irradiation processes on the mechanical properties and polymerisation kinetics of bulk-fill resin based composites. Journal of dentistry, 2013; 41:695–702.

23. Lovell LG, Lu H, Elliott JE, Stansbury JW and Bowman CN. The effect of cure rate on the mechanical properties of dental resins. Dental materials, 2001; 17:504–511.

24. Truffier-Boutry D, Gallez XA, Demoustier-Champagne S, Devaux J, Mestdagh M, Champagne B and Leloup G. Identification of free radicals trapped in solid methacrylated resins. J. Polym. Sci. A Polym. Chem., 2003; 41:1691–1699.

25. Rueggeberg FA, Hashinger D and Fairhurst C. Calibration of FTIR conversion analysis of contemporary dental resin composites. Dental materials, 1990; 6:241–249.

26. Teshima W, Nomura Y, Tanaka N, Urabe H, Okazaki M, Nahara Y. ESR study of camphorquinone/amine photoinitiator systems using blue light-emitting diodes, Biomaterials, 2003; 24: 2097–2103.

27. G.G. Odian, Principles of Polymerization, 3rd ed, 1991, Wiley, New York.

28. Feng L, Suh BI. Exposure reciprocity law in Photopolymerization of multifunctional acrylates and methacrylates. Macromolecular Chemistry and Physics. 2007;208:295-306.

1
2
3
List of tables
4
5
6
7
8
Table 1 Investigated composites and used light curing units Table 1 Investigated
9
10
11
12
13
14
15
Table 2 Characteristic parameters of the curing kinetics from direct evaluation
16
17
18
19
20
21
Table 3 Fit parameters of Arabesk and Grandio according to equation (11) determined for fit
22
23
intervals of 15 s, 40 s and 160 s
24
25
26
27
28
29
30
Table 4 Irradiance dependent $DC_{final}^{primary\ curing}$ values according to equation (11) for fit intervals
31
32
of 1.5 τ_{reac}^0
33

1
2
3
List of figures
4
5
6
7
Figure 1: Experimental setup to determine the degree of cure using FT-IR
8
9
10
11
12
13
Figure 2: Evaluation of DC curves to determine the characteristic parameters of the curing
14
15
kinetics
16
17
18
19
20
21
Figure 3: Effects of irradiance on DC curves during the initial cuing reaction – measured data
22
23
(dots) and fits (lines) – time range of fits is 15 s. (For better visibility curves are shifted by
24
25
20% along DC-axis each.)
26
27
28
29
30
31
32
Figure 4: Dependency of reaction time constant τ_{reac}^0 on irradiance
33
34
35
36
37
38
39
Figure 5: Comparison of fit curves using equation (4) – black line – and equation (11) – red
40
41
line – to measured data – symbols
42

111

Table 1 Investigated composites and used light curing units					
Dental Composite	**Producer**	**Type**	**Initiator**	**Matrix/ Filler content**	
Arabesk TOP OA2	Voco GmbH, Cuxhaven, Germany	Light-curing microhybrid composite	CQ/DABE	BisGMA	
				UDMA	
				TEGDMA	
				77%	
Grandio OA2		Light-curing nanohybrid restorative		BisGMA	
				TEGDMA	
				86%	
LCU		**Peak Wavelength [nm]**	**Peak Wavelength range [nm]**	**Irradiance Total Area [mW/cm²]**	**Irradiance Ø 4 mm Area [mW/cm²]**
Celalux I	Voco GmbH, Cuxhaven, Germany	450	410-510	1172 (5.8)	1655 (42.7)
Monowave					
Bluephase 16i		455	410-520	954 (1.5)	950 (1.0)
Monowave					
High Mode					
Bluephase 20i	Ivoclar Vivadent AG, Schaan, Lichtenstein				
Polywave					
Low Mode			380-435	666 (6.9)	661 (1.9)
			435-530		
High Mode		410 460	390-430	1281 (8.7)	1460 (5.4)
			430-530		
Turbo Mode			390-430	2222 (24.2)	2196 (9.3)
			430-530		

Table 2 Characteristic parameters of the curing kinetics from direct evaluation						
		Bluephase 20i Low	Bluephase 16i	Bluephase 20i High	Celalux I	Bluephase 20i Turbo
Arabesk	$m_{initial}$ [%/s]	10.5 (0.5)	13.2 (1.4)	15.4 (1.4)	17.4 (0.4)	21.4 (0.8)
	R^2 ($m_{initial}$)	0.927	0.941	0.943	0.913	0.943
	$\tau_{reaction}$ [s]	6.8 (1.8)	4.8 (0.8)	4.1 (0.5)	3.9 (0.4)	2.9 (0.4)
	DC_{3min} [%]	68.5 (3.0)	67.3 (1.2)	67.6 (2.1)	68.0 (1.1)	69.0 (1.1)
Grandio	$m_{initial}$ [%/s]	8.2 (2.0)	10.6 (0.4)	12.3 (0.4)	12.5 (0.8)	16.1 (0.9)
	R^2 ($m_{initial}$)	0.955	0.937	0.940	0.943	0.940
	$\tau_{reaction}$ [s]	6.9 (0.8)	5.1 (0.2)	4.9 (0.4)	4.6 (0.6)	3.5 (0.5)
	DC_{3min} [%]	61.6 (0.6)	64.5 (0.6)	65.3 (0.9)	64.7 (1.4)	64.5 (2.0)

Table 3 Fit parameters of Arabesk and Grandio according to equation (11) determined for fit intervals of 15 s, 40 s and 160 s

	Bluephase 20i Low	Bluephase 16i High	Bluephase 20i High	Celalux I	Bluephase 20i Turbo
Irradiance [mW/cm²]	661 (1.9)	950 (1.0)	1460 (5.4)	1655 (43)	2196 (9.3)
Arabesk					
Fit 15 s					
τ^0_{reac}	7.9 (0.6)	6.3 (0.4)	5.3 (0.4)	4.9 (0.2)	4.3 (0.3)
Θ	0.64 (0.23)	0.49 (0.13)	0.54 (0.09)	0.50 (0.13)	0.28 (0.05)
τ_{grow}	2.2 (0.1)	1.8 (0.06)	1.8 (0.1)	1.6 (0.1)	1.3 (0.1)
DC_{3min}	52.3 (1.1)	53.8 (2.07)	55.8 (0.9)	55.4 (0.9)	57.0 (1.3)
Fit 40 s					
Θ	1.70 (0.32)	1.26 (0.27)	1.30 (0.13)	1.06 (0.36)	0.75 (0.10)
τ_{grow}	4.0 (0.2)	3.2 (0.1)	3.1 (0.1)	2.7 (0.3)	2.2 (0.1)
DC_{3min}	58.8 (1.0)	59.5 (1.9)	61.2 (0.8)	60.2 (0.5)	62.0 (1.1)
Fit 3min					
Θ	3.78 (0.44)	2.70 (0.47)	2.55 (0.26)	2.19 (0.33)	1.59 (0.22)
τ_{grow}	7.4 (0.3)	5.5 (0.3)	5.1 (0.3)	4.4 (0.3)	3.6 (0.3)
DC_{3min}	65.2 (0.8)	64.9 (1.9)	66.4 (0.7)	64.9 (0.4)	66.5 (0.9)
Grandio					
Fit 15 s					
τ^0_{reac}	9.7 (1.1)	7.4 (0.2)	6.7 (0.5)	6.5 (0.5)	5.3 (0.3)
Θ	0.62 (0.17)	0.58 (0.05)	0.56 (0.13)	0.54 (0.15)	0.44 (0.07)
τ_{grow}	2.4 (0.1)	2.1 (0.1)	2.0 (0.1)	1.9 (0.1)	1.6 (0.1)
DC_{3min}	50.2 (0.9)	52.1 (0.6)	53.0 (0.2)	53.0 (1.3)	53.9 (0.5)
Fit 40 s					
Θ	1.81 (0.29)	1.54 (0.07)	1.38 (0.17)	1.29 (0.20)	1.07 (0.08)
τ_{grow}	4.5 (0.3)	3.7 (0.1)	3.3 (0.1)	3.2 (0.1)	2.6 (0.1)
DC_{3min}	57.5 (1.0)	58.3 (0.4)	58.7 (0.1)	58.3 (1.3)	58.8 (0.6)
Fit 3 min					
Θ	3.90 (0.54)	3.12 (0.11)	2.69 (0.17)	2.46 (0.25)	2.09 (0.11)
τ_{grow}	7.8 (0.9)	6.1 (0.1)	5.4 (0.1)	5.0 (0.2)	4.2 (0.1)
DC_{3min}	63.5 (1.6)	63.5 (0.3)	63.5 (0.1)	62.9 (1.4)	63.3 (0.5)

Table 4 Irradiance dependent $DC_{final}^{primary\ curing}$ values according to equation (11) for fit intervals of $1.5\ \tau^0_{reac}$

LCU	Type	Irradiance [mW/cm²]	$DC_{final}^{primary\ curing}$ [%]	
			Arabesk	Grandio
Bluephase 20i Low	Polywave	661	49.8 (1.4)	51.1 (1.1)
Bluephase 16i	Monowave	950	50.6 (1.7)	50.6 (0.2)
Bluephase 20i High	Polywave	1460	51.3 (1.2)	50.7 (0.6)
Celalux I	Monowave	1655	51.2 (1.3)	50.7 (1.0)
Bluephase 20i Turbo	Polywave	2196	52.3 (1.2)	49.2 (0.9)

1
2
3
4
5
6
7
8
9
10
11
12
13
14
15
16
17
18
19
20
21
22
23
24
25
26
27
28
29
30
31
32
33
34
35
36
37
38
39
40
41
42
43
44
45
46
47
48
49
50
51
52
53
54
55
56
57
58
59
60

Experimental setup to determine the degree of cure using FT-IR
Figure 1
82x79mm (300 x 300 DPI)

1
2
3
4
5
6
7
8
9
10
11
12
13
14
15
16
17
18
19
20
21
22
23
24
25
26
27
28
29
30
31
32
33
34
35
36
37
38
39
40
41
42
43
44
45
46
47
48
49
50
51
52
53
54
55
56
57
58
59
60

Evaluation of DC curves to determine the characteristic parameters of the curing kinetics
Figure 2
63x47mm (300 x 300 DPI)

115

Effects of irradiance on DC curves during the initial cuing reaction – measured data (dots) and fits (lines) – time range of fits is 15 s. (For better visibility curves are shifted by 20% along DC-axis each.)
Figure 3
127x191mm (300 x 300 DPI)

116

Dependency of reaction time constant on irradiance
Figure 4
84x84mm (300 x 300 DPI)
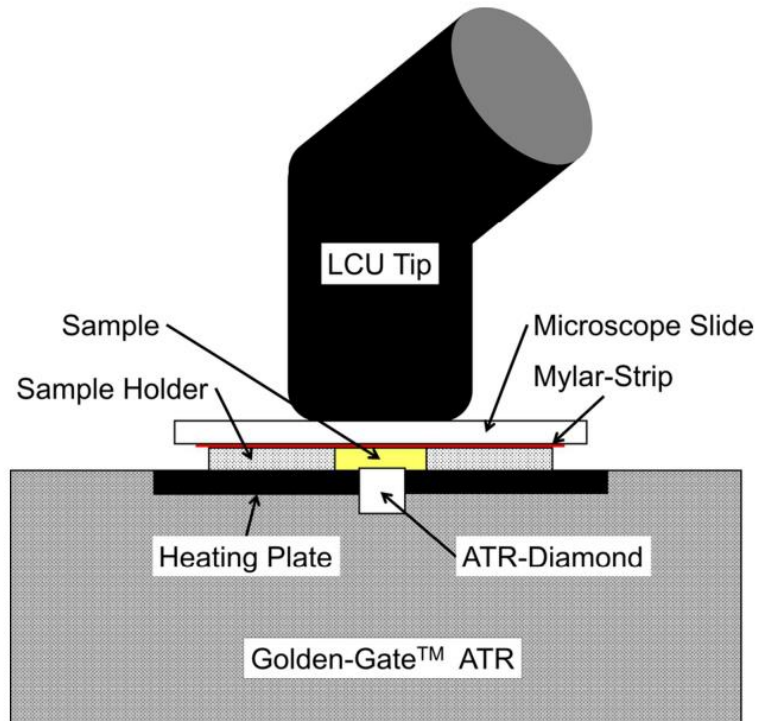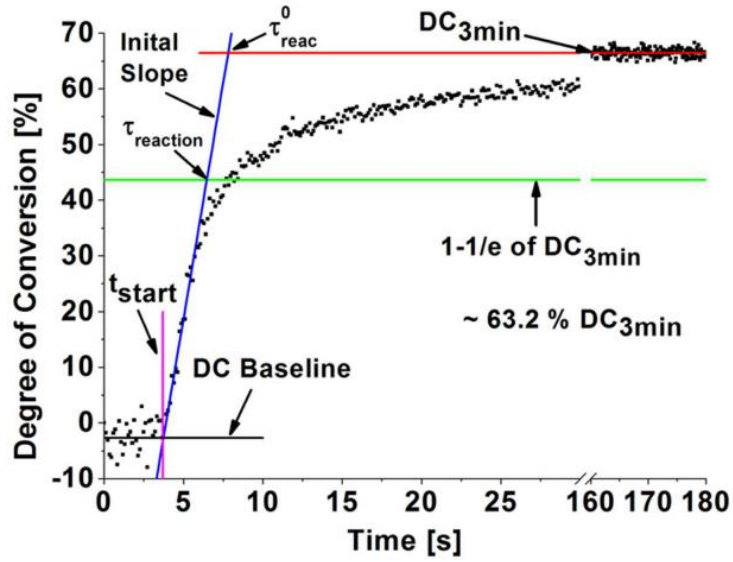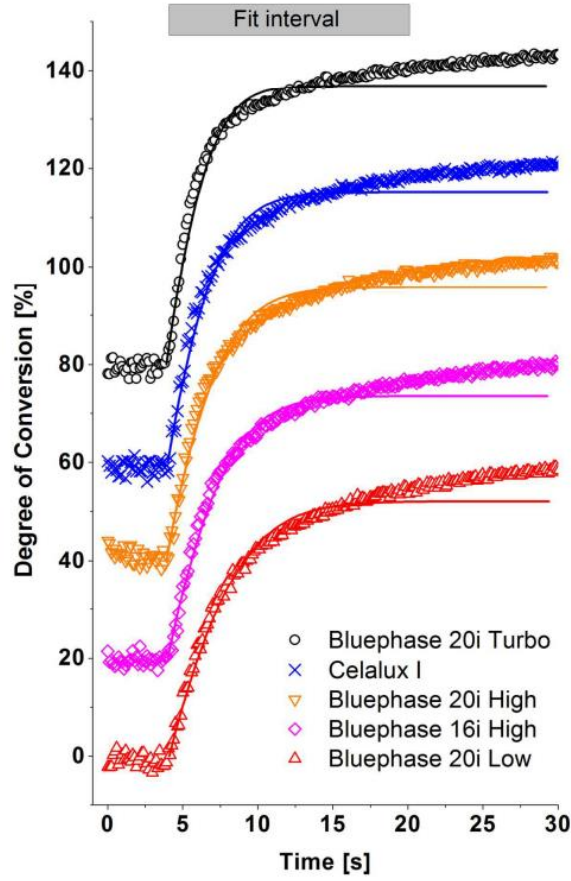
1
2
3
4
5
6
7
8
9
10
11
12
13
14
15
16
17
18
19
20
21
22
23
24
25
26
27
28
29
30
31
32
33
34
35
36
37
38
39
40
41
42
43
44
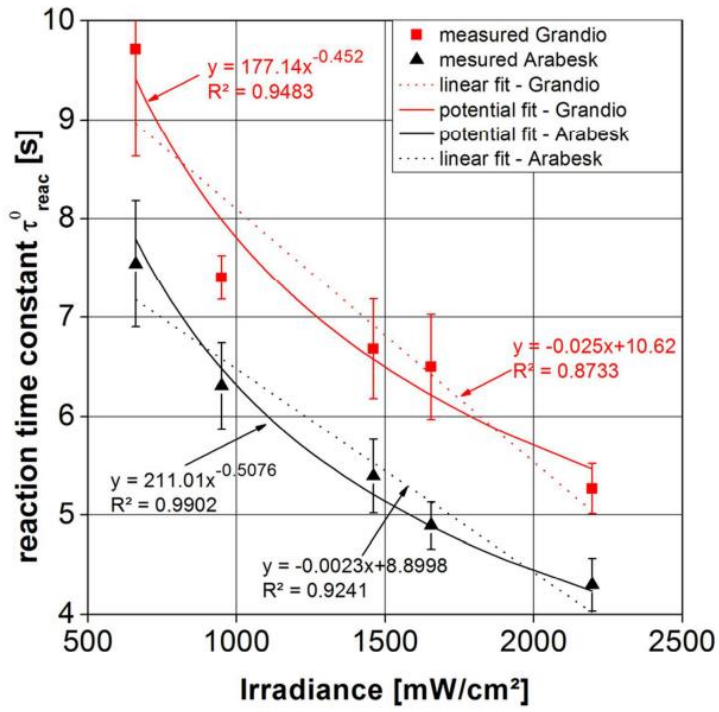45
46
47
48
49
50
51
52
53
54
55
56
57
58
59
60
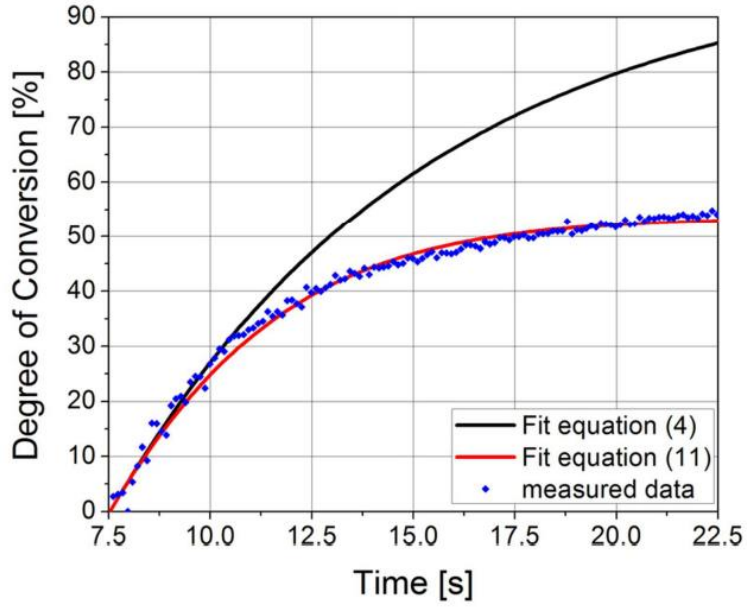
Comparison of fit curves using equation (4) – black line – and equation (11) – red line – to measured data –
symbols
Figure 5
72x61mm (300 x 300 DPI)

118

PAPER III

Examining exposure reciprocity in a resin based composite using high irradiance levels and real-time degree of conversion values

Daniela Selig [a,b,c], Thomas Haenel [a,b,d,e], Berenika Hausnerová [d,e], Bernhard Moeginger [b], Daniel Labrie [f], Braden Sullivan [a], Richard B.T. Price [a,*]

[a] Dalhousie University, Department of Dental Clinical Sciences, Faculty of Dentistry, Halifax, Canada
[b] Bonn-Rhein-Sieg University of Applied Sciences, Department of Natural Sciences, Rheinbach, Germany
[c] FH Aachen University of Applied Sciences, Department of Natural Sciences, Jülich, Germany
[d] Tomas Bata University in Zlin, Faculty of Technology, Department of Production Engineering, Zlin, Czech Republic
[e] Tomas Bata University in Zlin, University Institute, Centre of Polymer Systems, Zlin, Czech Republic
[f] Dalhousie University, Department of Physics and Atmospheric Sciences, Halifax, Canada

ARTICLE INFO

ABSTRACT

Objective. Exposure reciprocity suggests that, as long as the same radiant exposure is delivered, different combinations of irradiance and exposure time will achieve the same degree of resin polymerization. This study examined the validity of exposure reciprocity using real time degree of conversion results from one commercial flowable dental resin. Additionally a new fitting function to describe the polymerization kinetics is proposed.

Methods. A Plasma Arc Light Curing Unit (LCU) was used to deliver 0.75, 1.2, 1.5, 3.7 or 7.5 W/cm^2 to 2 mm thick samples of Tetric EvoFlow (Ivoclar Vivadent). The irradiances and radiant exposures received by the resin were determined using an integrating sphere connected to a fiber-optic spectrometer. The degree of conversion (DC) was recorded at a rate of 8.5 measurements a second at the bottom of the resin using attenuated total reflectance Fourier Transform mid-infrared spectroscopy (FT-MIR). Five specimens were exposed at each irradiance level. The DC reached after 170 s and after 5, 10 and 15 J/cm^2 had been delivered was compared using analysis of variance and Fisher's PLSD post hoc multiple comparison tests (alpha = 0.05).

Results. The same DC values were not reached after the same radiant exposures of 5, 10 and 15 J/cm^2 had been delivered at an irradiance of 3.7 and 7.5 W/cm^2. Thus exposure reciprocity was not supported for Tetric EvoFlow ($p < 0.05$).

Significance. For Tetric EvoFlow, there was no significant difference in the DC when 5, 10 and 15 J/cm^2 were delivered at irradiance levels of 0.75, 1.2 and 1.5 W/cm^2. The optimum combination of irradiance and exposure time for this commercial dental resin may be close to 1.5 W/cm^2 for 12 s.

© 2015 Academy of Dental Materials. Published by Elsevier Ltd. All rights reserved.

---

* *Corresponding author at*: Dalhousie University, Dental Clinical Sciences, 5981 University Avenue, Halifax, NS B3H 4R2, Canada.
Tel.: +1 902 494 1226; fax: +1 902 494 1662.
E-mail address: rbprice@dal.ca (R.B.T. Price).

1. Introduction

Photo-polymerizable resin-based composites (RBCs) have become the material of choice for direct restorations [1]. The radiant exposure (RE), namely the product of irradiance and exposure time, is an important factor that determines the degree of conversion (DC) and mechanical properties of photo-polymerizable RBCs [2–7]. The RE required to adequately polymerize a 1–2 mm thick increment of RBC is considered to be between 18 and 24 J/cm^2. This is based on studies using quartz-tungsten-halogen (QTH) light-curing units (LCUs), which found that it was necessary to deliver a minimum irradiance of 300–400 mW/cm^2 for 60 s [8,9]. To obviate the need to spend 30 to 60 seconds light curing light curing each increment of RBC, high power curing lights have been introduced to reduce light exposure times and thus shorten chairside procedures. Several authors have investigated what they have described as the 'Exposure Reciprocity Law' [10–12], which proposes that there exists reciprocity between irradiance and exposure time to achieve equivalent polymerization of RBCs. Consequently, some contemporary LCUs now deliver irradiance levels up to 6 W/cm^2, which, their manufacturers' claim, can allow for very short exposure times (1–3 s) to be used [13,14]. This makes these high output LCUs attractive to dentists who wish reduce the time they spend light curing. It is possible many resins appear to follow exposure reciprocity simply because they have been cured to a high DC [12], but this does not necessarily mean that their physical properties will be the same. Depending on the rate of cure, it has been reported that some RBCs may have different physical properties even when a similar DC is achieved [12]. It has been reported that curing a resin at a higher irradiance with a shorter exposure time can increase the shrinkage stress [15]. It also results in a lower degree of cure, lower flexural strength and lower modulus than curing with a lower irradiance for a longer time [2].

It has been reported that the greater the viscosity of the RBC, the more likely it is to exhibit exposure reciprocity compared to its flowable counterpart [11]. In the very early phase of polymerization the RBC has yet to develop a polymeric network to effectively trap the radicals [12]. Thus during this phase the principle of exposure reciprocity is likely violated. Near the end of polymerization, the principle should hold because almost all of the radicals are now trapped in the glassy network. For each resin system, there appears to be an optimum rate of initiation that produces the highest quantum yield. If the initiation rate is too high, more of the generated free radicals are prematurely spent via bimolecular termination because the medium has yet to develop a polymeric network to trap these free radicals effectively. Conversely, if the initiation rate is too low, many photons may be wasted if the network has already been well established, as this network will trap and annihilate the primary radicals, preventing them from producing polymers [12,16]. When the resin receives a high irradiance, the reaction rates between production and destruction of intermediate molecular species may not be in balance, and steady-state assumptions may not hold [17].

In some cases the irradiance and exposure time can influence the polymer chain length, extent of cross-linking, and mechanical properties of the resin [2,10–12,18–22]. At high irradiance levels only short polymer chain lengths can be achieved before cross-linking occurs [18,19]. Hadis et al. [11] examined 10 RBCs and reported that a reciprocal relationship between irradiance and the exposure time was observed for five commercial paste RBCs, but only for three out of the five flowable products. They delivered a RE of 18 J/cm^2 to verify the applicability of the exposure reciprocity concept using irradiance values between 400 and 3000 mW/cm^2. Using a Fourier Transform near-infrared spectrometer (FT-NIR) in the transmission mode, the time dependent DC and rates of polymerization R_p were measured through 1.4 mm thick RBC specimens. Two of the flowable resins exhibited a lower degree of conversion when exposed to 3000 mW/cm^2 for 6 s, compared to 400 mW/cm^2 for 45 s. Using differential scanning calorimetry, Feng et al. [12] reported that for experimental resins with an oligomer/monomer mass ratio equal to or greater than 6:4, the degree of double bond conversion followed a reciprocal arrangement when low irradiance levels between 3.1 mW/cm^2 and 50 mW/cm^2 were delivered to the resins. Since most commercial dental resins are similar binary systems, containing mostly viscous oligomers, they concluded that the 'exposure reciprocity law' might also apply to dental RBCs.

The available evidence for exposure reciprocity at any irradiance level is contradictory, most likely because different research groups have used different resins, ranges of irradiance and radiant exposures to investigate this phenomenon [2,10–12,23]. One study used very low irradiance levels (3–24 mW/cm^2) to investigate the relationship between the radiant exposure and the DC [23]. Using a kinetic model, the authors reported that the polymerization kinetics should not be expected to follow the reciprocity law behavior. At these low levels, as the irradiance increased, the overall radiant exposure required to achieve full conversion also increased. The ultimate conversion did not only depend on the radiant exposure, but also on the irradiation intensity and corresponding polymerization rate [23]. Another study using irradiance levels between 50 and 1000 mW/cm^2 described a parabolic relationship between irradiance and both flexural strength and flexural modulus [2] for Tetric Ceram (Ivoclar-Vivadent, Schaan, Liechtenstein). For this RBC, the maximum flexural strength and flexural modulus occurred at an intermediate irradiance level. This relationship may be applicable to other resins [12,16]. Other reports examining the concept of exposure reciprocity have based their conclusions on properties such as the elastic modulus [5], the micro-hardness [7], or the depth of cure [10] of the resin measured at a fixed time point after light exposure that ranged from 180 s to 1 week.

Fourier Transform mid-infrared spectroscopy (FT-MIR) is often used to measure the DC of dental resins by assessing the change in ratio of characteristic absorbance peaks of the cured and uncured resin. Commonly the methacrylate aliphatic C—C double bond peak height or area at 1638 cm^{-1} is compared to the aromatic C—C double bond peak height or area at 1608 cm^{-1}. Additionally, although not commonly carried out, it is recommended that the equipment response be determined using different mixtures of known molar ratios of aliphatic to aromatic groups [24]. Depending on the irradiance level, most of the polymerization reaction occurs within the first 5 s of light exposure [23,25,26]. Previous studies have

reported DC results based on conclusions drawn from curve fitting all the data using a single fitting function [27–30], or more recently a five parameter bi-exponential fitting function [26,31]. However, these fitting functions often do not fit the DC data gathered in the first few seconds very well and this is the time period of greatest interest. Also, as these studies collected relatively few data points during the first 5 s, they were unable to accurately follow the early changes in the DC.

Currently there is no research available to support the existence of exposure reciprocity for high output lights delivering more than 3 W/cm^2, even though there are LCUs on the market that deliver 6 W/cm^2 [14]. Therefore, the use of such high output lights may introduce the risk of under-curing photo-polymerizable RBCs. Given that more than 261 million RBC restorations and sealants are placed annually [1], this could have great health and financial implications. There is good indirect evidence that under-curing a RBC restoration may result in more bulk fracture, greater wear of the restoration, or more secondary caries [8,9,32–37]. Class II restorations are especially at risk of undercuring at the gingival portion of the proximal box [38–41]. This is the region that is the most difficult to reach with the curing light and interestingly it is the region where most failures occur [42]. Under-cured dental RBCs are also more likely to leach unwanted chemicals into the mouth [43–47]. Arbitrarily increasing light exposure times in an effort to prevent under-curing is not the answer as this may cause unacceptable thermal trauma to the pulp and surrounding tissues [48–52]. Thus, both dentists and manufacturers of dental light curing units (LCU) need to know if it is appropriate to use high irradiance values of 6 W/cm^2 and above to photo-cure dental resins in a short time.

This study exposed one commercial RBC to different levels of irradiance from 0.75 to 7.5 W/cm^2 and adjusted the time to deliver similar radiant exposures. The DC was measured in real time at a rate of approximately 8.5 DC measurements a second. A new curve fitting function was developed to better address the early polymerization kinetics (primary curing) as well as the long term curing in the glassy state (post-curing). The hypothesis is that the same DC will be reached when the same radiant exposures of 5, 10 and 15 J/cm^2 has been received at irradiance levels from 0.75 to 7.5 W/cm^2.

2. Materials and methods

A flowable resin, Tetric EvoFlow (Ivoclar Vivadent, Amherst, NY, USA) shade T, from the same lot was used to make all the specimens. According to the manufacturer, Tetric EvoFlow has a resin content of 38 wt% and a total filler content of 62 wt%. The resin contains 0.25 wt% camphorquinone (CQ) and 0.4 wt% 2,4,6-trimethylbenzoyl-diphenylphosphine oxide (TPO) photo-initiators. To ensure adequate spectral overlap, the spectral emission from the LCU (Fig. 1) was compared to the relative absorbance spectrum for these two photo-initiators (obtained from Aldrich Chemical Co., Milwaukee, WI, USA) using a UV–visible spectrophotometer (Helios Alpha, Thermo Spectronic, Rochester, NY, USA).

The RBC specimens were exposed to light from a Sapphire Plus Plasma Arc LCU (DenMat, Lompoc, CA, USA) with a 4-mm diameter turbo light guide. This turbo light guide
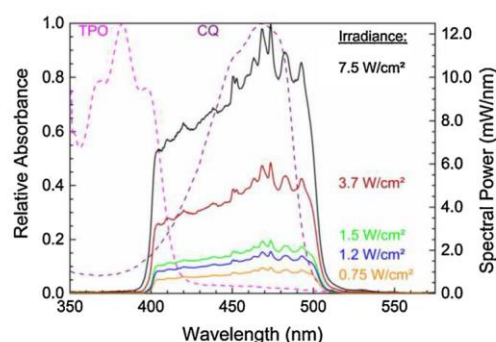
Fig. 1 – Emission spectra of the Sapphire Plus Plasma Arc LCU (right axis) at five different irradiance levels with relative absorbance spectra of TPO (magenta) and CQ (violet) measured in methyl methacrylate as a solvent (left axis).

delivered a maximum irradiance of 7.5 W/cm^2 to the RBC. To provide five different irradiance values to the RBC, the distance between the RBC and the end of the light guide was adjusted by predetermined amounts using an adjustable stage with a 0.1-millimeter vernier scale (#55024, Edmund Optics, Barrington, NJ). Five distances were used: 0 mm, 4.5 mm, 9.0 mm, 10.5 mm, and 13.5 mm. The irradiance, radiant exposure and spectral emission from the LCU at each distance were measured using an integrating sphere (Labsphere, North Sutton, NH, USA) connected to a fiber-optic spectrometer (USB 4000, Ocean Optics, Dunedin, FL, USA). There was a 4 mm aperture into the integrating sphere, which matched the diameter of the specimens and the diameter of the light guide. Thus, the sphere measured the total spectral radiant power that would be received by the specimens at each distance. This fiber-optic system was calibrated before the experiment using the internal reference lamp contained within the sphere. Spectrasuite v2.0.162 software (Ocean Optics) was used to collect and analyze the data.

Fig. 2 illustrates how the DC at the bottom of the specimens was measured before, during and after light exposure using Fourier Transform mid-infrared (FT-MIR) spectroscopy. The spectrometer (Tensor 27, Bruker, Billerica, MA, USA) was equipped with a temperature controlled attenuated total reflectance (ATR) unit (Golden Gate, Specac, Orpington, Kent, UK) containing a single reflection monolithic 2.0 mm × 2.0 mm diameter diamond prism with a 0.8 mm diameter active sampling area. Prior to the start of the experiment, mixtures with known molar ratios of aliphatic to aromatic groups were prepared using a technique previously described to calibrate the equipment [24]. These mixtures were made from TEGDMA (Sigma Aldrich, St. Louis, MO, USA), BisGMA (Sigma Aldrich), bisphenol-A-diglycidylether (Sigma Aldrich) and hydrogenated BisGMA (provided by Dr. J. Stansbury). These mixtures were measured using the FT-MIR equipment used in this study. A second order polynomial relationship with an excellent degree of correlation (R^2) of 0.999 between

the molar ratio and the absorption ratio was achieved using Eq. (1).

2.1. Equation 1: Degree of conversion

$$DC_{exp} = 100\% \times \left[1 - \frac{0.141 \left(\frac{Abs_{Aliphatic}}{Abs_{Aromatic}} \right)^2_{Polymer} + 1.1424 \left(\frac{Abs_{Aliphatic}}{Abs_{Aromatic}} \right)_{Polymer}}{0.141 \left(\frac{Abs_{Aliphatic}}{Abs_{Aromatic}} \right)^2_{Monomer} + 1.1424 \left(\frac{Abs_{Aliphatic}}{Abs_{Aromatic}} \right)_{Monomer}} \right] \quad (1)$$

where $Abs_{Aliphatic}$ and $Abs_{Aromatic}$ are the absorbances of the aliphatic and aromatic double bonds of polymer and monomer, respectively.

The specimens of Tetric EvoFlow were prepared in 2 mm thick aluminum rings with an inner diameter of 4 mm, which matched the diameter of the light guide and the aperture into the integrating sphere. A 50 μm thick Mylar Strip (Patterson, Montreal, Quebec, Canada) covered the top surface of the uncured composite. The uncured RBC was allowed to stabilize by resting on the temperature controlled ATR for 2 min in the dark before light curing. Based on a pilot study, this was sufficient time to achieve a stable temperature of 30 °C. Five specimens ($n = 5$) were irradiated at each irradiance level for 3 s, 6 s, 12 s, 15 s, and 23 s according to the digital timer of the LCU.

The DC was determined as follows:

1. Mid-IR data collection was started at a rate of approximately 8.5 measurements per second to determine the baseline of the uncured RBC.
2. After 10 s, the LCU was switched on for the predetermined time.
3. Data were collected for 170 s after the start of light exposure to determine the DC both during and after light exposure [11].
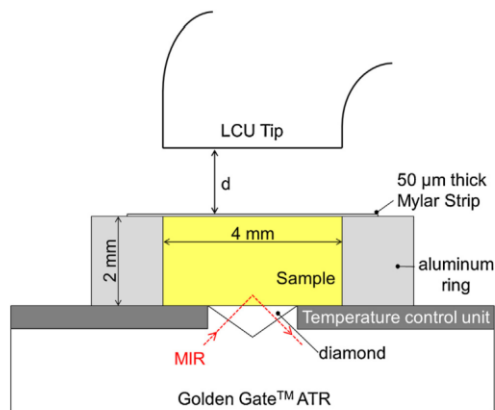
Fig. 2 – Schematic of equipment used for the Fourier Transform mid-infrared (FT-MIR) spectroscopy with the temperature controlled attenuated total reflectance (ATR) unit. ↔ describes the variable distance between the RBC and LCU tip.

The spectrometer acquired all spectra at a resolution of 8-wavenumbers. For each data point, the forward and backward scans of six interferograms were resolved and averaged. This procedure achieved a final acquisition rate of 8.5 DC points per second. The last 20 data points of each FT-MIR run, corresponding to a time range of approximately 2.4 s, were averaged to determine the static DC_{exp} at 170 s for each light exposure protocol.

Using Eq. (1), the DC values at any given time were calculated using the aliphatic carbon–carbon double bond peak at 1638 cm^{-1} ($Abs_{Aliphatic}$) and the aromatic carbon–carbon double bond peak at 1608 cm^{-1} ($Abs_{Aromatic}$). The area of each peak was calculated using a straight baseline between the minima on either side of the peak. The Bruker Opus software v.6.5 used a proprietary concave rubber band baseline correction with five iterations.

From the calculated DC results, a new fitting function given by Eq. (2) was developed. This equation consists of two factors describing the two curing processes. The first factor takes into account the primary curing phase from the liquid resin up to the glass transition, or vitrified state, and is an exponential function. The second factor takes into account the slow post-curing processes that occur in the glassy state and is a logarithmic function.

2.2. Equation 2: Fitting function

$$DC(t) = \underbrace{\left(1 - \exp\left(-\frac{t - t_{LCU}}{\tau^0_{reac}} \right) \right)}_{primary\ curing} * A * \underbrace{\left(1 + B * \ln \frac{t}{t_{LCU}} \right)}_{post\text{-}curing} \quad (2)$$

where τ^0_{reac} is the reaction time constant of the primary curing reaction, the fitting parameter A can be interpreted as the achievable DC of the primary curing, and the fitting parameter B describes the further increase of DC due to post-curing reactions. The fitting procedure starts at the time t_{LCU}, when the LCU was turned on. To provide standard deviations (SD) for the parameters τ^0_{reac}, A and B, each DC(t) curve of a light exposure protocol was fitted individually with Eq. (2) using the Excel solver tool (Microsoft, Redmond, WA, USA). Since primary curing predominates during the first few seconds of light exposure, highly resolved DC data are required. The fitting procedure of the DC curves was performed in three steps:

i) To determine the reaction time constant τ^0_{reac} in the liquid state, the primary curing data were fitted for the first few seconds during the rapid increase of DC while the post-curing data were disregarded.
ii) The fit was repeated for the time range 0–170 s to determine the parameters A and B while the reaction time constant τ^0_{reac} determined in step 1 was kept constant.
iii) Steps 1 and 2 provide the start values for the last fit in which all three parameters were finally determined.

To demonstrate the performance of Eq. (2), it was compared to two other fitting functions, a single exponential with three parameters (Eq. (3)) and a double exponential with five parameters according to Ilie et al. [31] (Eq. (4)).

2.3. Equation 3: A single exponential fitting function with three parameters

$$DC(t) = A + B * \exp\left(-\frac{t - t_{LCU}}{\tau_{reac}^{0}}\right) \qquad (3)$$

2.4. Equation 4: A double exponential with five parameters [31]

$$DC(t) = A + B * \exp\left(-\frac{t - t_{LCU}}{\tau_{reac}^{0}}\right) + D * \exp\left(-\frac{t - t_{LCU}}{\tau_{reac}^{1}}\right) \qquad (4)$$

where τ_{reac}^{0} is the reaction time constant of the primary curing and τ_{reac}^{1} is the reaction time constant of the post-curing. The fitting parameters A, B and D can be interpreted as maximum DC, extent of primary curing and extent of post-curing.

When the DC values were related to the RE (J/cm^2), a 7-point adjacent average smoothing function was used (Origin Pro v9.0, OriginLab, Northampton, MA, USA). Outlier tests (Grubbs test, $\alpha = 0.05$) were performed to compare the DC$_{exp}$ values at 170 s of the five specimens made at each irradiance level. They confirmed that the raw DC$_{exp}$ results could be compared to the DC$_{fitted}$ values. The mean DC$_{exp}$ values achieved at the time in which the resin received a RE of 5, 10 and 15 J/cm^2, respectively, and the final DC value measured at 170 s were compared using a one way analysis of variance (ANOVA) test followed by the post hoc Fisher's protected least significant difference (PLSD) test ($\alpha = 0.05$) with the corresponding light exposure protocol as the independent variable.

3. Results

Table 1 reports the exposure time, the distance from the light tip to the RBC, the irradiance, and radiant exposure for the five different light exposure protocols. Upon completion of the study, the LCU timer was found to be imprecise and it was also noted that the output from the LCU was not constant during exposure (Supplemental Fig. 1). After repeating the measurements five times, it was determined that the RBC specimens had been exposed to light for a mean of 2.6 s at a distance of 0 mm, 5.7 s at 4.5 mm, 11.7 s at 9.0 mm, 14.7 s at 10.5 mm, and 22.5 s at 13.5 mm (Table 1). Fig. 1 displays the emission spectra from the LCU at the five different irradiances. The spectral emission was relatively uniform for wavelengths
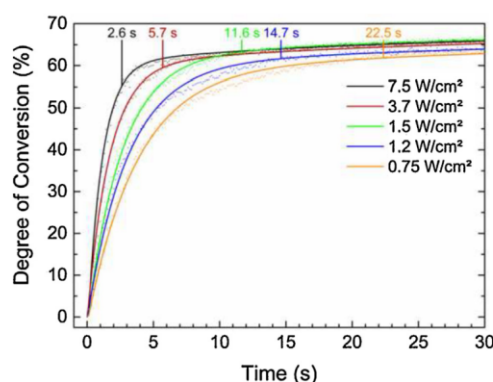
Fig. 3 – Time dependent measured DC$_{exp}$ and fitted DC$_{fit}$ curves of Tetric EvoFlow shown for the first 30 s when exposed to irradiance levels of 0.75, 1.2, 1.5, 3.7 and 7.5 W/cm^2. The times when the LCU turned off are indicated on each curve.

from 400 to 500 nm, and covered the CQ absorbance spectrum. The emission covered only a small part of the absorption spectrum of TPO because the majority of its absorbance is in the ultra-violet region below 400 nm.

Supplementary Fig. 1 related to this article can be found, in the online version, at http://dx.doi.org/10.1016/j.dental.2015.02.010.

When Eqs. (2) and (4) were applied to a set of data, they provided an excellent fit of the measured DC(t). Both fitting curves coincide almost completely with the data points while it can be seen that Eq. (3) provides an unsatisfactory fit (Supplemental Fig. 2). Of note, Eq. (2) requires only three fitting parameters and it provides a better fit with respect to the error sum (Table 2). Due to its design, Eq. (2) always determines a DC of zero for $t = t_{LCU}$, which is not the case for Eq. (4). This is necessary because there is no reaction at the precise moment when the LCU is turned on.

Supplementary Fig. 2 related to this article can be found, in the online version, at http://dx.doi.org/10.1016/j.dental.2015.02.010.

Fig. 3 shows both the measured DC points (DC$_{exp}$) and the fitted (DC$_{fit}$) time dependent DC curves of Tetric EvoFlow for the first 30 s when exposed to the five irradiance levels of 0.75, 1.2, 1.5, 3.7 and 7.5 W/cm^2. The initial slopes of the DC(t) curve increase with increasing irradiance levels. For all light exposure protocols, the fitting function represented by

Table 1 – Mean exposure time, distance to sample, irradiance and calculated radiant exposure as determined using the real time measurements made with the spectrometer.			
Mean exposure time (s)	Distance to RBC (mm)	Mean irradiance (W/cm^2)	Mean radiant exposure (J/cm^2)
2.6 (0.3)	0	7.5 (0.8)	19.6 (2.2)
5.7 (0.2)	4.5	3.7 (0.2)	21.1 (0.7)
11.7 (0.2)	9.0	1.5 (0.1)	17.4 (0.3)
14.7 (0.1)	10.5	1.2 (0.1)	17.5 (0.2)
22.5 (0.2)	13.5	0.75 (0.1)	16.7 (0.2)

Table 2 – Comparison of the fit parameters determined by Eqs. (2)–(4) with t_{LCU} = 1 s.

Parameter	Unit	Single exponential – Eq. (3) $DC(t) = A + B \times e^{-\frac{t-t_{LCU}}{\tau_{reac}^0}}$					Double exponential – Eq. (4) $DC(t) = A + B \times e^{-\frac{t-t_{LCU}}{\tau_{reac}^0}} + D \times e^{-\frac{t}{\tau_{reac}^1}}$					Single exponential and logarithmic – Eq. (2) $DC(t) = \left(1 - e^{-\frac{t-t_{LCU}}{\tau_{reac}^0}}\right) \times A \times \left(1 + B \times \ln\frac{t}{t_{LCU}}\right)$				
Irradiance (mW/cm²)		7500	3700	1500	1200	750	7500	3700	1500	1200	750	7500	3700	1500	1200	750
τ_{reac}^0	s	1.89	2.93	4.00	4.62	5.98	1.13	1.85	2.61	3.04	3.92	0.89	1.60	2.28	2.66	3.44
A	1	0.66	0.68	0.69	0.67	0.66	0.71	0.71	0.72	0.70	0.70	0.54	0.55	0.55	0.53	0.51
B	1	−0.56	−0.60	−0.61	−0.59	−0.59	−0.589	−0.608	−0.620	−0.597	−0.591	0.055	0.054	0.058	0.060	0.069
D	1	–	–	–	–	–	−0.103	−0.094	−0.098	−0.097	−0.104	–	–	–	–	–
τ_{reac}^1	s	–	–	–	–	–	101.2	65.2	69.6	72.1	76.8	–	–	–	–	–
Error sum		7149	5920	5664	5098	5051	158.4	28.5	19.8	14.8	10.4	19.7	7.1	3.9	2.9	2.2
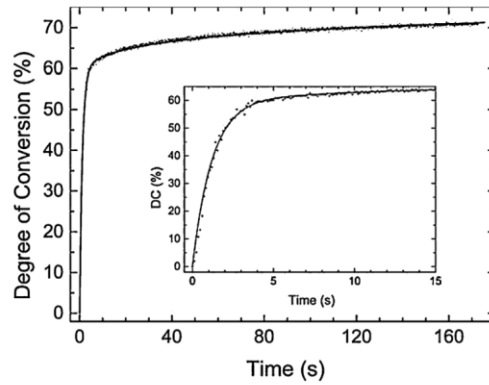
Fig. 4 – Mean DC(t) curves of five specimens exposed to the highest irradiance level (7.5 W/cm²) for the entire 170 s after the start of light exposure, with the first 15 s also shown on a larger scale in the insert. The measured data (dots) and fitted data (solid line) according to Eq. (2); degree of correlation $R^2 = 0.995$.

Eq. (2) provided an excellent correlation to the experimental data with correlation coefficients (R^2) between 0.995 and 0.996. To demonstrate this, Fig. 4 shows the DC(t) curve of the specimens exposed to the highest irradiance level (7.5 W/cm²) for the entire 170 s after the start of light exposure, with the first 15 s also shown on a larger scale in the insert. The three parameters: "reaction time constant τ_{reac}^0", "parameter A", and "parameter B" are reported in Table 3 together with the product $A \times B$ being a measure of the DC increase in the post-curing range.

Table 3 shows that the reaction time constant τ_{reac}^0 decreases when the irradiance levels increase. Fig. 3 shows that the primary curing reaction lasts between 2 and 8 s depending on the irradiance level and a DC of 0.5 (50%) is achieved after approximately 8 s even for the lowest irradiance level. The mean values of the achievable DC of primary curing expressed by parameter A decrease from 0.601 (60.1%) to 0.555 (55.5%) with decreasing irradiance level (Table 3). After the end of primary curing the DC is further increased by slow post-curing processes which are quantified by parameter B. Its values increase from 0.055 (5.5%) to 0.068 as the irradiance decreased.

The five light exposure protocols delivered similar total radiant exposures (RE) to the specimens, but over different exposure times. Table 4 reports the static DC_{exp} and the DC_{fit} at 170 s. The static DC_{exp} (170 s) values ranged between 68.5% and 71.1%. The one way ANOVA reported no significant differences in the five DC results, although there was a small decrease of the mean DC_{exp} (170 s) when 0.75 and 1.2 W/cm² were delivered.

Fig. 5 shows the achieved DC versus the corresponding time dependant RE received in real time by the RBC at each irradiance level up to 17 J/cm². Table 5 shows that within the accuracy of the measurement expressed by the standard
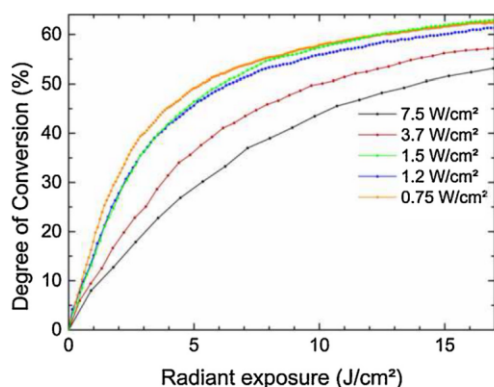
Fig. 5 – Real time DC as a function of radiant exposure (J/cm²) delivered at irradiance levels of 0.75, 1.2, 1.5, 3.7 and 7.5 W/cm².

deviation (SD) of the results, the specimens exposed to irradiance levels of 1.5, 1.2 and 0.75 W/cm² exhibited the same radiant exposure dependency on the DC achieved ($p > 0.05$, Fisher's PLSD). Fig. 5 illustrates that the same degree of conversion was not reached at the point that the same radiant exposures had been delivered for irradiance levels of 3.7 W/cm² and 7.5 W/cm² ($p < 0.05$, Fisher's PLSD) and, as the irradiance increased above 1.5 W/cm², the DC decreased significantly ($p < 0.05$, Fisher's PLSD).

4. Discussion

This study is the first to examine the effect on polymerization of high irradiance values, similar to those from LCUs now on the market [14], using mid-IR spectroscopy collected at 8.5 data points a second. It shows that, using static end point results (at 170 s), the same DC was reached if similar radiant exposures (RE) were delivered using the five irradiance levels. This supports the assumption that many resins will appear to follow exposure reciprocity simply because they have received a high RE and, consequently, have been cured to a high DC [12]. This is partly contrary to the results reported by Wydra et al. [23] who reported that the RE required to achieve full conversion also increased if the irradiation intensity is increased. However, that study used a data collection rate of two scans a second and very low irradiance levels (3–24 mW/cm²). Unlike previous studies that collected only a few data points during the first few seconds [10,23,26–31,53], the present study collected data in real time at a rate of approximately 8.5 DC measurements a second using the average of the forward and backward scans of six interferograms at each time point. When looking at these real time DC results (Fig. 5), it is evident that, although the final static DC (170 s) values are the same for all irradiance values, exposure reciprocity did not exist at the higher irradiance levels of 3.7 and 7.5 W/cm² during the early curing process up to the point where 17 J/cm² was delivered. This supports the

results reported by Wydra et al. [23]. At these high irradiance levels, the irradiation times are short and the initial lag time before the start of free radical initiation plays an important role when assessing exposure reciprocity. Thus, the hypothesis that the same DC will be reached when the same radiant exposure (RE) is delivered by all five different irradiance levels between 0.75 and 7.5 W/cm² was rejected.

4.1. Fitting function

Ilie et al. [26,31] has reported in a study of the kinetics of resin curing that the sum of two exponential functions with five parameters, Eq. (4), could provide a better fit than a single exponential function with three parameters, Eq. (3), for data collected at a rate of 2 DC values per second. According to their interpretation, the first exponential term describes the curing of the resin and the second exponential term describes the curing processes in the gel and the glassy states. However, Eqs. (3) and (4) provide a DC > 0 for $t = t_{LCU}$ (Table 2). This means that something is amiss with the fitting function, the fitting procedure, or the data, e.g. too much scatter or insufficient time resolution.

In this study, a new fitting function, Eq. (2), is proposed to describe the curing kinetics of commercial dental RBC. This new fitting function consists of two factors. The first factor of Eq. (2) describes the primary curing process of the resin and has an exponential time dependency. The second term of the Eq. (2) accounts for the post-curing reactions in the glassy state and has a logarithmic time dependency [54,55]. As shown in Eq. (2) there are three fitting parameters τ_{reac}^0, A and B. The parameter t_{LCU} is determined experimentally and represents the moment when the LCU is turned on. The parameter $1/\tau_{reac}^0$ is a measure of the reaction constant and corresponds to the initial slope of the DC(t) curve. The reaction time constant τ_{reac}^0 characterizes the reaction kinetics of the primary curing process and it defines the time in which 63% of the monomers are consumed during the polymerization process. After $3\,\tau_{reac}^0$, 95% of the reaction has happened and the exponential approaches zero, meaning that the reaction is ending because all consumable monomers have been polymerized during the primary curing. The DC would approach "1" (or 100%) unless deceleration processes limit the DC of the primary curing to a value which is given by the parameter "A". These deceleration processes are related to the immobilization of resin monomers and the polymer chain segments that occur when the liquid resin transfers into gel and then into the vitrified glassy state. Interestingly, the parameter A does not change significantly within the range of irradiance levels used and can be considered to be constant. This means that primary curing ends at a DC value w, which is between 55% and 60% for Tetric EvoFlow.

With decreasing irradiance level the reaction time constant τ_{reac}^0 increases from 1.07 s for an irradiance of 7.5 W/cm² to 3.52 s for an irradiance of 0.75 W/cm² (Table 2). Thus, the primary curing phase lasts between 3.3 and 10.5 s depending on the irradiance levels. After the primary curing phase, post-curing processes caused by trapped resin monomers and un-reacted chain segments are responsible for structural changes leading to a further increase of DC having the following logarithmic time dependency.

Table 3 – Mean fitting parameters according to Eq. (2) of the DC(t) curves with the correlation coefficients (R^2) at the five different irradiance levels.

Mean exposure time (s)	Mean irradiance (W/cm^2)	Reaction time constant τ_{reac}^0 (s)	Parameter A	Parameter B	Product A × B	R^2
2.6 (0.3)	7.5 (0.8)	1.07 (0.13)	0.593 (0.20)	0.0544 (0.0040)	0.0325	0.995
5.7 (0.2)	3.7 (0.2)	1.61 (0.18)	0.588 (0.39)	0.0563 (0.0066)	0.0331	0.995
11.7 (0.2)	1.5 (0.1)	2.47 (0.29)	0.601 (0.019)	0.0518 (0.0093)	0.0311	0.996
14.7 (0.1)	1.2 (0.1)	2.91 (0.11)	0.577 (0.11)	0.0557 (0.0051)	0.0321	0.996
22.5 (0.2)	0.75 (0.1)	3.51 (0.39)	0.555 (0.012)	0.0679 (0.0024)	0.0377	0.995

4.2. Equation 5: Post-curing fitting function

$$DC_{post-curing}(t) = A \times \left(1 + B \times \ln \frac{t}{t_{LCU}}\right)$$
$$= A + A \times B \times \ln \left(\frac{t}{t_{LCU}}\right) \tag{5}$$

The first term A on the right side of the equation represents the DC generated by primary curing. The second term describes the kinetics of post-curing phase. Its time dependency is determined by the product of A and B, which is relatively constant with values between 0.031 and 0.037 (Table 3). The mean value of parameter B seems to exhibit a weak irradiance dependency, possibly due to thermal effects caused by different irradiance levels. Even with a slightly higher mean value of 0.068 at the lowest irradiance of 0.75 W/cm^2, the other four values were between 0.052 and 0.056. Thus parameter B could also be considered to be a constant. The assumption "The parameters A and B are constant" has the consequence that the curing kinetics are determined only by the reaction time constant τ_{reac}^0 and thus by the primary curing. The post-curing is then only added on the primary curing and does not depend on the irradiance delivered. However, this assumption should be investigated further using other light activated RBCs and over longer measurement times.

The concept of exposure reciprocity assumes that the DC will be identical if the same amount of radiant exposure is delivered to the RBC [4,10–12]. In the very early stages of polymerization, the principle of exposure reciprocity is unlikely to be followed because a bimolecular process terminates most of the free radicals and a more reactive and viscous monomer is required to rapidly reach the pseudo-first order stage in the polymerization reaction [12]. Then later, exposure reciprocity may occur because the monomolecular pathway immobilizes almost all of the radicals. Consequently, the lack of exposure

reciprocity may only be apparent when low REs are delivered, or in the first few seconds of light exposure. This supposition is supported by Fig. 5 and the observation that the static DC$_{exp}$ (170 s) values do not differ significantly, although there was a small decrease of the mean DC$_{exp}$ (170 s) values at the lower irradiance levels of 0.75 and 1.2 W/cm^2 (Table 3). This result illustrates the limitations of using static DC values instead of collecting multiple DC values within the first few seconds of light exposure to characterize the effect of different irradiances if more than sufficient RE is delivered.

This study cannot provide a model for the vitrification process because the DC(t) curves, which are determined by the concentration of aliphatic double bonds, do not contain any information about the molecular mobility of the growing polymer chains in a resin environment. However, Fig. 3 shows that high irradiance levels (>3 W/cm^2) lead to a very fast increase in the DC of the resin, although this increase is insufficient to initially maintain reciprocity. The greater increase in DC at the higher irradiance levels can be explained by the very high generation rate of radicals and the initial decrease in viscosity as the temperature increases [29,53,55,56]. These radicals continue to cross-link at the higher temperature such that the DC$_{exp}$ values of ~70% achieved by all five irradiance levels after 170 s were not significantly different. The commercial flowable RBC used in the present study contains a TPO/CQ-amine photo-initiator system and more trapped radicals are produced by the use of a multiple initiator system. This may account for the greater post-curing increase at higher irradiance levels especially at 7.5 W/cm^2 (as shown in Fig. 3) because TPO shows a high molar absorptivity [57,58]. TPO also has a shortened intermediate step leading to a faster initiation progress compared to CQ.

For this flowable RBC, the post-curing effects compensated for differences in the irradiance level within 3 min after light exposure when the radiant exposure exceeded 17 J/cm^2. On the other hand, the DC values reported in Table 4 and the real time degree of conversion/radiant exposure curves in Fig. 5

Table 4 – Mean measured DC$_{exp}$ and fitted DC$_{fit}$ values measured at 170 s with standard deviation (SD) when Tetric EvoFlow was exposed at the five different irradiance levels. There was no significant difference in the DC values measured at 170 s.

Exposure time (s)	Mean irradiance (W/cm^2)	Mean calculated radiant exposure (J/cm^2)	DC$_{exp}$ (170 s) (%)	DC$_{fit}$ (170 s) (%)
2.6 (0.3)	7.5 (0.8)	19.6 (2.2)	70.9 (2.1)	71.0 (2.4)
5.7 (0.2)	3.7 (0.2)	21.1 (0.7)	70.2 (3.7)	70.5 (4.1)
11.7 (0.2)	1.5 (0.1)	17.4 (0.3)	71.1 (2.7)	71.1 (3.2)
14.7 (0.1)	1.2 (0.1)	17.5 (0.2)	69.0 (1.2)	69.0 (1.3)
22.5 (0.2)	0.75 (0.1)	16.7 (0.2)	68.5 (1.6)	68.9 (1.7)

Table 5 – Mean measured DC_{exp} with standard deviation (SD) when Tetric EvoFlow received 5, 10 and 15 J/cm² at the five different irradiance levels.

Mean exposure time (s)	Mean irradiance (W/cm²)	DC @ (5 J/cm²) (%)	DC @ (10 J/cm²) (%)	DC @ (15 J/cm²) (%)
2.6 (0.3)	7.5	27.6 (2.4)	43.4 (2.3)	50.7 (2.5)
5.7 (0.2)	3.7	37.3 (3.1)	50.2 (3.1)	56.4 (3.8)
11.6 (0.2)	1.5	47.1 (2.7)[a,b]	57.7 (2.8)[a]	61.4 (2.8)[a]
14.6 (0.2)	1.2	46.8 (0.9)[a]	56.2 (1.2)[a]	60.2 (1.3)[a]
22.4 (0.2)	0.75	49.8 (1.4)[b]	58.3 (1.6)[a]	61.9 (1.5)[a]

ANOVA test of DC_{exp} (radiant exposure of 5 J/cm²): means are significantly different ($p > 0.05$):

	DF	Sum of squares	Mean square	F value		p value
Energy	4	1698.132	424.533	83.474		<.0001
Residual	20	101.716	5.086			

ANOVA test of DC_{exp} (radiant exposure of 10 J/cm²): means are significantly different ($p > 0.05$):

	DF	Sum of squares	Mean square	F value		p value
Energy	4	800.703	200.176	38.087		<.0001
Residual	20	105.116	5.256			

ANOVA test of DC_{exp} (radiant exposure of 15 J/cm²): means are significantly different ($p > 0.05$):

	DF	Sum of squares	Mean square	F value		p value
Energy	4	439.015	109.754	16.809		<.0001
Residual	20	130.589	6.529			

Post hoc Fisher's PLSD: similar superscript letters a, b indicate no significant difference in mean values within the column ($p > 0.05$).

illustrate that Tetric EvoFlow did not reach the same DC for all five irradiance levels when the REs below 17 J/cm² were delivered. Thus, the real time exposure reciprocity does not hold for the higher irradiance levels of 3.7 and 7.5 W/cm², but it seems to hold for irradiance levels from 0.75 to 1.5 W/cm². This suggests that this commercial RBC may have a window of irradiance and exposure time for which exposure reciprocity holds. Based on the RE dependent DC results shown in Fig. 5, an irradiance level of approximately 1.5 W/cm² for 12 s seems to be a good compromise with respect to exposure time for this RBC. This supports the concept that there is an optimum rate of initiation that produces the highest quantum yield and if the initiation rate is too high, many of the free radicals that are generated are prematurely spent via bimolecular termination. Further study is required to determine if other commercial RBCs have windows of irradiance and exposure times in which exposure reciprocity holds.

Based on the LCU timer, the exposure times should have been 3.0 s, 6.0 s, 12.0 s, 15.0 s, and 23.0 s, but when the exposure times were recorded with the integrating sphere-fiberoptic spectrometer measurement system the timer was found to be imprecise. Timing errors of 0.3–0.5 s found in this study would have minimal impact on a 20 s exposure time, but these errors will have a greater impact on short exposure durations both in research and in the dental office. Short irradiation times will require greater accuracy in the positioning of the LCU by the dentist over the resin and more accurate timers on the LCU. Future studies should not rely upon the timer on the LCU. Instead the exposure times and the actual RE received by the specimen should be measured in real time.

In this study, the authors worked closely with the manufacturer of the FT-MIR equipment (Bruker) to find the best method to achieve a low scatter of the data in the order of

1–2%. Therefore, the DC(t) curves reproduced by the fitting function show correlation coefficients (R^2) that were always greater than 0.995 using only a three parameter fitting function. In comparison, Ilie et al. [31] used a fitting function with two exponential terms having a five parameter fitting function and yet achieved lower correlation coefficients (R^2) that were between 0.68 and 0.93. This was partly attributed to the 10% or more scatter in their data. As the reaction rate is very fast in the liquid phase, the effects of different irradiance levels on early differences in the reaction rate require a faster data collection rate compared to previous studies that collected 'real time' data at a rate of 1 [29,30], 2 to 3 scans a second [10,23,26,27,31,53,28]. Now that it is possible to collect highly time resolved mid-IR data, the reasons for the deviation from exposure reciprocity at higher irradiance levels and the effects of delivering lower overall, but clinically relevant, REs on exposure reciprocity require further study.

5. Conclusion

Within the limitations of this study that used one commercial flowable RBC, the results confirms previous reports that, provided the RBC receives an amount of RE that is more than sufficient (17+J/cm²), then the static DC values measured at 170 s will support the principle of exposure reciprocity. However, the same degree of conversion was not reached at the point that the same radiant exposures had been delivered for irradiance levels of 3.7 W/cm² and 7.5 W/cm² ($p < 0.05$, Fisher's PLSD). Thus the principle of exposure reciprocity was not supported above 1.5 W/cm² and the research hypothesis was rejected. Dentists should be cautious when using irradiance

levels above 1.5 W/cm^2 with correspondingly shorter exposure times.

Acknowledgements

REFERENCES

[1] Heintze SD, Rousson V. Clinical effectiveness of direct class II restorations – a meta-analysis. J Adhes Dent 2012;14:407–31.

[2] Peutzfeldt A, Asmussen E. Resin composite properties and energy density of light cure. J Dent Res 2005;84:659–62.

[3] Emami N, Soderholm KJ. How light irradiance and curing time affect monomer conversion in light-cured resin composites. Eur J Oral Sci 2003;111:536–42.

[4] Halvorson RH, Erickson RL, Davidson CL. Energy dependent polymerization of resin-based composite. Dent Mater 2002;18:463–9.

[5] Sakaguchi RL, Ferracane JL. Effect of light power density on development of elastic modulus of a model light-activated composite during polymerization. J Esthet Restor Dent 2001;13:121–30.

[6] Emami N, Soderholm KJ, Berglund LA. Effect of light power density variations on bulk curing properties of dental composites. J Dent 2003;31:189–96.

[7] Price RB, Felix CA, Andreou P. Effects of resin composite composition and irradiation distance on the performance of curing lights. Biomaterials 2004;25:4465–77.

[8] Rueggeberg FA, Caughman WF, Curtis Jr JW. Effect of light intensity and exposure duration on cure of resin composite. Oper Dent 1994;19:26–32.

[9] Fan PL, Schumacher RM, Azzolin K, Geary R, Eichmiller FC. Curing-light intensity and depth of cure of resin-based composites tested according to international standards. J Am Dent Assoc 2002;133:429–34.

[10] Leprince JG, Hadis M, Shortall AC, Ferracane JL, Devaux J, Leloup G, et al. Photoinitiator type and applicability of exposure reciprocity law in filled and unfilled photoactive resins. Dent Mater 2011;27:157–64.

[11] Hadis M, Leprince JG, Shortall AC, Devaux J, Leloup G, Palin WM. High irradiance curing and anomalies of exposure reciprocity law in resin-based materials. J Dent 2011;39:549–57.

[12] Feng L, Suh BI. Exposure reciprocity law in photopolymerization of multi-functional acrylates and methacrylates. Macromol Chem Phys 2007;208:295–306.

[13] EMS Swiss Master Light Product description. EMS, Nyon, Switzerland.

[14] FlashMax2 Product description. Copenhagen, Denmark: CMS Dental, 2011.

[15] Unterbrink GL, Muessner R. Influence of light intensity on two restorative systems. J Dent 1995;23:183–9.

[16] Kurdikar DL, Somvarsky J, Dusek K, Peppas NA. Development and evaluation of a Monte Carlo technique for the simulation of multifunctional polymerizations. Macromolecules 1995;28:5910–20.

[17] Watts DC. Reaction kinetics and mechanics in photo-polymerised networks. Dent Mater 2005;21:27–35.

[18] Lovell LG, Lu H, Elliott JE, Stansbury JW, Bowman CN. The effect of cure rate on the mechanical properties of dental resins. Dent Mater 2001;17:504–11.

[19] Pfeifer CS, Wilson ND, Shelton ZR, Stansbury JW. Delayed gelation through chain-transfer reactions: mechanism for stress reduction in methacrylate networks. Polymer 2011;52:3295–303.

[20] Feng L, Carvalho R, Suh BI. Insufficient cure under the condition of high irradiance and short irradiation time. Dent Mater 2009;25:283–9.

[21] Dewaele M, Asmussen E, Peutzfeldt A, Munksgaard EC, Benetti AR, Finne G, et al. Influence of curing protocol on selected properties of light-curing polymers: degree of conversion, volume contraction, elastic modulus, and glass transition temperature. Dent Mater 2009;25:1576–84.

[22] Musanje L, Darvell BW. Polymerization of resin composite restorative materials: exposure reciprocity. Dent Mater 2003;19:531–41.

[23] Wydra JW, Cramer NB, Stansbury JW, Bowman CN. The reciprocity law concerning light dose relationships applied to BisGMA/TEGDMA photopolymers: theoretical analysis and experimental characterization. Dent Mater 2014;30:605–12.

[24] Rueggeberg FA, Hashinger DT, Fairhurst CW. Calibration of FTIR conversion analysis of contemporary dental resin composites. Dent Mater 1990;6:241–9.

[25] Randolph LD, Palin WM, Genet M, Devaux J, Leloup G, et al. The effect of ultra-fast photopolymerisation of experimental composites on shrinkage stress, network formation and pulpal temperature rise. Dent Mater 2014;30:1280–9.

[26] Ilie N, Durner J. Polymerization kinetic calculations in dental composites: a method comparison analysis. Clin Oral Investig 2014;18:1587–96.

[27] Zhang Y, Wang Y. Photopolymerization of phosphoric acid ester-based self-etch dental adhesives. Dent Mater J 2013;32:10–8.

[28] Frauscher KE, Ilie N. Degree of conversion of nano-hybrid resin-based composites with novel and conventional matrix formulation. Clin Oral Investig 2013;17:635–42.

[29] Oliveira M, Cesar PF, Giannini M, Rueggeberg FA, Rodrigues J, Arrais CA. Effect of temperature on the degree of conversion and working time of dual-cured resin cements exposed to different curing conditions. Oper Dent 2012;37:370–9.

[30] Arrais CA, Rueggeberg FA, Waller JL, de Goes MF, Giannini M. Effect of curing mode on the polymerization characteristics of dual-cured resin cement systems. J Dent 2008;36:418–26.

[31] Ilie N, Kessler A, Durner J. Influence of various irradiation processes on the mechanical properties and polymerisation kinetics of bulk-fill resin based composites. J Dent 2013;41:695–702.

[32] Hammouda IM. Effect of light-curing method on wear and hardness of composite resin. J Mech Behav Biomed Mater 2010;3:216–22.

[33] Ferracane JL, Mitchem JC, Condon JR, Todd R. Wear and marginal breakdown of composites with various degrees of cure. J Dent Res 1997;76:1508–16.

[34] Shortall A, El-Mahy W, Stewardson D, Addison O, Palin W. Initial fracture resistance and curing temperature rise of ten

contemporary resin-based composites with increasing radiant exposure. J Dent 2013;41:455–63.

[35] Ferreira SQ, Costa TR, Klein-Junior CA, Accorinte M, Meier MM, Loguercio AD, et al. Improvement of exposure times: effects on adhesive properties and resin-dentin bond strengths of etch-and-rinse adhesives. J Adhes Dent 2011;13:235–41.

[36] Xu X, Sandras DA, Burgess JO. Shear bond strength with increasing light-guide distance from dentin. J Esthet Restor Dent 2006;18:19–27 [discussion 8].

[37] Price RB, Ferracane J. Effect of energy delivered on the shear bond strength to dentin. Can J Restor Dent Prosthodont 2012;5:48–55.

[38] Akova T, Ozkomur A, Uysal H. Effect of food-simulating liquids on the mechanical properties of provisional restorative materials. Dent Mater 2006;22:1130–4.

[39] Corciolani G, Vichi A, Davidson CL, Ferrari M. The influence of tip geometry and distance on light-curing efficacy. Oper Dent 2008;33:325–31.

[40] Felix CA, Price RB. The effect of distance from light source on light intensity from curing lights. J Adhes Dent 2003;5:283–91.

[41] Price RB, Derand T, Sedarous M, Andreou P, Loney RW. Effect of distance on the power density from two light guides. J Esthet Dent 2000;12:320–7.

[42] Mjör IA. Clinical diagnosis of recurrent caries. J Am Dent Assoc 2005;136:1426–33.

[43] Chen RS, Liuiw CC, Tseng WY, Hong CY, Hsieh CC, Jeng JH. The effect of curing light intensity on the cytotoxicity of a dentin-bonding agent. Oper Dent 2001;26:505–10.

[44] Knezevic A, Zeljezic D, Kopjar N, Tarle Z. Cytotoxicity of composite materials polymerized with LED curing units. Oper Dent 2008;33:23–30.

[45] De Carvalho RV, Fernandez MR, Poli-Frederico RC, Guiraldo RD, Lopes MB, Berger SB, et al. Influence of different photo-activation distances on cytotoxicity of a dental adhesive model resin. Minerva Stomatol 2013;62:199–205.

[46] Sigusch BW, Pflaum T, Volpel A, Gretsch K, Hoy S, Watts DC, et al. Resin-composite cytotoxicity varies with shade and irradiance. Dent Mater 2012;28:312–9.

[47] Durner J, Obermaier J, Draenert M, Ilie N. Correlation of the degree of conversion with the amount of elutable

substances in nano-hybrid dental composites. Dent Mater 2012;28:1146–53.

[48] Gomes M, DeVito-Moraes A, Francci C, Moraes R, Pereira T, Froes-Salgado N, et al. Temperature increase at the light guide tip of 15 contemporary LED units and thermal variation at the pulpal floor of cavities: an infrared thermographic analysis. Oper Dent 2013;38:324–33.

[49] Aksakalli S, Demir A, Selek M, Tasdemir S. Temperature increase during orthodontic bonding with different curing units using an infrared camera. Acta Odontol Scand 2014;72:36–41.

[50] Oberholzer TG, Makofane ME, du Preez IC, George R. Modern high powered led curing lights and their effect on pulp chamber temperature of bulk and incrementally cured composite resin. Eur J Prosthodont Restor Dent 2012;20:50–5.

[51] Leprince J, Devaux J, Mullier T, Vreven J, Leloup G. Pulpal-temperature rise and polymerization efficiency of LED curing lights. Oper Dent 2010;35:220–30.

[52] Baroudi K, Silikas N, Watts DC. In vitro pulp chamber temperature rise from irradiation and exotherm of flowable composites. Int J Paediatr Dent 2009;19:48–54.

[53] Price RB, Whalen JM, Price TB, Felix CM, Fahey J. The effect of specimen temperature on the polymerization of a resin-composite. Dent Mater 2011;27:983–9.

[54] Steinhaus J, Frentzen M, Rosentritt M, Möginger B. Dielectric analysis of short-term and long-term curing of novel photo-curing dental filling materials. Macromol Symp 2010;296:622–5.

[55] Goodner MD, Bowman CN. Development of a comprehensive free radical photopolymerization model incorporating heat and mass transfer effects in thick films. Chem Eng Sci 2002;57:887–900.

[56] Andrzejewska E. Photopolymerization kinetics of multifunctional monomers. Prog Polym Sci 2001;26:605–65.

[57] Neumann MG, Schmitt CC, Ferreira GC, Correa IC. The initiating radical yields and the efficiency of polymerization for various dental photoinitiators excited by different light curing units. Dent Mater 2006;22:576–84.

[58] Chen YC, Ferracane JL, Prahl SA. Quantum yield of conversion of the photoinitiator camphorquinone. Dent Mater 2007;23:655–64.

Manuscript Number:

Title: Determining depth of cure (DoC) of VLC RBC intrinsically using a new evaluation procedure to profiles of depth dependent hardness, mass loss after solvent extraction and post-reaction enthalpy

Article Type: Full Length Article

Keywords: Determination of an intrinsic depth of cure, dental composites, radiant exposure, depth dependent hardness, depth dependent mass loss, depth dependent post-reaction enthalpy

Corresponding Author: Mr. Thomas Haenel, M.Sc.

Corresponding Author's Institution: Bonn-Rhein-Sieg, University of Applied Sciences

First Author: Thomas Haenel, M.Sc.

Order of Authors: Thomas Haenel, M.Sc.; Berenika Hausnerová, Ph.D.; Martin Dopadlo, M.Sc.; Johannes Steinhaus, Ph.D.; Bernhard Moeginger, Dr.-Ing.

Abstract: Abstract
Objectives
The determination of depth of cure (DoC) of VLC RBC is usually performed in a heuristic manner. Therefore, the aim of this study is develop an evaluation procedure for depth properties e.g. hardness, mass loss after solvent extraction, and post-reaction enthalpy which produces DoC-values intrinsically without using arbitrary threshold values.
Methods
Two commercially available composites - Arabesk®TOP OA2 and Grandio®OA2 - were cured by the following curing protocols: exposure times were 5, 20 and 80 s with LCU irradiances of 650, 1200, and 2200 mW/cm². To investigate the depth dependent changes of hardness, mass loss after solvent extraction post-reaction enthalpy ($\Box HR$), glass transition temperature (T_g), and post-reaction temperature (T_R), samples having a thickness of 0.5 mm and a diameter of 8 mm were piled to a total height of 5 mm. Then, the samples were stored at 23°C for one week either in a dry and dark environment or in tetrahydrofuran (THF).
Results
The depth dependent profiles of hardness, mass loss after solvent extraction and post-reaction enthalpy could be well fitted using a hyperbola tangent function containing three parameters. The evaluation procedure defines an intrinsic DoC using only the two fit parameters "depth of inflection point" and slope at the inflection point". Inserting the DoC-definition in the fit functions shows that the plateau values of properties have decreased to 88%. The DoC-values from hardness profiles depend logarithmically on the radiant exposure. The hardness profiles exhibit maximum hardness not at the surface but somewhere deeper in the sample what is usually attributed to oxygen inhibition. As the samples were prepared in a way that allowed oxygen inhibition at every measured surface the lower surface hardness has to be explained differently. Due

to a one-way ANOVA (p=0.05) glass transition temperature Tg and post-reaction temperature TR showed no significant differences with respect to exposure time and depth.

Significance

The new evaluation procedure allows for determining an intrinsic DoC of VLC RBC which takes into account all data points of measured depth dependent property profiles and does not depend on the experimentalist, thus, increasing the reliability of DoC-values. No arbitrary threshold values are required anymore and the evaluation procedure can easily be installed as a macro on computers what is very helpful for scientists developing VLC RBC.

134

Determining depth of cure (DoC) of VLC RBC intrinsically using a new evaluation procedure to profiles of depth dependent hardness, mass loss after solvent extraction and post-reaction enthalpy

Thomas Haenel[1,2], Berenika Hausnerová[1,3], Martin Dopadlo[2], Johannes Steinhaus[1,2], Bernhard Moeginger[2]

[1] Centre of Polymer Systems, University Institute, Tomas Bata University in Zlin, Zlin, Czech Republic

[2] Bonn-Rhein-Sieg University of Applied Sciences, Department of Natural Sciences, Rheinbach, Germany

[3] Tomas Bata University in Zlin, Faculty of Technology, Department of Production Engineering, Zlin, Czech Republic

Corresponding author:

Bernhard Moeginger

Bonn-Rhein-Sieg University of Applied Sciences,

Faculty of Applied Natural Sciences

Von Liebig Str. 20

53359 Rheinbach, Germany

Phone: +49 2241/865 531

Fax: +49 2241/865 8531

bernhard.moeginger@h-brs.de

1 Introduction

The depth of cure (DoC) is an important property of visible light curing resin based composites (VLC-RBC) in dentistry as well as in composites' development mainly in order to evaluate and compare their curing behavior [1]. The DoC depends on light intensity and intensity distribution of the LCU, spectrum of the curing light, exposure time and filling technique [2–7]. It is influenced by shade, composition formulation, and translucency of the VLC-RBC [7–11]. It is an important information for dentists because insufficiently cured restorations due to too thick layers may cause health problems because of elution of residual monomers and inadequate mechanical properties reducing the longevity of restorations [1,2,6,7,12].

The curing process of VLC-RBC was often investigated [3,13–15]. The energy introduced by the LCU activates camphorquinone molecules to an excited state in which they can react with accelerator molecules to radicals. These radicals may attack the carbon-double bonds of the resin monomers and initiate the polymerization reaction. The monomers of VLC-RBC have at least two carbon double bonds to allow for i) polymerization and ii) cross-linking between the polymer chains. One of the main factors that affect both degree of conversion and depth of cure (DoC) is the radiant exposure RE representing the delivered energy to the VLC-RBC. Some researchers found that equal amounts of energy introduced to the VLC RBC generate the same degrees of conversion and mechanical properties irrespective of the chosen exposure times as long as they are not too short [16–19]. Due to Lambert-Beer absorption the number of available photons decreases exponentially with depth [20,21]. Less initiator molecules can be activated and as a consequence the density of radicals decreases. Thus, more polymerization steps are required before cross-linking can occur [22]. Therefore, Leprince et al. [6] assumed that the thermo-mechanical properties have to change from glassy to liquid behavior with depth somewhere. This means that the amount of extractable substance (monomers, oligomers and short polymers) has to increase at a certain depth.

During the curing process, the rate of reaction decreases with time because of a decreasing monomer concentration and an increasing glass transition temperature T_g [6,16,23,24]. The mobility of the remaining monomers and radicals is more and more restricted until they are finally trapped in the vitrified polymer network. In that state radicals may exist for days or month [24–26]. This "freezing in process" limits the degree of conversion to values significantly less than 100% (besides steric hindrances due to molecular structures). The trapped radicals can promote post-curing in the vitrified polymer network or restart the curing process if temperature is increased above T_g because chain segments become mobile again. This leads to further curing,

135

and a DSC trace shows a post-reaction peak. During the curing process the molecular weight of the polymer chains is increased. As a consequence, the glass transition temperature T_g is shifted to higher temperatures until it exceeds ambient or process temperature [27–30].

Many methods can be applied to determine quantitative DoC-values, e.g. ISO 4049 scratch test, hardness profiles, atomic force microscopy, penetration depth of an indenters, determination of degree of conversion, or change of ion viscosity [2,4,6,7,22,31,32]. All these methods require a criterion for "sufficient cure". Therefore, arbitrary threshold values chosen in a heuristic manner are applied to determine DoC.

From a scientific point of view it is desirable to determine the DoC by applying an evaluation procedure to depth dependent properties, e.g. hardness profiles, without using threshold values. Thus, the hypothesis of this paper is that the DoC of VLC RBCs can be determined by fitting depth dependent property profiles with an appropriate function which generates the DoC-value intrinsically.

2 Materials and Methods

2.1 Materials and light curing units (LCU)

The two investigated VLC-RBC (Arabesk TOP OA2, Lot-No.:1246483 and Grandio OA2, Lot-No.: 1303489, Voco, Cuxhaven, Germany [33,34]) and the used LCU are described in table 1. In the further text to the VLC-RBC is refered as Arabesk and Grandio, respectively. The power output of the LCUs was checked with a laser power meter (Thor Labs, PM100D).

The sample discs were made in steel rings having an outside diameter $D_{out} = 18$ mm, an inside diameter $D_{in} = 8$ mm and a thickness of 0.5 mm. The steel rings were flattened to ensure reproducible positioning in the sample holders of both curing device and hardness tester. The sample preparation is described in Table 2. After curing the samples were stored in a dry and dark environment at room temperature for 1 week. After storage, the thickness of each sample was measured with a micrometer (Mitutoyo Europe GmbH, Neuss, Germany) having a resolution of 0.01 mm. At least three samples were investigated for each data point

2.2 Methods

Hardness testing

The hardness testing was performed using a cross pattern of five indentation on the top and the bottom surface of each sample using a Vickers hardness tester (SemiMakroVickers 5112; Buehler LTD., USA) Table 2. A test force of 0.2 N was applied for an indentation time of 10 s. The hardness of the top surface (x = 0) is the mean of

5 hardness measurements while the hardness values at other depths represent the means of 5 bottom hardness values and 5 top hardness values of the neighboring sample slide.

Determination of the mass loss

After hardness testing, the samples were taken out of the sample holder in order to determine the sample mass using a balance (Precisa 92SM-202A, Precica Gravimetrics AG, Dietikon, Switzerland). Then, the samples were stored in tetrahydrofuran THF (Rotisolv HPLC 99,9 %, Carl Roth, Germany) for 1 week in a dark environment at room temperature. After storage, the samples were dried in open black micro-tubes at room temperature until the sample mass reached constancy. The difference to the mass before storing in THF represents the mass loss. It is related to the resin fraction of Arabesk and Grandio, respectively, yielding the relative mass loss.

Determination of the post-reaction enthalpy

The samples were taken out of the sample holder and cut to pieces having a mass between 10 and 25 mg. The post-reaction enthalpy of the samples was determined using a DSC (DSC 8000, Perkin Elmer Inc., USA) with starting temperature -60°C, heating rate of 20K/min, end temperature of +200°C and nitrogen purge flow of 20 mL/min. Three samples (n=3) were measured for both Arabesk and Grandio. The glass transition temperature T_g was determined by the inflection point of the glass transition step of the DSC curve. The temperature of starting post-reaction T_R was determined by the peak at the end of the glass transition. The post-reaction enthalpy ΔH_R was determined as the integral between the DSC-curve and the baseline above T_g. The evaluation scheme to determine T_g, T_R and ΔH_R using the first runs of the corresponding DSC measurements is shown in Figure 1. The depth of the post-reaction enthalpies was determined as averages of top and bottom coordinates of the corresponding slices. A Nalimov outlier test was used to validate the T_g and T_R results. A one-way ANOVA with a Tukey test (p = 0,05) was performed to compare the results of T_g and T_R of each exposure time sample group.

2.3   Determination of the depth of cure (DoC)

The investigated properties show a sigmoidal depth dependency. Close to the surface the DC is maximal what corresponds to a high hardness, a high post-reaction enthalpy due to trapped radicals and almost no mass loss. At a certain depth the DC starts to decrease and as a consequence both hardness and post-reaction enthalpy decrease while mass loss increases. In large depths where most of the light is absorbed the DC approaches zero and thus hardness and post-reaction enthalpy also approach zero while mass loss becomes 100%. If one assumes a Lambert-Beer-like absorption of light in the VLC-RBC the large depth bounds should be achieved gradually. In

order to fit the depth dependent data the fit function has to have an inflection point at a certain depth x_0 and a large depth behavior similar to the light absorption behavior. Therefore, a tangent hyperbola depth dependency of the investigated properties was chosen:

1. Hardness
$$HV(x) = \frac{HV^{Plateau}}{2} \cdot \{1 + tanh[-a_1(x - x_{0,1})]\} \tag{1}$$

with surface hardness $HV^{Plateau}$, slope at the inflection point a_1, and depth of the inflection point $x_{0,1}$

2. Relative mass loss
$$\Delta m(x) = \frac{\Delta m_{max}}{2} \cdot \{1 + tanh[a_2(x - x_{0,2})]\} \tag{2}$$

with slope at the inflection point a_2 and depth of the inflection point $x_{0,2}$

3. Post-reaction enthalpy
$$\Delta H_R(x) = \frac{\Delta H_{R,max}}{2} \cdot \{1 + tanh[-a_3(x - x_{0,3})]\} \tag{3}$$

with post-reaction enthalpy $\Delta H_{R,\ max}$ at the surface, slope at the inflection point a_3, and depth of the inflection point $x_{0,3}$

The DoC is determined by the 3 steps:

- Fit of the measured data to determine values for surface property ($HV^{Plateau}$ or ΔM_{max} or $\Delta H_{R,\ max}$), slope at the inflection point, and depth of the inflection point,

- Determination of the interception of inflection tangents with the corresponding surface properties,

- The depth coordinate of the interception point is considered as the depth of cure (DoC) given by

$$DoC_i = x_{0,i} - \frac{1}{a_i}, \quad i = HV, \Delta M, \Delta H_R \tag{4}$$

The DoC defined by equation (4) depends only on the depth of the inflection point and the slope at the inflection point. The hardness profiles were also evaluated using the definition that the depth of cure is represented by the depth at which 80% of the hardness plateau $HV^{Plateau}$ ($DoC_{0.8HV}$) is reached, see also Figure 2. This allows for comparing DoC_{HV} to $DoC_{0.8HV}$.

3   Results

Hardness profiles

With increasing exposure times and irradiances of the LCU the hardness profiles change in two ways, Figure 3:

- The maximum Vickers hardness HV_{max} and the hardness plateau $HV^{Plateau}$ are shifted to higher hardness values.

- The inflection points of the fit curves are shifted to higher depth values.

The maximum values of the hardness plateaus were determined to 63 HV for Arabesk and 120 HV for Grandio. This is due to the difference in filler content leading also to standard deviations being typically 3 times larger for Grandio than for Arabesk. The mean values of the hardness plateaus increase for longer exposure times. However, the hardness increase of samples irradiated 20 s to those irradiated 80 s is not significant with respect to the standard deviations. After an exposure time of 20 s the maximum hardness is almost reached in the plateau range for both VLC RBCs. Longer exposure times mainly shift the inflection points $x_{0,1}$ to deeper depths and thus also the DoC. The slope a_1 at the inflection points $x_{0,1}$ has values between 0.8 and 1.3 mm^{-1} for both composites showing no specific dependency on the irradiation conditions, Table 3.

The DoC determination according to equation (4) shows that the DoC_{HV} increases from 0.5 mm (Bluephase 20i low, 5 s) to 2.5 mm (Bluephase 20i turbo, 80 s) for Arabesk. Grandio shows DoC_{HV} of 0.8 mm (Bluephase 20i low, 5 s) to 3.5 mm (Bluephase 20i turbo, 80 s,), respectively. The lower resin content of Grandio leads also to an increase of DoC, Table 3.

Profiles of mass loss

With increasing exposure times and irradiances of the LCU the inflection points $x_{0,2}$ are shifted to higher depth values and the standard deviations of the relative mass loss is increased, Figure 4 and Table 4. The increase of the standard deviation is due to additional loss of filler particles for depths exceeding the $DoC_{\Delta m}$. This is also reflected in fact that the slopes a_2 at the inflection points $x_{0,2}$ range from 0.7 to 1.5 mm^{-1}, Table 4, and showed no a specific dependency on the irradiation conditions. The depths were calculated as averages of top and bottom coordinates of the discs whose relative mass losses were determined.

The DoC determination according to equation (4) showed that for Arabesk the $DoC_{\Delta m}$ increases from 0.3 mm (Bluephase 20i low, 5 s) to 3 mm (Bluephase 20i turbo, 80 s). Grandio shows $DoC_{\Delta m}$ of 1.1 mm (Bluephase 20i low, 5 s) to 3.9 mm (Bluephase 20i turbo, 80 s,), respectively, Table 4.

The samples showed different states of dissolving after one week storage in THF depending on the depth of the sample disc, Figure 5. Sample discs taken from depths of no mass loss showed no visible effect of the solvent. Sample discs taken from depths with mass loss exhibited white dots and fissures with a dim white surface before disintegration. Furthermore, the shapes of samples taken at the deepest depths indicate also the inhomogeneity of the intensity distribution of the LCU.

Profiles of post-reaction enthalpies

With increasing exposure times and irradiances of the LCU the inflection points $x_{0,3}$ of Arabesk are shifted to higher depth values, Figure 5 and Table 5. The slopes a_3 at the inflection points $x_{0,3}$ range from 1.0 to 1.8 mm^{-1} with reasonable standard deviations. Only the samples irradiated with the Celalux for 5 s showed a slope a_3 of 2.3 mm^{-1} but with a standard deviation of 1.9 mm^{-1}, Table 5. In general, the slopes a_3 showed no a specific dependency on the irradiation conditions. Post-reaction measurements couldn't be performed for 0.5 mm thick discs of Grandio because of the low resin content and corresponding small enthalpy peaks.

The glass transition temperatures T_g and the post-reaction temperatures T_R of all measurements passing the Nalimov outlier test were determined to 50.3 (1.5)°C and 56.8 (1.1)°C, respectively, as averages over all samples. A one-way ANOVA showed no significant differences of T_g and T_R with respect to depths and irradiation conditions.

The DoC determination according to equation (4) showed that for Arabesk the $DoC_{\Delta m}$ increased from 0 mm (Bluephase 20i low, 5 s) to 2 mm (Bluephase 20i turbo, 80 s), Table 5. The high post-reaction enthalpies of the top sample discs irradiated with Celalux and Bluephase 20i Low indicate an insufficient degree of curing.

Comparison of DoC determined according to different methods

In Table 6 the DoC determined according to equation (4) are compared to the $DoC_{0.8HV}$, the depth at which 80% of the plateau hardness is reached. The DoC_{HV} values are typically 0.3 mm smaller than the $DoC_{0.8HV}$ and can be interpreted as the depth where the hardness plateau ends. The $DoC_{\Delta m}$ values are similar to the $DoC_{0.8HV}$ values while the $\mathbf{DoC_{\Delta HR}}$ values produce the smallest values.

4 Discussion

The depth of cure (DoC) represents the thickness of a sufficiently cured layer of VLC RBCs. Although its meaning is intuitively clear the quantitative determination is challenging as it is usually done in a heuristic manner. In most cases the DoC is determined by applying two methods:

1. **ISO 4049 scratch test** which measures the depths to which some curing took place. It is clear that this depth represents a maximum DoC. As there is a less cured range within VLC RBCs within this maximum DoC it is divided by „2" in order to exclude only less cured ranges. This gives more realistic DoCs to be used by dentists in their daily work.

2. **measuring of depth dependent hardness profiles** and evaluating the depth at which the hardness has dropped to a certain hardness value which is to represent „sufficient cure". The choice of this hardness

value is a bit arbitrary and in literature one can find values of 90%, 85% and 80% of the maximum hardness as limits. Mostly 80% is used.

Both methods do a relatively good job as long as one is only interested in comparing VLC RBCs. However, if the DoC should be a defined physical quantity the considered depth dependent change of properties has to be taken into account and effects of the experimentalist have to be limited.

Fitting the data of depth dependent changes of hardness, relative mass loss after storage in a solvent and post-reaction enthalpy using equations (3) shows that the data are nicely fitted, Fig. 3, 4 and 6, and that the DoC is determined by the two parameters „depth of inflection point“ and „slope at the inflection point“ of the fit function, Fig. 2. Thus, the DoC determination itself is not affected by experimentalists anymore. Furthermore, if one introduces the definition of the DoC according to equation (4) to equation (3) the argument of tanh-function becomes „1“ and $\tanh(1) \cong 0.76$. This means that the property values have decreased to 88% of their maximum values at DoC irrespective of the considered property. In that context one can say that the DoC determined according to equation (4) represents the depth in a VLC RBC to which light curing has generated a constant property level. Interestingly, the evaluation provides different DoC for the three investigated properties. The comparison of the DoC determined by equation (4) to $DoC_{0.8HV}$, Table 6, shows the ranking:

$$DoC_{\Delta HR} < DoC_{HV} < DoC_{0.8HV} <\approx DoC_{\Delta m} \tag{5}$$

indicating that the light curing process affects them in a different manner.

The light introduced to a VLC RBC generates radicals starting the curing reaction of dimethylacrylate monomers. As the light intensity decreases in a Lambert-Beer-manner both concentration of radicals and reaction rate should exhibit a corresponding behavior. Thus, the time dependency of degree of conversion depends on the amount of energy delivered by the LCU to the VLC RBC [3,16,28] on one hand side and on the depth within the VLC RBC [22,35] on the other. The reaction rate decreases drastically if the glass transition temperature of the curing resin exceeds ambient temperature due to the loss of molecular mobility [6,23,26]. As the glass transition depends on the degree of polymerization it is crucial whether the transition to the glassy state takes place via cross-linking leading to a sudden transition because cross-linking doubles on average the degree of polymerization or polymerization leading to a rather gradual transition.

Due to the high radical concentration close to the surface the resin is transferred very quickly to the glassy state as cross-linking is the dominant process. This may lead to rather disordered network structures in which comparatively many monomer molecules and radicals are quickly trapped. With increasing depth the times to

glass transition increase due to the decreasing radical concentration. This has the consequence that a single radical has to form longer molecule chains before cross-linking can occur the deeper it is in the VLC RBC. At first network formation may occur in a more regular manner but with a little bit reduced cross-linking density trapping less monomers and radicals. In spite of a lower cross-linking density a higher hardness is measured because of less softening due to less trapped monomers and radicals.

In a certain depth the radical concentration has decreased to a level that the glass transition is reached during the polymerization process. This means that there are regions in which polymer chains are already in the glassy state neighbored by liquid resin regions. Further polymerization is only possible if radicalized polymer chains are fed by monomers from the liquid phase or if new radicals are generated by ongoing irradiation. After irradiation the radicals undergo termination reactions if not trapped in the glassy network [13,14]. The loosely cross-linked glassy regions can be swollen by monomer molecules from the remaining liquid regions. This promotes at least three effects: i) post-curing reactions with trapped radicals, ii) decrease of stiffness as the monomer molecules may act as softeners, and iii) annihilation of trapped radicals because of the higher mobility in the softened regions. With this picture of the curing process in mind one can understand the findings of this investigation.

The samples irradiated for 5 s did not achieve a sufficient degree of conversion yet as all investigated properties have reached the final plateau values in the surface layer only after an irradiation of 20 s, Fig. 3, 4 and 6. The relative mass loss of the samples irradiated in the Bluephase Turbo mode for 5 s is close to zero. This leads to the conclusion that sufficient cure of Arabesk and Grandio requires an energy delivery of at least 4.6 J. Bluephase Low mode and Celalux delivered only 1.4 or 2.3 J, respectively, what is obviously too few for a sufficient cure. Results of samples irradiated for 20 s support this conclusion. Samples irradiated in the Bluephase Low mode received 5.5 J and had a sufficiently cured first layer showing no mass loss in contrast to the second layer. Further increase of the irradiation time to 80 s does not affect the plateau values anymore but leads to larger DoC, Table 6. If sufficient cure is established only diffusion controlled reactions lead to a small increase of degree of conversion. In the network theory the stiffness e.g. Young's modulus is reciprocal to the mean chain length between two cross-links [36]. Thus, the small increase of degree of conversion in sufficiently cured regions due to longer irradiation times has only little effect on stiffness or hardness. In insufficiently or uncured regions, however, longer irradiation times compensate for Lambert-Beer-absorption increasing the thickness of the sufficiently cured layer. If depth of cure DoC_{HV} is plotted versus radiant exposure RE one can nicely fit the data points ($R^2 = 0.966$) with the function

$$DoC_{HV}(RE) = A * \ln(RE) + B .$$
(6)

whereas A and B are materials constants. They were determined for i) Arabesk to A=0.487 and B=0.379 and for ii) Grandio to A=0.635 and B=0.440. Interestingly it requires a minimum RE of 0.459 J (Arabesk) and 0.500 J(Grandio) to generate a none-negative DoC what can be attributed to effects generated by inhibitors added to VLC RBCs. Equation (6) expresses in principle that the DoC is limited because both irradiation time and intensity of LCUs are restricted for practical reasons. Very high intensities may harm patients and very long irradiation times are not accepted by them either.

Several studies observed the maximum hardness HV_{max} not at the top surface but in deeper layers [1,21]. Usually, this effect is attributed to oxygen inhibition of the top surface [1,15]. The samples in this study consisted of stacked 0.5 mm thick discs separated by Mylar strips. Therefore, oxygen inhibition should occur in each layer but the hardness increase from the surface to deeper layers was also found, Fig. 3. This means that oxygen inhibition may play a role but it cannot be the main explanation. Another explanation was given by Lovell et al [19] who assumed that a certain amount of short polymer chains is generated at high reaction rates reducing stiffness and hardness. However, the simplest explanation for the reduced surface hardness is to assume that a rather disordered network is formed quickly due to the high reaction rate at the surface in which more monomer molecules and radicals are trapped in a higher concentration than in deeper depths.

The evaluation of the investigated depth dependent property changes shows that the determined DoCs depend on the considered property. To understand this one has to figure out how the curing process may affect the properties and their change. If one determines the depth dependent hardness profile of a VLC RBC one knows that the decreasing hardness occurring at a certain depth is due to reduced cross-linking density and higher contents of monomers and oligomers. Both facts reduce mechanical properties such as stiffness, strength and hardness. The DoC_{HV} is determined as the depth in which the hardness has reached a predefined limit. The question is: What is different if another property is used to determine DoC?

Usually the samples are cured and stored for some time, e.g. 24 hours or a week, under defined conditions. Thus, post-curing processes shift the boundary of sufficiently cured VLC RBC to deeper depths while radical annihilation reduces the concentration of trapped radicals in not optimally cured regions. If DoC is determined after some time one can expect that hardness profiles produce larger DoC-values than post-reaction enthalpy profiles. Storage in THF leads to swell of the network and increases the mobility locally. In these regions the glass temperature can be reduced to ambient temperature. Trapped and immobilized monomers and radicals regain mobility and restart polymerization and cross-linking [26]. This shifts the boundary of sufficiently cured VLC RBC further to deeper depths. If relative mass loss profiles are determined after drying larger DoC-values

143

should be produced than for hardness profiles. This consideration explains the difference between DoC_{HV}, $DoC_{\Delta m}$ and $DoC_{\Delta HR}$ in Table 6.

The glass transition temperatures were found to be 50 to 51°C independently of the curing protocols. As VLC RBCs are almost isothermally cured the process temperature during curing is not much above ambient temperature. Each step of chain growth increases the glass transition temperature of the resin until it exceeds the process temperature. Then the curing rate decreases drastically and the curing process freezes in. If glass transition temperatures do not depend on radiant exposure (or curing conditions), one can conclude that all samples were cured to the same degree of conversion but may differ in cross-linking density.

The post-curing enthalpy ΔH_R informs about the concentration of trapped radicals in the cured network. The top layer always showed maximum post-curing enthalpy because a large number of radicals was generated close to the surface leading to high reaction rates and a fast and partly sudden vitrification of the resin matrix trapping many radicals in the network. With increasing depth the concentration of generated radicals decreases due to Lambert-Beer-absorption and correspondingly the number of radicals trapped by the vitrification process. In large depths vitrification does not occur anymore and radicals annihilate in the liquid resin. Without trapped radicals there is no post-reaction if temperature exceeds post-reaction temperature of 56 to 57°C.

5 Conclusion

The new evaluation method using a hyperbola tangent function to fit depth dependent property profiles yields an intrinsic definition for the quantity "depth of cure" (DoC) in equation (4). The DoC is completely determined by the two parameter **inflection point $x_{0,i}$** and the **slope a_i at the inflection point** of the hyperbola tangent function not involving any threshold values. Thus, the hypothesis of the paper is stated. Furthermore, it turned out that at the DoC the plateau values of the considered property have decreased to 88% at a consequence of the evaluation procedure, no matter which property is considered. The evaluation produced different DoC-values for the considered hardness, mass loss and post-reaction enthalpy profiles, but these differences can be consistently explained with property specific processes happening between sufficiently cured and uncured sample regions. Furthermore, the hardness profiles state results of many other researchers that the maximum hardness does not occur at the surface but somewhere deeper in the sample. Usually this fact is explained by oxygen inhibition. As the experiments of this study were performed using samples of stacked 0.5 mm thick discs, oxygen inhibition can take place at every surface. Thus, oxygen inhibition cannot be the main reason that the maximum hardness occurs somewhere deeper in the sample.

List of Figures

List of Tables

References

1. Asmussen E and Peutzfeldt A. Influence of specimen diameter on the relationship between subsurface depth and hardness of a light-cured resin composite. Eur J Oral Sci, 2003; 111:543–546.
2. Ruyter IE and Oysaed H. Conversion in different depths of ultraviolet and visible light activated composite materials. Acta Odontol. Scand., 1982; 40:179–192.
3. Watts DC. Reaction kinetics and mechanics in photo-polymerised networks. Dental materials : official publication of the Academy of Dental Materials, 2005; 21:27–35.
4. Lindberg A, Peutzfeldt A and van Dijken, Jan W V. Effect of power density of curing unit, exposure duration, and light guide distance on composite depth of cure. Clin Oral Investig, 2005; 9:71–76.
5. Li J, Fok, Alex S L, Satterthwaite J and Watts DC. Measurement of the full-field polymerization shrinkage and depth of cure of dental composites using digital image correlation. Dental materials : official publication of the Academy of Dental Materials, 2009; 25:582–588.
6. Leprince JG, Levêque P, Nysten B, Gallez B, Devaux J and Leloup G. New insight into the "depth of cure" of dimethacrylate-based dental composites. Dent Mater, 2012; 28:512–520.
7. Alrahlah A, Silikas N and Watts DC. Post-cure depth of cure of bulk fill dental resin-composites. Dent Mater, 2014; 30:149–154.
8. Ferracane JL, Aday P, Matsumoto H and Marker VA. Relationship between shade and depth of cure for light-activated dental composite resins. Dental Materials, 1986; 2:80–84.
9. Cook WD. Factors affecting the depth of cure of UV-polymerized composites. J. Dent. Res., 1980; 59:800–808.
10. Shortall AC, Palin WM and Burtscher P. Refractive Index Mismatch and Monomer Reactivity Influence Composite Curing Depth. Journal of Dental Research, 2008; 87:84–88.
11. Leprince JG, Palin WM, Hadis MA, Devaux J and Leloup G. Progress in dimethacrylate-based dental composite technology and curing efficiency. Dent Mater, 2013; 29:139–156.
12. Schmalz G and Arenholt-Bindslev D. Biocompatibility of Dental Materials. s.l., 2009.
13. Green GE, Stark BP and Zahir SA. Photocross-Linkable Resin Systems. Polym Rev (Phila Pa), 1981; 21:187–273.
14. Cook WD. Photopolymerization kinetics of dimethacrylates using the camphorquinone/amine initiator system. Polymer, 1992; 33:600–609.
15. Fouassier J, Allonas X and Burget D. Photopolymerization reactions under visible lights: principle, mechanisms and examples of applications. Progress in Organic Coatings, 2003; 47:16–36.
16. Halvorson RH, Erickson RL and Davidson CL. Energy dependent polymerization of resin-based composite. Dent Mater, 2002; 18:463–469.
17. Miyazaki M, Oshida Y, Moore BK and Onose H. Effect of light exposure on fracture toughness and flexural strength of light-cured composites. Dent Mater, 1996; 12:328–332.
18. Emami N and Soderholm KM. How light irradiance and curing time affect monomer conversion in light-cured resin composites. Eur. J. Oral Sci., 2003; 111:536–542.
19. Lovell LG, Lu H, Elliott JE, Stansbury JW and Bowman CN. The effect of cure rate on the mechanical properties of dental resins. Dental Materials, 2001; 17:504–511.
20. Arikawa H, Fujii K, Kanie T and Inoue K. Light transmittance characteristics of light-cured composite resins. Dental Materials, 1998; 14:405–411.
21. Flury S, Hayoz S, Peutzfeldt A, Hüsler J and Lussi A. Depth of cure of resin composites: Is the ISO 4049 method suitable for bulk fill materials? Dent Mater, 2012; 28:521–528.
22. Steinhaus J, Moeginger B, Grossgarten M, Rosentritt M and Hausnerova B. Dielectric analysis of depth dependent curing behavior of dental resin composites. Dent Mater, 2014; 30:679–687.
23. Ferracane JL. Correlation between hardness and degree of conversion during the setting reaction of unfilled dental restorative resins. Dental Materials, 1985; 1:11–14.
24. Truffier-Boutry D, Gallez XA, Demoustier-Champagne S, Devaux J, Mestdagh M, Champagne B and Leloup G. Identification of free radicals trapped in solid methacrylated resins. J. Polym. Sci. A Polym. Chem., 2003; 41:1691–1699.
25. Burtscher P. Stability of radicals in cured composite materials. Dental Materials, 1993; 9:218–221.
26. Leprince J, Lamblin G, Truffier-Boutry D, Demoustier-Champagne S, Devaux J, Mestdagh M and Leloup G. Kinetic study of free radicals trapped in dental resins stored in different environments. Acta Biomaterialia, 2009; 5:2518–2524.
27. Fox TG and Loshaek S. Influence of molecular weight and degree of crosslinking on the specific volume and glass temperature of polymers. J. Polym. Sci., 1955; 15:371–390.
28. Leung RL, Fan PL and Johnston WM. Post-irradiation Polymerization of Visible Light-activated Composite Resin. Journal of Dental Research, 1983; 62:363–365.
29. Ferracane JL and Greener EH. The effect of resin formulation on the degree of conversion and mechanical properties of dental restorative resins. Journal of biomedical materials research, 1986; 20:121–131.
30. Santos GB, Medeiros IS, Fellows CE, Muench A and Braga RR. Composite depth of cure obtained with QTH and LED units assessed by microhardness and micro-Raman spectroscopy. Operative dentistry, 2007; 32:79–83.
31. Aravamudhan K, Rakowski D and Fan P. Variation of depth of cure and intensity with distance using LED curing lights. Dent Mater, 2006; 22:988–994.
32. Moore BK, Platt JA, Borges G, Chu TG and Katsilieri I. Depth of cure of dental resin composites: ISO 4049 depth and microhardness of types of materials and shades. Operative dentistry, 2008; 33:408–412.
33. Voco GmbH. Arabesk Top instructions for use. Cuxhaven, 2011.
34. Voco GmbH. Grandio instructions for use. Cuxhaven, 2010.
35. Haenel T, Hausnerova B, Price RB and Moeginger B. Kinetics of primary curing of visible light curing resin based dental composites.
36. Gordon M. The Physics of Rubber Elasticity (Third Edition). L. R. G. Treloar, Clarendon Press, Oxford. 1975 pp. xii + 370. Price: £14.00. Brit. Poly. J., 1976; 8:39.

Figure 1 Evaluation of DSC curves
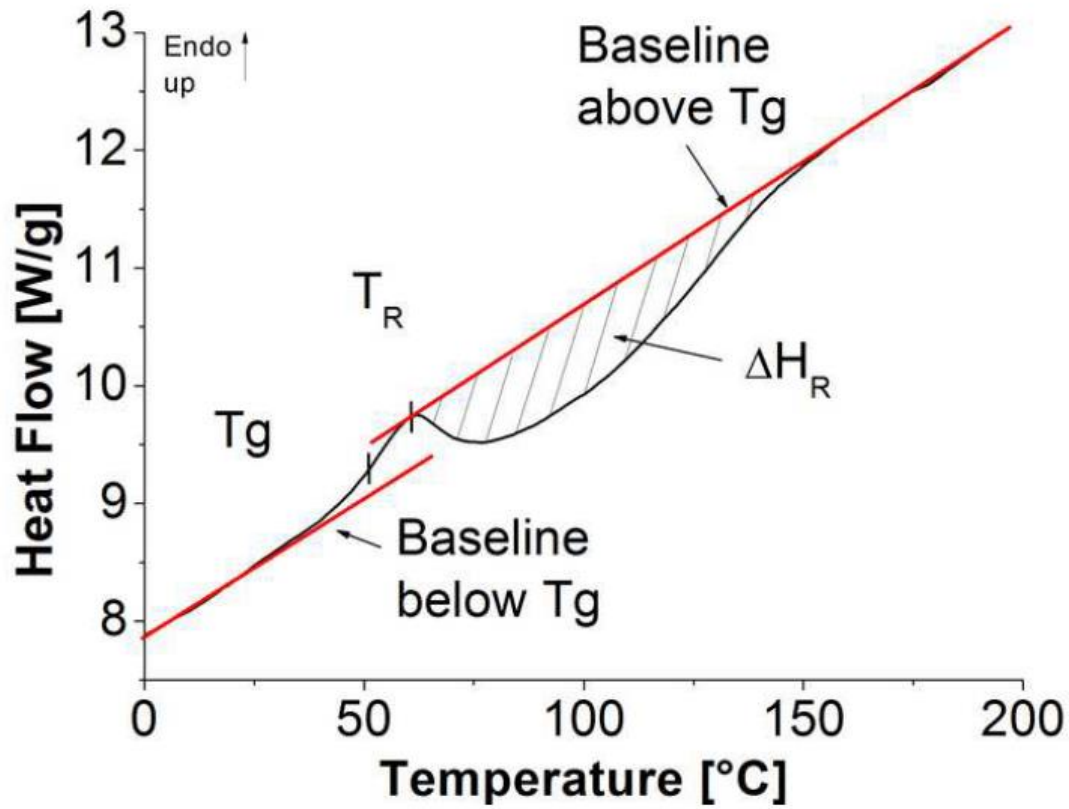
Figure 2 Scheme of evaluation of depth dependent hardness

148
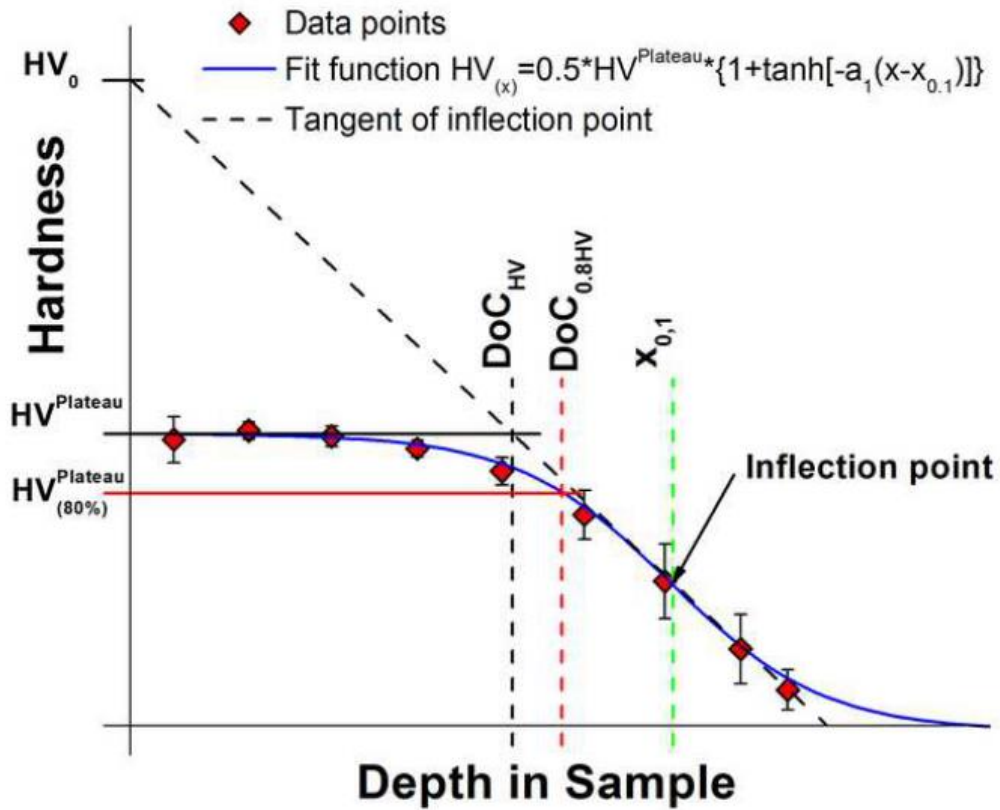
Figure 3 Depth dependent hardness of Arabesk and Grandio
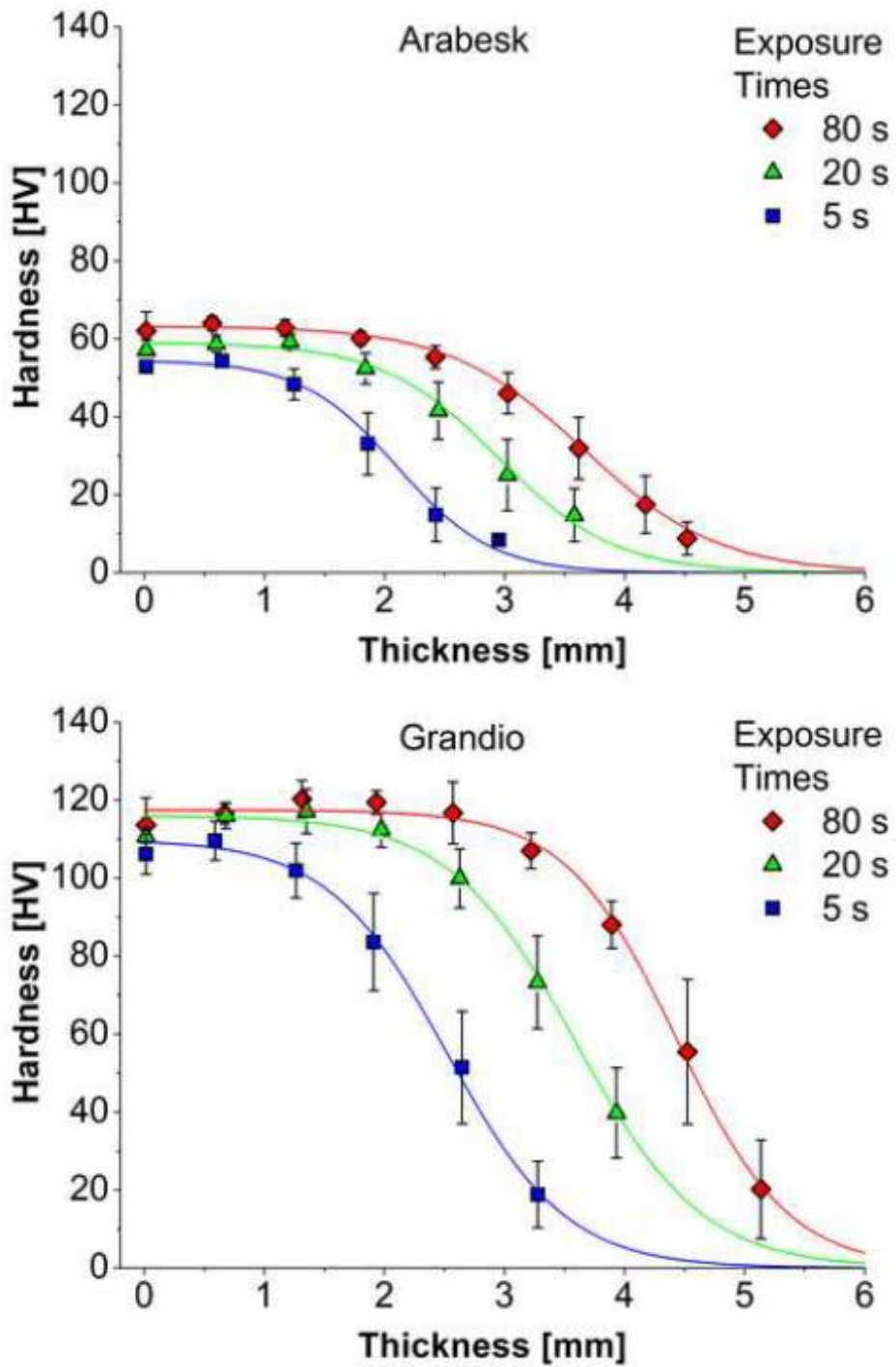
Figure 4 Depth dependent relative mass loss of Arabesk and Grand
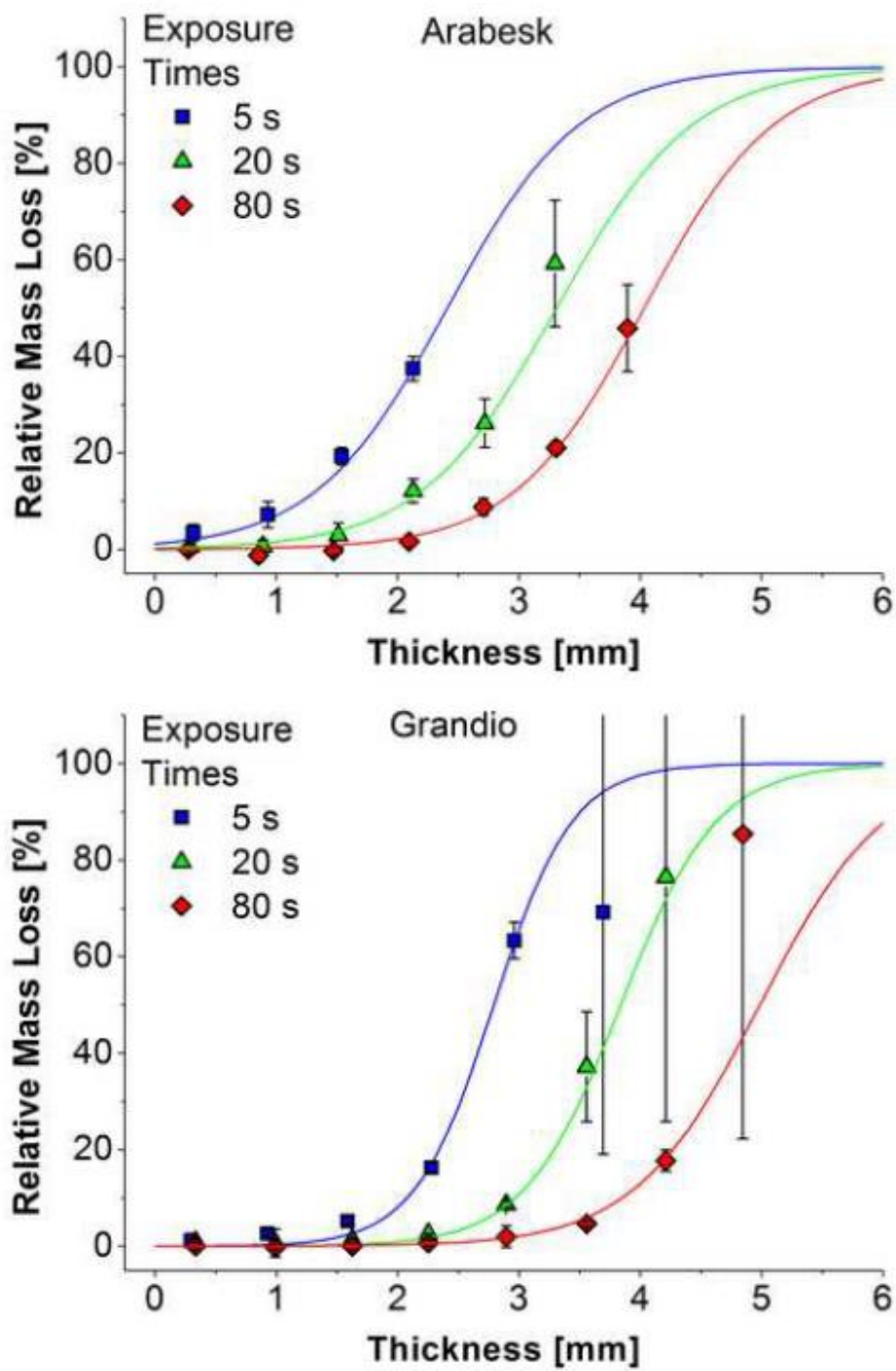
Figure 5 Samples after storage in THF
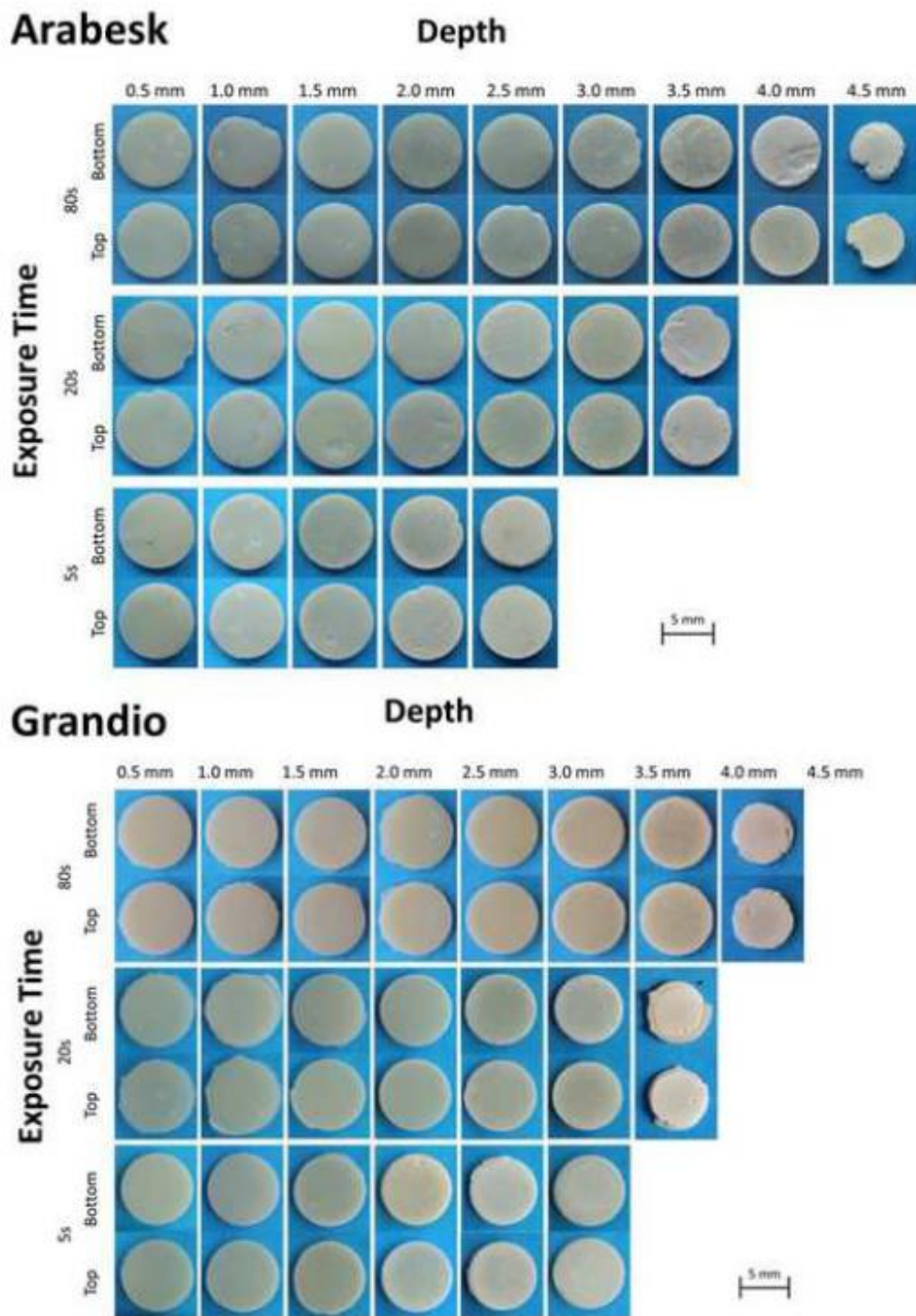
151

152
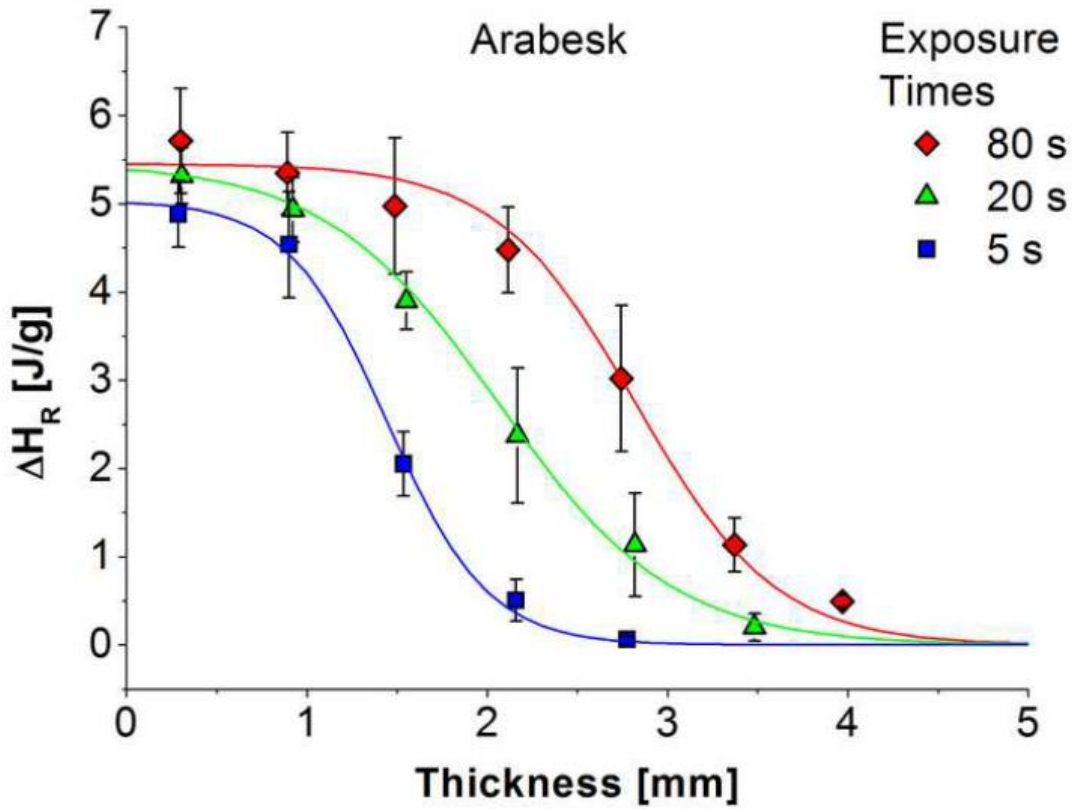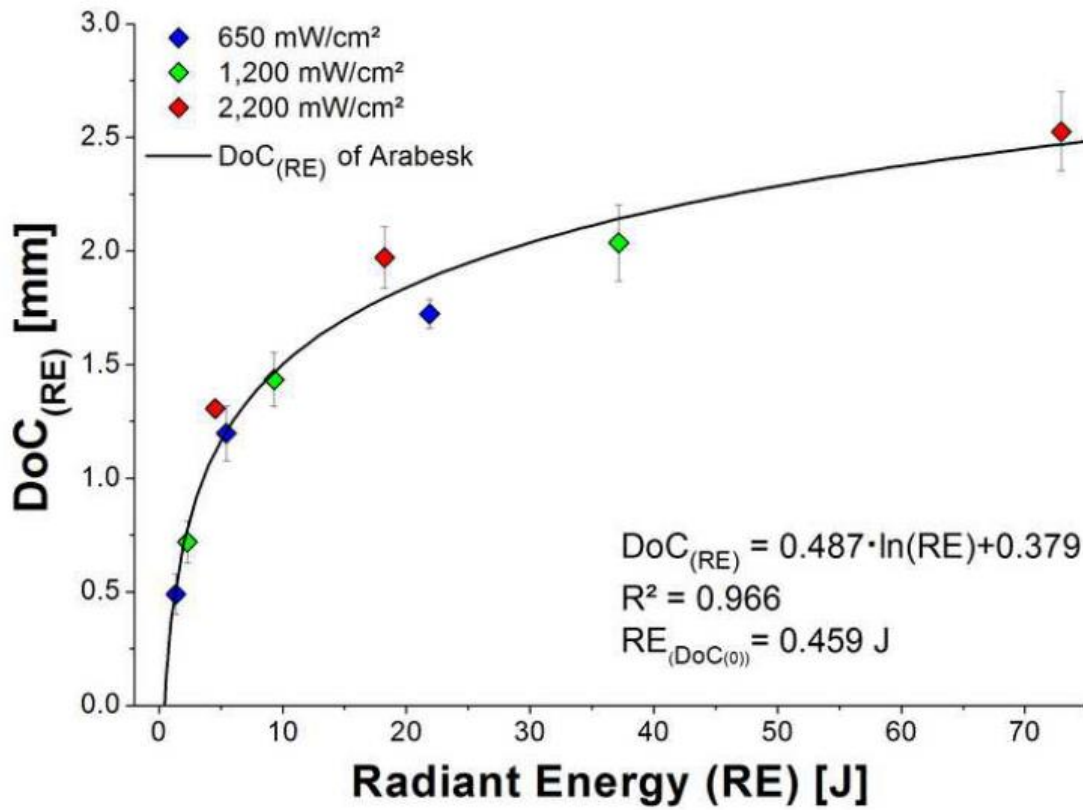
Table 1 Materials and LCU Properties

Dental Composite	Producer	Type	Initiator	Matrix/ Filler content		
Arabesk TOP OA2	Voco GmbH, Cuxhaven, Germany	Light-curing microhybrid composite	CQ/DABE	BisGMA UDMA TEGDMA 77%		
Grandio OA2	Voco GmbH, Cuxhaven, Germany	Light-curing nanohybrid restorative	CQ/DABE	BisGMA TEGDMA 86%		
LCU		Peak Wavelength [nm]	Peak Wavelength range [nm]	Irradiance Total Area [mW/cm²]	Delivered energy over 5, 20 and 80 s [J]	
Celalux 2 Monowave	Voco GmbH, Cuxhaven, Germany	450	415-500	1264 (9.5)	2.3; 9.3; 37.2	
Low Mode Polywave	Ivoclar Vivadent AG, Schaan, Lichtenstein	410 460	380-435 435-530	666 (6.9)	1.4; 5.5; 21.9	
Turbo Mode Polywave		410 460	390-430 430-530	2222 (24.2)	4.6; 18.2; 72.9	

Table 2 Description of experimental setup and sample preparatio
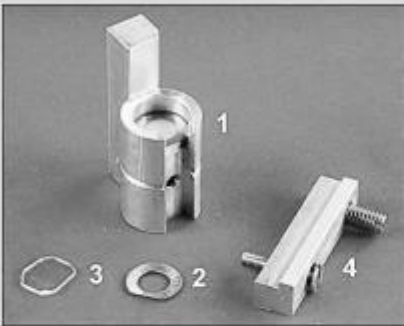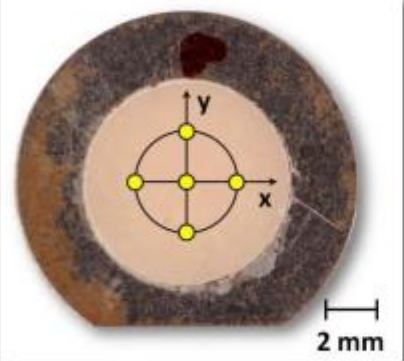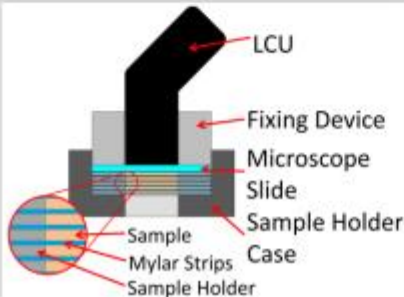
Table 2 Description of experimental setup and sample preparation

Description

Tool to cure the samples
1 Sample holder device
2 Sample holder
3 Microscope slide
4 Position fixing device

Sample holder
The VLC RBC was placed in the middle of the rings (2) and covered with a Mylar stripe on top and bottom. The samples were flattened with a microscope slide (3) and consecutively placed in the sample holder device (1). After putting the desired number of samples in the sample holder device, the top layer was covered with a microscope slide.

The LCU was centered over the sample holder device. The exposure times were 5, 20 and 80s.

Table 3 Evaluation of depth dependent hardness curves

Table 3 Evaluation of depth dependent hardness curves with the fit parameters hardness plateau $HV^{Plateau}$, depth of inflection point $x_{0,1}$, and slope at inflection point a_1; the depth of cure DoC_{HV} determined according to equation (4)

		Time [s]	$HV^{Plateau}$ [HV]		$x_{0,1}$ [mm]		a_1 [HV/mm]		$DoC_{(HV)}$ [mm]	
Arabesk	Celalux 2	5	50.8	(4.2)	1.6	(0.1)	1.2	(0.1)	0.7	(0.1)
		20	53.7	(2.2)	2.4	(0.1)	1.1	(0.1)	1.4	(0.1)
		80	56.8	(2.7)	3.1	(0.2)	0.9	(0.0)	2.0	(0.2)
	Bluephase 20i Low	5	50.3	(1.4)	1.3	(0.0)	1.2	(0.1)	0.5	(0.1)
		20	56.4	(1.1)	2.2	(0.1)	1.0	(0.1)	1.2	(0.1)
		80	58.4	(1.5)	2.9	(0.1)	0.9	(0.1)	1.7	(0.1)
	Bluephase 20i Turbo	5	54.5	(0.9)	2.1	(0.1)	1.3	(0.1)	1.3	(0.0)
		20	59.1	(1.8)	2.9	(0.1)	1.0	(0.0)	2.0	(0.1)
		80	63.3	(2.5)	3.7	(0.1)	0.9	(0.1)	2.5	(0.2)
Grandio	Celalux 2	5	104.6	(2.9)	1.9	(0.1)	1.1	(0.1)	1.0	(0.1)
		20	119.4	(7.5)	2.7	(0.1)	0.8	(0.1)	1.4	(0.1)
		80	120.7	(11.4)	3.7	(0.2)	0.9	(0.1)	2.5	(0.0)
	Bluephase 20i Low	5	104.0	(4.5)	1.7	(0.1)	1.3	(0.4)	0.8	(0.4)
		20	116.7	(4.8)	2.5	(0.3)	1.0	(0.1)	1.5	(0.4)
		80	118.2	(4.2)	3.3	(0.3)	0.9	(0.0)	2.2	(0.3)
	Bluephase 20i Turbo	5	109.9	(2.6)	2.5	(0.0)	1.0	(0.2)	1.5	(0.3)
		20	116.1	(1.1)	3.6	(0.1)	0.9	(0.2)	2.5	(0.1)
		80	117.4	(2.8)	4.4	(0.1)	1.1	(0.1)	3.5	(0.0)

Table 4 Evaluation of mass loss curves

Table 4 Evaluation of mass loss curves with fit parameters depth of inflection point $x_{0,2}$ and slope a_2; depth of cure $DoC_{\Delta m}$ according to equation (4)

		Time [s]	$x_{0,2}$ [mm]		a_2 [1/mm]		$DoC_{(\Delta m)}$ [mm]	
Arabesk	Celalux	5	2.0	(0.1)	0.7	(0.1)	0.5	(0.1)
		20	2.4	(0.1)	1.0	(0.1)	1.5	(0.1)
		80	3.4	(0.4)	0.9	(0.2)	2.3	(0.1)
	Bluephase 20i Low	5	1.7	(0.1)	0.7	(0.1)	0.3	(0.1)
		20	2.5	(0.1)	0.8	(0.1)	1.3	(0.1)
		80	3.3	(0.2)	0.8	(0.1)	2.1	(0.1)
	Bluephase 20i Turbo	5	2.4	(0.1)	0.9	(0.3)	1.2	(0.2)
		20	3.3	(0.1)	0.9	(0.1)	2.2	(0.1)
		80	4.0	(0.2)	0.9	(0.1)	3.0	(0.2)
Grandio	Celalux	5	2.3	(0.4)	0.9	(0.4)	1.2	(0.0)
		20	3.0	(0.3)	1.1	(0.1)	2.1	(0.2)
		80	3.7	(0.5)	1.4	(0.5)	2.9	(0.3)
	Bluephase 20i Low	5	2.2	(0.1)	0.9	(0.1)	1.1	(0.1)
		20	3.2	(0.0)	0.8	(0.1)	1.9	(0.2)
		80	3.5	(0.2)	1.4	(0.2)	2.8	(0.3)
	Bluephase 20i Turbo	5	2.8	(0.1)	1.5	(0.1)	2.1	(0.1)
		20	3.8	(0.2)	1.3	(0.4)	3.0	(0.1)
		80	5.0	(0.2)	1.0	(0.2)	3.9	(0.1)

Table 5 Evaluation of post-reaction curves

Table 5 Evaluation of post-reaction curves with fit parameters maximum post-reaction enthalpy ΔH_{max}, depth of inflection point $x_{0.3}$, slope at inflection point a_3; depth of cure $DoC_{\Delta HR}$ according to equation (4)

		Time [s]	$\Delta H_{(max)}$ [J/g]		$x_{0.3}$ [mm]		a_3 [J/g*mm]		$DoC_{(\Delta HR)}$ [mm]	
Arabesk	Celalux	5	4.8	(3.0)	1.0	(0.5)	2.8	(1.9)	0.5	(0.8)
		20	5.5	(1.1)	1.7	(0.1)	1.5	(0.5)	1.0	(0.2)
		80	5.7	(0.6)	2.2	(0.1)	1.3	(0.1)	1.5	(0.1)
	Bluephase 20i Low	5	4.6	(2.2)	0.6	(0.2)	1.5	(0.3)	-0.1	(0.2)
		20	6.2	(1.5)	1.3	(0.2)	1.7	(0.3)	0.7	(0.3)
		80	4.9	(0.1)	2.1	(0.1)	1.5	(0.4)	1.4	(0.1)
	Bluephase 20i Turbo	5	5.0	(0.5)	1.4	(0.1)	1.8	(0.1)	0.9	(0.1)
		20	5.5	(0.2)	2.1	(0.2)	1.0	(0.3)	1.0	(0.2)
		80	5.5	(0.8)	2.8	(0.1)	1.3	(0.3)	2.0	(0.3)

Table 6 Comparison of depth of cure

Table 6 Comparison of depth of cure at 80% of the plateau hardness $DoC_{0.8HV}$ to depth of cure DoC_{HV}, depth of cure for mass loss $DoC_{\Delta m}$, and depth of cure for post-reaction enthalpy $DoC_{\Delta HR}$ according to equation (4)

		Time [s]	$DoC_{0.8HVmax}$ [mm]		DoC_{HV} [mm]		$DoC_{\Delta m}$ [mm]		$DoC_{\Delta HR}$ [mm]	
Arabesk	Celalux	5	1.1	(0.1)	0.8	(0.1)	0.8	(0.1)	0.5	(0.8)
		20	1.8	(0.1)	1.5	(0.1)	1.8	(0.1)	1.0	(0.2)
		80	2.4	(0.2)	2.1	(0.2)	2.6	(0.1)	1.5	(0.1)
	Bluephase 20i Low	5	0.7	(0.2)	0.5	(0.2)	0.6	(0.1)	-0.1	(0.2)
		20	1.6	(0.1)	1.3	(0.2)	1.6	(0.1)	0.7	(0.3)
		80	2.1	(0.1)	1.8	(0.1)	2.4	(0.1)	1.4	(0.1)
	Bluephase 20i Turbo	5	1.6	(0.1)	1.4	(0.1)	1.5	(0.2)	0.9	(0.1)
		20	2.3	(0.1)	2.1	(0.1)	2.5	(0.1)	1.0	(0.2)
		80	2.9	(0.2)	2.6	(0.2)	3.3	(0.2)	2.0	(0.3)
Grandio	Celalux	5	1.3	(0.1)	1.0	(0.1)	1.5	(0.1)		
		20	1.9	(0.1)	1.6	(0.1)	2.5	(0.2)		
		80	2.9	(0.1)	2.6	(0.1)	3.7	(0.6)		
	Bluephase 20i Low	5	1.2	(0.3)	0.9	(0.4)	1.1	(0.1)		
		20	1.9	(0.4)	1.6	(0.4)	1.9	(0.2)		
		80	2.6	(0.3)	2.3	(0.3)	2.8	(0.3)		
	Bluephase 20i Turbo	5	1.9	(0.2)	1.6	(0.3)	2.1	(0.1)		
		20	2.9	(0.1)	2.6	(0.2)	3.1	(0.1)		
		80	3.8	(0.1)	3.5	(0.2)	3.9	(0.1)		

ELSEVIER

Effect of the irradiance distribution from light curing units on the local micro-hardness of the surface of dental resins

CrossMark

Thomas Haenel[a,b], Berenika Hausnerová[a,c], Johannes Steinhaus[a,b], Richard B.T. Price[d], Braden Sullivan[d], Bernhard Moeginger[b,]*

[a] Centre of Polymer Systems, University Institute, Tomas Bata University in Zlin, Zlin, Czech Republic
[b] Bonn-Rhein-Sieg, University of Applied Sciences, Department of Natural Sciences, Rheinbach, Germany
[c] Tomas Bata University in Zlin, Faculty of Technology, Department of Production Engineering, Zlin, Czech Republic
[d] Dalhousie University, Department of Dental Clinical Sciences, Faculty of Dentistry, Halifax, Canada

ARTICLE INFO

ABSTRACT

Objective. An inhomogeneous irradiance distribution from a light-curing unit (LCU) can locally cause inhomogeneous curing with locally inadequately cured and/or over-cured areas causing e.g. monomer elution or internal shrinkage stresses, and thus reduce the lifetime of dental resin based composite (RBC) restorations. The aim of the study is to determine both the irradiance distribution of two light curing units (LCUs) and its influence on the local mechanical properties of a RBC.

Methods. Specimens of Arabesk TOP OA2 were irradiated for 5, 20, and 80 s using a Bluephase® 20i LCU in the Low mode (666 mW/cm^2), in the Turbo mode (2222 mW/cm^2) and a Celalux® 2 (1264 mW/cm^2). The degree of conversion (DC) was determined with an ATR-FTIR. The Knoop micro-hardness (average of five specimens) was measured on the specimen surface after 24 h of dark and dry storage at room temperature.

Results. The irradiance distribution affected the hardness distribution across the surface of the specimens. The hardness distribution corresponded well to the inhomogeneous irradiance distributions of the LCU. The highest reaction rates occurred after approximately 2 s light exposure. A DC of 40% was reached after 3.6 or 5.7 s, depending on the LCU. The inhomogeneous hardness distribution was still evident after 80 s of light exposure.

Significance. The irradiance distribution from a LCU is reflected in the hardness distribution across the surface. Irradiance level of the LCU and light exposure time do not affect the pattern of the hardness distribution – only the hardness level. In areas of low irradiation this may result in inadequate resin polymerization, poor physical properties, and hence premature failure of the restorations as they are usually much smaller than the investigated specimens. It has to be stressed that inhomogeneous does not necessarily mean poor if in all areas of the restoration enough light intensity is introduced to achieve a high degree of cure.

© 2014 Academy of Dental Materials. Published by Elsevier Ltd. All rights reserved.

* *Corresponding author at*: Bonn-Rhein-Sieg, University of Applied Sciences, Department of Natural Sciences, Justus-von-Liebig Str. 20, 53359 Rheinbach, Germany. Tel.: +49 2241 865 531; fax: +49 2241 865 8531.
E-mail address: bernhard.moeginger@fh-brs.de (B. Moeginger).

1.   Introduction

Visible light cured (VLC) resin based composites (RBCs) are commonly used as restorative materials [1]. Adequate curing of these materials depends on the initiator receiving sufficient energy at correct wavelengths [2]. Adjusting the optimum curing conditions by choosing correct light exposure time and irradiance level, precise positioning of the light curing unit (LCU) over the restoration site and not attempting to cure too much resin at one time make the difference between a resin that is properly cured and an inadequately cured restoration [3–5]. The irradiance from the LCU has a significant influence on the surface hardness as well as on depth of cure (DoC) and degree of conversion (DC) [6–9].

The reactive radicals are created by the exposure of VLC RBCs. A photo-sensitive initiator, such as camphor quinone (CQ), absorbs light energy and changes into an excited state. The excited state is transferred to a reducing agent, usually an amine molecule e.g. dimethylaminobenzoate (DABE). The CQ–DABE-pair (exiplex) creates two free radicals. They attack the free carbon double bonds of the monomers and start the photo-polymerization. The number of generated radicals depends on the emitted irradiance of a LCU and affects thus directly the attainable DC [2,10–13].

The highest reaction rates and highest changes in DC were observed as long as the resin is below the glass-transition temperature (T_g) [2]. During the curing process T_g increases because it is linked to the degree of polymerization of the resin molecules or the corresponding molecular weight, respectively. Therefore, T_g exceeds the polymerization temperature after some time [14]. The matrix transfers to the glassy state in which the mobility of the radicals and monomers is drastically reduced and the reaction rate tends to zero [15–18]. Therefore, the existing radicals are trapped in the cured polymer matrix [19]. After the exposure the trapped radicals either react very slowly with remaining carbon double bonds or deactivate over termination reactions over a long period of time. This effect known as "post-curing" [20–22] leads to a further and slow increase of DC. It depends on the numbers of trapped radicals in the cured polymer matrix. Halverson et al. showed that the photo-polymerization process has an energy absorption limit. Over a specific energy level no improving of the mechanical behavior was observed [10].

Mechanical properties such as hardness, Young's modulus or shrinkage depend directly on the DC [13,23]. Several studies showed that a high DC corresponds to high hardness, high Young's modulus, and high shrinkage [15,24–26]. Therefore, possible irradiance distributions of LCU may produce inhomogeneous shrinkage resulting in internal stress distributions and/or debonding [18,27–30].

Several authors have described the problem of inhomogeneous irradiance output from LCUs, the effect on the curing of VLC RBCs and the consequences of the light output measurement as part of the quality management [31–34]. Currently two different types of light-emitted diode (LED) LCUs are in use: Firstly, monowave blue-LED units emitting a relatively sharp blue light peak and secondly, polywave LED units emitting a broader spectrum with at least two peaks at different wavelengths. Some studies reported higher curing efficiencies in terms of hardness, elastic modulus or DC for polywave LCUs with the same or lower irradiance than for monowave LCUs [35–38].

Tungsten halogen lights and plasma arc lights also emit a broad range of wavelengths that cover the effective spectra of the commonly used photo-initiators [6,39]. However, the classical tungsten halogen lights are being rapidly replaced by LED units due to convenience reasons and higher irradiances [1,7].

The surface hardness (Knoop or Vickers) has been used to characterize the mechanical properties of VLC RBCs [39]. The DC within the resin was determined using Fourier transform infrared spectroscopy (FTIR) [40]. Arikawa et al. and Price et al. found a correlation between the irradiance distribution and the hardness distribution [31,41].

However, the effects of prolonged exposure times on the hardness distribution requires further study as it is assumed that additional curing will occur in areas of lower DC as initiator radicals will have a slightly higher mobility there. This allows additional cross-links to be created in these areas leading to a more homogeneous polymer network. In most cases the exposure time will be between 5 and 40 s [31,41]. The primary problems of current RBCs are inadequate polymerization, shrinkage and corresponding shrinkage stress as well as elution of low molecular substances. This restricts the durability of restorations and may induce allergies or other health implications [26,42,43].

Therefore, the hypotheses of this study were the follows:

1. Each LCU has a specific irradiance distribution leading to a corresponding pattern of the hardness distribution of a dental composite surface.
2. The number of radicals depends on the irradiance level and/or on the exposure time. A higher irradiance creates sufficient radicals to activate all carbon double bounds forming a more homogeneous network and longer exposure times provide radicals over a longer period. Thus, the effects of differences of irradiance distributions of LCUs are compensated by longer exposure time.

2.   Materials and methods

2.1.   Materials and sample preparation

A camphorquinone based VLC RBC – the micro-hybrid composite Arabesk TOP OA2, VOCO, LOT 1114471 (in the following text abbreviated Arabesk) – containing 22 wt.% bisphenol A glycidyl methacrylate (Bis-GMA), triethylene glycole dimethacrylate (TEGDMA), and urethane dimethacrylate (UDMA), and 77 wt.% of bi-ceramic system filler was used in this study [44,45].

2.2.   Methods

2.2.1.   Measurement of power and beam-profiles of the LCU

Two LED LCU with different emission spectra were used in this study, Fig. 1:
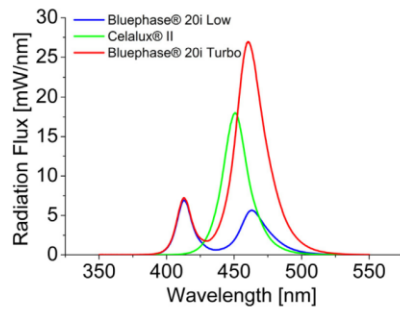
Fig. 1 – Spectral distribution of the Celalux® 2, Bluephase® 20i in the Low mode and the Turbo mode.

Fig. 2 – Schematic experimental setup of the beam profiler measurement.

1. The monowave blue-LED LCU "Celalux® 2" (Voco, Cuxhaven, Germany) delivering an irradiance of 1000–1500 mW/cm^2, depending on the light guide tip (manufacturer information) [11] and
2. The polywave poly-LED LCU "Bluephase® 20i" (Ivoclar Vivadent, Schaan, Liechtenstein) is used in Low mode with an irradiance of 650 mW/cm^2 and in Turbo mode with an irradiance of 2200 mW/cm^2 (manufacturer information) (in the following text abbreviated Low mode and Turbo mode) [46].

Both LCUs had a 10 mm entrance diameter and an 8 mm exit diameter turbo light guide tip.

The power output from each LCU was determined using an integrating sphere (LabSphere 6″) connected to an UV–vis spectrometer (Ocean Optics USB4000, Dunedin, FL). The power output P_{out} was calculated by integrating the spectra between the wavelengths $\lambda_{min} = 350$ nm and $\lambda_{max} = 550$ nm, Fig. 1.

The irradiance distributions across the tip of each light guide were determined using a Laser Beam Profiler (LBA USB-L070 Beam Profiler, Ophir-Spiricon, Logan, UT, USA) and evaluated with the Beam Gage software (Ophir-Spiricon). The LCUs were placed directly on a frosted glass shield (DG2X2-1500, Thor Laboratories, Newton, NJ, USA) in front of the camera lens, Fig. 2. The intensity image of the beam-profiler in arbitrary intensity units has to be transferred to intensities with the calibration factor f_{cal}:

$$f_{cal} = \frac{P_{out}}{I_{total} \cdot A_{pixel}} \tag{1}$$

with the intensity value I_{total} of the measured beam-profiler data and the area of a pixel A_{pixel} with a linear dimension of 29.2 μm. Eq. (1) expresses f_{cal} as irradiance per count.

Then the irradiance per pixel Ir_{pixel} is given by

$$Ir_{pixel} = f_{cal} \cdot I_{pixel} \tag{2}$$

with I_{pixel} as intensity per pixel in arbitrary intensity units.

The radiance exposure H_e provides the information in which time the same amount of energy was delivered to the specimen surface for different LCU modes. It is defined by Eq. (3):
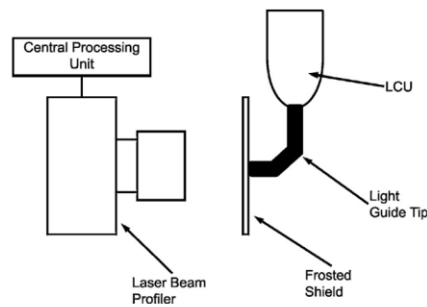
$$H_e = I_r \cdot t_e \tag{3}$$

with the irradiance I_r and exposure time t_e.

2.2.2. Determination of the top hardness distribution

Micro-hardness specimens were made in 1 mm thick circular aluminum rings ($D_{out} = 20$ mm, $D_{in} = 8$ mm). The aluminum rings were marked by a flat edge to ensure a defined and comparable position for each sample with respect to the light beam and so that they could be repeatedly placed in the same orientation in the Knoop micro-hardness tester. The Arabesk was carefully placed incrementally with a dental plugger into the center hole of the ring and covered with a Mylar® strip to reduce air inhibition of the resin. A 1 mm thick microscope slide was used to press and flatten the sample to the thickness of 1 mm. The light guide tips were placed directly on the microscope slide over the center of the sample. The specimens were irradiated for 5, 20 and 80 s through the microscope slide and the Mylar strip using each LCU. For light exposure times exceeding the available time program, the LCU had to be restarted. Five specimens ($n = 5$) were made at each light exposure time and with each LCU. The microscope slide and the Mylar strips were removed from the specimens 10 min after exposure.

Each specimen for the hardness tests was measured 24 h after exposure. They were stored in a dry and dark room at a temperature of (23 °C) for 24 h before Knoop micro-hardness was measured.

The micro-hardness (in the following text abbreviated hardness) distribution on the top surface of the specimens was measured with a Knoop micro-hardness tester (Mitutoyo, HM 101) equipped with an automatic xy-stage. The mapping was performed with 45 indentations with a lateral resolution of 1 mm on 5 specimens ($n = 5$) according to Fig. 3 in order to calculate mean hardness and standard deviation for each coordinate point. The lateral resolution of 1 mm was chosen to affirm a threefold distance of the longest edges of the Knoop indentations being around 300 μm. This affirms that the indentations do not affect each other. The indentation

Fig. 3 – Overlay of hardness measurement grid (red dots) and the irradiated sample area. The lateral distance of the indentation points in x and y direction is 1 mm. (For interpretation of the references to color in this figure legend, the reader is referred to the web version of the article.)

force of 490.3 mN was applied for 8 s generating maximum indentation depths of 7 μm. The hardness was measured on the top surface because the inte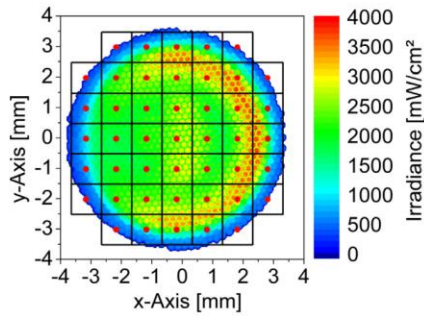nsity distribution of the LCU is most pronounced at the surface. Light scattering at the filler resin interfaces will partly change the lateral intensity distribution within the sample and complicate a correlation.

The results of the hardness mapping were compared with a two-sample test of variance (significant level $\alpha = 0.05$) and the mean hardness was calculated as the arithmetic average for each indentation position. For each exposure time the mean of the hardness maps was compared with a two-sample t-test ($\alpha = 0.05$) to verify a significant difference between the different exposure times.

2.2.3. Determination of the DC by FTIR Spectroscopy

DC specimens were prepared in 1 mm thick Delrin® rings ($D_{out} = 15$ mm, $D_{in} = 4$ mm). The Delrin® rings for the DC specimens were placed centrically over the Golden Gate ATR diamond (Bruker Tensor 27, Mid IR, FTIR). The Arabesk was carefully incrementally placed with a dental plugger into the center hole of the Delrin® rings and covered with a Mylar® strip to reduce air inhibition of the resin. A 1 mm thick microscope slide was used to press and flatten the sample to the thickness of 1 mm. The light guide tips were placed directly on the microscope slide over the center of the sample. The specimens were exposed with the Low and Turbo mode for 5, 20 and 80 s through the microscope slide and the Mylar strip using each LCU. For light exposure times exceeding the available time program, the LCU had to be restarted. The Mylar strip typically absorbed 5% of the LCU irradiation. Five specimens ($n = 5$) were made at each light exposure time and with each LCU. Due to the experimental setup the DC had to be recorded

at the bottom surface of the specimen on the ATR in real time for 180 s.

The curing process was investigated using a FTIR spectrometer (Bruker Tensor 27) equipped with an ATR-Golden-Gate camber (attenuated total reflection) under the following conditions:

Measuring time:	180 s to determine the final DC
Sample scan time:	6 recording spectra in double side mode
Resolution with respect to the wave number:	8 cm^{-1}
Scan rate:	10 scans/s.

A measure for the time dependent DC is in principle the ratio of the change of the absorbance band of the aliphatic C=C double bound ($Abs_{(Aliphatic)}$) with respect to the absorbance of the uncured state in the wave number range 1645–1620 cm^{-1}. Due to scatter between two measurements the absorbance of the aliphatic band is mostly normalized to the absorbance of the aromatic band ($Abs_{(Aromatic)}$) in the wave number range 1620–1590 cm^{-1} because this band is not affected by the curing process.

DC determination is affected by the relationship between the molar ratio (M_r) of Bis-GMA, TEGDMA, UDMA and their corresponding absorption ratio (A_r).

$$A_r = \frac{Abs_{(Aliphatic)}}{Abs_{(Aromatic)}} \tag{4}$$

The FT-IR equipment was calibrated based on a technique reported by Rueggeberg et al. [47] using hydrogenated BIS-GMA and TEGDMA with different M_r. The regression analysis of M_r against A_r showed a second order polynomial.

$$M_r = 0.141 \cdot A_r^2 + 1.142 \cdot A_r \tag{5}$$

Then the DC is given by

$$DC = 100\% \times \left[1 - \frac{0.141[(Abs_{(Aliphatic)})/(Abs_{(Aromatic)})]^2_{Polymer} + 1.1424[(Abs_{(Aliphatic)})/(Abs_{(Aromatic)})]_{Polymer}}{0.141[(Abs_{(Aliphatic)})/(Abs_{(Aromatic)})]^2_{Monomer} + 1.1424[(Abs_{(Aliphatic)})/(Abs_{(Aromatic)})]_{Monomer}} \right] \tag{6}$$

The rate of $DC_{(t)}$ was determined by calculating the derivative of the $DC_{(t)}$-curves.

3. Results

3.1. Measurements of power output and irradiance distribution

The LCUs were chosen to have significant differences with respect to power output: the ratio "Bluephase Low:Celalux® 2:Bluephase®Turbo is 1:1.7:3.3. However, the relevant quantity for the dentist is the total irradiance as it determines the locally introduced amount of energy. The ratio of the total irradiance of the LCUs is 1:1.9:3.3. The differences for the LCU Celalux® 2 were attributed to the smaller tip area of the light guide (Table 1).

The irradiance distributions of Celalux® 2 and Bluephase® 20i are very different although Low mode and Turbo mode

Table 1 – Power outputs, calculated irradiances, radiant exposure and spectral information from each LCU.

	Unit	Celalux® 2	Low mode	Turbo mode
Power	mW	465 (3.5)	273 (2.8)	912 (9.9)
Relative power		1.7	1	3.3
Effective tip area of LCU	cm^2	0.37 (1.8 × 10^{-5})	0.41 (5.0 × 10^{-5})	0.41 (3.5 × 10^{-5})
Irradiance	mW/cm^2	1264 (9.5)	666 (6.9)	2222 (24.2)
Relative irradiance		1.9	1	3.3
Peak wavelength	nm	450	413	413
			463	460
Peak wavelength range	nm	415–500	390–435	395–430
			435–495	430–495

varied only in the intensity level, Fig. 4. The Celalux® 2 exhibited three regions of different irradiance levels, Fig. 4a. Region I is a square shaped-area of approximately 9 mm^2 in the center of the light guide with an average irradiance of 1400 mW/cm^2, Table 2a. Region II is an annular-shaped area around the center region with a width of approximately 1 mm and an average irradiance of 760 mW/cm^2. Region III is a ring with a diameter of 3 mm and a width of approximately 1 mm with an average irradiance of 980 mW/cm^2. The irradiance distribution has a maximum between 1 and 2 o'clock position and a minimum between 7 and 8 o'clock, Table 2a.

The beam-profile irradiance patterns from the Low and Turbo modes were similar in shape, Fig. 4b and c. After normalization to the highest irradiance value, the irradiance maps show almost no differences between them, Table 3. In the center of the light beam there was a rectangular area of approximately 4 mm^2 with an irradiance of 660 mW/cm^2 in the Low mode and 2200 mW/cm^2 in the Turbo mode, respectively. A ⊃-shaped area on the right side occurs around the center with a radius of 2.5 mm and a width of 1 mm. The highest irradiance within this ⊃-shaped area was 730 mW/cm^2 in the Low mode and 2500 mW/cm^2 in the Turbo mode, Table 2b and c. Nevertheless, a ring with 3 mm diameter and a width of approximately 1 mm exhibited relatively low average irradiances of 360 mW/cm^2 and 1130 mW/cm^2 in the Low and Turbo modes, respectively. The "low irradiance region" left of the center had irradiances of 550 mW/cm^2 in the Low mode and 1500 mW/cm^2 in the Turbo mode.

The radiant exposure H_e for the Low and Turbo mode was calculated in a time interval of 80 s in steps of 0.5 s to determine the exposure times having the same H_e of 3.3, 13.3 and 53.3 J/cm^2. These H_e were delivered after exposure times of 5, 20 and 80 s for the Low mode. The corresponding exposure times for the Turbo mode were determined to be 1.5, 6 and 24 s while after exposure times of 5, 20 and 80 s the H_e for the Turbo mode were 11.1, 44.4 and 177.8 J/cm^2

3.2. Measurement of the hardness distribution and mapping

The hardness mapping revealed differences in the hardness distributions with respect to minimum and maximum hardness values, Table 4. As anticipated, the mean hardness of the surface increased with exposure time. The increase of the mean hardness was typically 25–30% when the light exposure time was prolonged from 5 to 80 s, Table 5. The Celalux® 2 and the Turbo mode showed the largest increase in hardness between 5 and 20 s, while the largest increase occurred between 20 s and 80 s for the Low mode, Table 5. Interestingly, for each light exposure condition the mean hardness of the Low mode was higher than for the Celalux® 2. The two-sample t-test showed a significant difference between the mean hardness of the different exposure times for all LCUs (α = 0.05).

The local hardness values of the specimens are plotted as hardness maps in Fig. 5. For the Celalux® 2, the hardness map after 5 s of light exposure shows a region of greater hardness in the middle of the sample which corresponds to the position of the high irradiance square region in the center of the light beam, Fig. 5. This region expands with light exposure time from the middle to the periphery of the specimens. Furthermore, the maps show greater hardness values on the right half of the specimens. The hardness map after 20 s of
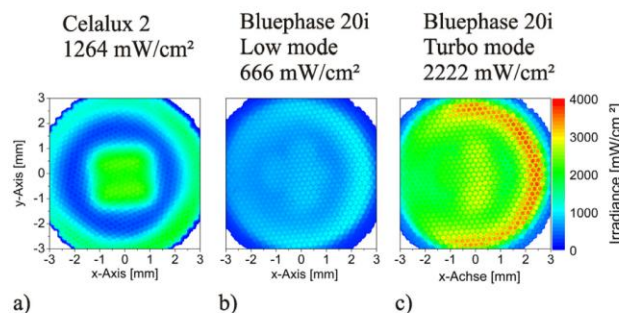

Fig. 4 – Irradiance distributions of Celalux® 2 (a), Low mode (b) and Turbo mode (c) in a color representation. (For interpretation of the references to color in this figure legend, the reader is referred to the web version of the article.)

Table 2 – Irradiance distribution of areas with 1 mm² around the indentation points.

(a) Celalux® 2 Irradiance [mW/cm²]

y-Axis [mm] \ x-Axis [mm]	−3	−2	−1	0	1	2	3
3		1109	1193	1281	1408	1058	
2	991	984	499	460	758	1556	905
1	902	419	1386	1766	1070	928	1196
0	879	420	1732	2173	677	929	1145
−1	907	477	1007	1363	834	1219	1067
−2	771	919	572	528	834	589	571
−3		721	960	989	956		

(b) Low mode

y-Axis [mm] \ x-Axis [mm]	−3	−2	−1	0	1	2	3
3		263	503	594	439	211	
2	258	631	721	730	794	629	195
1	417	638	630	742	661	867	383
0	483	618	676	732	655	816	468
−1	424	657	618	682	619	850	370
−2	256	612	724	723	798	600	194
−3		251	445	527	414	220	

(c) Turbo mode

y-Axis [mm] \ x-Axis [mm]	−3	−2	−1	0	1	2	3
3		858	1708	1955	1387	602	
2	719	1995	2409	2672	2479	1945	539
1	1143	1881	2079	2544	2166	2873	1126
0	1314	1842	2149	2495	2062	2791	1450
−1	1221	2041	2081	2435	2113	2903	1103
−2	751	2048	2567	2622	2853	1938	533
−3		775	1564	1878	1350	659	

light exposure shows greater hardness values that are more homogeneously distributed across the surface. The hardness map after 80 s of light exposure is almost entirely homogeneous. The maximum hardness value was 25.1 KHN, and 85% of the hardness values exceeded 23 KHN. The min–max-ratio decreased from 63% after 5 s to 16% after 80 s of light exposure time, Table 5.

For the Low mode as well as for the Turbo mode, the hardness maps show a ⊃-shaped region with a radius of 2 mm around the middle of the specimens of greater hardness values in the right half, Fig. 5b and c. This region corresponds to the higher ⊃-shaped irradiance region of Bluephase® 20i shown in Fig. 4b and c. On the left half of the map, there is a region of lower hardness. This region corresponds to the LED chip that emits light close to 410 nm. The min–max-ratio of the hardness decreased from 61.5% to 20.9% between 5 and 80 s of light exposure from the Low mode while for the Turbo mode the min–max-ratio decreased from 42.4 to 23.9% between 5 and 20 s of light exposure time, but increased again to 29.8% between 20 s and 80 s of light exposure time. Even after 80 s of light exposure, the complete homogenization across the surface hardness was not observed.

The comparison of the irradiance and hardness distribution was calculated as the difference of the normalized irradiance maps and normalized hardness distribution maps, Table 3. Three factors: irradiance inhomogeneity factor (IIF), hardness inhomogeneity factor (HIF), and comparison inhomogeneity factor (CIF) represent inhomogeneity of irradiance, hardness and comparison of both, Table 4.

IIF as an arithmetic mean value of the normalized irradiance map specifies inhomogeneity of the irradiance distribution. HIF as an arithmetic mean value of the normalized hardness map specifies the inhomogeneity in the hardness distribution. IIF and HIF values of 1 correspond to homogeneous irradiance and hardness distributions, respectively. The HIFs of the Celalux® 2 and the Low modes indicate that the inhomogeneity in the hardness distribution decrease with increasing exposure time, while the Turbo mode shows a decrease in homogeneity between 5 and 20 s and between 20 and 80 s increasing inhomogeneity.

CIF is an arithmetic mean value of the comparison map and reveals the congruence of irradiance and hardness distribution. A value of zero implies no difference between irradiance and hardness distribution.

The obtained CIF value indicates an increasing difference between irradiance and hardness distribution at longer exposure time for each LCU.

3.3. Measurement of the degree of conversion (DC)

The penetration depth of the IR radiation in the ATR mode is in the order of the wavelengths that are up to 2 μm [48]. Therefore, the DC was measured in a depth of 1 mm below the surface corresponding to one half of typical depths of cure of the investigated VLC RBC. At this depth one may expect a representative reaction rate to get some information about how much time is required to reach the beginning vitrification. After an exposure time of 5–6 s the DC exceeded 40% for the Low mode and after 3–4 s for the Turbo mode, Table 6

Table 3 – Normalized irradiance and hardness distribution of the Low and Turbo mode for 5 s of exposure time.

Normalized irradiance

	(a) Low mode 5 s x-Axis [mm]							(b) Turbo mode 5 s x-Axis [mm]						
y-Axis [mm]	−3	−2	−1	0	1	2	3	−3	−2	−1	0	1	2	3
3		0.3	0.6	0.7	0.5	0.2			0.3	0.6	0.7	0.5	0.2	
2	0.3	0.7	0.8	0.8	0.9	0.7	0.4	0.2	0.7	0.8	0.9	0.9	0.7	0.4
1	0.5	0.7	0.7	0.9	0.8	1.0	0.8	0.4	0.6	0.7	0.9	0.7	1.0	0.8
0	0.6	0.7	0.8	0.9	0.8	1.0	1.0	0.5	0.6	0.7	0.9	0.7	1.0	1.0
−1	0.5	0.8	0.7	0.8	0.7	1.0	1.0	0.4	0.7	0.7	0.8	0.7	1.0	1.0
−2	0.3	0.8	0.9	0.9	1.0	1.0	1.0	0.3	0.7	0.9	0.9	1.0	1.0	1.0
−3		0.2	0.3	0.4	0.3	0.2			0.4	0.8	1.0	1.0	1.0	

Hardness [KHN]

	(a) Low mode 5 s x-Axis [mm]							(b) Turbo mode 5 s x-Axis [mm]						
y-Axis [mm]	−3	−2	−1	0	1	2	3	−3	−2	−1	0	1	2	3
3		16.8	21.0	21.4	20.4	16.0			20.5	22.1	22.9	21.3	18.4	
2	15.3	21.2	22.8	23.2	23.3	20.8	15.2	18.8	22.0	22.6	21.3	22.6	21.7	20.6
1	20.3	20.5	20.0	21.3	23.9	20.6	20.2	21.4	20.5	18.8	21.0	22.4	22.7	20.8
0	19.7	20.8	21.0	23.2	23.4	24.1	19.9	21.0	20.3	22.0	23.8	23.1	22.0	17.2
−1	18.3	23.0	21.8	22.9	23.3	23.9	18.1	20.9	14.7	21.6	22.6	18.7	20.6	19.3
−2	11.1	20.0	21.5	23.1	21.8	20.4	11.1	13.7	22.2	21.8	22.0	20.2	14.7	18.7
−3		10.9	16.2	18.7	17.6	9.3			19.7	21.0	18.9	19.9	21.1	

Normalized hardness

	(a) Low mode 5 s x-Axis [mm]							(b) Turbo mode 5 s x-Axis [mm]						
y-Axis [mm]	−3	−2	−1	0	1	2	3	−3	−2	−1	0	1	2	3
3		0.7	0.9	0.9	0.8	0.7			0.9	0.9	1.0	0.9	0.8	
2	0.6	0.9	0.9	1.0	1.0	0.9	0.6	0.8	0.9	0.9	0.9	0.9	0.9	0.9
1	0.8	0.9	0.8	0.9	1.0	0.9	0.8	0.9	0.9	0.8	0.9	0.9	1.0	0.9
0	0.8	0.9	0.9	1.0	1.0	1.0	0.8	0.9	0.9	0.9	1.0	1.0	0.9	0.7
−1	0.8	1.0	0.9	1.0	1.0	1.0	0.8	0.9	0.6	0.9	0.9	0.8	0.9	0.8
−2	0.5	0.8	0.9	1.0	0.9	0.8	0.5	0.6	0.9	0.9	0.9	0.8	0.6	0.8
−3		0.5	0.7	0.8	0.7	0.4			0.8	0.9	0.8	0.8	0.9	

Comparison of irradiance and hardness

	(a) Low mode 5 s x-Axis [mm]							(b) Turbo mode 5 s x-Axis [mm]						
y-Axis [mm]	−3	−2	−1	0	1	2	3	−3	−2	−1	0	1	2	3
3		0.4	0.3	0.2	0.3	0.4			0.6	0.3	0.3	0.4	0.6	
2	0.3	0.2	0.1	0.1	0.1	0.1	0.2	0.5	0.2	0.1	0.0	0.0	0.2	0.5
1	0.4	0.1	0.1	0.0	0.2	−0.1	0.0	0.5	0.2	0.1	0.0	0.2	0.0	0.1
0	0.2	0.1	0.1	0.1	0.2	0.0	−0.2	0.4	0.2	0.2	0.1	0.3	0.0	−0.3
−1	0.3	0.2	0.2	0.1	0.2	0.0	−0.2	0.5	−0.1	0.2	0.1	0.1	−0.1	−0.2
−2	0.1	0.1	0.0	0.1	−0.1	−0.2	−0.5	0.3	0.2	0.0	0.0	−0.2	−0.4	−0.2
−3		0.3	0.4	0.4	0.4	0.2			0.4	0.0	−0.2	−0.2	−0.1	

and Fig. 6. The maximum rate of $DC_{(t)}$ of 13.3%/s for the Low mode occurred after 1.8 s. For the Turbo mode the maximum rate of $DC_{(t)}$ occurred after 1.9 s with 20.6%/s. This shows that most of the curing process happened within this very short time range. The analysis of H_e also shows a higher DC for the Low mode between 5 and 80 s than for the Turbo mode in the corresponding time range from 1.5 to 24 s.

The final degree of conversion after 180 s of measurement $DC_{(3\,min)}$ exhibited lower DCs for the Low mode specimens than for the Turbo mode specimens. For example, in the Low mode an exposure time of 5 s leads to a $DC_{(3\,min)}$ of 54.2% while after 80 s of exposure time a DC of 65.2% is reached. In the Turbo mode the corresponding $DC_{(3\,min)}$ values are 62.5% and 67.3%, respectively, Table 6.
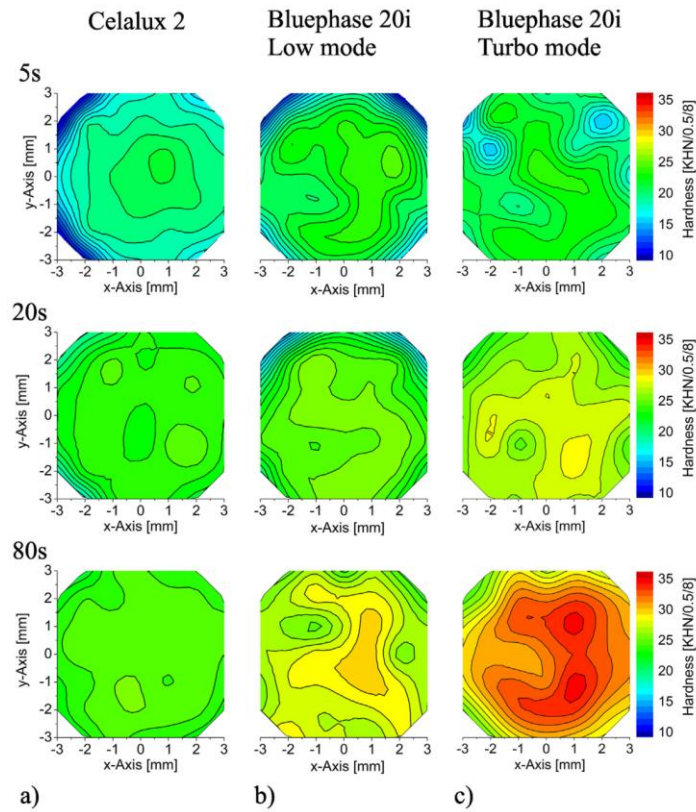
Fig. 5 – Surface hardness distributions of Arabesk specimens after 5, 20 and 80 s exposure time using the Celalux® 2 (a), Low mode (b) and Turbo mode (c).

Table 4 – Mean, minimum and maximum hardness according to the Knoop hardness mapping after 24 h, irradiance inhomogeneity factor (IIF), the comparison inhomogeneity factor (CIF) and the hardness inhomogeneity factor (HIF).

	Celalux® 2 exposure time			Low mode exposure time			Turbo mode exposure time		
	5 s	20 s	80 s	5 s	20 s	80 s	5 s	20 s	80 s
Mean hardness [KHN]	17.8 (3.2)	22.6 (1.6)	23.9 (0.9)	20.0 (3.8)	22.8 (3.5)	26.9 (1.5)	20.5 (2.5)	26.2 (1.6)	30.2 (2.6)
Minimum hardness [KHN]	7.9 (1.6)	17.5 (1.0)	21.2 (1.2)	9.3 (1.8)	11.2 (3.0)	22.4 (1.3)	12.2 (3.4)	21.6 (2.3)	24.9 (1.2)
Maximum hardness [KHN]	21.6 (0.7)	24.1 (1.0)	25.1 (1.1)	24.8 (2.6)	26.4 (4.3)	29.6 (2.6)	23.9 (2.9)	28.4 (1.6)	34.6 (1.7)
Hardness ratio Min/max [%]	63.4	27.4	15.5	62.5	57.6	24.3	49	23.9	28
IIF	0.45	0.45	0.45	0.69	0.69	0.69	0.73	0.73	0.73
HIF	0.82	0.94	0.95	0.82	0.88	0.91	0.86	0.92	0.87
CIF	0.37	0.48	0.5	0.13	0.2	0.22	0.13	0.19	0.15

Table 5 – Increase of the mean hardness with increasing exposure times.

	Hardness change in %		
	From 5 to 20 s	From 20 to 80 s	From 5 to 80 s
Celalux® 2	21.1	5.6	25.5
Low mode	12.6	15.0	25.7
Turbo mode	21.9	13.1	32.1

4. Discussion

The curing rate of a VLC RBC depends on the level of exposure, Fig. 6. High exposure creates a large number of radicals in the irradiated areas (in contrast to areas of a low exposure). A large number of radicals leads to a high rate of reaction. Therefore, at areas of high exposure, the T_g exceeds the polymerization temperature faster than in areas of a low exposure, and the
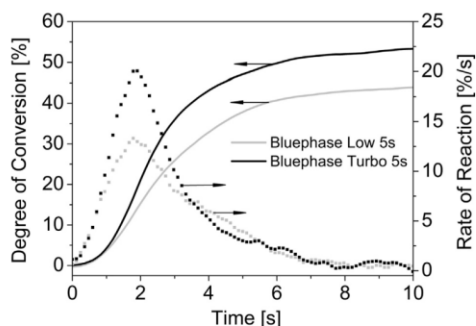
Fig. 6 – Degree of conversion (DC) and rate of DC$_{(t)}$ of Arabesk cured with Bluephase® 20i in Low and Turbo mode for 5 s.

radicals are immobilized earlier. Consequently, T_g exceeds the curing temperature later in areas of low exposure, leading to a longer curing time without radical immobilization. Hereby, prolonged exposure time may give the curing reaction at areas of low exposure enough time to reach the same cross-linking state as in areas of high exposure. Therefore, a longer exposure time is expected to enhance homogeneity of the hardness distribution.

The results of beam-profiling and other studies have shown that all LCUs have a specific irradiance distribution [30–32,37]. The corresponding irradiance and spectral distributions depend on the construction of the light source, reflector, lenses or other light interacting parts [33]. The LCUs used in this study have four LED chips. The arrangement of the LED chips is recognizable in the centers of each beam-profile, Fig. 4. The square of high irradiance in the center of the light beam of the Celalux® 2 is caused by the four LED chip areas that emit light with the same wavelength at the same power output. Broad-spectrum, poly-LED units attempt to overcome the problem of a narrow spectral emission from monowave LEDs using a combination of two different types of LED chips. The Bluephase® 20i shows a diffuse area of four superimposed spots caused by three LED chips, emitting at a wavelength of 460 nm above, to the right and below the center of the light beam and one LED chip emitting at a wavelength of 410 nm left of the center [33,46]. The low irradiance from the 410 nm

LED chip is widely separated from the high irradiance delivered from the 460 nm LED chips. Due to the design, the outer ring of the Celalux® 2 and the ⊃-shaped ring of the Bluephase® 20i are caused by the reflection of the light from the parabolic mirror within these units [33]. The area of high irradiance at the right edge of the beam profile of the Bluephase® 20i is caused by the superposition of the three LEDs emitting at a wavelength of 460 nm. The fact that the normalized irradiance values in the Low mode and Turbo mode do not differ. This confirms the assumption that the irradiance distribution is only generated by the internal optics of the LCU and not by the power output from the LED chips.

As long as there are radicals capable to react with acrylate groups of any kind the DC is increased and a denser resin network is formed shown by the increasing mean hardness with extended exposure time for each LCU. However, a complete homogenization was not observed for higher irradiance or longer exposure time. Thus, the irradiance distribution was not compensated by a longer exposure time.

The specific irradiance distribution of each LCU generates a corresponding distribution of the radical concentration [49]. Regions having a higher radical concentration reach a higher DC and as a consequence a greater local surface hardness. Therefore, regions with a long and high irradiance history end up with greater hardness values. Thus, long-term light exposure is increasing the level of hardness values but it is not affecting the hardness distribution. A homogeneous hardness distribution cannot be achieved simply by increasing the light exposure time.

This fact can be explained by considering the DC$_{(t)}$ rates of Arabesk. They reach the maximum after a light exposure time of 2–2.5 s and the DC reaches 40% after 5–6 s, Fig. 6. Such fast curing kinetics form the basic structure of the 3-dimensional polymer network within a few seconds. The mobility of the radicals and monomers is drastically reduced when the polymer network transfers to the glassy state [16,18]. Lovell et al. [14] showed that the T_g of a standard BisGMA/TEGDMA resin system exceeds the ambient temperature at a DC of approximately 40%. At this point, the irradiance distribution is frozen into the surface in terms of the hardness distribution. Below the glass temperature T_g further curing processes occur mainly in regions of high radical concentrations with available acrylate groups [50].

The specimens cured with the Celalux® 2 showed a more homogeneous hardness distribution than those cured with the Bluephase® 20i. Their hardness increase seems to spread

Table 6 – Result of the ATR-FTIR measurement, maximum reaction rate DC$_{(t)}$, time of maximum reaction rate, time to a DC of 40%, DC after 5, 20 and 80 s and DC$_{(3\ min)}$ for 5, 20 and 80 s exposure times after 180 s measurement time.

	Unit	Low mode	Turbo mode
Maximum reaction rate DC$_{(t)}$	%/s	13.3 (1.8)	20.6 (1.4)
Time to maximum of rate of DC	s	1.8 (0.1)	1.9 (0.1)
time to a DC of 40%	s	5.7 (0.1)	3.5 (0.1)
Low mode DC 5 s; turbo mode DC 1.5 s	%	41.6 (1.9)	31.4 (3.6)
Low mode DC 20 s; turbo mode DC 6 s	%	56.8 (1.3)	51.2 (2.3)
Low mode DC 80 s; turbo mode DC 24 s	%	63.6 (1.0)	60.8 (2.5)
DC$_{(3\ min)}$ 5 s [%]	%	54.2 (1.7)	62.5 (2.1)
DC$_{(3\ min)}$ 20 s [%]	%	62.3 (1.4)	64.7 (2.7)
DC$_{(3\ min)}$ 80 s [%]	%	65.2 (1.0)	67.3 (2.2)

from the center to the periphery of the specimens with longer light exposure times. The minimum hardness values correspond to minimum irradiances and vice versa. This can be seen for the positions (−2;−3) and (1;2) of Table 2c having irradiance values of 775 mW/cm^2 and 2672 mW/cm^2, respectively, while the corresponding hardness values are 23 KHN and 33 KHN on the Turbo mode hardness map after 80 s of exposure, Fig. 5c.

The comparison of irradiance and hardness in Table 3 for the Low mode and the Turbo mode shows that the irradiance distributions mirror the hardness distributions of the specimen surface. The CIF values show that this effect becomes less evident if the exposure time increases from 5 to 80 s, Table 4. This implies that the correlation between the irradiance and hardness decreases as the exposure time increases.

The hardness distributions in the sample surface are caused by the corresponding distributions of the DC [23]. Furthermore, shrinkage depends also on DC [15,24]. Thus, any hardness distribution implies an inhomogeneous shrinkage behavior [25]. The consequence is a distribution of internal stresses leading to unfavorable conditions and possible reduction in the longevity of restorations [26–29].

The mean top surface hardness of the Low mode specimen was greater than the Celalux® 2 specimens although it has only 50% of the Celalux® 2 irradiance. Increasing hardness and DC were reported in studies comparing the curing performance of mono- and polywave LCUs [34,36,51].

Miletic et al. assume that the differences in the polymerization are due to the differences of emitted wavelengths for various LCUs [34]. The Celalux® 2 has a peak maximum wavelength of 450 nm in contrast to the Low mode with 463 nm, Table 1. This wavelength fits better to the absorption peak maximum of CQ (470 nm) [41]. Park et al. suppose that the additional wavelength range of polywave LCUs in the lower range has an additional effect on the curing process [36]. This would explain the enhanced state of curing of the Low mode, which has an additional wavelength range of 390–435 nm, Table 1. Summarizing this, the differences in peak maxima and additional wavelength range explain the different curing performance from the Celalux® 2 and the Low mode.

The Turbo mode shows a lower DC value at each equivalent energy-time point, Table 6. The radiant exposure H_e of 3.3 J/cm^2 was reached after 1.5 s for the Turbo mode and after 5 s for the Low mode, respectively. The time range is 3.3 times longer for the Low mode. The maximum rate of $DC_{(t)}$ for the Turbo mode was not exceeded in contrast to the Low mode, Table 6. Therefore, the network formation for the Low mode has more time to proceed with the polymerization process. Equal DCs are reached after 2.7, 12.7 and 42.9 s for the Turbo mode and after 5, 20 and 80 s for the Low mode. For the Turbo mode both mean hardness after 80 s and mean $DC_{(3\,min)}$ after 180 s reached slightly higher values than for the Low mode, Table 6. These results may imply that the maximum DC depends on the irradiance level for similar spectra's of LCUs.

5. Conclusion

The first hypothesis "Each LCU has a specific irradiance distribution leading to a corresponding pattern of the hardness distribution of a dental composite surface." was confirmed in this study. The hardness distribution reflects the irradiance distribution of each LCU's.

The second hypothesis "The effects of differences of irradiance distributions of LCUs are compensated by longer exposure times." was rejected since longer exposure times do not lead to a complete homogenization of the hardness distribution, despite the observation of an improvement of homogeneity.

The results confirm findings of other researchers that exposure reciprocity is not a valid rule [11,45,46].

For clinical practice the effect of imaging the pattern of the irradiance distribution into the local mechanical properties is relevant. However, the majority of restoration cavities are smaller than the samples in this study, i.e. appearing with better homogeneity of irradiation, an optimal positioning of the LCU with respect to the restoration is more difficult. This may lead to more inadequate curing due to irradiance spots over a restoration. Locally insufficient curing of the VLC RBCs is the consequence causing not only mechanical instability, but further problems such as the elution of residual monomers or other substances [42].

REFERENCES

[1] Rueggeberg FA. State-of-the-art. Dental photocuring – a review. Dent Mater 2011;27:39–52.
[2] Leprince JG, Palin WM, Hadis MA, Devaux J, Leloup G. Progress in dimethacrylate-based dental composite technology and curing efficiency. Dent Mater 2013;29:139–56.
[3] Feng L, Carvalho RM, Suh BI. Insufficient cure under the condition of high irradiance and short irradiation time. Dent Mater 2009;25:283–9.
[4] Price RBT, McLeod ME, Felix CM. Quantifying light energy delivered to a Class I restoration. J Can Dent Assoc 2010;76:a23.
[5] Li J, Fok AS, Satterthwaite J, Watts DC. Measurement of the full-field polymerization shrinkage and depth of cure of dental composites using digital image correlation. Dent Mater 2009;25:582–8.
[6] D'Alpino PHP, Svizero NR, Pereira JC, Rueggeberg FA, Carvalho RM, Pashley DH. Influence of light-curing sources on polymerization reaction kinetics of a restorative system. Am J Dent 2007;20:46–52.

[7] Jandt KD, Mills RW. A brief history of LED photopolymerization. Dent Mater 2013;29:605–17.

[8] Bennett AW, Watts DC. Performance of two blue light-emitting-diode dental light curing units with distance and irradiation-time. Dent Mater 2004;20:72–9.

[9] Aravamudhan K, Rakowski D, Fan P. Variation of depth of cure and intensity with distance using LED curing lights. Dent Mater 2006;22:988–94.

[10] Halvorson RH, Erickson RL, Davidson CL. Energy dependent polymerization of resin-based composite. Dent Mater 2002;18:463–9.

[11] Peutzfeldt A, Asmussen E. Resin composite properties and energy density of light cure. J Dent Res 2005;84:659–62.

[12] Watts DC. Reaction kinetics and mechanics in photo-polymerised networks. Dent Mater 2005;21:27–35.

[13] Stansbury JW. Dimethacrylate network formation and polymer property evolution as determined by the selection of monomers and curing conditions. Dent Mater 2012;28:13–22.

[14] Lovell LG, Lu H, Elliott JE, Stansbury JW, Bowman CN. The effect of cure rate on the mechanical properties of dental resins. Dent Mater 2001;17:504–11.

[15] Amirouche-Korichi A, Mouzali M, Watts DC. Effects of monomer ratios and highly radiopaque fillers on degree of conversion and shrinkage-strain of dental resin composites. Dent Mater 2009;25:1411–8.

[16] Gonçalves F, Kawano Y, Pfeifer C, Stansbury JW, Braga RR. Influence of BisGMA, TEGDMA, and BisEMA contents on viscosity, conversion, and flexural strength of experimental resins and composites. Eur J Oral Sci 2009;117:442–6.

[17] Kloosterboer JG, Lijten G. Photopolymers exhibiting a large difference between glass transition and curing temperatures. Polymer 1990;31:95–101.

[18] Sideridou I, Tserki V, Papanastasiou G. Effect of chemical structure on degree of conversion in light-cured dimethacrylate-based dental resins. Biomaterials 2002;23:1819–29.

[19] Leprince J, Lamblin G, Truffier-Boutry D, Demoustier-Champagne S, Devaux J, Mestdagh M, et al. Kinetic study of free radicals trapped in dental resins stored in different environments. Acta Biomater 2009;5:2518–24.

[20] Watts D, McNaughton V, Grant A. The development of surface hardness in visible light-cured posterior composites. J Dent 1986;14:169–74.

[21] Uhl A, Mills RW, Jandt KD. Photoinitiator dependent composite depth of cure and Knoop hardness with halogen and LED light curing units. Biomaterials 2003;24:1787–95.

[22] Truffier-Boutry D, Demoustier-Champagne S, Devaux J, Biebuyck J, Mestdagh M, Larbanois P, et al. A physico-chemical explanation of the post-polymerization shrinkage in dental resins. Dent Mater 2006;22:405–12.

[23] Ferracane JL. Correlation between hardness and degree of conversion during the setting reaction of unfilled dental restorative resins. Dent Mater 1985;1:11–4.

[24] Stansbury JW, Trujillolemon M, Lu H, Ding X, Lin Y, Ge J. Conversion-dependent shrinkage stress and strain in dental resins and composites. Dent Mater 2005;21:56–67.

[25] Li J, Li H, Fok AS, Watts DC. Multiple correlations of material parameters of light-cured dental composites. Dent Mater 2009;25:829–36.

[26] Cramer NB, Stansbury JW, Bowman CN. Recent advances and developments in composite dental restorative materials. J Dent Res 2011;90:402–16.

[27] Schneider LFJ, Cavalcante LM, Silikas N. Shrinkage stresses generated during resin-composite applications: a review. J Dent Biomech 2010;1:1–14.

[28] Thompson VP, Watson TF, Marshall GW, Blackman BRK, Stansbury JW, Schadler LS, et al.

Outside-the-(cavity-prep)-box thinking. Adv Dent Res 2013;25:24–32.

[29] Xiong J, Sun X, Li Y, Chen J. Polymerization shrinkage, stress, and degree of conversion in silorane- and dimethacrylate-based dental composites. J Appl Polym Sci 2011;122:1882–8.

[30] Vandewalle KS, Roberts HW, Andrus JL, Dunn WJ. Effect of light dispersion of LED curing lights on resin composite polymerization. J Esthet Restor Dent 2005;17: 244–54.

[31] Arikawa H, Kanie T, Fujii K, Takahashi H, Ban S. Effect of inhomogeneity of light from light curing units on the surface hardness of composite resin. Dent Mater J 2008;27: 21–8.

[32] Vandewalle KS, Roberts HW, Rueggeberg FA. Power distribution across the face of different light guides and its effect on composite surface microhardness. J Esthet Restor Dent 2008;20:108–17.

[33] Price RBT, Rueggeberg FA, Labrie D, Felix CM. Irradiance uniformity and distribution from dental light curing units. J Esthet Restor Dent 2010;22:86–101.

[34] Miletic V, Santini A. Micro-Raman spectroscopic analysis of the degree of conversion of composite resins containing different initiators cured by polywave or monowave LED units. J Dent 2012;40:106–13.

[35] Neumann MG, Miranda WG, Schmitt CC, Rueggeberg FA, Correa IC. Molar extinction coefficients and the photon absorption efficiency of dental photoinitiators and light curing units. J Dent 2005;33:525–32.

[36] Park H, Son S, Hur B, Kim H, Kwon Y, Park J. Effect of the difference in spectral outputs of the single and dual-peak LEDs on the microhardness and the color stability of resin composites. J Korean Acad Conserv Dent 2011;36:108.

[37] Ilie N, Hickel R. Can CQ be completely replaced by alternative initiators in dental adhesives? Dent Mater J 2008;27: 221–8.

[38] Price RBT, Labrie D, Rueggeberg FA, Felix CM. Irradiance differences in the violet (405 nm) and blue (460 nm) spectral ranges among dental light-curing units. J Esthet Restor Dent 2010;22:363–77.

[39] Ilie N, Hickel R, Watts DC. Spatial and cure-time distribution of dynamic-mechanical properties of a dimethacrylate nano-composite. Dent Mater 2009;25:411–8.

[40] Emami N, Soderholm KM. How light irradiance and curing time affect monomer conversion in light-cured resin composites. Eur J Oral Sci 2003;111:536–42.

[41] Price RBT, Fahey J, Felix CM. Knoop microhardness mapping used to compare the efficacy of LED, QTH and PAC curing lights. Oper Dent 2010;35:58–68.

[42] Durner J, Obermaier J, Draenert M, Ilie N. Correlation of the degree of conversion with the amount of elutable substances in nano-hybrid dental composites. Dent Mater 2012;28:1146–53.

[43] Furche S, Hickel R, Reichl FX, van Landuyt K, Shehata M, Durner J. Quantification of elutable substances from methacrylate based sealers and their cytotoxicity effect on with human gingival fibroblasts. Dent Mater 2013;29: 618–25.

[44] Salzmann AC. Mikromechanischer Verschleiß dentaler Füllungsstoffe. Dissertation. Tübingen; 2006.

[45] Musanje L, Darvell B. Polymerization of resin composite restorative materials: exposure reciprocity. Dent Mater 2003;19:531–41.

[46] Leprince JG, Hadis M, Shortall AC, Ferracane JL, Devaux J, Leloup G, et al. Photoinitiator type and applicability of exposure reciprocity law in filled and unfilled photoactive resins. Dent Mater 2011;27:157–64.

[47] Rueggeberg FA, Hashinger D, Fairhurst C. Calibration of FTIR conversion analysis of contemporary dental resin composites. Dent Mater 1990;6:241–9.

[48] Specac Ltd. MK II Golden Gate Single Reflection ATR System User Manual; 2008.

[49] Leprince JG, Lamblin G, Devaux J, Dewaele M, Mestdagh M, Palin WM, et al. Irradiation modes' impact on radical entrapment in photoactive resins. J Dent Res 2010;89:1494–8.

[50] Anseth KS, Newman SM, Bowman CN. Polymeric dental composites: properties and reaction behavior of multimethacrylate dental restorations. Adv Polym Sci 1995:177–217.

[51] Leprince J, Devaux J, Mullier T, Vreven J, Leloup G. Pulpal-temperature rise and polymerization efficiency of LED curing lights. Oper Dent 2010;35:220–30.

PAPER VI

Corresponding Author: Mr. Thomas Haenel, M.Sc.

Corresponding Author's Institution: Bonn-Rhein-Sieg, University of
Applied Sciences

First Author: Thomas Haenel, M.Sc.

Order of Authors: Thomas Haenel, M.Sc.; Berenika Hausnerová, Ph.D.; Lara
Kehret, M.Sc.; Johannes Steinhaus, Ph.D.; Bernhard Moeginger, Dr.-Ing.

Abstract: Abstract
Objectives
Post-curing is a well-known phenomenon of cured dental composites leading
to an increase of mechanical properties such as stiffness, strength or
hardness. However, little attention has been paid to the kinetics of
post-curing. The present study investigates the post-curing behavior of a
dental composites cured with different curing protocols using time
resolved hardness data to express the kinetics of post-curing
quantitatively.
Methods
Three light curing units, a QTH, a monowave LED and a polywave LED were
characterized with respect to their emission spectra and compared to the
absorbance spectrum of CQ to determine the spectrum overlap. The
absorption behavior of the VLC RBC (Arabesk TOP OA2) was measured with an
integrating sphere to determine the attenuation of light. The samples
having a diameter of 8 mm and a height of 1 mm were cured for 5, 10, 20
and 40 s (polywave LED) or 20, 40 and 80 s (QTH and monowave LED). The
collecting of hardness data started 10 minutes after irradiation and
ended after 7 days using a Vickers hardness tester.
Results
With increasing irradiation time and irradiance of the LCU higher
hardness values were measured. The corresponding hardness curves became
straight lines if plotted versus logarithm of time allowing for
constructing master curves meaning that the kinetics of post-curing has a
logarithmic time dependency. The slopes are a measure for the rate of
post-curing in terms of HV/decade. For all the LCU the rate of post-
curing was higher in the top surface compared to the bottom surface
showing that post-curing does not level out property differences with
time and depends on the cross-sectional distance from the surface.
Furthermore, the total energy concept does not hold for Arabesk.
Significance

The derived master curve concept based on hardness evolution allows for predicting long term hardness due to post-curing processes. This gives the chance to compare effects of different curing protocols on post-curing kinetics and to estimate the long term properties of composites and their tolerance against mishandling. Furthermore, there is a high probability that the master curve concept also applies to other properties affected by post-curing extending the prediction possibilities.

Investigation of the Post-curing Behavior and Kinetics of a Dental Composite

Thomas Haenel[1,2,3], Berenika Hausnerová[1,3], Lara Kehret[2], Johannes Steinhaus[1,2,3], Bernhard Moeginger[2]

[1] Tomas Bata University in Zlin, Faculty of Technology, Department of Production Engineering, Zlin, Czech Republic

[2] Bonn-Rhein-Sieg University of Applied Sciences, Department of Applied Natural Sciences; Rheinbach, Germany

[3] Centre of Polymer Systems, University Institute, Tomas Bata University in Zlin, Zlin, Czech Republic

Keywords: visible light curing dental composites, degree of conversion, Vickers hardness, hardness change, post-curing kinetics, spectrum overlap to camphorquinone

Corresponding author:

Bernhard Moeginger

Bonn-Rhein-Sieg, University of Applied Sciences,

Department of Natural Sciences

Justus-von-Liebig Str. 20

53359 Rheinbach, Germany

Phone: +49 2241/865 531

bernhard.moeginger@h-brs.de

1. Introduction

Post curing processes in visible light curing resin based composites (hereinafter abbreviated by VLC RBC) sum up all changes of physical and chemical properties occurring after irradiation [1,2]. Cured VLC RBCs are highly cross-linked polymer networks in the glassy state which represents a thermodynamic non-equilibrium state [3–6]. Basically one can distinguish two driving forces of post-curing in VLC RBC: i) a slow increase of the degree of conversion due to diffusion controlled polymerization and cross-linking reactions [4,7] and ii) physical ageing due to relaxation processes towards the thermodynamic equilibrium [4,5] whereas the first is considered to be the dominant one. Both post-curing processes lead to an increase of stiffness and strength as well as hardness due to the denser and more cross-linked network [4].

In order to investigate post-curing or other long term processes of VLC RBC different methods such as time dependent hardness measurements [8], shrinkage measurements [9], measurement of degree of conversion using Fourier Transformation Infrared Spectroscopy (FTIR) [10,11], or dynamic mechanical analysis (DMA) [12] were used to gain insight in their kinetics. In dentistry hardness measurements are commonly used to characterize the mechanical property changes as it can be easily employed to small samples [13–15]. A further advantage is that the hardness of a VLC RBC is correlated to its degree of conversion under certain conditions [16–18].

During the curing reaction of a VLC RBCs the molecular weight increases with every monomer added to the polymer chain as well as the degree of conversion. With ongoing chain growth, viscosity [19] and mechanical properties [12,17,20–22] of a polymer change. Furthermore, the mobility of the polymer chains decreases with increasing molecular weight leading to the consequence that the glass transition temperature T_g exceeds ambient or process temperature [16,18,19,23,24]. Thus, the mobility of monomers and initiator molecules is

drastically inhibited within the polymer network and correspondingly the curing reaction. Now the radicals are trapped in the frozen matrix in which they can exist for weeks or months [24,25].

Due to Lovell et al [12] the liquid resin transfers to the glassy state if the degree of conversion approaches 40%. This degree of conversion is reached after 4 to 9 s after irradiation using LCUs with more 800 mW/cm² [26]. As there remain trapped immobile radicals a slow diffusion of monomers is still possible in the glassy state promoting further curing reactions via post-curing. This means that all properties related to degree of conversion should exhibit a corresponding time dependency.

For many VLC RBCs a reciprocity law called "total energy concept[27]" or "exposure reciprocity[28,29]" was empirically found stating that a long irradiation time with a low irradiance LCU leads to the same degree of conversion and mechanical properties as half the irradiation with a LCU having the double irradiance. The basic idea behind the total energy concept is that a certain amount of energy has to be introduced to a sample to "fully" cure it. Then the final curing state is only energy determined if introduced by the identical LCU of different power. The advantage is the total energy concept is that it allows predictions of the mechanical properties of VLC RBC to a certain extent. The concept is supported by the fact that a given VLC RBC achieved the same hardness value independently of the applied curing protocols if the same amount of energy was introduced [30,31].

However, long term DEA and DMA investigations show that post-curing is a long lasting process that does stop if sufficient energy is introduced [32]. In contrast, it seems to be an ongoing long term process which can level out reduced mechanical properties because not optimal curing procedures.

The aim of this study is to investigate the post-curing behavior of a VLC RBC depending on the curing conditions determined by LCUs and irradiation time. The hypothesis is that the kinetics of a post-curing process can be quantitatively determined by measuring time dependent hardness increase after irradiation.

2. Materials and methods

Materials and Light Curing Units (LCU)

The light curing dental composites Arabesk TOP OA2 (Voco, Cuxhaven, Germany, Lot-No.: 1040470), a micro-hybrid resin based composites with a filler content of 77%, was used for these investigation as the resin content of 23% allows for a better detection of hardness changes of the cured resin due to post-curing effects. In the following text to the composite is referred by "Arabesk". Three LCUs were used to cure the composites with irradiation times of 5 s, 10 s, 20 s, 40 s, and 80 s, Table 1.

Determination of LCU spectra, spectrum overlap and light absorption behavior

The spectra $I(\lambda)$ of the LCU lights between 350 to 550 nm were measured using an UV-VIS Micro-Spectrometer (Boehringer Ingelheim® microParts GmbH, Dortmund, Germany). These spectra were compared to the CQ absorbance spectrum to calculate the light intensities of the LCUs in the range of effective wavelengths. The range of effective wavelengths is determined by the lower (λ_a) and upper wavelength (λ_b) at the halfwidth of the CQ absorbance peak, Figure 1. Subsequently the spectrum overlap $O_{spectrum}$ of LCU can be calculated. It represents a measure for the radicalization efficiency of an LCU and is the ratio of its intensity between lower and upper wavelength to its total intensity.

$$O_{spectrum} = \frac{\int_{\lambda_a}^{\lambda_b} I(\lambda) * d\lambda}{\int_{350nm}^{550nm} I(\lambda) * d\lambda} \qquad (1)$$

At the surface of the samples the light coming from the LCU is partly reflected and does not contribute to the activation of initiator molecules. In order to know the real radiant exposure introduced to a sample the absorption behavior in terms of the depth dependent decrease of light intensity has to be determined. Therefore, Al-rings ($D_{out} = 21$ mm, $D_{in} = 10$ mm) having heights of 0.5, 1.0 and 1.5 mm were packed with Arabesk, covered with Mylar strips on top and bottom, and flattened between two microscope slides. The Al-rings were placed in the front entry of an integrating sphere (LabSphere 6″) equipped with UV-VIS spectrometer (USB 4000, Ocean Optics, Dunedin, Florida, USA). The light guide tip of the LCU was positioned in front of the sample directly on the Mylar strip, Figure 1a. The transmitted light intensity was measured for each thickness for 10 s through the cross section of the sample (n=3) and fitted with an exponential function due to Lambert-Beer-absorption.

Sample preparation and hardness measurement

Steel rings ($D_{out}= 20$ mm, $D_{inner}= 8$ mm, h = 1 mm) were packed with Arabesk and covered with microscope slides on the top and bottom to affirm flat surfaces for hardness measurements. The samples were irradiated from the top through the microscope slide for the times given in Table 1 with 8 samples (n=8) for each irradiation time. The experimental setup is shown in Figure 1b. After removal of the microscope slides the samples are ready for the hardness testing.

A Vickers hardness tester (Macro Vickers 5100 Series, Buehler GmbH, Düsseldorf, Germany) was used with a load of 200 gf (1.961 N) and 15 s indentation time. The hardness measurements started 10 min after irradiation whereas the indentations were randomly distributed on the top and bottom surface. The hardness measurements were repeated as often as possible for the first 2 h with a time protocol. Further hardness measurements were performed after 4, 8, 24, and 170 h with 5 indentations each. The samples were stored in a dry and dark environment at room temperature between the measurements.

Evaluation method

Mean values and standard deviations of the hardness measurements were calculated for 3 min intervals during the first 2 h. The hardness measurements after 4, 8, 24, and 170 h were verified using a Nalimov outlier test before calculating mean hardness and standard deviation for each time group. A normality test was performed to verify a comparison between top and bottom hardness values. Sample groups which passed this normality test were tested by a one-way ANOVA with a Tukey test ($\alpha = 0.05$) to compare the data of top and bottom surface.

3. Results

The maximum absorbance of CQ is at a wavelength of 469 nm reported as the most efficient wavelength [11] Due to the intercepts of half-width and absorbance peak of CQ the lower and upper wavelength were determined to 444 nm and 504 nm, respectively, Figure 2. It can be seen that the area given by height of absorbance peak A_{max} and half-width corresponds approximately to the area under the absorbance curve of CQ. The radicalization efficiency of LCUs may be quantified by the area of its spectrum between lower and upper wavelength. Table 1 shows that the spectrum overlap $O_{spectrum}$ differs for the three LCUs between 70% (QTH) and 90% (Celalux). This has to be taken into account if the radiant exposure is calculated using the irradiances provided by the manufacturers.

The light intensity within the sample depends on the distance from the surface, and thus, on the thickness of the sample, Figure 3. The data can be fitted using an exponential function due to Lambert-Beer-absorption with a R^2=0.950. The difference between the irradiance of the LCU (1512 mW/cm²) and the extrapolated irradiance at the sample surface (1148 mW/cm²) indicates that approximately 25% of the light are reflected. The attenuation coefficient of 0.821/mm corresponds to a penetration depth of the light of 1.22 mm, a value similar to those found by other researchers [33].

The hardness values of top and bottom surface increase approximately a factor 2 in the considered time range of 7 days, Table 2 The top surface hardness values increased from 25 HV after 10 min (20s – Celalux) to 55 . The bottom surface hardness values increased from 21 HV (5s – Bluephase 20i Turbo) 54 HV (80 s – Polofil Lux). The maximum hardness increase of around 15 HV was found during the first 110 minutes after irradiation, Figure 4. With respect to standard deviations the hardness after 24 hours and 7 days are identical. This means that further property changes due to post-curing processes – if there are any – are not detectable by hardness measurements anymore.

The Bluephase 20i Turbo is a high irradiance LCU especially developed for composites containing a further initiator system besides CQ which can then be cured at irradiation times between 5 and 10 s [34]. However, if composites containing only a CQ initiator system are cured with the Bluephase 20i Turbo an irradiation time of 5 s can be too short for sufficient cure. Although the hardness values at the top surface after an irradiation time of 5 s are comparable to those cured for 20 s with the Celalux and Polofil Lux, Table 2, the hardness values at the bottom surface are significantly lower. Furthermore, the hardness values at the bottom surface increase slower compared to those cured for 20 s with the Celalux and Polofil Lux. This means post-curing did not compensate in the long term if the bottom surface was undercured.

In most cases, the normality test was not passed for the hardness values of top and bottom surface for the first 110 min, Table 2. Thus, the hardness data of top and bottom surface have to be handled separately if the one-way ANOVA test is applied. The comparisons of the top and bottom hardness values with the one-way ANOVA test were not passed. Therefore, the bottom hardness values are differ from each and cannot combine to mean hardness values.

The increasing hardness values seem to have a logarithmic time dependency. If the hardness values are plotted versus logarithm of time the hardness values lay on straight lines, Figure 4. It can be seen that the hardness values of the top surface are always larger than those of the bottom surface although the difference between them is decreasing for longer irradiation times.

On first sight the slopes of the hardness increase on the logarithmic time scale seem to be similar for the different irradiation times. This suggests the presence of a superposition principle for the post-curing process – short term hardness values of long irradiation times correspond to long term hardness values of short irradiation times – allowing for constructing a master curve using the function

$$HV\left(\lg\left(a_{t_{irrad}} * t\right)\right) = a * \lg\left(a_{t_{irrad}} * t\right) + b = a * \left(\lg t + \lg a_{t_{irrad}}\right) + b \qquad (2)$$

with Vickers hardness HV, time t, shift factor $a_{t_{irrad}}$, slope a and intercept b.

Figure 5 shows that the hardness values of different irradiation times can be shifted nicely to master curves if shifted with the shift factors given in Table 3a and b. If the master curves are fitted linearly it is found that the slopes of the hardness of the top surface are slightly larger than those of the bottom surface, Figure 6 and Table 4. The construction of master curves requires the definition of reference measurements which are given by hardness curves irradiated for 20 s (Polofil Lux and Celalux) and 10 s (Bluephase 20i Turbo) as these irradiation conditions correspond to radiant exposures of approximately 20 J/cm².

With increasing irradiance the hardness values become higher for the same post-curing time, Figure 7. Furthermore, the slopes of the master curves differ not much but they are found to be slightly larger if the samples have a smaller initial hardness expressed by interception b and thus a lower degree of conversion when post-curing starts.

181

4. Discussion

The correlation of degree of conversion, irradiance and mechanical properties is well-known for VLC-RBCs [16–18]. Therefore, hardness is often measured due to its simple and quick performance to characterize the state of cure after irradiation as a final hardness seems to be reached if the VLC RBC has "fully" cured.

The hardness data of both top and bottom surface reveals different curing efficiencies ranking the LCUs according to increasing hardness as follows: Celalux, Polofil Lux Bluephase 20i Turbo, Table 2. That the Celalux produces samples of the lowest hardness is surprising as it has almost the same irradiance as the Polofil Lux but a much higher spectrum overlap of 90% compared to 70%. This means that the Polofil Lux, a QTH LCU, cures in a different way than the Celalux, a LED LCU. One can identify two possible differences. Firstly, a QTH LCU introduces more heat to the sample leading to higher curing temperatures or process temperatures although an IR filter is to absorb most of the IR radiation. This gives the curing reaction more time before the glass transition temperature T_g exceeds the process temperature freezing in the initial curing reaction [19]. As a consequence, degree of conversion as well as hardness becomes higher. Secondly, the spectrum of the Polofil Lux shows still a lot of intensity in the wavelength range of 360 to 444 nm. Thus, it could be possible that inelastic light scattering processes may either increase the intensity in the range of spectrum overlap or the temperature due to photo-thermal effects [35–37].

Due to Figure 4 the hardness values increase logarithmically with time after irradiation allowing for constructing master curves. This is surprising as the hardness is related rather to the strength of a material than to the stiffness (Young's modulus) [38]. Furthermore, it turns out that the hardness values of top and bottom surface distinguish even after 7 days of post-curing showing that there is no levelling out of hardness differences due to post-curing. If the master curves are fitted linearly the slope of the hardness increase is a measure of the kinetics

of the post-curing processes in terms of hardness increase per decade of time. For Arabesk the slope is 6 to 7 HV/decade of time, Table 4a and b, predicting a hardness increase from 55 HV after 7 days to 61 HV after 70 days. As the slope depends on the time interval of evaluation – the hardness increase is around 7 HV/decade for a time interval of 24 h, Table 4a, while it is around 6 HV/decade for a time interval of 7 days – one can conclude that the kinetics of the post-curing process slows down with time more than predicted by the logarithmic time dependency. However, this assumption has to be verified with experiments and methods which are more sensitive to resin changes induced by post-curing.

For all three LCUs the slopes of the master curves determined for the bottom surface are always smaller than those for the top surface. In spite of the fact that both top and bottom hardness increase with time due to post-curing the rate at the bottom surface is 0.2 to 0.5 HV/decade less. This means that post-curing processes do not level out local differences of hardness due to local differences of degree of conversion generated by the initial curing conditions. This corresponds to findings of Haenel et al [26] showing that the intensity distribution of LCU is mirrored in the hardness distribution of resin composites even after long irradiation times.

In principle, the interpretation of this result is that the kinetics of post-curing processes are determined by the conditions under which the liquid resin was transferred to the glassy state. At the bottom surface in a depth of 1 mm the light intensity is approximately half that of the top surface. If one assumes that radical concentration is proportional to irradiance the cured Arabesk resin has roughly the double cross-linking density at the top surface compared to bottom surface. Both surfaces are in glassy state, however, the molecular mobility at the bottom surface is a little bit higher due to the less cross-linked network. On first sight this should lead to a higher rate of post-curing. However, the rate of radical annihilation is also increased especially if further irradiation generates new radicals via initiation reactions. The

decrease of radical concentration subsequently decreases the rate of post-curing. Thus, "high" rates of post-curing can be expected only if the cured resin consists of a highly cross-linked network in which the radicals are bound to immobile chain ends and hardly subjected to termination reactions.

The rate of post-curing depends on irradiance as the master curves are shifted to higher hardness values, Figure 7. The slopes of the master curves are slightly larger if the initial hardness and thus the degree of conversion are smaller when post-curing starts. This means on one hand side less cured samples show more post-curing. But on the other hand side for all 3 LCUs the post-curing rate at the bottom surface is smaller where the degree of conversion is lower. This contradictive result can only mean that all LCUs transfer the resin network at the surface to a degree of cross-linking at which all radicals are completely immobilized. Because of lower irradiances the degree of conversion is slightly lower with a higher molecular mobility leading to a higher rate of post-curing whereas at the bottom surface the above described process takes place.

Conclusion

The investigation of the post-curing behavior the VLC RBC Arabesk shows clearly that the hardness curves depend both on irradiation times and LCU irradiances. Surprisingly for each LCU the hardness curves of each irradiation time could be superposed to a master curve as they exhibited similar slopes if plotted versus logarithm of time. The kinetics of post-curing has to depend logarithmically on time for at least 7 days after irradiation. Fitting the hardness curves produced higher rates of post-curing for the top surfaces than for the bottom surfaces. Although the hardness increased the rate of post-curing differs cross-sectional distance from the surface, differences in the degree of curing and the corresponding hardness were not leveled out. This means that the network structure achieved in the moment in which the resin

transfers from the liquid to the glassy state determines the post-curing kinetics to a large extent.

As the QTH LCU Polofil Lux and LED LCU Celalux have almost identical irradiances they should produce samples with very similar hardness curves due to the total energy concept. However, the samples cured with Celalux showed lower hardness values although its spectrum overlap to CQ is 90% compared to 70% for the QTH LCU. Thus, the total energy concept fails for Arabesk and should be considered only as a rough estimate.

The post-curing curves of hardness vs. logarithmic time show a self-similar behavior. This allowed to develop a master curve concept by superimpose the several post-curing curves by shifting on the x-axis. The hardness vs. logarithmic time curves show a linear progress and allow predicting the post-curing behavior of an expanding time scale. The results of the master curves show that the Top and Bottom post-cuing have a slightly different progress which is not compensate by the post-curing which reflects the influence of the absorbance energy with increase thickness of the samples.

References

[1] Cook WD and Johannson M. The influence of postcuring on the fracture properties of photo-cured dimethacrylate based dental composite resin. J. Biomed. Mater. Res., 1987; 21:979–989.

[2] Stansbury JW. Curing Dental Resins and Composites by Photopolymerization. J Esthet Restor Dent, 2000; 12:300–308.

[3] Simon F. Über den Zustand der unterkühlten Flüssigkeiten und Gläser. Z. Anorg. Allg. Chem., 1931; 203:219–227.

[4] Treloar, L. R. G. The physics of rubber elasticity. Oxford, New York, 2005.

[5] Hutchinson JM. Physical aging of polymers. Progress in Polymer Science, 1995; 20:703–760.

[6] Sideridou I, Tserki V and Papanastasiou G. Effect of chemical structure on degree of conversion in light-cured dimethacrylate-based dental resins. Biomaterials, 2002; 23:1819–1829.

[7] Leprince JG, Lamblin G, Devaux J, Dewaele M, Mestdagh M, Palin WM, Gallez B and Leloup G. Irradiation modes' impact on radical entrapment in photoactive resins. Journal of Dental Research, 2010; 89:1494–1498.

[8] Ozcan S, Yikilgan I, Uctasli MB, Bala O and Kurklu, Zeliha Gonca Bek. Comparison of time-dependent changes in the surface hardness of different composite resins. European journal of dentistry, 2013; 7:S20-5.

[9] Uhl A, Mills RW, Rzanny AE and Jandt KD. Time dependence of composite shrinkage using halogen and LED light curing. Dental materials : official publication of the Academy of Dental Materials, 2005; 21:278–286.

[10] Halvorson RH, Erickson RL and Davidson CL. Energy dependent polymerization of resin-based composite. Dental Materials, 2002; 18:463–469.

[11] Nomoto R. Effect of light wavelength on polymerization of light-cured resins. Dent Mater J, 1997; 16:60–73.

[12] Lovell LG, Lu H, Elliott JE, Stansbury JW and Bowman CN. The effect of cure rate on the mechanical properties of dental resins. Dental Materials, 2001; 17:504–511.

[13] Asmussen E. Restorative resins: hardness and strength vs. quantity of remaining double bonds. Eur J Oral Sci, 1982; 90:484–489.

[14] Greener EH, Greener CS and Moser JB. The hardness of composites as a function of temperature. J Oral Rehabil, 1984; 11:335–340.

[15] Alrahlah A, Silikas N and Watts DC. Post-cure depth of cure of bulk fill dental resin-composites. Dental materials : official publication of the Academy of Dental Materials, 2014; 30:149–154.

[16] Leung RL, Fan PL and Johnston WM. Post-irradiation Polymerization of Visible Light-activated Composite Resin. Journal of Dental Research, 1983; 62:363–365.

[17] Ferracane JL. Correlation between hardness and degree of conversion during the setting reaction of unfilled dental restorative resins. Dental Materials, 1985; 1:11–14.

[18] Santos GB, Medeiros IS, Fellows CE, Muench A and Braga RR. Composite depth of cure obtained with QTH and LED units assessed by microhardness and micro-Raman spectroscopy. Operative dentistry, 2007; 32:79–83.

[19] Fox TG and Loshaek S. Influence of molecular weight and degree of crosslinking on the specific volume and glass temperature of polymers. J. Polym. Sci., 1955; 15:371–390.

[20] Eliades GC, Vougiouklakis GJ and Caputo AA. Degree of double bond conversion in light-cured composites. Dental Materials, 1987; 3:19–25.

[21] Lovell LG, Berchtold KA, Elliott JE, Lu H and Bowman CN. Understanding the kinetics and network formation of dimethacrylate dental resins. Polym. Adv. Technol., 2001; 12:335–345.

[22] Beun S, Glorieux T, Devaux J, Vreven J and Leloup G. Characterization of nanofilled compared to universal and microfilled composites. Dent Mater, 2007; 23:51–59.

[23] Wu W and Fanconi BM. Post-curing of dental restorative resin. Polym. Eng. Sci., 1983; 23:704–707.

[24] Leprince J, Lamblin G, Truffier-Boutry D, Demoustier-Champagne S, Devaux J, Mestdagh M and Leloup G. Kinetic study of free radicals trapped in dental resins stored in different environments. Acta Biomaterialia, 2009; 5:2518–2524.

[25] Watts DC. Reaction kinetics and mechanics in photo-polymerised networks. Dent Mater, 2005; 21:27–35.

[26] Haenel T, Hausnerová B, Steinhaus J, Price, Richard B T, Sullivan B and Moeginger B. Effect of the irradiance distribution from light curing units on the local micro-hardness of the surface of dental resins. Dental materials : official publication of the Academy of Dental Materials, 2015; 31:93–104.

[27] Peutzfeldt A and Asmussen E. Resin Composite Properties and Energy Density of Light Cure. Journal of Dental Research, 2005; 84:659–662.

[28] Leprince JG, Hadis M, Shortall AC, Ferracane JL, Devaux J, Leloup G and Palin WM. Photoinitiator type and applicability of exposure reciprocity law in filled and unfilled photoactive resins. Dental materials : official publication of the Academy of Dental Materials, 2011; 27:157–164.

[29] Selig D, Haenel T, Hausnerová B, Moeginger B, Labrie D, Sullivan B and Price RBT. Examining exposure reciprocity in a resin based composite using high irradiance levels and real-time degree of conversion values. Dent Mater, 2015; 31:583–593.

[30] Emami N and Soderholm K-JM. How light irradiance and curing time affect monomer conversion in light-cured resin composites. Eur. J. Oral Sci., 2003; 111:536–542.

[31] Abate PF, Zahra VN and Macchi RL. Effect of photopolymerization variables on composite hardness. The Journal of prosthetic dentistry, 2001; 86:632–635.

[32] Steinhaus J, Frentzen M, Rosentritt M and Möginger B. Dielectric Analysis of Short-Term and Long-Term Curing of Novel Photo-Curing Dental Filling Materials. Macromol. Symp., 2010; 296:622–625.

[33] Steinhaus J, Moeginger B, Grossgarten M, Rosentritt M and Hausnerova B. Dielectric analysis of depth dependent curing behavior of dental resin composites. Dent Mater, 2014; 30:679–687.

[34] Ivoclar Vivadent. Bluephase 20i. Licence to cure. LED for every use. LED for every use.

[35] Knezevic A, Tarle Z, Meniga A, Sutalo J, Pichler G and Ristic M. Degree of conversion and temperature rise during polymerization of composite resin samples with blue diodes. J Oral Rehabil, 2001; 28:586–591.

[36] Howard B, Wilson ND, Newman SM, Pfeifer CS and Stansbury JW. Relationships between conversion, temperature and optical properties during composite photopolymerization. Acta Biomaterialia, 2010; 6:2053–2059.

[37] Jung H, Friedl K-H, Hiller K-A, Furch H, Bernhart S and Schmalz G. Polymerization efficiency of different photocuring units through ceramic discs. Operative dentistry, 2006; 31:68–77.

[38] Ferry JD. Viscoelastic properties of polymers. New York, 1980.

List of figures

List of tables

Table 1 Properties of LCUs

Table 1: Properties of the used LCUs and applied exposure radiants				
LCU	Polofil® Lux	Celalux®	Bluephase® 20i	
Manufacturer	Voco GmbH Cuxhaven, Germany		Ivoclar Vivadent, Schaan, Lichtenstein	
LCU Type	QTH	LED Monowave	LED Polywave, Turbo Mode	
Peak Wavelength [nm]	450	450	410	460
Peak Width [nm]	370-520	380-435	395-430	430-495
Irradiance Total Area [mW/cm²]	1179 (6)	1156 (2)	2222 (24)	
Radiant Exposure [J] Irradiation Times 5s, 10s, 20s, 40s, 80s	9.6; 19.2; 38.4	9.0; 18.0; 35.9	4.5; 9.1; 18.1; 36.2	
Spectrum Overlap	70%	90%	82%	

Table 2 Change of top and bottom hardness

Table 2: Change of top and bottom hardness with time after irradiation								
		Irradiation Time [s]	Post-Curing Time					
			10 min [HV]	110 min [HV]	240 min [HV]	480 min [HV]	1400 min [HV]	10000 min [HV]
Top	Polofil Lux	20	29.6 (1.0)	40.9 (0.3)	42.6 (0.6)	44.5 (0.8)	49.2 (1.1)	50.2 (1.5)
		40	33.9 (0.7)	43.3 (0.4)	45.6 (1.1)	48.0 (1.2)	52.1 (0.8)	54.8 (1.2)
		80	39.6 (2.7)	48.1 (0.3)	49.1 (2.2)	50.7 (1.5)	55.8 (1.7)	54.2 (0.7)
	Celalux	20	25.1 (0.0)	37.8 (1.2)	41.4 (1.8)	43.1 (0.7)	46.3 (0.9)	47.5 (1.5)
		40	31.3 (1.2)	39.0 (1.5)	41.6 (1.8)	44.0 (1.1)	47.1 (1.7)	47.0 (0.3)
		80	35.8 (3.5)	41.5 (0.8)	44.2 (0.8)	46.6 (1.4)	48.9 (1.7)	52.0 (0.9)
	Bluephase 20i Turbo	5	28.7 (1.3)	39.5 (0.8)	42.3 (1.4)	42.6 (1.0)	47.6 (1.8)	48.2 (2.4)
		10	34.5 (1.5)	42.4 (0.2)	44.6 (0.5)	47.7 (0.6)	51.9 (1.2)	52.3 (1.1)
		20	39.0 (0.7)	44.4 (0.7)	47.8 (1.8)	50.3 (1.0)	53.8 (1.7)	55.2 (1.4)
		40	43.5 (1.3)	47.9 (0.3)	50.1 (0.9)	52.3 (0.8)	55.1 (0.9)	54.6 (0.6)
Bottom	Polofil Lux	20	26.6 (1.0)	36.3 (0.8)	39.2 (0.7)	39.7 (0.5)	43.5 (1.6)	44.9 (1.8)
		40	30.3 (1.4)	41.7 (0.4)	43.6 (1.1)	46.2 (1.8)	50.4 (0.9)	53.2 (1.8)
		80	39.3 (5.3)	46.4 (0.7)	47.1 (3.2)	49.8 (1.7)	55.1 (1.6)	53.0 (0.9)
	Celalux	20	25.6 (1.2)	36.3 (0.7)	40.1 (1.7)	40.8 (1.3)	44.4 (1.3)	45.8 (1.0)
		40	31.7 (0.9)	40.1 (0.7)	42.2 (1.2)	44.4 (1.0)	48.1 (1.0)	47.5 (0.9)
		80	36.7 (4.2)	42.7 (0.6)	44.6 (0.7)	47.3 (1.1)	49.6 (1.1)	52.1 (0.6)
	Bluephase 20i Turbo	5	21.0 (1.2)	31.1 (0.9)	33.0 (0.8)	32.9 (0.7)	36.5 (1.7)	36.9 (3.1)
		10	32.2 (1.7)	41.0 (0.5)	42.2 (1.1)	45.2 (1.2)	49.3 (1.9)	50.2 (0.4)
		20	37.3 (2.0)	43.6 (0.5)	46.7 (1.7)	49.1 (1.9)	52.2 (2.5)	53.5 (1.1)
		40	43.2 (1.7)	46.9 (0.5)	49.4 (0.8)	51.4 (0.5)	53.8 (0.9)	53.4 (1.2)

Table 3 a and b loagrithm of shift factor

Table 3a: Logarithm of shift factors determined using data of 7 days						
	QTH		Celalux		Turbo	
Irradiation time	Top	Bottom	Top	Bottom	Top	Bottom
5					-0.55	-1.65
10					0.00	0.00
20	0.00	0.00	0.00	0.00	0.44	0.64
40	0.48	0.84	0.20	0.56	0.99	1.28
80	1.26	1.63	0.72	1.14		

Table 3b: Logarithm of shift factors determined using data of 24 h						
	QTH		Celalux		Turbo	
Irradiation time	Top	Bottom	Top	Bottom	Top	Bottom
5					-0.50	-1.46
10					0.00	0.00
20	0.00	0.00	0.00	0.00	0.39	0.58
40	0.43	0.73	0.18	0.50	0.89	1.15
80	1.16	1.45	0.63	1.00		

Table 4 a and b fit parameter

Table 4a: Fit parameter slope a and interception b of master curves with corresponding R^2 using data of 7 days				
	LCU	Slope a	Interception b [HV]	R^2
Top	QTH	6.41	26.5	0.933
	Celalux	6.51	23.7	0.940
	Turbo	6.12	29.8	0.956
Bottom	QTH	6.27	23.0	0.950
	Celalux	6.23	22.9	0.956
	Turbo	5.65	28.4	0.980

Table 4b: Fit parameter slope a and interception b of master curves with corresponding R^2 using data of 24 h				
	LCU	Slope a	Interception b [HV]	R^2
Top	QTH	7.15	25.2	0.944
	Celalux	7.41	22.1	0.952
	Turbo	6.95	28.4	0.970
Bottom	QTH	7.10	21.6	0.962
	Celalux	7.16	21.3	0.970
	Turbo	6.38	27.2	0.990

Integrating Sphere

Sample

UV-Vis Detektor

Light Guide Tip

Sample Holder

a)

Light Guide

Microscope slides

Sample

Sample holder

∅8 mm

1 mm

b)
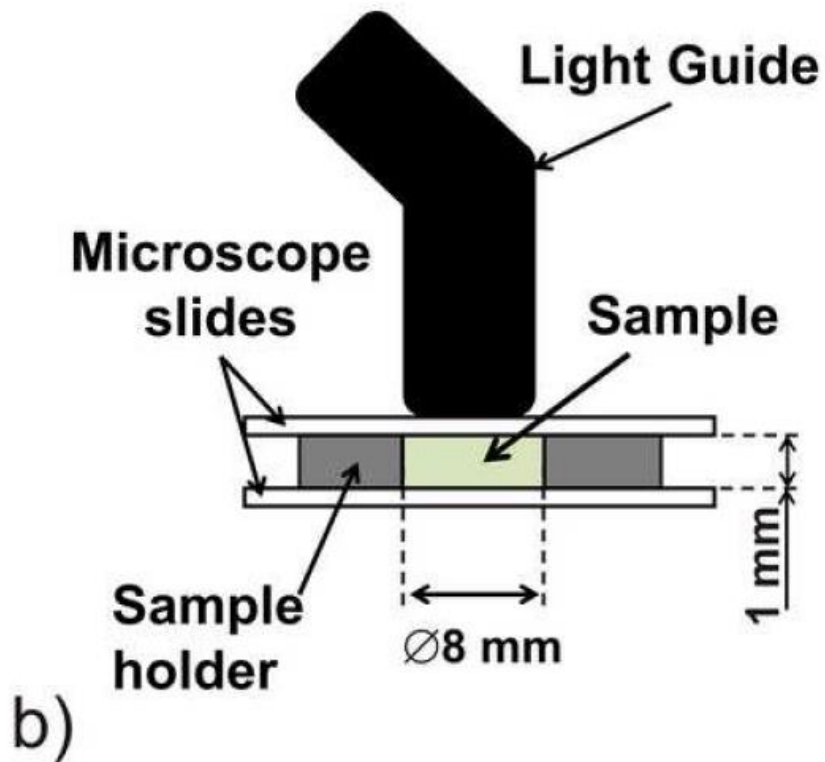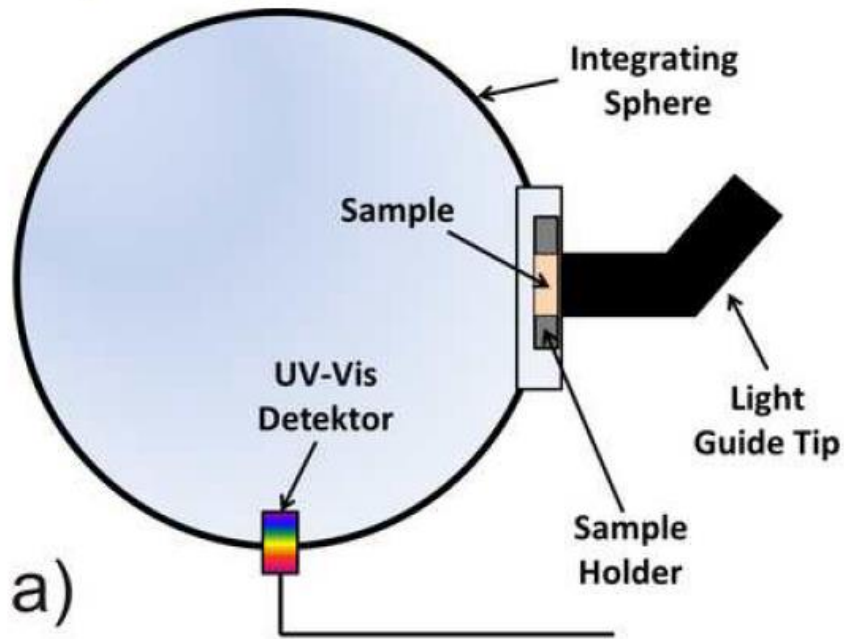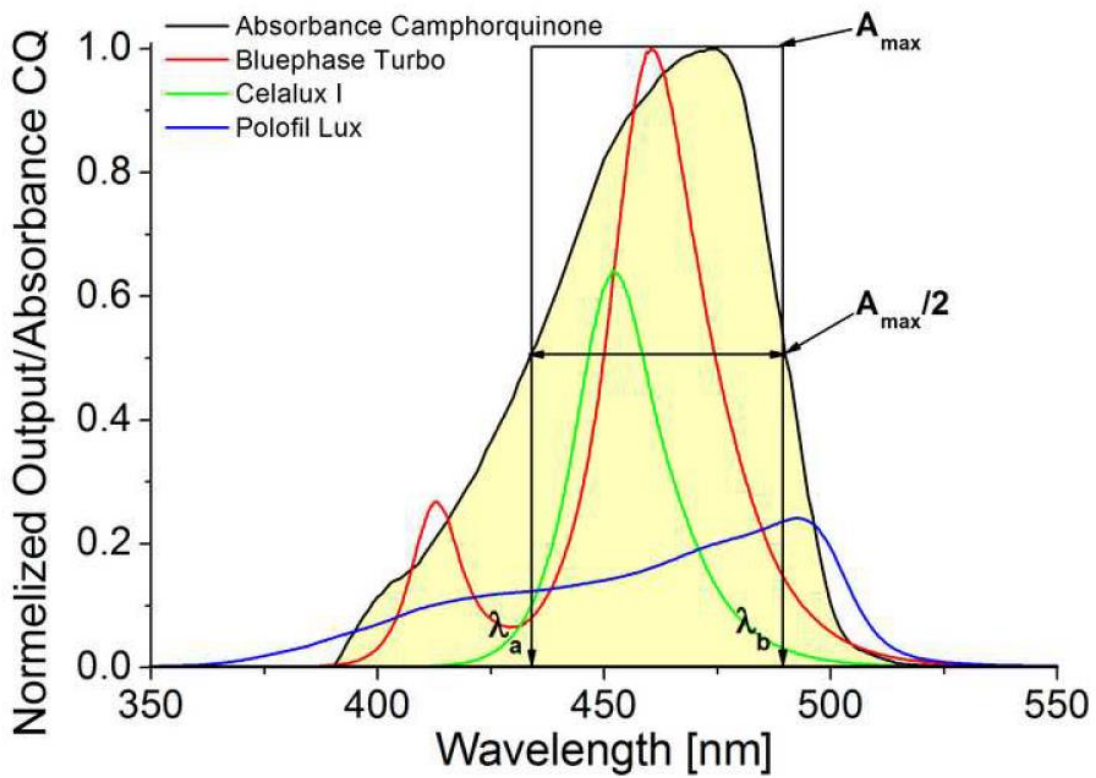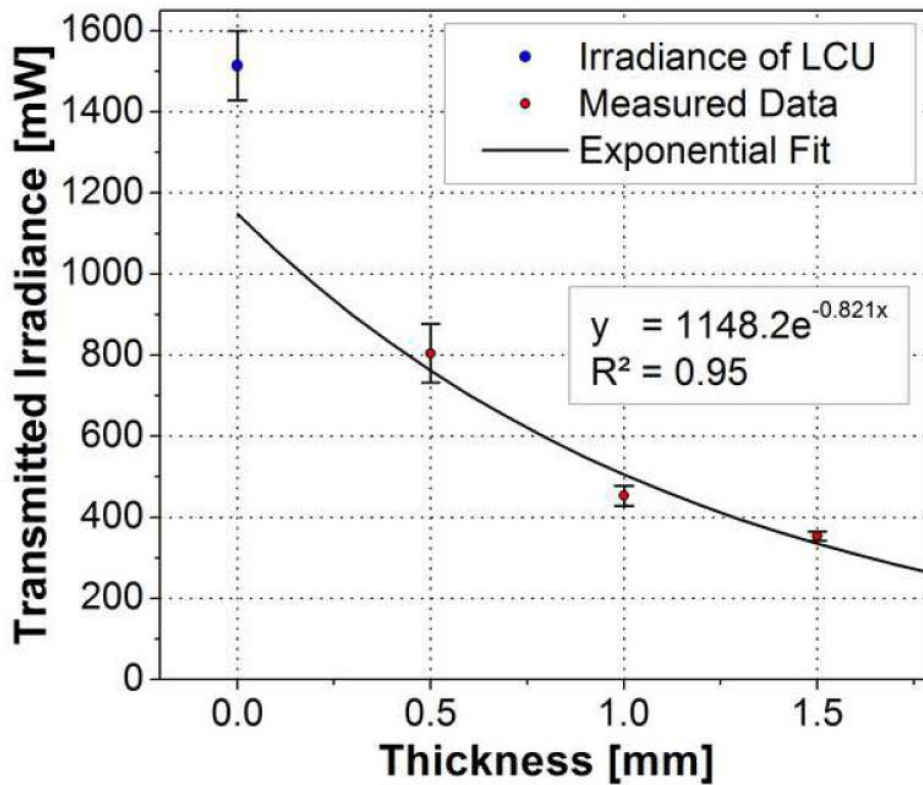
Figure 4 Time dependent hardness